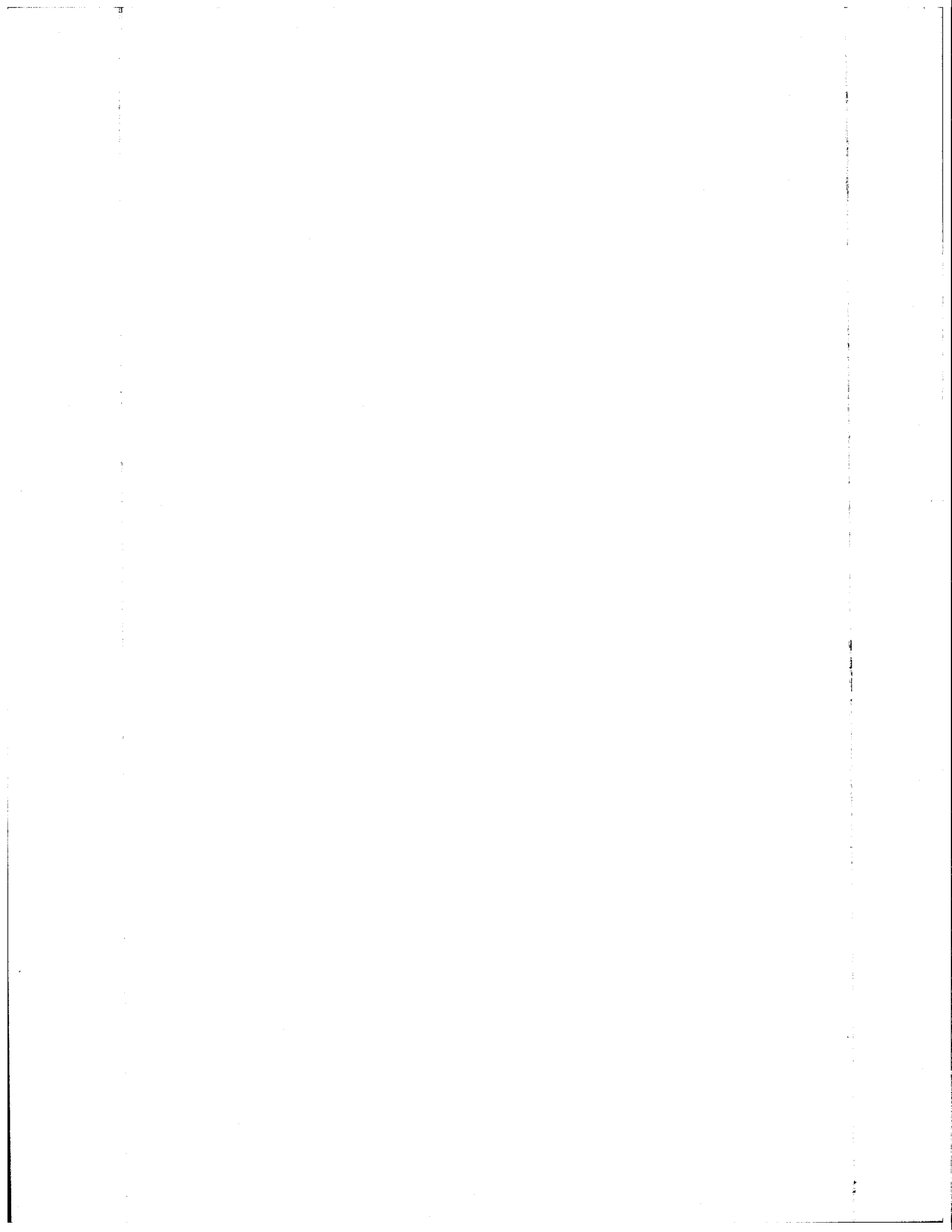


NOTE TO USERS

This reproduction is the best copy available.

UMI[®]



UNIVERSITY OF SASKATCHEWAN, REGINA CAMPUS

FACULTY OF GRADUATE STUDIES

CERTIFICATION OF THESIS WORK

We, the undersigned, certify thatThemistocles P. Paradellis.

.....

candidate for the Degree of Doctor of Philosophy in Nuclear Physics

has presented his thesis on the subject ...A Study of the Excited

.....States of Some Spheroidal Nuclei.....

.....

that the thesis is acceptable in form and content, and that the student

demonstrated a satisfactory knowledge of the field covered by his thesis

in an oral examination held onApril 17, 1970.....

External Examiner R. E. Bell

Professor of Physics, McGill University.

Internal Examiners J. X. Walston

S. H. Nagi
~~.....~~

C. P. Bell

John J. Gagnon

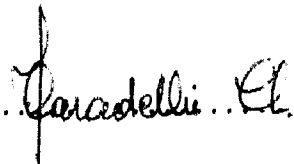
A. B. MacClellan

.....
.....
.....

PERMISSION TO USE POSTGRADUATE THESES

Title of thesis ... A Study of the Excited States of Some
..... Spheroidal Nuclei
.....
Name of Author ... Themistocles P. Paradellis
Division or College ... Physics, Division of Natural Sciences & Mathemat.
Degree ... Doctor of Philosophy in Nuclear Physics

In presenting this thesis in partial fulfillment of the requirements for a postgraduate degree from the University of Saskatchewan, I agree that the Libraries of this University shall make it freely available for inspection. I further agree that permission for extensive copying of this thesis for scholarly purposes may be granted by the professor or professors who supervised my thesis work or, in their absence, by the Chairman of the Division, the Head of the Department or the Dean of the College in which my thesis work was done. It is understood that any copying or publication or use of this thesis or parts thereof for financial gain shall not be allowed without my written permission. It is also understood that due recognition shall be given to me and to the University of Saskatchewan, Regina Campus, in any scholarly use which may be made of any material in my thesis.

Signature 
Date April 17, 1970

27/9/66
100 c.

A STUDY OF
THE
EXCITED STATES OF SOME
SPHEROIDAL NUCLEI

A Thesis

Submitted to the Faculty of Graduate Studies
In Partial Fulfilment of the Requirements
For the Degree of
Doctor of Philosophy
in Physics
Division of Natural Sciences and Mathematics
University of Saskatchewan, Regina Campus

by

Themistocles P. Paradellis

March, 1970

UMI Number: DC52120

UMI[®]

UMI Microform DC52120

Copyright 2006 by ProQuest Information and Learning Company.
All rights reserved. This microform edition is protected against
unauthorized copying under Title 17, United States Code.

ProQuest Information and Learning Company
300 North Zeeb Road
P.O. Box 1346
Ann Arbor, MI 48106-1346

ABSTRACT

The decay of ^{75}Se , ^{78}As and ^{92}Y has been investigated by means of high resolution Ge(Li) detectors. The accurate relative efficiency calibration of a variety of Ge(Li) detectors has been used to test a semi-empirical relative efficiency equation. It was found that the relative efficiency of a particular detector may be expressed through an equation relating the efficiency with the photoelectric and Compton coefficients of Germanium, the active volume of the detector and the energy of the detected photons.

Single and coincidence spectra revealed the existence of three previously unobserved gamma rays in ^{75}As at 24.4, 81.0 and 468.6 KeV. The accurate intensity data obtained here have been combined with conversion electron intensity and half life data available in the literature to obtain accurate conversion coefficients and transition rates in ^{75}As .

The ^{78}As activity has been produced via the $^{78}\text{Se}(n,p)^{78}\text{As}$ and $^{81}\text{Br}(n,\alpha)^{78}\text{As}$ reactions using the 14 MeV flux of a neutron generator. Thirty one gamma rays have been observed in the decay of ^{78}As , most of them for the first time. A decay scheme is proposed including 16 excited states in ^{78}Se .

The ^{92}Y activity has been produced via the $^{92}\text{Zr}(n,p)^{92}\text{Y}$ reaction. The decay of ^{92}Y has been investigated for the first time by means of high resolution Ge(Li) detectors. Twelve transitions have been observed in the decay of ^{92}Y and an improved decay scheme is presented including

six excited states.

The intermediate coupling model has been used to interpret the obtained data. The model is formulated, extended and tested on the odd Xe isotopes. It was found that the model describes well the observed properties of these isotopes.

A good description of both positive and negative parity states in ^{75}As is obtained if an extra term $H' = g\bar{l}\cdot\bar{R}$ is added in the Hamiltonian of the intermediate coupling model, where g is a constant and \bar{l}, \bar{R} the angular momenta of the extra core particle and core, respectively. This term gives rise to several positive parity states which have been recently observed in ^{83}Rb .

Finally, it was found that the observed excited states of ^{92}Zr can be well reproduced by the intermediate coupling model. The ^{92}Zr nucleus is considered to be described by a ^{90}Zr vibrating core to which two $2d_{5/2}$ neutrons are coupled. The observed half life of the first 2^+ collective state in ^{92}Zr is reproduced well by the model.

The level structure of ^{78}Se is interpreted in terms of collective and quasiparticle excitations.

ACNOWLEDGMENTS

I would like to thank Dr. S. Hontzeas for his guidance, his constant interest and endless discussions during the present work.

I would also like to thank the members of the Physics Department for their interest and especially Dr. G. Papini and Dr. I. Naqvi for occasional discussions.

My thanks are due to Chemcell of Canada for the scholarship granted me. My thanks are also extended to the University of Saskatchewan for the summer scholarships granted me. This work has been partially supported by the National Research Council.

The help of Mr. B. Ramadan in operating the neutron generator is appreciated. The help of Mr. H. Block in the computer work is acknowledged.

TABLE OF CONTENTS

ABSTRACT	(ii)
ACKNOWLEDGMENT	(iv)
LIST OF FIGURES	(viii)
LIST OF TABLES	(xii)
1. INTRODUCTION	1
2. THE INTERMEDIATE COUPLING APPROACH IN THE FRAMEWORK OF THE UNIFIED MODEL	3
2.1 Historical	3
2.2 Even-even nuclei in the collective vibrational model	4
2.3 Even-even nuclei in the unified model	9
2.4 Odd nuclei in the unified model	11
2.5 Detailed treatment of the even-odd spherical nuclei	14
2.6 Magnetic dipole and electric quadrupole moments	18
2.7 Electromagnetic transitions	23
2.8 Quasiparticles	26
2.9 Introduction of quasiparticles in the unified model	32
3. APPLICATION OF THE INTERMEDIATE COUPLING MODEL	35
3.1 Positive parity states in odd Xe isotopes	35
3.2 Even-even Xe isotopes	37
3.3 Computational procedure	44
3.4 Level structure of ^{127}Xe	46
3.5 Level structure of ^{129}Xe	54
3.6 Level structure of ^{131}Xe	61
3.7 Level structure of ^{133}Xe	73
3.8 General remarks	78

4.	EXPERIMENTAL FACILITIES	83
4.1	Detectors and associated electronics	83
4.2	Relative efficiency calibration of the Ge(Li) detectors	86
4.2.1	A semi-empirical efficiency equation for Ge(Li) detectors	97
4.2.2	Application of the semi-empirical equation	100
4.3	Energy calibration	111
4.4	The neutron generator	111
5.	EXPERIMENTAL WORK	113
5.1	The decay of ^{75}Se	113
5.1.1	Single gamma ray spectroscopy	115
5.1.2	Coincidence experiments	125
5.1.3	Internal conversion coefficients	133
5.1.4	The disintegration of ^{75}Se	138
5.1.5	Transition rates in ^{75}As	147
5.2	The decay of ^{78}As	150
5.2.1	Low energy single spectroscopy (<1 MeV)	153
5.2.2	Intermediate energy region singles spectroscopy (1-2 MeV)	161
5.2.3	High energy region singles spectroscopy (>2 MeV)	173
5.2.4	Coincidence measurements	176
5.2.5	Construction of the decay scheme of ^{78}As	189
5.3	The decay of ^{92}Y	201
5.3.1	Gamma ray singles spectra for $E < 1$ MeV	204
5.3.2	Gamma ray singles spectra for $E > 1$ MeV	208
5.3.3	Coincidence experiment	212
5.3.4	Construction of the decay scheme of ^{92}Y	216
5.3.5	The disintegration of ^{92}Y	222
6.	GENERAL DISCUSSION	226
6.1	A modified intermediate coupling model for ^{75}As	226
6.1.1	Positive parity states in ^{75}As and related nuclei in the framework of a modified intermediate coupling model	229
6.1.2	Excited states in ^{75}As in the framework of the modified intermediate coupling model	236
6.2	The level structure of ^{78}Se	246
6.3	The level structure of ^{92}Zr	249
6.3.1	The coupling of two neutrons to the ^{90}Zr core	251

7. SUMMARY AND CONTRIBUTION TO KNOWLEDGE	259
APPENDIX A	268
APPENDIX B	271
APPENDIX C	274
APPENDIX D	279
APPENDIX E	281
APPENDIX F	284
REFERENCES	287

LIST OF FIGURES

Number	Title	Page
1	The calculated spectrum of ^{127}Xe in comparison with the experimental spectrum	47
2	The calculated spectrum of ^{129}Xe in comparison with the experimental spectrum	55
3	The calculated spectra of ^{131}Xe	63
4	The calculated spectrum of ^{133}Xe in comparison with the experimental spectrum	75
5	Calculated single particle spacing in odd Xe isotopes as a function of the mass number	79
6	The calculated coupling constant of odd Xe isotopes as a function of the mass number	80
7	Block diagram of the coincidence arrangement	85
8	Log-log dependence of the relative efficiency of the $29 \text{ cm}^3 \text{ Ge(Li)}$ detector on the energy	90
9	Relative efficiency curve of the $0.39 \text{ cm}^3 \text{ Ge(Li)}$ detector	92
10	Relative efficiency curve of the $2 \text{ cm}^3 \text{ Ge(Li)}$ detector	93
11	Relative efficiency curve of the $29 \text{ cm}^3 \text{ Ge(Li)}$ detector	94
12	Relative efficiency curve of the $0.39 \text{ cm}^3 \text{ Ge(Li)}$ detector for $E < 100 \text{ KeV}$	96
13	Relative efficiency curve of the $17 \text{ cm}^3 \text{ Ge(Li)}$ detector	102
14	Relative efficiency curve of the $42 \text{ cm}^3 \text{ Ge(Li)}$ detector	108
15	Horizontal cross section of a source and detector	110
16	Gamma ray spectrum of ^{75}Se observed with the $0.39 \text{ cm}^3 \text{ Ge(Li)}$ detector (Energy up to 100 KeV)	116

Number	Title	Page
17	Gamma ray spectrum of ^{75}Se obtained with the 2 cm ³ Ge(Li) detector (Energy region from 75 to 100 KeV)	119
18	Gamma ray spectrum of ^{75}Se obtained with the 29 cm ³ Ge(Li) detector (Energy region 100-400 KeV)	121
19	Gamma ray spectrum of ^{75}Se obtained with the 29 cm ³ Ge(Li) detector (Energy region 400-700 KeV)	122
20	Expanded gamma ray spectrum of ^{75}Se in the energy region 400-620 KeV as obtained with the 29 cm ³ Ge(Li) detector (48 hours counting period)	123
21	The spectrum of Fig.20 after a 32 hours subtraction period	124
22	Gamma rays in ^{75}Se in coincidence with the 198.6 KeV transition	129
23	Gamma rays in ^{75}Se in coincidence with the 198.6 KeV transition	
24	Gamma rays of ^{75}Se in coincidence with the 279.5 KeV transition	132
25	The proposed decay scheme of ^{75}Se	141
26	Gamma ray spectrum of ^{78}As observed with the 29 cm ³ Ge(Li) detector in the energy region 0.5-1.0 MeV	154
27	The decay curves of some ^{78}As gamma rays	156
28	The decay of the composite 828 KeV gamma ray as observed in the activity produced by irradiation of a SeO ₂ target	157
29	Gamma ray spectrum of ^{78}As .Activity produced by irradiation of a Br target (0.5-1.0 MeV)	158
30	Gamma ray spectrum of ^{78}As observed with the 29 cm ³ Ge(Li) detector.Activity produced by irradiation of a Se target (Energy region 1.0-1.6 MeV)	164
31	Gamma ray spectrum of ^{78}As observed with the 29 cm ³ Ge(Li) detector.Activity produced by irradiation of Se target (Energy region 1.6-2.1 MeV)	165
32	The decay curves of some ^{78}As gamma rays	166

Number	Title	Page
33	The decay curves of some ^{78}As gamma rays	167
34	Gamma ray spectrum of ^{78}As observed with the 29 cm^3 Ge(Li) detector. Activity produced by irradiation of a Br target (Energy region 1.0-1.4 MeV)	169
35	Gamma ray spectrum of ^{78}As observed with the 29 cm^3 Ge(Li) detector. Activity produced by irradiation of a Br target (Energy region 1.4-1.95 MeV)	172
36	Gamma ray spectrum of ^{78}As observed with the 29 cm^3 Ge(Li) detector. Activity produced by irradiation of a Se target (Energy region 2.1-3.1 MeV)	174
37	Gamma ray spectrum of ^{78}As observed with the 29 cm^3 Ge(Li) detector. Activity produced by irradiation of a Br target. Energy region 1.9-2.3 MeV	175
38	^{78}As gamma rays with $E < 700$ KeV in coincidence with a 100 KeV wide gate centered at the 614 KeV transition	178
39	^{78}As gamma rays in coincidence with the gate which includes the 614 KeV transition (Energy region 0.8-1.5 MeV)	179
40	^{78}As gamma rays in coincidence with the gate which includes the 614 KeV transition (Energy region 1.5-3.0 MeV)	180
41	^{78}As gamma rays in coincidence with the gate which include the 1373 and 1308 KeV transitions (Energy region 0.5-1.2 KeV)	186
42	^{78}As gamma rays in coincidence with the gate which includes the 1373 and 1308 KeV transitions (Energy region 1.3-1.9 MeV)	187
43	The proposed decay scheme of ^{78}As	196
44	The excited states of ^{78}Se observed in the present work in comparison with (d,p), (d,d') and (p,p') reaction data	198
45	Gamma ray spectrum of ^{92}Y as observed with the 29 cm^3 Ge(Li) detector (Energy region 0.4-1.0 MeV)	205

Number	Title	Page
46	The 909 and 934 KeV transitions observed in the irradiated Zr target	207
47	Gamma ray spectrum of ^{92}Y as observed with the 29 cm^3 Ge(Li) detector (Energy region 1.0-1.5 MeV)	209
48	Gamma ray spectrum of ^{92}Y as observed with the 29 cm^3 Ge(Li) detector (Energy region 1.5-2.1 MeV)	210
49	Gamma ray spectrum of ^{92}Y in coincidence with the gate which include the 934 KeV transition	214
50	The proposed decay scheme of ^{92}Y	220
51	The coupling of a $g_{9/2}$ state to the vibrational core	230
52	Calculated positive parity states in ^{83}Rb in comparison with the experimental spectrum (gh=50 KeV)	233
53	Calculated positive parity states in ^{83}Rb in comparison with the experimental spectrum (gh=70 KeV)	235
54	Calculated states in ^{75}As	237
55	Calculated states in ^{92}Zr	253
56	Calculated electromagnetic properties of the excited states in ^{92}Zr in comparison with the experimental available data	257

LIST OF TABLES

Number	Title	Page
1	Excited states of some even-even Xe nuclei	38
2	Electromagnetic properties of some even-even nuclei	40,41
3	Calculated state vectors in ^{127}Xe	50
4	Calculated properties of some ^{127}Xe nuclear states	52,53
5	Calculated state vectors of some ^{129}Xe excited states	57
6	Calculated properties of some ^{129}Xe nuclear states	59,60
7	Calculated state vectors of some excited states in ^{131}Xe (I)	64
8	Calculated properties of some ^{131}Xe nuclear states (I)	65,66
9	Calculated state vectors of some excited states in ^{131}Xe (II)	70
10	Calculated properties of some ^{131}Xe nuclear states (II)	71,72
11	Calculated state vectors of some ^{133}Xe nuclear states	76
12	Calculated properties of some ^{133}Xe excited states	77
13	Single particle energies and G values for some Xe isotopes	81
14	Radioactive sources used in efficiency calibration of the Ge(Li) detectors	88
15	Calculated parameters of various detectors	103
16	Relative efficiency values for several Ge(Li) detectors	105

Number	Title	Page
17	Experimental and calculated relative efficiency values for the 42cm ³ Ge(Li) detector	107
18	Energy and intensity of the low energy gamma rays in ⁷⁵ Se	117
19	Energy and intensity of gamma rays in ⁷⁵ Se	126
20	Internal conversion electron intensities	134
21	K conversion coefficients of the transitions in ⁷⁵ As	136
22	Experimental and theoretical K conversion coefficients in ⁷⁵ As	137
23	Conversion intensity ratios and internal conversion coefficients in ⁷⁵ As	139
24	Electron capture branching ratios in ⁷⁵ Se	144
25	Absolute intensities of the ⁷⁵ As gamma rays	146
26	Transition rates of M1 and E2 gamma rays observed in ⁷⁵ As	149
27	Gamma rays observed in the decay of ⁷⁸ As produced via the ⁸¹ Br(n, α) ⁷⁸ As reaction	162
28	Gamma rays observed in the decay of ⁷⁸ As produced via the ⁷⁸ Se(n,p) reaction	163
29	Contributions of the 1228.0 KeV ⁷⁶ As photopeak to the 1228.0 KeV ⁷⁸ As photopeak	171
30	Coincidence intensities of gamma rays in ⁷⁸ As	182
31	Coincidence intensities of gamma rays in ⁷⁸ As	188
32	Energy and intensity of gamma rays observed in the decay of ⁹² Y	211
33	Intensity of ⁹² Zr gamma rays observed in coincidence with the gate which include the 934.5 KeV transition	215

Number	Title	Page
34	Beta branching and logft values in the decay of ^{92}Y	223
35	Computed wave functions for some positive parity states in ^{75}As	239
36	Computed wave functions for some negative parity states in ^{75}As	240
37	Electromagnetic transition probabilities in ^{75}As	242
38	Solution of BCS equations for ^{75}As	245
39	Calculated state vectors for some excited states in ^{92}Zr	256

1. INTRODUCTION

This work presents a combined experimental and theoretical investigation of the nuclear properties of some nuclei. In the experimental part of the work, the techniques of high resolution gamma spectroscopy are used to investigate the excited states of the ^{75}As , ^{78}Se and ^{92}Zr . Single and coincidence gamma ray measurements using a variety of Ge(Li) detectors have been extensively used to determine the excited states of the above mentioned nuclei. The ^{78}Se and ^{92}Zr nuclei were investigated by following the beta decay of the parent ^{78}As and ^{92}Y activity. These two nuclei have a relatively short half life, and they have been produced locally using the 14 MeV neutron flux of a Texas Nuclear neutron generator. The excited states of ^{75}As have been determined by following the decay of ^{75}Se , which has a long half life and therefore was obtained from a commercial supplier.

The interpretation of the data obtained in this work is done mainly in terms of the intermediate coupling approach of the unified model. This model is fully developed and extensively treated in Chapter 2. An attempt is also made to give a physical interpretation of the otherwise adjustable constants of the model. In Chapter 3 the model is tested using the data available in the literature on the odd Xe nuclei with A ranging from 127 to 133.

In Chapter 4 a brief description of the equipment used in the present work is given. In this same chapter original work concerning relative efficiency calibrations of Ge(Li) detectors is also given, that is, the possibility of expressing the relative efficiency of a Ge(Li) detector with a semi-empirical equation which relates the efficiency with the geometric and physical properties of the germanium crystal of the detectors.

In Chapter 5 the results of the experimental work are presented. The experimental techniques used and the construction of the decay schemes of the isotopes under consideration are discussed in detail.

The interpretation of the level structure and other properties of the nuclei under investigation in terms of the adopted model is given in Chapter 6. The present work is reviewed in Chapter 7.

The available literature on the subjects treated in this work has been reviewed extensively up to the 20th of February, 1970.

2. THE INTERMEDIATE COUPLING APPROACH IN THE FRAMEWORK OF THE UNIFIED MODEL

2.1. Historical

Despite the success of the shell and independent particle models in explaining many nuclear properties, experimental evidence indicated that there are many nuclear properties which cannot be described by a model which considers the pair-wise filling of nuclear orbits. Large quadrupole moments, the observed spheroidal shape of some nuclei, the vibrational spectra of the even-even nuclei, indicated that the cooperative contribution of all the nucleons present in a nucleus should be taken into account in the interpretation of the nuclear structure. The significance of the nuclear collective effects found expression in 1936 in the liquid drop model ^(1,2).

The introduction of the intrinsic particle degrees of freedom in ⁽³⁾ the collective model was suggested by Bohr and Mottelson in the early 1950's. The mathematical treatment of the coupling of the intrinsic ⁽⁴⁾ with the collective degrees of freedom was treated in detail by Choudhury ⁽⁷⁻⁹⁾. In recent years a few papers appeared in the literature with specific application of the unified model to some nuclei.

In the following sections the model is reviewed in detail. The mathematical treatment of the coupling of the individual particle degrees of freedom to the collective oscillations of the nuclei is extensively treated.

2.2 Even even nuclei in the collective vibrational model

In the collective vibrational model the nucleus is considered to undergo shape oscillations in analogy with a liquid drop. The shape of the surface of the nucleus, which has constant density throughout its volume, can be described by the parameters $a_{\lambda\mu}$ in the equation

$$R(\theta, \varphi) \equiv R_0 \left[1 + \sum_{\lambda, \mu} a_{\lambda\mu} Y_{\lambda\mu}(\theta, \varphi) \right] \dots \dots \dots 2.1$$

where $0 \leq \lambda \leq \infty$ and $-\lambda \leq \mu \leq +\lambda$.

As is known, the nuclear density ⁽⁵⁾ is not constant and has a radial dependence. In the following it is assumed that the nuclear density oscillations are volume conserving. In this way the expression for $R(\theta, \varphi)$ given by equation 2.1 can be applied to each equidensity surface. Under these postulated conditions the coefficients $a_{\lambda\mu}$ in equation 2.1 may serve as the collective coordinate variables and suitable expressions for the kinetic and dynamic energy of the nucleus may be obtained in terms of these new variables.

The potential energy of the nucleus possessing $A/2$ pairs of nucleons (A is the mass number) will be associated with the collective potential energy exhibited by the oscillating nucleons and may be written

$$V \equiv \frac{1}{2}C \left| \frac{R-R_0}{R_0} \right|^2 \equiv \frac{1}{2} \sum_{\lambda, \mu} C_{\lambda\mu} |a_{\lambda\mu}|^2 \dots \dots \dots 2.2$$

In equation 2.2 $C_{\lambda\mu}$ is the nuclear surface deformation parameter and is a constant characteristic of the particular nucleus. For a quantized liquid drop the following expression may be derived ⁽³⁾ for the parameter C_λ and is given by

$$C_\lambda = C_\lambda^{(1)} + C_\lambda^{(2)} \dots \dots \dots 2.3$$

where $C_\lambda^{(1)} = SR_0^2 (\lambda - 1) (\lambda + 2) \dots \dots \dots 2.4$

is the term in the deformation parameter which depends on the surface tension S in absence of electric charges

and $C_\lambda^{(2)} = - \frac{3}{2\pi} \frac{Z^2 e^2}{R_0} \frac{(\lambda - 1)}{(2\lambda + 1)} \dots \dots \dots 2.5$

expresses the contributions to the deformation parameter arising from the Coulomb energy.

Equation 2.2 expresses clearly the fact stated earlier, that the coefficients $a_{\lambda\mu}$ may serve as the collective coordinate variables.

The collective kinetic energy of the nucleus may be derived in the same way and is given by

$$T \equiv \frac{1}{2} B \left| \frac{d}{dt} \left(\frac{R - R_0}{R} \right) \right|^2 \equiv \frac{1}{2} \sum_{\lambda\mu} B_\lambda \left| \dot{a}_{\lambda\mu} \right|^2 \dots \dots \dots 2.6$$

where B is an inertial parameter. In the case of a nucleus of constant nuclear density possessing an irrotational* flow, Bohr (3) has derived an expression for B_λ given by

$$B_\lambda \equiv \frac{1}{\lambda} \cdot \frac{3}{4\pi} \cdot A \cdot M \cdot R_0^2 \dots \dots \dots 2.7$$

where M is the nucleon mass.

The quantization of the system requires the introduction of the variable conjugate to $a_{\lambda\mu}$ which is defined as

* The expression "irrotational" implies that the elementary volume is not rotating about an axis moving with its own center.

$$\pi_{\lambda, \mu} \equiv \frac{\partial T}{\partial \dot{a}_{\lambda \mu}} \equiv B_{\lambda} \dot{a}_{\lambda \mu} \dots \dots \dots 2.8$$

The appropriate commutators are given by

$$[a_{\lambda \mu}, \pi_{\lambda' \mu'}]_{-} = \frac{\hbar}{i} \delta_{\lambda \lambda'} \delta_{\mu \mu'} \dots \dots \dots 2.9$$

$$[\pi_{\lambda \mu}, \pi_{\lambda' \mu'}]_{-} = [a_{\lambda \mu}, a_{\lambda' \mu'}]_{-} = 0$$

with the reality conditions

$$\pi_{\lambda, \mu}^{+} = (-1)^{\mu} \pi_{\lambda, -\mu} \quad a_{\lambda, \mu}^{+} = (-1)^{\mu} a_{\lambda, -\mu} \dots \dots \dots 2.10$$

The collective Hamiltonian for the system of A nucleons may be written with the help of equations 2.2 and 2.6 and is given by

$$H_{col} \equiv \frac{1}{2} \sum_{\lambda \mu} B_{\lambda} |a_{\lambda \mu}|^2 + \frac{1}{2} \sum_{\lambda \mu} C_{\lambda \mu} |\dot{a}_{\lambda \mu}|^2 \dots \dots \dots 2.11$$

Equation 2.11 is a characteristic equation of a set of decoupled simple harmonic oscillators of frequencies

$$\omega_{\lambda} \equiv \left(\frac{C_{\lambda}}{B_{\lambda}} \right)^{1/2} \dots \dots \dots 2.12$$

This suggests that a transformation of the collective variables into an N representation would be more useful.

The transformation is accomplished through the introduction of the creation and annihilation operators $b_{\lambda \mu}^{+}$ and $b_{\lambda \mu}$ for phonons* of angular momentum λ and z-component of angular momentum μ .

The transformations are specified through the following equations

* Here and hereafter the term "phonon" refers to a mechanical quantum of energy.

$$\pi_{\lambda,\mu} \equiv i \left(\frac{B_\lambda \hbar \omega_\lambda}{2} \right)^{1/2} \left[b_{\lambda,\mu}^+ - (-1)^\mu b_{\lambda,-\mu} \right] \dots \dots \dots 2.13$$

$$a_{\lambda,\mu} \equiv \left(\frac{\hbar}{2\omega_\lambda B_\lambda} \right)^{1/2} \left[b_{\lambda,\mu} + (-1)^\mu b_{\lambda,-\mu}^+ \right] \dots \dots \dots 2.14$$

Using the commutators of equation 2.9 and the equations 2.3 and 2.4 commutation relations are obtained for $b_{\lambda\mu}^+$ and $b_{\lambda\mu}$ given by

$$\left[b_{\lambda\mu}, b_{\lambda'\mu'}^+ \right]_- = \delta_{\lambda\lambda'} \delta_{\mu\mu'} \dots \dots \dots 2.15(a)$$

$$\left[b_{\lambda\mu}, b_{\lambda'\mu'} \right]_- = \left[b_{\lambda\mu}^+, b_{\lambda'\mu'}^+ \right]_- = 0 \dots \dots \dots 2.15(b)$$

Some important properties of the creation and annihilation operator are given by

$$N_{\lambda,\mu}^{ob} = b_{\lambda\mu}^+ b_{\lambda\mu} \dots \dots \dots 2.16(a)$$

$$N_{\lambda\mu}^{ob} | \eta_{\lambda\mu} \rangle = b_{\lambda\mu}^+ b_{\lambda\mu} | \eta_{\lambda\mu} \rangle = \eta_{\lambda\mu} | \eta_{\lambda\mu} \rangle \dots \dots \dots 2.16(b)$$

$$b_{\lambda\mu} | \eta_{\lambda\mu} \rangle = \sqrt{\eta_{\lambda\mu}} | \eta_{\lambda,\mu}^{-1} \rangle \dots \dots \dots 2.16(c)$$

$$b_{\lambda\mu}^+ | \eta_{\lambda\mu} \rangle = \sqrt{\eta_{\lambda\mu}+1} | \eta_{\lambda,\mu}^{+1} \rangle \dots \dots \dots 2.16(d)$$

where $N_{\lambda,\mu}^{ob}$ is the number operator which commutes with the Hamiltonian, $\eta_{\lambda\mu}$ specifies the number of phonons with angular momentum λ and z-component μ present, and $| \eta_{\lambda,\mu} \rangle$ denotes the state vector of the system in the N representation.

The ground state vector is defined by

$$b_{\lambda\mu} | 0 \rangle \equiv 0 \dots \dots \dots 2.17$$

for all λ,μ . Using the properties of $b_{\lambda\mu}^+$ and $b_{\lambda\mu}$ and the commutation

relations it can be easily shown that the collective Hamiltonian in equation 2.11 may assume the form given by

$$H_{col} \equiv \sum_{\lambda, \mu} \hbar \omega_{\lambda} (b_{\lambda \mu}^{\dagger} b_{\lambda \mu} + \frac{1}{2}) \dots \dots \dots 2.18$$

In the case where even-even nuclei are considered, excitations described by $\lambda = 0, 1$ do not occur for low excitation energies. More specifically, excitations of the $\lambda = 0$ type describe density oscillations since in a first approximation the volume is given by

$$V = V_0 (1 + \frac{3a_0}{\sqrt{4\pi}}) \dots \dots \dots 2.19$$

In this case it can be shown (6) that excitations of this type occur for energies $E \approx 10$ MeV and hence are irrelevant to the discussion of lower lying excited nuclear states. The term with $\lambda = 1$ describes the vibrations of the neutron medium relative to the proton medium and is of the order of 15 MeV.

Thus the first realistic situation arises from the quadrupole ($\lambda = 2$) vibrations of the nucleus.

Since quadrupole phonons have five degrees of freedom $-2 < \mu < +2$ the energy of the ground state, i.e. the state containing no phonons, has an energy $E = 5/2 \hbar \omega$ as can be readily verified from equation 2.18. The angular momentum of this ground state is $\lambda = 0$ and the parity $(-1)^{\lambda}$ is positive.

The first excited state of an even-even nucleus is the state which arises from one quadrupole phonon. The energy of such a state is $H_{col} |1_2\rangle \equiv (1 + 5/2) \hbar \omega_2 |1_2\rangle$. The state has angular momentum $\lambda = 2$ and parity $(-1)^2 =$ positive. The next excited states arise from the

coupling of two phonons of angular momentum 2. The energy of these states is $E = (2 + 5/2) \hbar\omega_2$ and in general they are degenerate states. If weak perturbations are applied the degeneracy is removed and the three states which result from the coupling of the angular momentum of the two phonons may be observed with corresponding spin and parity 0^+ , 2^+ and 4^+ .

At approximately the same excitation energy a 3^- state can be observed which arises from the presence of a octupole ($\lambda = 3$) phonon (parity $(-1)^3 = \text{negative}$) since from equation 2.3 and 2.7 it may be inferred that $\omega_3 \approx 2\omega_2$.

The nuclear structure of the even-even nuclei described previously has been verified experimentally, ⁽⁵⁾ and this structure is common to all the nuclei which do not belong to the deformed region.

2.3 Even-even nuclei in the unified model

The motion of the independent particle in the shell model is determined by the average static nuclear field. In turn the shape of the field is determined by the distribution of the nuclear density. In the case of volume conserving nuclear vibrations it is expected that the motion of the independent particle will reflect the change of the field which in turn is related to the oscillations of the nuclear density.

The Hamiltonian of the shell model in the case under discussion is related to the deviation of the shape of the nucleus from sphericity, i.e. it will be a function of the deformation parameter a . The parameter a is analogous to the variables $a_{\lambda\mu}$ discussed in the previous section and the reason will become clear later. The modified shell model Hamiltonian

$H_s(a(t))$ is expanded in terms of a and \dot{a} and in a first approximation is written

$$H_s(a(t)) = H_0 + \frac{1}{2}B\dot{a}^2 + \frac{1}{2}Ca^2 + \dots \quad 2.20$$

The wave functions $\varphi(t)$ of $H(a(t))$ follow the self consistency requirement that their dependence on the nuclear deformation oscillates in phase with the field

$$\varphi = \varphi_0 e^{-i\omega t} \dots \quad 2.21$$

where ω is the frequency of the field oscillation. Then the energy expectation value may be written

$$\langle E \rangle = E_0 + \frac{1}{2} \langle B \rangle \dot{a}^2 + \frac{1}{2} \langle C \rangle a^2 + \dots \quad 2.22$$

where $E_0 = \langle \varphi_0 | H_0 | \varphi_0 \rangle$, $\langle B \rangle = \langle \varphi_0 | B | \varphi_0 \rangle$ and $\langle C \rangle = \langle \varphi_0 | C | \varphi_0 \rangle$.

Under these conditions it follows that

$$\omega = \left(\frac{C}{B} \right)^{\frac{1}{2}} \text{ and } a = k \cdot \cos \omega t$$

are the equations describing free, small amplitude oscillations.

The first postulate of the unified model is that a , along with $\Pi = B\dot{a}^*$ are dynamical variables and obey the commutator

$$[a, \Pi]_- = \frac{\hbar}{i} \dots \quad 2.23$$

The problem then is treated in exactly the same way as was done in the collective model discussed in the previous section.

A very important problem must be pointed out concerning the quantization procedure. In the unified model the parameters a and \dot{a}

are parameters determining the shape of the shell model field. As such they do not obey the uncertainty principle ⁽⁵⁾ and actually

$$[a, \pi] = 0 \neq \frac{\hbar}{i} \dots \dots \dots 2.24$$

In the classical limit the approximation should lead to the correct results since $\hbar \rightarrow 0$. In view of this fact the above mentioned approximations resemble a semi-classical description. Nevertheless the assumption of the unified model is that the results remain in general valid.

The success of the unified model lies mostly in the fact that it does predict the normal modes of the nuclear field thus allowing the coupling of shape oscillations to other intrinsic modes. This subject is investigated in the following section.

2.4 Odd nuclei in the unified model

The case of odd mass nuclei may be viewed within the framework of the unified model as the coupling of an odd nucleon to the collective vibrations of an even-even nucleus.

The spin \bar{I} of the nucleon state which arises from the coupling of the nucleon of spin \bar{j} to the vibrating core which possesses a spin \bar{R} is given by

$$\bar{I} = \bar{R} + \bar{j} \dots \dots \dots 2.25$$

The Hamiltonian of the system is considered to be separable and is expressed by the equation

$$H = H_{col} + H_j + H_{int} \dots \dots \dots 2.26$$

where H_{col} is the Hamiltonian of the vibrating core as given by

equations (2.22) and (2.18), H_j is the Hamiltonian of the single particle given by

$$H_j |j\rangle = E_j |j\rangle \dots \dots \dots 2.27$$

and H_{int} is the interaction Hamiltonian for the system particle-core.

An approximate expression for the interaction Hamiltonian may be obtained from the nuclear one body potential V .

According to the previous discussion (section 2.3) the nuclear potential is considered to be a function of the nuclear shape. More precisely, we may identify the equipotential surfaces of the potential $V_a(\vec{r})$ with the surfaces of constant density given by

$$r_\theta = r \left[1 + \sum_{\lambda\mu} a_{\lambda\mu} Y_{\lambda\mu} \right] \dots \dots \dots 2.28$$

where r is considered to be constant.

Hence we have

$$V(a_{\lambda\mu}; r_\theta) = V_o(r) = V_o \left(\frac{r_\theta}{1 + \sum_{\lambda\mu} a_{\lambda\mu} Y_{\lambda\mu}} \right) \dots \dots \dots 2.29$$

where $V_o(r)$ is the equipotential surface for $V_o(\vec{r})$. The following expression for $V(a_{\lambda\mu}; r)$ may be derived from equation (2.29) and is given by

$$V(a_{\lambda\mu}; r) \equiv V_o \left(\frac{r}{1 + \sum_{\lambda\mu} a_{\lambda\mu} Y_{\lambda\mu}} \right) \dots \dots \dots 2.30$$

As a next step the nuclear potential $V(a_{\lambda\mu}; r)$ is expanded around the spherical surface $a_{\lambda\mu} = 0$ as follows

$$V(a_{\lambda\mu}; r) = V(o; r) + \sum_{\lambda\mu} \left(\frac{\partial V}{\partial a_{\lambda\mu}} \right)_o a_{\lambda\mu} \dots \dots \dots 2.31$$

or

$$\begin{aligned}
 V(a_{\lambda\mu}; r) &= V(o; r) + \sum_{\lambda\mu} \frac{\partial V_o}{\partial r} \left(\frac{\partial r}{\partial a_{\lambda\mu}} \right)_o a_{\lambda\mu} = \\
 &= V(o; r) + \sum_{\lambda\mu} \frac{\partial V_o}{\partial r} \left(\frac{\partial}{\partial a_{\lambda\mu}} \left\{ \frac{r_\theta}{1 + \sum_{\lambda\mu} a_{\lambda\mu} Y_{\lambda\mu}} \right\} \right)_o a_{\lambda\mu} \dots\dots\dots 2.32
 \end{aligned}$$

and

$$V(a_{\lambda\mu}; r) = V_o(r) + \sum_{\lambda\mu} \frac{\partial V_o}{\partial r} \left\{ \frac{\partial}{\partial a_{\lambda\mu}} \left[r_\theta (1 - \sum_{\lambda\mu} a_{\lambda\mu} Y_{\lambda\mu}) \right] \right\}_o a_{\lambda\mu} \dots\dots\dots 2.33$$

In deriving equation 2.33 use was made of the fact that $V(o; r) = V_o(r)$ and equation 2.28 was expanded keeping the first term only. Equation 2.33 may be written

$$V(a_{\lambda\mu}; r) = V_o(r) - \sum_{\lambda\mu} \frac{\partial V_o}{\partial r} [r \cdot Y_{\lambda\mu}] a_{\lambda\mu} \dots\dots\dots 2.34$$

since $[r_\theta]_o = r$ and the final expression is

$$V(a_{\lambda\mu}; r) = V_o(r) - r \frac{\partial V_o}{\partial r} \sum_{\lambda\mu} a_{\lambda\mu} Y_{\lambda\mu} \dots\dots\dots 2.35$$

Hence the interaction Hamiltonian may be written

$$H_{int} = -k(r) \sum_{\lambda\mu} a_{\lambda\mu} Y_{\lambda\mu} \dots\dots\dots 2.36$$

where $k(r) = r \partial V_o / \partial r$ is usually treated as a constant and its value is of the order of 40 MeV.

The expression for k shows that the interaction Hamiltonian is appreciable near the surface of the nucleus where the nuclear density changes drastically. In the case of a square well potential $k(r)$ may be written

$$k(r) = V_o^k R_o \delta(r - R_o) \dots\dots\dots 2.37$$

where V_o^k is the potential depth.

By using the expression for $a_{\lambda\mu}$ taken from equation 2.14, equation 2.36 may be written

$$H_{\text{int}} = -k(r) \sum_{\lambda\mu} \left(\frac{\hbar}{2\omega_\lambda B_\lambda} \right)^{\frac{1}{2}} \left[b_{\lambda\mu} + (-1)^\mu b_{\lambda, -\mu}^+ Y_{\lambda\mu} \right] \dots \dots \dots 2.38$$

or by taking into account equation 2.12

$$H_{\text{int}} = -k(r) \sum_{\lambda\mu} \hbar\omega_\lambda \left(\frac{1}{2\hbar\omega_\lambda C_\lambda} \right)^{\frac{1}{2}} \left[b_{\lambda, \mu} + (-1)^\mu b_{\lambda, -\mu}^+ Y_{\lambda\mu} \right] \dots \dots \dots 2.39$$

In the case in which more than one particle is coupled to the vibrating core the interaction Hamiltonian of equation 2.39 should be replaced with the sum of the interaction Hamiltonians over all extra core particles given by

$$H_{\text{int}} = - \sum_i k(r_i) \sum_{\lambda\mu} \hbar\omega_\lambda \left(\frac{1}{2\hbar\omega_\lambda C_\lambda} \right)^{\frac{1}{2}} \left[b_{\lambda, \mu} + (-1)^\mu b_{\lambda, -\mu}^+ Y_{\lambda\mu}(r_i) \right] \dots \dots \dots 2.40$$

2.5 Detailed treatment of the even-odd spherical nuclei

In the present treatment of the even-odd nuclei, only quadrupole oscillations of the even-even core are considered. The extra-core particle (proton or neutron) is coupled to the surface quadrupole phonons. The interaction Hamiltonian (equation 2.39) can be written

$$H_{\text{int}} = -k \hbar\omega_2 \left(\frac{1}{2\hbar\omega_2 C_2} \right)^{\frac{1}{2}} \sum_{\mu} (b_{2, \mu} + (-1)^\mu b_{2, -\mu}^+) Y_{2\mu} \dots \dots \dots 2.41$$

In the following, a dimensionless constant ξ is introduced defined by

$$\xi \equiv k \left(\frac{5}{2\pi\hbar\omega_2 C_2} \right)^{\frac{1}{2}} \dots \dots \dots \dots \dots \dots \dots 2.42$$

The numerical factor $5/\pi$ is introduced in the above expression simply to avoid the same factor in later expressions. In addition to the

introduction of the constant ξ in equation 2.42, the subscript 2 is dropped from the quantities C , ω and b_μ , b_μ^+ , since only quadrupole phonons are considered. Equation 2.41 is written now in the form

$$H_{\text{int}} = - \sqrt{\frac{\pi}{5}} \xi \hbar \omega \sum_{\mu} \left[b_{\mu} + (-)^{\mu} b_{-\mu}^+ \right] Y_{2\mu} \dots \dots \dots 2.43$$

The constant ξ will be called the coupling constant.

For nuclei close to the closed shells, the interaction Hamiltonian is small compared to the collective Hamiltonian and usual perturbation theory may be applied (weak coupling limit). But in regions far removed from the closed shells the interaction Hamiltonian is comparable with the level spacing $\hbar\omega$ and hence an exact diagonalization of the coupled system is necessary (intermediate coupling model). In this case $1 \leq \xi \leq 4$. Finally in the case of a deformed nucleus the nucleus obtains a permanent deformation and the model is modified properly to take account of this deformation.

The state vector of the odd particle is denoted by $|jm\rangle$ where j is the total angular momentum $\vec{j} = \vec{\ell} + \vec{s}$ of the particle and m the z -component of the angular momentum. In the following calculation it is very important to define the sequence in which the coupling of momenta is done. Therefore the following procedure is adopted. The spin \vec{s} is coupled to the angular momentum $\vec{\ell}$, to a total angular momentum \vec{j} , in that order. Hence the following identity may be written for the state vector $|jm\rangle$

$$|jm\rangle \equiv \left| \frac{1}{2} \ell, j, m \right\rangle \dots \dots \dots 2.44$$

The state vector of the even-even core will be denoted by $|NRm'\rangle$ where

N is the number of quadrupole phonons present with total angular momentum R and z-component m'.

In the present calculations the angular momentum representation is used and the eigenvectors of the uncoupled system are used as the basis vectors such that

$$\frac{1}{(2I+1)^{\frac{1}{2}}} |j;NR;IM\rangle = \sum_{m,m'} (-1)^{j-R-M} \begin{pmatrix} j & R & I \\ m & m' & -M \end{pmatrix} |jm\rangle |NRm'\rangle \dots 2.45$$

where the 3j symbol $\begin{pmatrix} j & R & I \\ m & m' & -M \end{pmatrix}$ is defined in Appendix A; and $I = \bar{R} + \bar{j}$ is the total angular momentum of the state. The eigenvectors of the total Hamiltonian are expressed as linear combinations of the basis vectors and are denoted by $|E;IM\rangle$ where

$$|E;IM\rangle = \sum_{j;N;R} C_{jNR} |j;NR;IM\rangle \dots 2.46$$

where E is the energy eigenvalue of the state of total angular momentum I.

The matrix elements of the secular equation

$$(H - E_i) |j;NR;IM\rangle = 0 \dots 2.47$$

where H is the total Hamiltonian of the system as given by Equation 2.26, can be obtained using the techniques of Racah Algebra. A brief outline of these techniques along with several definitions and useful relations is given in Appendix A.

To calculate the matrix elements of the total Hamiltonian it is useful to separate the Hamiltonian into two parts as follows:

$$H = (H_{col} + H_j) + H_{in} \dots 2.48$$

The matrix elements of the first part of the Hamiltonian are easily obtained and are given by

$$\begin{aligned}
\langle j'; N'R'; IM | H_{col} + H_j | j; NR; IM \rangle &= (\hbar\omega + \epsilon_j) \langle j'; N'R'; IM | j; NR; IM \rangle = \\
&= (\hbar\omega + \epsilon_j) \delta_{NN'} \delta_{RR'} \delta_{jj'} \dots \dots \dots 2.49
\end{aligned}$$

where the zero point energy of the collective Hamiltonian is neglected. As can be easily seen, Equation 2.49 contributes only to the diagonal elements of the secular equation.

The matrix elements of the second part of the Hamiltonian are more difficult to evaluate. Making use of Equation A-14

$$\begin{aligned}
\langle j'; N'R'; IM | -\sqrt{\frac{\pi}{5}} \xi \hbar\omega \sum_{\mu} [b_{\mu} + (-1)^{\mu} b_{-\mu}^{\dagger}] Y_{2\mu} | j; NR; IM \rangle &\equiv \\
= -\sqrt{\frac{\pi}{5}} \xi \hbar\omega (-1)^{I+j} \left\{ \begin{matrix} j' & R' & I \\ R & j & 2 \end{matrix} \right\} (j' || Y_2 || j) \left[(-1)^{R'} (N'R' || b || NR) + \right. \\
&\quad \left. + (-1)^R (NR || b || N'R') \right] \dots \dots \dots 2.50
\end{aligned}$$

In this equation $\left\{ \begin{matrix} j' & R' & I \\ R & j & 2 \end{matrix} \right\}$ stands for the 6j symbol and is defined in Appendix A while $(j' || Y_2 || j)$ indicates the reduced matrix elements of the tensors Y_2 as defined in Appendix A. The reduced matrix elements of the annihilation tensor operator b are discussed in Appendix B, where an extensive tabulation is also given.

Substitution in Equation 2.50 of the expression for the reduced matrix elements of the spherical harmonic operator obtained from Equation A-12) leads to an expression for the matrix elements of the interaction Hamiltonian given by

$$\begin{aligned}
\langle j'; N'R'; IM | H_{int} | j; NR; IM \rangle &= -\frac{1}{2} \xi \hbar\omega (-1)^{I+j'+j-\frac{1}{2}} \times \left\{ \begin{matrix} j & R & I \\ R' & j' & 2 \end{matrix} \right\} \times \\
&\times \left(\begin{matrix} j' & 2 & j \\ -\frac{1}{2} & 0 & \frac{1}{2} \end{matrix} \right) \left[(-1)^{R'} (N'R' || b || NR) + (-1)^R (NR || b || N'R') \right] \times \\
&\times \delta_{\text{even}}^{\ell+\ell'} \dots \dots \dots 2.51
\end{aligned}$$

Several selection rules result from the elements of Equation 2.51. The $3j$ and the δ symbols lead to the rules $\Delta l \leq 0, 2$ $\Delta j \leq 2$. This shows that admixtures of states are allowed only for states of the same parity. The reduced matrix elements of the annihilation operator show that $\Delta R \leq 2$ and $N' < N$. This explains the symmetric form of the matrix elements of the tensor b in Equation 2.51.

In the diagonalization process, the quantities ξ and ϵ are treated as unknown parameters which are adjusted to give a good description of the experimental spectra of the nuclei under consideration. The quantity $\hbar\omega$, although treated as an unknown, has a value which is usually close to the experimental value of the first 2^+ excited state of the neighbouring even-even nuclei.

2.6 Magnetic dipole and electric quadrupole moments

The state vectors which are derived from the application of the intermediate coupling model to the nuclei under consideration, may be used to calculate the magnetic dipole and electric quadrupole moments of these nuclear states. The magnetic dipole moment of a nuclear state $|E, IM\rangle$ is defined as

$$\mu \equiv \langle E^{\alpha}, IM = I | \left(\frac{4\pi}{3}\right)^{1/2} \mathcal{M}_{\mu}(M1, \mu = 0) | E^{\alpha}, IM = I \rangle \dots 2.52$$

where $\mathcal{M}(M1, \mu)$ is the magnetic dipole operator and is given ⁽⁸⁾ by

$$\mathcal{M}(M1, \mu) = \left(\frac{3}{4\pi}\right)^{1/2} \{ g_l l_{\mu} + g_s s_{\mu} + g_R R_{\mu} \} \text{ n.m} \dots 2.53$$

where g_l , g_s and g_R are the g factors for the orbital angular momentum spin and core respectively, and (n.m) is the nuclear magneton given by

$$n.m \equiv \frac{eh}{2M_0C} \equiv 0.505 \cdot 10^{-23} \text{erg.gauss}^{-1} \dots \dots \dots 2.54$$

In order to evaluate the magnetic moment, the expression for the state vector from Equation (2.46) and the magnetic operator for $\mu = 0$ are substituted into Equation (2.52). Then an expression is obtained for μ which is given by

$$\mu = \sum_{\ell' j j' N N' R R'} C_{\ell' j' N' R'} C_{\ell j N R} \langle \ell' j'; N' R'; I M | g_{\ell} \bar{L} + g_S \bar{S} + g_R \bar{R} | j; N R; I M \rangle \dots \dots \dots 2.55$$

On applying the Wigner-Eckart theorem (equation A-10) one obtains

$$\begin{aligned} \mu &= \begin{pmatrix} I & 1 & I \\ -I & 0 & I \end{pmatrix} \sum_{\ell' j j' N N' R R'} C_{\ell' j' N' R'} C_{\ell j N R} \langle \ell' j'; N' R'; I | g_{\ell} \bar{L} + g_S \bar{S} + g_R \bar{R} || j; N R; I \rangle \times \\ &\times C_{\ell' j' N' R'} C_{\ell j N R} = \frac{I}{\{I(2I+1)(I+1)\}^{\frac{1}{2}}} \sum_{\ell' j j' N N' R R'} C_{\ell' j' N' R'} \langle \ell' j'; N' R'; I | \\ &|| g_{\ell} \bar{L} + g_S \bar{S} + g_R \bar{R} || j; N R; I \rangle C_{\ell' j' N' R'} C_{\ell j N R} \dots \dots \dots 2.56 \end{aligned}$$

where the analytical expression equation (A-7) for the 3j symbol was used.

The evaluation of the reduced matrix elements in equation (2.56) requires the successive application of the relations given by equations (A-11), (A-16) and (A-17). Application of equations (A-16) and (A-17) yields the following expressions:

$$\begin{aligned} \langle \frac{1}{2} \ell' j'; N' R'; I | | g_{\ell} \bar{L} | | \frac{1}{2} j; N R; I \rangle &= (-1)^{j'+R+I+1} g_{\ell} (\sqrt{2I+1})^2 \times \\ &\times \langle \frac{1}{2} \ell' j' || \ell || \frac{1}{2} j \rangle \times \left\{ \begin{matrix} j & I & R \\ I & j & I \end{matrix} \right\} \delta_{N N'} \delta_{R R'} \dots \dots \dots 2.57 \end{aligned}$$

$$\begin{aligned} \langle \frac{1}{2} \ell' j'; N' R'; I | | g_S \bar{S} | | \frac{1}{2} j; N R; I \rangle &= (-1)^{j'+R+I+1} g_S (\sqrt{2I+1})^2 \langle \frac{1}{2} \ell' j' || S || \frac{1}{2} j \rangle \times \\ &\times \left\{ \begin{matrix} j' & I & R \\ I & j & I \end{matrix} \right\} \delta_{N N'} \delta_{R R'} \dots \dots \dots 2.58 \end{aligned}$$

$$(j'; N'R'; I \| g_R \bar{R} \| j; NR; I) = (-1)^{j'+R+I+1} (\sqrt{2I+1})^2 (N'R' \| R \| NR) \times$$

$$\times \begin{Bmatrix} R & I & j' \\ I & R' & I \end{Bmatrix} \delta_{jj'} \dots \dots \dots 2.59$$

In analogy with equation (A-11) it is found that

$$(N'R' \| R \| NR) = \left\{ R(R+1)(2R+1) \right\}^{1/2} \delta_{RR'} \delta_{NN'} \dots \dots \dots 2.60$$

The reduced matrix elements of the operators \bar{l} and \bar{s} are obtained using equation (A-16) and are given by

$$\left(\frac{1}{2} \ell' j' \| \bar{l} \| \frac{1}{2} \ell j \right) = (-1)^{\frac{1}{2} + \ell + j' + 1} \left\{ (2j+1)(2j'+1) \right\}^{1/2} (\ell \| \bar{l} \| \ell) \begin{Bmatrix} \ell' & j' & \frac{1}{2} \\ j & \ell & 1 \end{Bmatrix} =$$

$$= (-1)^{\ell + j' - \frac{1}{2}} \left\{ (2j+1)(2j'+1) \right\}^{1/2} \left\{ \ell(\ell+1)(2\ell+1) \right\}^{1/2} \begin{Bmatrix} \ell & j' & \frac{1}{2} \\ j & \ell & 1 \end{Bmatrix} \delta_{\ell\ell'} \dots \dots \dots 2.61$$

and

$$\left(\frac{1}{2} \ell' j' \| \bar{s} \| \frac{1}{2} \ell j \right) = (-1)^{\frac{1}{2} + \ell' + j' + 1} \left\{ (2j+1)(2j'+1) \right\}^{1/2} (s \| \bar{s} \| s) \begin{Bmatrix} \frac{1}{2} & j' & \ell \\ j & \frac{1}{2} & 1 \end{Bmatrix} \delta_{\ell\ell'} =$$

$$= (-1)^{\ell + j - \frac{1}{2}} \left\{ (2j+1)(2j'+1) \right\}^{1/2} \left\{ \frac{1}{2}(\frac{1}{2}+1)(2\frac{1}{2}+1) \right\}^{1/2} \begin{Bmatrix} \frac{1}{2} & j' & \ell \\ j & \frac{1}{2} & 1 \end{Bmatrix} \delta_{\ell\ell'} =$$

$$= (1)^{\ell + j - \frac{1}{2}} \left\{ (2j+1)(2j'+1) \right\}^{1/2} \left(\frac{3}{2} \right)^{1/2} \begin{Bmatrix} \frac{1}{2} & \frac{1}{2} & 1 \\ j & j' & \ell \end{Bmatrix} \delta_{\ell\ell'} \dots \dots \dots 2.62$$

The final expression for the magnetic moment becomes

$$\mu = \left\{ \frac{I(2I+1)}{(I+1)} \right\}^{1/2} \sum_{\ell j j' NR} C_{\ell j j' NR} C_{\ell j j' NR; I} (-1)^{R+I+j'} \times$$

$$\times \begin{Bmatrix} j' & j & 1 \\ I & I & R \end{Bmatrix} (-1)^{\frac{1}{2}} \left\{ (2j+1)(2j'+1) \right\}^{1/2} \left[(-1)^{j'+\frac{1}{2}} g_{\ell} \left\{ \ell(\ell+1)(2\ell+1) \right\}^{1/2} \times \right.$$

$$\times \left. \begin{Bmatrix} \ell & \ell & 1 \\ j & j' & \frac{1}{2} \end{Bmatrix} + (-1)^{j+\frac{1}{2}} g_s \left(\frac{3}{2} \right)^{1/2} \begin{Bmatrix} \frac{1}{2} & \frac{1}{2} & 1 \\ j & j' & \ell \end{Bmatrix} - g_R \left\{ R(R+1)(2R+1) \right\}^{1/2} \times \right.$$

$$\times \left. \begin{Bmatrix} R & R & I \\ I & I & j \end{Bmatrix} \delta_{jj'} \right] \text{ n.m. } \dots \dots \dots 2.63$$

The g_{ℓ} ratio is taken consistently to be 1 for a proton and 0 for a neutron. The g_R ratio is usually taken as $g_R = Z/A$ but its value may

vary within reasonable limits. Finally the g_s ratio is $g_s = +5.5856$ for free protons and $g_s = -3.8263$ for free neutrons. Usually g_s is replaced by an effective g_s value to account for possible polarization effects of the core.

An expression for the electric quadrupole moment may be obtained in a similar way. The electric quadrupole moment q is defined as

$$q = \langle E^\alpha; IM = I \mid \left(\frac{16\pi}{5}\right)^{1/2} \mathcal{M}_\mu(E_{2\mu} = 0) \mid E^\alpha; IM = I \rangle \dots 2.64$$

where $\mathcal{M}_\mu(E_{2,\mu})$ is the electric quadrupole operator and is given by

$$\mathcal{M}_\mu(E_{2,\mu}) \equiv \frac{3}{4\pi} ZeR_0^2 \left(\frac{\hbar\omega}{2C}\right)^{1/2} \left[(-1)^\mu b_{-\mu} + b_\mu^+ \right] + \left(e_i + \frac{Ze}{A^2} r^2 Y_{2\mu} \right) \dots 2.65$$

Substituting the expression for the state vectors and the electric quadrupole operator for $\mu = 0$ from equation 2.46 one obtains

$$q = \left(\frac{16\pi}{5}\right)^{1/2} \sum_{jj' NN' RR'} C_{j'N'R'} C_{jNR} \langle j'; N'R'; IM = I \mid \frac{3Ze}{4\pi} R_0^2 \left(\frac{\hbar\omega}{2C}\right)^{1/2} \left[b_\mu^+ + (-1)^\mu b_{-\mu} \right]_{\mu=0} + \left(e_i + \frac{Ze}{A^2} \right) r^2 (Y_{2\mu})_{\mu=0} \mid j; NR; IM = I \rangle \dots 2.66$$

This expression is decomposed according to the Wigner Eckart theorem equation A-10 as follows:

$$q = \left(\frac{16\pi}{5}\right)^{1/2} \begin{pmatrix} I & 2 & I \\ -I & 0 & I \end{pmatrix} \sum_{jj' NN' RR'} C_{j'N'R'}^\alpha C_{jNR}^\alpha \times \left[\langle j'; N'R'; I \mid \frac{3}{4\pi} ZeR_0^2 \times \left(\frac{\hbar\omega}{2C}\right)^{1/2} b_2 \mid j'; NR; I \rangle + \langle j'; N'R'; I \mid \left(e_i + \frac{Ze}{A^2} r^2 Y_2 \right) \mid j; NR; I \rangle \right] \dots 2.67$$

The expressions for the reduced matrix elements may be worked out with the same methods as described in the case of the magnetic moment using the equations A-11, A-16, A-17 and the relation of equation A-8 for the

pertinent 3j symbol. Thus the final expression is given by

$$\begin{aligned}
 q &= \left\{ \frac{I(2I-1)(2I+1)}{(2I+3)(I+1)} \right\}^{1/2} \sum_{jNR} C_{\ell' j' N' R'}^{\alpha} C_{\ell j NR}^{\alpha} \times \\
 &\times \left\{ \frac{3}{(5\pi)^{1/2}} ZeR_0^2 \left(\frac{\hbar\omega}{2C} \right)^{1/2} (-1)^{j+I} \begin{Bmatrix} j' & N' & R' \\ I & I & j \end{Bmatrix} \left[(-1)^{R'} \langle NR \| b \| N' R' \rangle + \right. \right. \\
 &\quad \left. \left. + (-1)^R \langle N' R' \| b \| NR \rangle \delta_{\ell\ell'} \delta_{jj'} + 2 \left(e_i + \frac{Ze}{A^2} \right) (-1)^{R+I+\frac{1}{2}} \right] \times \right. \\
 &\times \left. \left\{ (2j+1)(2j'+1) \right\}^{1/2} \begin{Bmatrix} j' & j & 2 \\ I & I & R \end{Bmatrix} \begin{Bmatrix} j' & 2 & j \\ -\frac{1}{2} & 0 & \frac{1}{2} \end{Bmatrix} \langle r^2 \rangle \delta_{\text{even}}^{\ell+\ell'} \delta_{NN'} \delta_{RR'} \dots \right. \quad 2.68
 \end{aligned}$$

where

$$\langle r^2 \rangle = \langle \ell' j' \| r^2 \| \ell j \rangle \dots \dots \dots 2.69$$

The evaluation of $\langle r^2 \rangle$ requires the use of shell model wave functions. Usually one assumes that both initial and final states are constant throughout the interior of the nucleus and vanish outside. On the basis of this constant density model, the value of the radial integral $\langle r^\lambda \rangle$ is

$$\langle r^\lambda \rangle = \frac{\int_0^R r^\lambda r^2 dr}{\int_0^R r^2 dr} = \frac{3}{(\lambda+3)} \frac{R^{\lambda+3}}{R^3} = \frac{3}{(\lambda+3)} R^\lambda \dots \dots \dots 2.70$$

where R is the nuclear radius.

In using equation 2.68 it is found that the charge of the extra core particle differs from the charge of the free nucleon and for this reason an effective charge is used to account for polarization effects. Frequently (7-9) the effective charge of the proton is taken as $e_p = 2e$ and that of the neutron as $e_n = e$.

2.7 Electromagnetic transitions

The real test for the nuclear models is their ability to predict the correct transition probability and the multiplicities of the nuclear electromagnetic radiation. The probability of an electromagnetic transition between two nuclear states, is known to be strongly dependent upon the choice of the state vector of the nuclear states involved. A successful nuclear model should predict correctly the experimental transition probabilities.

The most frequent transitions occurring in the nuclei of the spherical region are the E-2 and M-1 transitions as well as their mixtures. Fortunately, for these two transitions it is easy to derive somewhat exact expressions for their transition probabilities within the frame of the present model.

The most general magnetic and electric multipole operators for a 2^λ -radiation in a space fixed system are respectively given by (10)

$$M_m(\lambda, \mu) = \frac{eh}{2Mc} (g_s \mathcal{S} + \frac{2}{\lambda+1} g_l \bar{L}) \bar{\nabla} (r^\lambda Y_{\lambda\mu}) + \frac{eh}{Mc} \frac{1}{\lambda+1} g_R \int \bar{R}(r) \bar{\nabla} (r^\lambda Y_{\lambda\mu}) d\tau \dots \dots \dots 2.71$$

where $\bar{R}(r)$ is the collective angular momentum satisfying the condition $\int \bar{R}(r) d\tau = \bar{R}$ and the other quantities are as in equation 2.53

and

$$M_e(\lambda, \mu) = \left[e_i + (-1)^\lambda \frac{Ze}{A} \right] r^\lambda Y_{\lambda\mu} + \frac{3}{4\pi} ZeRo^\lambda a_{\lambda\mu}^\lambda \dots \dots \dots 2.72$$

where the quantities involved have been defined in equation 2.65.

In both expressions the first part represents the transition of the extra core particle which is assumed to be individually excited while the last terms represent the contribution of the core to the transition (the multipole moments generated by the collective motion in the core).

In general the magnetic moment operator is difficult to evaluate because of the form of the collective part. Nevertheless for M-1 transitions the evaluation is easy and the M-1 operator assumes the form of equation 2.52.

The expression for the electric operator reduces to the electric quadrupole moment operator given in equation 2.65 in the case that quadrupole phonons exist. For the case of E- λ radiation with $\lambda \neq 2$ the collective part of the equation should be zero since no phonons with $\lambda \neq 2$ are assumed to exist. In that case the electric 2- λ radiation operator is an approximate operator which describes the extra core particle, while the collective effects (phonon decoupling, existence of $\lambda \neq 2$ phonons) are neglected.

The transition probability $T(\lambda)$ for the emission photon of multipole order λ and energy E is given by ⁽⁷⁾

$$T(\lambda) = \frac{8\pi(\lambda+1)}{\lambda [(2\lambda+1)!!]^2} \frac{1}{h^{2(\lambda+1)}} \left(\frac{E}{c}\right)^{2\lambda+1} B(\lambda) \dots\dots\dots 2.73$$

where $B(\lambda)$ is the reduced transition probability and is given by

$$B(\lambda) = \frac{1}{2I+1} \sum_{M'\mu M} \left| \langle E^{\lambda}; I'M' | M(\lambda, \mu) | E^{\lambda}; IM \rangle \right|^2 \equiv \\ \equiv \frac{1}{2I+1} \left| \langle E^{\lambda}; I' || M(\lambda, \mu) || E^{\lambda}; I \rangle \right|^2 \dots\dots\dots 2.74$$

where β and α denote the transition from the initial state of eigenvalue E^α and spin I to the state β with spin I' and energy E^α .

The evaluation of the matrix elements proceeds in the same way the derivation of the expressions of the magnetic and electric moments described in the previous section.

The final expression for the magnetic dipole and electric quadrupole reduced transition probabilities are respectively given by

$$\begin{aligned}
 B_m(1) = & \frac{3}{4\pi} (n.m)^2 (2I'+1) \left| \sum_{jj'NR} C_\beta (\ell'j';NR;I') C_\alpha (\ell j;NR;I) \right. \\
 \alpha I \rightarrow \beta I' & \\
 \times \left\{ & (-1)^{R+I+j'+\ell} [(2j+1)(2j'+1)]^{\frac{1}{2}} \left\{ \begin{matrix} j' & j & 1 \\ I & I' & R \end{matrix} \right\} \left[(-1)^{j+\frac{1}{2}} \left\{ \begin{matrix} \ell & \ell & 1 \\ j & j' & \frac{1}{2} \end{matrix} \right\} g_\ell \right. \right. \\
 & \left. \left[(\ell(\ell+1)(2\ell+1)]^{\frac{1}{2}} + (-1)^{j-\frac{1}{2}} \left\{ \begin{matrix} \frac{1}{2} & \frac{1}{2} & 1 \\ j & j' & \ell \end{matrix} \right\} g_s \left(\frac{3}{2} \right)^{\frac{1}{2}} \right] + (-1)^{R+I+j} \right. \\
 & \left. \left. \left\{ \begin{matrix} R & R & 1 \\ I & I' & j \end{matrix} \right\} g_R \left\{ R(R+1)(2R+1) \right\}^{\frac{1}{2}} \delta_{jj'} \right\} \right|^2 \dots \dots \dots 2.75
 \end{aligned}$$

and

$$\begin{aligned}
 B(2) = & (2I'+1) \left| \sum_{\ell(j'j'NN'R'R')} C_\beta (\ell'j';N'R';I') C_\alpha (\ell j;NR;I) \right. \\
 \alpha I \rightarrow \beta I' & \\
 \times \left\{ & \frac{3}{4(5\pi)^{\frac{1}{2}}} ZeRo^2 \xi \frac{\hbar\omega}{k} (-1)^{j+I'} \left\{ \begin{matrix} R & R' & 2 \\ I & I' & j \end{matrix} \right\} \left[(-1)^{R'} (NR\|b\|N'R') + \right. \\
 & \left. + (-1)^R (N'R'\|b\|NR) \right] \delta_{\ell\ell'} \delta_{jj'} + \frac{\sqrt{5}}{2\sqrt{\pi}} (e_i + \frac{Ze}{A^2}) (-1)^{R+I+\frac{1}{2}} \times \\
 \times \left\{ & (2j+1)(2j'+1) \right\}^{\frac{1}{2}} \left\{ \begin{matrix} j' & j & 2 \\ I & I' & R \end{matrix} \right\} \left(\begin{matrix} j' & 2 & j \\ -\frac{1}{2} & 0 & \frac{1}{2} \end{matrix} \right) (j'\|r^2\|j) \delta_{\text{even}}^{+'} \delta_{NN'} \delta_{RR'} \left| \right. \\
 & \dots \dots \dots 2.76
 \end{aligned}$$

2.8 <<Quasiparticles>>

In sections 2.3 to 2.5 a general treatment was given of the odd A spherical nuclei in the frame of the unified model. The Hamiltonian of the system under consideration was given by eq. 2.26. This equation included the term H_j , the single particle Hamiltonian, given by

$$H_j |j\rangle = \epsilon_j |j\rangle \dots \dots \dots 2.77$$

where ϵ_j are the eigenvalues of the single particle states. The ϵ_j were treated as adjustable constants determined from the best fit of the model to the experimental data for a particular nucleus.

In previous works⁽⁷⁻⁹⁾ the intermediate coupling model was used and it was found that the E_j values derived from the best fit were considerably different from the single particle levels derived from a shell model. N. Glendenning⁽¹⁴⁾ has pointed out that this effect can be explained in terms of the pairing theory. This theory was first developed by S. T. Belyaev⁽¹¹⁾ and later elaborated by L. S. Kisslinger and R. A. Sorensen.^(12,13)

A fundamental assumption of the pairing theory is that within a nuclear shell all even particles are paired with zero total angular momentum. For simplicity, it is assumed that within a given shell all possible interactions are switched off and the only acting force is the pairing force. The index j is used to specify the angular momentum of a particle within the given shell and m is the z-component of the angular momentum. If the energy of a state j within the given shell (shell model energy) is denoted by ϵ_j then the Hamiltonian of the system of n particles in the shell under consideration is given by⁽¹³⁾

$$H_j = \sum_{jm} \epsilon_j b_{jm}^+ b_{jm} \dots \dots \dots 2.78$$

where $\sum b_{jm}^+$ is the operator of the number of particles that are present and b_{jm}^+ , b_{jm} are the respective creation and annihilation operators for fermions with the following properties

$$\begin{aligned} [b_{jm}^+, b_{j'm'}] &= \delta_{jj'} \delta_{mm'} \dots\dots\dots 2.79 \\ [b_{jm}^+, b_{j'm'}^+] &= [b_{jm}, b_{j'm'}] = 0 \dots\dots\dots 2.80 \\ b_{jm}^+ | 0 \rangle &= | jm \rangle \dots\dots\dots 2.81 \\ b_{j-m}^+ | 0 \rangle &= | j-m \rangle \dots\dots\dots 2.82 \end{aligned}$$

The independent particle Hamiltonian H_j given by equation 2.78 is diagonal for states containing a definite number of particles in each shell.

An additional term in the total Hamiltonian of the system is required now, to describe the pairing force.

After Kisslinger and Sorensen^(12,13) the pairing Hamiltonian is assumed to have the form given by

$$H_p = -\frac{1}{2} G \sum_{j,j',mm'} b_{j'm'}^+ b_{j'-m'}^+ b_{j-m} b_{jm} \dots\dots\dots 2.83$$

where G is the strength of the pairing force, which is assumed to be constant and independent of the particle state.

The treatment of the pairing part of the Hamiltonian is simplified by transformation to a system in which the number of particles is not conserved. An auxiliary Hamiltonian is introduced which is related to $(H_j + H_p)$ by the equation given by⁽¹²⁾

$$H = H_j + H_p - \lambda N = H_j + H_p - \lambda \sum_{jm} b_{jm}^+ b_{jm} \dots\dots\dots 2.84$$

An additional constraint is introduced for the solution Ψ of eq. 2.84.

$$\langle \Psi | N | \Psi \rangle = n \dots\dots\dots 2.85$$

Where n is the proper number of particles. In this way the choice of λ determines only the average number of particles in the system described by eq. 2.84.

An approximate solution of equation 2.84 may be obtained by introducing the Bogolubov-Valatin ^(11,12) canonical transformations

$$\alpha_{jm} = U_j b_{jm} - V_j b_{j-m}^+ \dots\dots\dots 2.86$$

$$\beta_{jm} = U_j b_{j-m}^+ + V_j b_{jm} \dots\dots\dots 2.87$$

The new Fermi operators α_{jm} and β_{jm} are called the <<quasi-particle>> creation and annihilation operators respectively and they are linear combinations of shell model particle and hole creation operators.

The coefficients U_j and V_j are real numbers. Their physical significance is that V_j^2 is the probability of the pair $(jm, j-m)$ occupying the state E_j while U_j^2 is the non occupation probability.

U_j and V_j are related by

$$U_j^2 + V_j^2 = 1 \dots\dots\dots 2.88$$

α_{jm} and β_{jm} satisfy the same commutation relations as b_{jm} and b_{jm}^+ .

$$[\beta_{jm}^+, \beta_{j'm'}]_+ = [\alpha_{jm}^+, \alpha_{j'm'}]_+ = \delta_{jj'} \delta_{mm'} \dots\dots\dots 2.89$$

The transformations inverse to eq. 2.86 and 2.87 are:

$$b_{jm}^+ = U_j \alpha_{jm}^+ + V_j \beta_{jm}^+ \dots\dots\dots 2.90$$

$$b_{j-m} = U_j \beta_{j-m} - V_j \alpha_{j-m}^+ \dots\dots\dots 2.91$$

If the transformations specified by eqs. 2.90 and 2.91 are used in eq. 2.84, the Hamiltonian H is transformed to ^(11,12)

$$H = V + H_{11} + H_{20} + H_{int} \dots\dots\dots 2.93$$

where V is a constant term,

$$H_{11} = \sum_j \left\{ (\epsilon_j - \lambda)(U_j^2 - V_j^2) + 2G\underline{\Omega}_j U_j^2 V_j^2 \right\} (\alpha_j^+ \alpha_j + \beta_j^+ \beta_j) \quad 2.94$$

$$H_{20} = \sum_j \left\{ (\epsilon_j - \lambda) 2U_j V_j - G\underline{\Omega}_j U_j V_j (U_j^2 - V_j^2) \right\} (\alpha_j^+ \beta_j^+ + \beta_j \alpha_j) \quad 2.95$$

and $2\underline{\Omega}_j = 2j+1$ is the multiplicity of the given state.

The term H_{11} describes one quasiparticle excitations while the term H_{20} describes two quasiparticle excitations. H_{int} contains terms with products of four quasiparticles and describes the interaction between quasiparticles. This term is dropped. ⁽¹¹⁾ The effect of neglecting this interaction term is negligible as Belyaev ⁽¹¹⁾ has pointed out, and mainly affects the strength G of the pairing force.

Neglecting this interaction term, the Hamiltonian 2.93 is written

$$H = V + H_{11} + H_{20} \dots \dots \dots 2.96$$

The Hamiltonian given by eq. 2.96 may be considered an independent particle Hamiltonian provided terms of the form $(\alpha_j^+ \beta_j^+ + \beta_j \alpha_j)$ vanish, since these terms describe the quasiparticle interaction, i.e. if

$$H_{20} = 0 \dots \dots \dots 2.97$$

By equating the coefficient of 2.97 to zero the following condition is obtained

$$\frac{G}{2} \sum_j \frac{\underline{\Omega}_j}{\sqrt{(\epsilon_j - \lambda)^2 + \Delta^2}} = 1 \dots \dots \dots 2.98$$

where

$$\Delta = G \sum_j \underline{\Omega}_j U_j V_j \dots \dots \dots 2.99$$

$$U_j^2 = \frac{1}{2} \left[1 + \frac{\epsilon_j - \lambda}{\sqrt{(\epsilon_j - \lambda)^2 + \Delta^2}} \right] \dots \dots \dots 2.100$$

$$\text{and } v^2 = \frac{1}{2} \left[1 - \frac{\epsilon_j - \lambda}{\sqrt{(\epsilon_j - \lambda)^2 + \Delta^2}} \right] \dots \dots \dots 2.101$$

The constraint condition given by eq. 2.85 imposes one more relation which is given by

$$n \equiv \langle \Psi_0 | N | \Psi_0 \rangle = \sum_j \frac{\Omega_j}{2} \left[1 - \frac{\epsilon_j - \lambda}{\sqrt{(\epsilon_j - \lambda)^2 + \Delta^2}} \right] \dots 2.102$$

If the number of particles n in a given shell, the pairing force G , and the single particle levels are given, then the equations 2.98 and 2.102 may be solved and thus the unknown parameters λ and Δ may be computed. The single particle levels may be obtained from a shell model (for example the Nilsson⁽¹⁰⁾ model for $\delta=0$.) The parameter G is chosen to fit the experimental data and is of the order of 0.25 MeV for $A \approx 100$. An iteration method was used and a numerical solution for the set of equations 2.98 and 2.102 was obtained. It was found that the iteration used, converged fast. In Appendix C the iteration program used to solve the above mentioned equations is given. In applying equations 2.98 and 2.102 in odd A nuclei it was assumed that short range forces do not account for neutron-proton pair interactions. This assumption is correct in cases where the neutrons and protons do not occupy the same levels. The energy of a quasiparticle state j in an odd A nucleus may be calculated from the expression

$$\langle \Psi | U + H_{11} | \Psi \rangle = U + \sqrt{(\epsilon_j - \lambda)^2 + \Delta^2} \equiv U + E_j \dots \dots \dots 2.103$$

where the corresponding Hamiltonian given by eq. 2.96 is used. Thus the energy of a quasiparticle state, neglecting the constant term v , is given by

$$E_j = \sqrt{(\epsilon_j - \lambda)^2 + \Delta^2} \dots \dots \dots 2.104$$

The separation energy between two one-quasi particle states in an odd A nucleus is given by

$$E_j - E_{j'} = \sqrt{(\epsilon_j - \lambda)^2 + \Delta^2} - \sqrt{(\epsilon_{j'} - \lambda)^2 + \Delta^2} \dots 2.105$$

The corresponding expression for the first excited state in an even nucleus is the state with two quasiparticles (both neutron or proton) and is given by

$$\langle \Psi(j_1 j_2) | H_{11} | \Psi(j_1 j_2) \rangle = \sqrt{(\epsilon_{j_1} - \lambda)^2 + \Delta^2} + \sqrt{(\epsilon_{j_2} - \lambda)^2 + \Delta^2} \dots 2.106$$

where the two quasiparticles have angular moments j_1 and j_2 respectively.

From the previous discussion it is clear that the pairing theory is capable of giving a semiquantitative description of the single particle (quasiparticle) spectrum of the nucleus.

This suggests that the introduction of quasiparticles in the unified model might improve considerably the capability of the unified model to account for the various nuclear properties especially in the case of the odd A spherical nuclei. This subject is treated in the following section.

2.9 Introduction of quasiparticles in the unified model.

In the present section the concept of quasiparticle states is introduced in the unified model.

The states of an odd-A nucleus are considered to result from the coupling of the quasiparticles states available to the last odd nucleon to the phonon vibrations of the core.

To begin with, it is assumed that the interaction between quasiparticle states and phonon is switched off and the Hamiltonian of the phonon-quasiparticles system is written

$$H = H_j + H_{col} \dots \dots \dots 2.107$$

where H_{col} is defined by eq. 2.18 and H_j is the quasiparticle Hamiltonian given by eq. 2.84. The state vector of a quasiparticle will be denoted $|jm\rangle$ and satisfies the relation

$$H_j |jm\rangle = E_j |jm\rangle \equiv \sqrt{(\epsilon_j - \lambda)^2 + \Delta^2} |jm\rangle \dots \dots 2.108$$

The basis vector $|j;NR;IM\rangle$ for the system under consideration is introduced as in eq. 2.45.

The matrix elements of the Hamiltonian given by eq. 2.107 in accordance with the previous discussion, as given by

$$\begin{aligned} \langle j';N'R';I'M' | H_{col} + H_j | j;NR;IM\rangle &= (\hbar\omega + E_j) \delta_{NN'} \delta_{RR'} \delta_{jj'} \equiv \\ &\equiv \left\{ \hbar\omega + \sqrt{(\epsilon_j - \lambda)^2 + \Delta^2} \right\} \delta_{NN'} \delta_{jj'} \delta_{RR'} \dots \dots \dots 2.109 \end{aligned}$$

Essentially the same notation as in section 2.5 is kept while the motion of quasiparticles has been introduced. Thus far the only change introduced is the substitution of the quasiparticle energy E_j in the matrix elements given by eq. 2.109 instead of the adjustable constant ϵ_j .

Now the interaction between quasiparticles and phonons is switched on. The interaction Hamiltonian is assumed to have exactly the same form as in equation 2.43.

The matrix elements of the interaction Hamiltonian will have the same form as in eq. 2.50. The only difference is that the matrix elements $\langle j;NR;IM | H | j';N'R';I'M \rangle$ are taken between quasiparticle states instead of particle states. In order to transform the one expression into the other, the general transformation of an operator from quasiparticle to particle representation is considered.

The same notation as in the previous section is used. An expression is obtained for the matrix elements of a general operator Q between quasiparticles states in terms of the corresponding expression in terms of particles states. This expression is given by

$$\langle \alpha_j^+ | Q | \alpha_j^+ \rangle = \sum_{\alpha, \beta} \langle \alpha | Q | \beta \rangle \langle \alpha_j^+ b_{\alpha}^+ b_{\beta}^+ | \alpha_j^+ \rangle \equiv \langle j | Q | j' \rangle (U_j U_{j'} - V_j V_{j'}) \dots \dots \dots 2.110$$

Thus the matrix elements of the interaction Hamiltonian may be calculated and are given by

$$\langle j';N'R';I'M | H_{int} | j;NR;IM \rangle = -\sqrt{\frac{\pi}{5}} \xi (U_j U_{j'} - V_j V_{j'}) \hbar \omega (-1)^{I+j} \times \left\{ \begin{matrix} j'R'I \\ R \ j \ 2 \end{matrix} \right\} \langle j' || Y_2 || j \rangle \left[(-1)^R \langle N'R' || b || NR \rangle + (-1)^R \langle NR || b || N'R' \rangle \right] 2.111$$

Equation 2.111 indicates that the matrix elements of the interaction Hamiltonian between single particles states must be multiplied by the statistical factor $(U_j U_{j'} - V_j V_{j'})$ which is based on the occupation number of the quasiparticle state.

This concept could have been introduced qualitatively in the earlier part of this work (section 2.5). In obtaining the off diagonal matrix element of the interaction Hamiltonian between particles states,

the expression eq. 2.50 is summed over all the magnetic substates. But since it might be possible that a certain level might not be completely empty and thus having available all the substates to the odd nucleon, a statistical factor is needed to account for this effect. This statistical factor based on the occupation probability of the given state, should account for the substates available to the extra core particle.

These qualitative assumptions are now, naturally introduced by considering the quasiparticle states instead of particle states.

In the present work, E_j , the single particle energy, is still treated as an adjustable constant. The E_j values derived from the best fit are compared with the predictions of the pairing theory as formulated in the last two sections. In the off diagonal elements of the interaction Hamiltonian an approximate statistical factor is introduced whenever necessary by considering the number of nucleons which may share a given state with the extra core nucleon.

This procedure has the advantage that it allows a more close and independent examination of the validity of the two submodels used in the present version of the unified model, that is the intermediate coupling model and the pairing model.

3. APPLICATION OF THE INTERMEDIATE COUPLING MODEL

3.1. Positive parity states in odd Xe isotopes

In recent years a considerable amount of information concerning the level structure of Xe isotopes has become available. Most of this information is based on the investigation of the gamma ray spectra of these isotopes with high resolution Ge(Li) detectors. These investigations provide very accurate information on the energy position and spins of the levels of most of these isotopes.

The majority of the states observed in the odd Xe isotopes have a positive parity. All the nuclei ⁽¹⁵⁾ of this isotopic region show a low lying $1/2^+$ or $3/2^+$ state. More specifically, ^{127}Xe and ^{129}Xe have a $1/2^+$ ground state ⁽¹⁵⁾ while a $3/2^+$ state is developed at 125 and 39 KeV respectively. In ^{131}Xe , ^{133}Xe and ^{135}Xe , the ground state is $3/2^+$. In ^{131}Xe it was long known that the first excited state is a $1/2^+$ state at 81 KeV. Very recently ⁽¹⁶⁾ the corresponding $1/2^+$ states in ^{133}Xe and ^{135}Xe have been reported at 264 and 288.6 KeV respectively.

In the previously mentioned five Xe isotopes, a group of positive parity states is observed at energies close to the energy of the first 2^+ states of the corresponding even-even Xe isotopes.

The shell model predicts that the last odd neutron in the ground state occupies the $3s_{1/2}$ state in ^{127}Xe and ^{129}Xe and the $2d_{3/2}$ state in the ground state of the other Xe isotope with $A \geq 131$. According to the shell model the first excited states in these isotopes are excitation states of the odd neutron. Thus the odd neutron in ^{127}Xe and ^{129}Xe

is excited to the $2d_{3/2}$ state while in $^{131,133,135}\text{Xe}$ the odd neutron is excited to the $3s_{1/2}$ state. According to a strict single particle picture⁽¹⁷⁾, the transition probabilities for the gamma transitions deexciting these $2d_{3/2}$ and $3s_{1/2}$ states are approximately half the predictions of the Moskowski⁽¹⁷⁾ estimates for these transitions. Actually the transition probabilities of the 39 and 81 KeV transitions deexciting the corresponding $3/2^+$ and $1/2^+$ levels in ^{129}Xe and ^{131}Xe have been measured experimentally^(15,18). The results show that these transitions which are predominantly M1 in character are retarded over the single particle estimates by a factor of 30, indicating that these states have a configuration quite different from the single particle predictions. One more weakness of a simple shell model view of the structure of these levels is the difficulty in explaining the gradual lowering of the $3/2^+$ states in $^{127,129}\text{Xe}$ with respect to the $1/2^+$ ground state. As mentioned before the $3/2^+$ state becomes the ground state in Xe isotopes with A 131 while the $1/2^+$ state rises from 80 KeV in ^{131}Xe to 283 KeV in ^{135}Xe with respect to the $3/2^+$ ground state.

Two transitions at 284 and 364 KeV have been observed to deexcite a 364 KeV level in ^{131}Xe . The half life of this level has been measured experimentally⁽¹⁹⁾. The results indicate that the 284 KeV (E2) transition in ^{131}Xe is enhanced by a factor of 10 over the single particle estimate. The 364 KeV transition is E2 in character with a 9% admixture of M1. From these data, it is deduced that the E2 component of the 364 KeV transition has an enhancement factor of 30 for the observed transition

probability over the single particle estimate, while the M1 component is similarly retarded by a factor of 10^3 over the single particle estimate.

(14)

Early in the 1960's, Glendenning pointed out that the structure of the Xe isotopes may be described in terms of a model in which the odd neutron in these isotopes is coupled to the vibrations of an even-even core. He applied these considerations to $^{127,129}\text{Xe}$ and found good agreement with the experimental data available. At that time very limited experimental data were available for a meaningful comparison. Most of these data were concerned with the energy position of a few known levels. In order to test the model described in the previous chapter, the four Xe isotopes with $127 \leq A \leq 133$ are investigated in this work.

First, the structure of the even-even Xe isotopes is examined. The results of this examination may give an indication of the extent to which the even-even Xe isotopes are good harmonic vibrators.

3.2. Even-even Xe isotopes

The level structure of several even Xe isotopes is quite well known. The first three excited states of the six Xe isotopes with $126 \leq A \leq 136$ are listed in Table 1. The states shown are the first 2^+ , and the 2^+ and 4^+ observed at energies twice that of the first 2^+ excited state. The 0^+ state usually observed in even-even nuclei has not been identified in any of the listed Xe isotopes. The center

Table 1

(a)
Excited states of some even-even Xe nuclei

Xe Nucleus A	One phonon state (in KeV) 2 ⁺	Two phonon states (in KeV)			Center of gravity	$R = \frac{E \text{ two phonons}}{E \text{ one phonon}}$
		0 ⁺	2 ⁺	4 ⁺		
126	389.0	-	881	943	920.8	2.37
128	443.0	-	970	1033	1010.8	2.28
130	536.1	-	1122.1	1204.1	1174.3	~2.19
132	667.8	-	1298.1	1440.7	1389.7	2.08
134	848.0	-	1615	1733	1690.1	2.00
136	1313	-	2582	2633	2614.8	1.98

(a) from ref. (15)

of gravity of the two states with spin 2^+ and 4^+ which should belong to the members of the 2 phonon excitation is also shown in Table 1. The ratio of the energy of the center of gravity of the 2 phonon states to the energy of the first 2^+ state is also listed in this table. This ratio is a good indicator of the anharmonicity of the even-even nucleus. A value of 2 is expected from a perfect harmonic vibrator for the ratio of the energy of the 2 phonons over the one phonon states.

The listed ratios in Table 1 indicate that the anharmonicity of the even-even nuclei decreases with increasing atomic number. In ^{134}Xe and ^{136}Xe this ratio is 2 and 1.98 respectively. In ^{134}Xe the nucleus is approaching the shell closure (80 neutrons) and in ^{136}Xe has a closed neutron shell.

In Table 2 the properties of some transitions in some Xe isotopes are presented. The measured transition probabilities of two E2 transitions deexciting the first 2^+ level in these nuclei are listed and compared with the single particle estimates ⁽¹⁷⁾. The ratio of these transition probabilities over the single particle estimate is found to be 44 and 16.0 in ^{126}Xe and ^{132}Xe respectively. The ratios of the reduced transition probabilities of the transitions deexciting the second 2^+ level and feeding the 0^+ ground and 2^+ first excited states are also presented in Table 1. This ratio is 0.011 in ^{126}Xe and decreases to a value of 0.0014 in ^{132}Xe .

If equation (2.76) is used to calculate the collective transition probability for an E2 radiation from a 2^+ one phonon state to the 0^+

Table 2

Nuclei	Level Initial J ^π KeV	Final J ^π KeV	Transition in KeV	(a)		Xe nuclei $\frac{T(E2)_{exp}}{A=T(E2)_{sp}}$	Branch	$\frac{B(2_2^+ \rightarrow 0_1^+)}{B(2_2^+ \rightarrow 2_1^+)}$	C in MeV
				T(E2)exp in tr/sec	T(E2)sp in tr/sec				
¹²⁶ Xe	(2 ⁺) 389	(0 ⁺) 0	389	1.7x10 ¹⁰	3.9x10 ⁸	44	1.0	---	20
	(2 ⁺) 881	(2 ⁺) 389	492	---	---	--	0.83	---	
	(2 ⁺) 881	(0 ⁺) 0	881	---	---	--	0.17	0.011	
¹²⁸ Xe	(2 ⁺) 443	(0 ⁺) 0	443	---	---	--	1.0	---	--
	(2 ⁺) 970	(2 ⁺) 443	527	---	---	--	0.84		
	(2 ⁺) 970	(0 ⁺) 0	970	---	---	--	0.16	0.0091	
¹³⁰ Xe	(2 ⁺) 536	(0 ⁺) 0	536	---	---	--	1.0		--
	(2 ⁺) 1121.1	(2 ⁺) 536	585.1	---	---	--	0.87		
	(2 ⁺) 1121.1	(0 ⁺) 0	1121.1	---	---	--	0.13	0.0056	
¹³² Xe	(2 ⁺) 667.8	(0 ⁺) 0	667.8	9.85x10 ¹⁰	6.10x10 ⁹	16.0	1.0		93
	(2 ⁺) 1298.1	(2 ⁺) 667.8	630.3	---	---	--	0.95		
	(2 ⁺) 1298.1	(0 ⁺) 0	1298.1	---	---	--	0.05	0.00136	
¹³⁴ Xe	(2 ⁺) 848	(0 ⁺) 0	848	---	---	--	1.0		
	(2 ⁺) 1615	(2 ⁺) 848	767	---	---	--	0.55		
	(2 ⁺) 1615	(0 ⁺) 0	1615	---	---	--	0.45	0.020	

Table 2 (continued)

Nuclei	Level Initial J ^π KeV	Final J ^π KeV	Transition in KeV	(a)		$\frac{T(E2)_{exp}}{A=T(E2)_{sp}}$	Branch	$\frac{B(2_{2}^{+} \rightarrow 0^{+})}{B(2_{2}^{+} \rightarrow 2_{1}^{+})}$	C in MeV
				T(E2)exp in tr/sec	T(E2)sp in tr/sec				
¹³⁶ Xe	(2 ⁺)1313	(0 ⁺) 0	1313	---	---	--	1.0	---	--
	(2 ⁺)2582	(2 ⁺)1313	1269	---	---	--	0.70		
	(2 ⁺)2582	(0 ⁺) 0	2582	---	---	--	0.30	0.013	

(a) from ref. (15)

ground state, then the ratio to the single particle estimate may be deduced.

The final expression for this ratio is given by

$$A \equiv \frac{T(2)2^+ \rightarrow 0^+}{T_{sp}} = \frac{5}{2\pi} \frac{Z^2 \hbar \omega}{C} \dots \dots \dots (3.1)$$

Because of the factor Z^2 the ratio A is usually $\gg 1$ and hence a collective state exhibits an enhanced E2 transition probability. Equation (3.1) is used to obtain the stiffness parameter C for ^{126}Xe and ^{132}Xe since in these cases the ratio A is known. The values obtained for the parameter C are presented in Table 2.

Equation (2.76) also indicates that no E2 transition occurs between states differing by more than 1 phonon. Thus in a perfect vibrator, transitions from the second 2^+ state to the ground state are forbidden. Observation of these transitions in even-even nuclei as very weak transitions may be considered as an indication of anharmonicity. Nevertheless, it is possible that the $|22^+\rangle$ phonon state, i.e., the state with 2 phonons of total angular momentum 2^+ , may interact with the $|12^+\rangle$ state. In this case the structure of the second 2^+ state contains some admixtures of the $|12^+\rangle$ state in a form given by

$$|22^+\rangle = |22^+\rangle + \beta |12^+\rangle \dots \dots \dots (3.2)$$

where β is very small.

If this happens, then the transition probability from the second 2^+ state to the 0^+ ground state is finite since matrix elements of the form $\langle 00|b|12^+\rangle$ are finite.

Through equation (2.76), it can easily be shown that the ratio of the reduced transition probability of the $2^+ \rightarrow 0^+$ to the $2^+ \rightarrow 2^+$ is given by

$$\frac{B(E2)_{2^+ \rightarrow 0^+}}{B(E2)_{2^+ \rightarrow 2^+}} = \frac{1}{2} \beta^2 \quad \dots \dots \dots (3.3)$$

With equation (3.3) and the data of Table 2, it is found, for example, in ^{132}Xe that $\beta^2 \approx 2.7 \times 10^{-3}$ indicating that a 3% admixture of $|12^+\rangle$ state in the $|22^+\rangle$ state is adequate to explain the observed forbidden $2^+ \rightarrow 0^+$ transition. The observed admixture in the case of ^{132}Xe indicates an interaction energy of the order of

$$\langle 12 | V | 22 \rangle \equiv \beta^2 \hbar \omega \approx 1.8 \text{ KeV} \quad \dots \dots \dots (3.4)$$

For the other nuclei which exhibit a larger anharmonicity, values of β^2 are larger and the interaction energy is about 10 KeV. As can be seen in Table 2, the same is observed in ^{134}Xe and ^{136}Xe . These two nuclei show no anharmonicity in their ratios of the phonons energies. However they show an appreciable mixing of the low lying states. This probably happens because the explicit particle structure of the levels interferes with the vibrations of the core. Some similar considerations are given in more detail in Chapter 6, section 4 where the level structure of ^{92}Zr is examined.

Finally it may be noted that equation (2.78) indicates that M1 transitions may not proceed between states which differ in their phonon number. Thus M1 transition probabilities are usually retarded between collective states as these states tend to share the strength of one particular phonon state.

From the above general discussion of the Xe even isotopes it can

be deduced that these nuclei clearly exhibit collective phenomena with some inevitable small anharmonicities. Thus the use of these nuclei as vibrating cores for coupling single particles is justified.

3.3. Computational procedure

The model has been applied to some odd Xe isotopes, namely ^{127}Xe , ^{129}Xe , ^{131}Xe and ^{133}Xe . In these cases the last odd neutron is considered to have available the $3s_{1/2}$ and $2d_{3/2}$ states. States of up to three phonons have been considered. Then the interaction matrix elements have been calculated between states of a given spin using equation (2.50). Values for the $3j$ and $6j$ symbols were obtained from ref. (20). The effective spacings $\epsilon_{3/2} - \epsilon_{1/2}$ have been treated as adjustable parameters. The other unknown parameters were the coupling constant ξ and the oscillation energy of the vibrating core (see Chapter 2, section 5).

The matrices corresponding to a given spin have been diagonalized with the aid of the IBM 1130 computer of the USRC. The best fit of the theoretical to the experimental spectrum was obtained using iteration procedures.

First the system was diagonalized for several values of the effective spacing parameter $\epsilon_{3/2} - \epsilon_{1/2}$. Then for each value of the effective spacing parameter the ξ and $\hbar\omega$ values that gave the best description of the first excited states were retained to reproduce the spectrum. From all spectra which corresponded to a specific set of $\epsilon_{3/2} - \epsilon_{1/2}$, ξ and $\hbar\omega$ values, the spectrum which gave a better description of the second and possibly of the

third excited state was retained as representing the best fit. More details about the computational work involved with the application of the model are given in Appendix D. The magnetic and electric moments as well as the transition probabilities of several transitions in the nuclei under investigation have been calculated using equations (2.63, 2.68, 2.73, 2.75 and 2.76) as described in Chapter 2. The parameters entering such calculations are the effective neutron g_e and g_s values, the effective neutron charge e_n , the magnetic moment of the core g_R and the parameter $\langle K \rangle$, which is the potential depth of the appropriate nuclei.

In the following calculations it was assumed that both g_e and e_n are zero in accordance with the properties of a free neutron. The potential parameter was assumed to be $\langle K \rangle = 40$ MeV. Probably this value might be as much as half of the value adopted in this work and is a function of the explicit structure of the assumed core. If the stiffness parameter C (last column of Table 2) was known for all the even-even nuclei considered in these calculations, a better choice of the constant K could have been made. Through equation (2.42) the constant $\langle K \rangle$ may be written in terms of the coupling constant ξ and the vibrational energy as

$$\langle K \rangle = \xi \left(\frac{2\pi\hbar\omega C}{5} \right)^{\frac{1}{2}} \dots \dots \dots (3.5)$$

The consequence of this equation in connection with the adopted $\langle K \rangle$ value are discussed later, individually for each examined nucleus.

The effective neutron spin magnetic moment g_s and the core magnetic moment $g_R \approx \frac{Z}{A}$ (see discussion in Chapter 2, section 6) have been assigned

the values $g_s = -2.3$ and $g_R = 0.3$. This particular set of values has been found to give a consistent description of the magnetic moment as well as the magnetic dipole transition probabilities in the nuclei under consideration. Many authors have pointed out that an effective g_s value for neutrons or protons which is half of the corresponding free particle g value, gives a better description of the magnetic nuclear properties. The value $g_s = -2.3$ used here is somewhat lower than the value $1/2 g^{\text{eff}} = -1/2 \times 3.8 = -1.9$. Finally the state vectors necessary to obtain the required nuclear properties have been obtained from the diagonalization of the matrices which corresponded to the best fit to the energy levels of the examined nuclei.

3.4. Level structure of ^{127}Xe

The calculated energy spectrum including states with spin up to $5/2^+$ is shown in Fig. (1), and is compared with the experimentally observed spectrum. The values of the constants obtained from the best fit of the model are $\epsilon_{1/2} - \epsilon_{3/2} = 250$ KeV, $\hbar\omega = 410$ KeV and $\xi \cong 2.75$.
(21)

The experimental data on the level structure of ^{127}Xe come from the investigation of the β^+ decay of ^{127}Cs . ^{127}Cs has a $1/2^+$ ground state spin, which favours transitions to $1/2^+$ and $3/2^+$ excited states in ^{127}Xe . Thus the comparison of the predictions of the model is limited by these observed spin assignments which unfortunately are tentative.

Except for the first $3/2^+$ level at 125 KeV, the model predicts a

1975 _____ $\leq \frac{3}{2}, (5^-)$

$\frac{3}{2}^+$ _____ 1925

1775 _____ $\leq \frac{3}{2}, (5^-)$

$\frac{3}{2}^+$ _____ 1770

1582 _____ $\leq \frac{3}{2}, (5^-)$

$\frac{1}{2}^+$ _____ 1620

1534 _____ $\leq \frac{3}{2}, (5^-)$

$\frac{3}{2}^+$ _____ 1550

1305 _____ $\leq \frac{3}{2}, (5^-)$

1195 _____ $\leq \frac{3}{2}, (5^-)$

$\frac{3}{2}^+$ _____ 1220
 $\frac{1}{2}^+$ _____ 1190
 $\frac{3}{2}^+$ _____ 1140

929 _____ $\frac{1}{2}^+, \frac{3}{2}^+, (5^-)$

$\frac{3}{2}^+$ _____ 1003
 $\frac{1}{2}^+$ _____ 962

$\frac{5}{2}^+$ _____ 825

586 _____ $\frac{3}{2}^+, (\frac{1}{2})^+$

$\frac{3}{2}^+$ _____ 676
 $\frac{1}{2}^+$ _____ 626
 $\frac{5}{2}^+$ _____ 600
 $\frac{3}{2}^+$ _____ 511

411 _____ $\frac{1}{2}^+, (\frac{3}{2})^+$

$\frac{5}{2}^+$ _____ 350

321 _____ $\frac{3}{2}^+$
300 _____ $\frac{3}{2}^+$

125 _____ $\frac{3}{2}^+$

$\frac{3}{2}^+$ _____ 125

0 _____ $\frac{1}{2}^+$

$\frac{1}{2}^+$ _____ 0

EXPERIMENTAL

THEORETICAL

Fig. 1. The calculated spectrum of ^{127}Xe in comparison with the experimental spectrum. Ref.(21).

low lying $5/2^+$ level at 350 KeV. The data shown in Fig. (1) indicate that no $5/2^+$ level has been observed in the experimental spectra. The first group of excited states in ^{127}Xe are observed at 321, 411 and 586 KeV. The 321 KeV level is tentatively assigned a $3/2^+$ spin ⁽²¹⁾ while the states at 411 and 586 KeV have a probable spin assignment of $1/2^+$ and $3/2^+$ respectively. However the order may be reversed. The model predicts a group of four excited states at 511, 600, 626 and 676 KeV with spin assignments $3/2^+$, $5/2^+$, $1/2^+$ and $3/2^+$ respectively. If the predicted 511 KeV $3/2^+$ state is assumed to correspond to the experimentally observed level at 321 KeV $3/2^+$, then the other two experimental levels are nicely explained by the $1/2^+$ and $3/2^+$ members of the calculated multiplet. Again the absence of a $5/2^+$ state from the experimental spectrum should be noted.

The reason for the higher calculated energy of this multiplet compared to the experimental one, may be found by considering some collective effects not accounted for by the present model. For example, anharmonicities have not been included in the model. Inclusion of anharmonicities may have resulted in a somewhat lower one phonon energy for the ^{127}Xe nucleus, thus improving the agreement with the experimental data.

The next state predicted by the model is a $5/2^+$ state again missing from the experimental spectrum.

The states developed at around 1 MeV in the calculated spectra correspond to the coupling of the neutron with 2 phonons. The experimental

spectra indicate two levels at 929 and 1195 KeV with probable $(1/2,3/2)^+$ spin assignments. Both these levels may be well accounted for by the members of the 2 phonons states of the calculated spectrum at about 1 MeV.

A state observed at 1305 KeV has a probable $(1/2,3/2)^+$ or $(5/2)^-$ spin assignment. In the calculated spectra no state is developed in this energy and probably this indicates that this state may be a $5/2^-$ state. If this state has a positive parity assignment then it must belong to one of the members of the two phonons states, and it may correspond to the $1/2^+$ state which is calculated to lie at about 1220 KeV.

Finally for the four states which are observed at 1534, 1582, 1775 and 1975 KeV no definite spin assignment is indicated from the experimental data. This fact indicates that a choice must be made between a $(1/2,3/2)^+$ and $5/2^-$ assignment for the spin of all these levels. As can be seen in the calculated spectra shown in Fig. (1), four excited states are developed at 1550, 1620, 1770 and 1925 KeV which compare favourably with these observed levels. If this good agreement of the calculated levels with the experimental is not accidental, then the model suggests the spin sequence $3/2^+$, $1/2^+$, $3/2^+$, $3/2^+$ for the four observed levels respectively.

The state vectors of some important levels in ^{127}Xe , as calculated from the best fit to the experimental data, are given in Table 3. With these wavefunctions several electromagnetic properties of

Table 3

Calculated state vectors in ^{127}Xe

$ E; I^\pi\rangle$	$ 0; 1/2^+\rangle$	$ 411; 1/2^+\rangle$	$ 929; 1/2^+\rangle$	$ 125; 3/2^+\rangle$	$ 321; 3/2^+\rangle$	$ 586; 3/2^+\rangle$
$ j; NR\rangle$						
$ 1/2; 00\rangle$	0.877	0.392	0.164			
$ 1/2; 12\rangle$				0.537	0.587	-0.312
$ 1/2; 20\rangle$	0.118	-0.616	0.627			
$ 1/2; 22\rangle$				-0.129	0.450	0.460
$ 1/2; 24\rangle$						
$ 1/2; 30\rangle$	-0.022	0.124	0.322			
$ 1/2; 32\rangle$				0.053	0.058	-0.191
$ 3/2; 00\rangle$				0.723	-0.174	0.593
$ 3/2; 12\rangle$	-0.447	0.479	0.356	-0.341	0.532	0.262
$ 3/2; 20\rangle$				0.149	0.011	-0.351
$ 3/2; 22\rangle$	0.117	0.358	-0.530	0.157	0.310	-0.230
$ 3/2; 24\rangle$						
$ 3/2; 30\rangle$				-0.036	0.023	0.136
$ 3/2; 32\rangle$	-0.041	0.304	-0.257	-0.042	0.059	0.180
$ 3/2; 33\rangle$				-0.004	-0.182	-0.064

the ^{127}Xe states are computed as described in section 3.3. These results are listed in Table 4.

Unfortunately, not many experimental data concerning the moments and the electromagnetic transitions in ^{127}Xe are available today. The only available data concern the branching ratios of some gamma transitions deexciting some levels in ^{127}Xe (see Table 4 (c)). The calculated data agree rather well with the experimental data. For instance, the level at 321 KeV with a $3/2^+$ spin assignment is deexciting through the 321 and the 196 KeV transitions with corresponding branching ratios of 0.70 and 0.30. These values may be compared with the calculated values of 0.52 and 0.48 respectively. The agreement for the branching ratios of the transitions deexciting the 411 KeV $1/2^+$ level is even better. The model predicts ratios of 0.975 and 0.025 respectively, which are in good agreement with the respective ratio values of 0.943 and 0.057 suggested by the experimental data. The calculated ratios for the 586 KeV level are not in very good agreement with the experimental data but the agreement may be considered satisfactory.

Finally the model predicts a quadrupole moment value of -0.11 barns for the 125 KeV $3/2^+$ state. However it is important to emphasize the significance of the right choice of the nuclear potential parameter $\langle K \rangle$. The value of -0.11 barns for the quadrupole moment was derived under the assumption that $\langle K \rangle \cong 40$ MeV. But if the value of the stiffness parameter C for ^{127}Xe is close to the value of 20 MeV suggested by the data on the ^{126}Xe nucleus (see Table 2) then the use of equation (3.5) gives a value

Table 4

Calculated properties of some ^{127}Xe nuclear states

a) Moments

State	I^π	μ calc in (nm)	μ exp in (nm)	q calc in barns	q exp in barns
ground	$1/2^+$	-0.89	---	---	---
125	$3/2^+$	+0.81	---	-0.11	---

b) Electromagnetic transitions

Initial state	Final state	E	T(M1)calc	T(M1)exp	T(E2)calc	T(E2)exp	δ^2 calc
E in KeV I^π	E in KeV I^π	in KeV	in tr/sec	in tr/sec	in tr/sec	in tr/sec	(a)
125 $3/2^+$	ground $1/2^+$	125	2×10^7		5×10^6		0.250
321 $3/2^+$	ground $1/2^+$	321	1.55×10^9		1.7×10^8		0.250
321 $3/2^+$	125 $3/2^+$	196	1.57×10^9		3.2×10^7		0.020
411 $1/2^+$	ground $1/2^+$	411	1.26×10^{11}				0.000
411 $1/2^+$	125 $3/2^+$	286	5.17×10^8		1.72×10^8		0.332
586 $3/2^+$	ground $1/2^+$	586	2.88×10^9		8.6×10^9		2.98
586 $3/2^+$	125 $1/2^+$	461	6.29×10^9		6.2×10^8		0.10
929 $1/2^+$	ground $1/2^+$	929	9.0×10^{11}				0.00

(a) The mixing ratio is defined as $\delta^2 = \frac{T(E2)}{T(M1)}$. $\delta^2 = 0$ indicates pure M1, while $\delta^2 = \infty$ indicates pure E2 radiation.

Table 4 (continued)

c) Branching ratios

Initial state		Final state		Transition in KeV	Branching calculated	Branching (a) experimental
E in KeV	I^π	E in KeV	I^π			
321	$3/2^+$	ground	$1/2^+$	321	0.520	0.70
		125	$3/2^+$	196	0.480	0.30
411	$1/2^+$	ground	$1/2^+$	411	0.975	0.943
		125	$3/2^+$	286	0.025	0.057
586	$3/2^+$	ground	$1/2^+$	586	0.618	0.463
		125	$1/2^+$	461	0.382	0.537

d) Total half lives of some excited states

Level in KeV	I^π	Calculated $T_{1/2}$ in sec	Experimental $T_{1/2}$ in sec
125	$3/2^+$	2.2×10^{-8}	---
321	$3/2^+$	2.1×10^{-10}	---
411	$1/2^+$	5.5×10^{-12}	---
586	$3/2^+$	1×10^{-10}	---
929	$1/2^+$	8×10^{-13}	---

(a) from ref. (21)

of $\langle K \rangle$ around 10 MeV. This value for the parameter $\langle K \rangle$ results in a quadrupole moment value of -0.44 barns. Thus the experimental determination of the quadrupole moment of the 125 KeV state in ^{127}Xe is of particular interest.

3.5. Level structure of ^{129}Xe

The calculated energy spectrum of ^{129}Xe containing states with spin up to $5/2^+$ is shown in Fig. (2) and is compared with the experimentally (18,22) observed spectrum. The values of the adjustable constants obtained from the best fit are $\epsilon_{3/2} - \epsilon_{1/2} = 82$ KeV, $\hbar\omega = 420$ KeV and $\xi \approx 3.00$. For almost all the calculated levels there is an experimental counterpart as shown in Fig. (2). The level calculated at 340 KeV with a $5/2^+$ spin may correspond to the observed 322 KeV $5/2^+$ level. A low lying $(1/2$ or $3/2)^+$ state at 318 KeV is not reproduced by the model. It is possible that this level corresponds to one of the higher calculated $1/2^+$, $3/2^+$ states which is lowered because of some additional interactions which have not been included in the Hamiltonian of the present model. But it is also very probable that this state may be due to an entirely different configuration, bearing very little collective character. Some indications about the nature of this level could have been drawn from a knowledge of the half life of this state, which unfortunately has not been measured as yet.

The experimental level at 411 KeV with a $1/2^+$, $3/2^+$ spin assignment may correspond to the calculated $3/2^+$ state at 481 KeV. The possibility

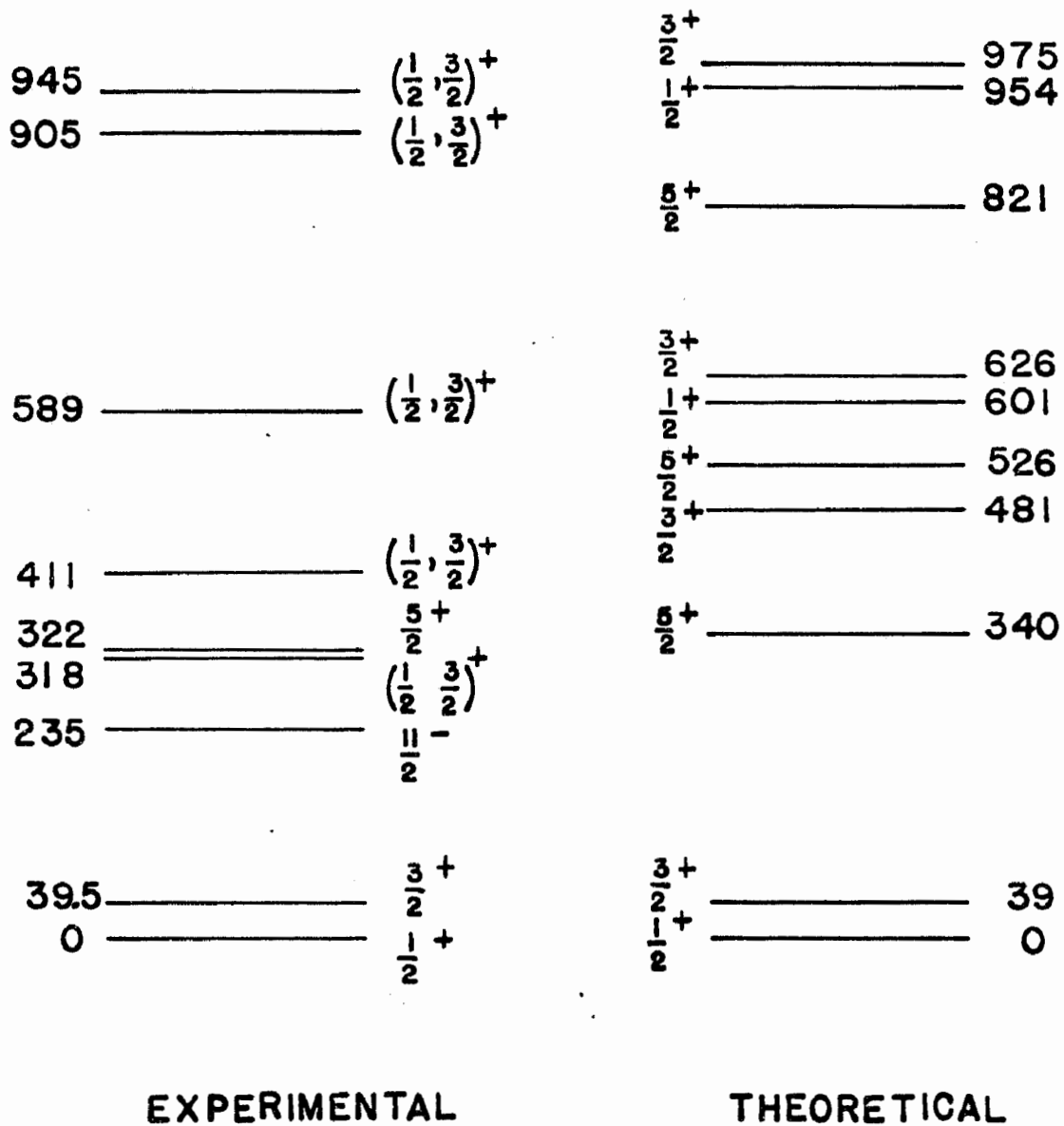


Fig. 2. The calculated spectrum of ^{129}Xe in comparison with the experimental spectrum as obtained from Refs (18,22).

that this level may correspond to the higher lying $1/2^+$ state at 601 KeV is not excluded. It is shown later that on the grounds of the observed branching ratios of the transitions deexciting the 411 KeV levels the $3/2^+$ assignment for this level is more likely. The experimental state at 589 KeV may correspond to one of the two predicted by the model states at 601 and 626 KeV with spins $1/2^+$ and $3/2^+$ respectively. A calculated $5/2^+$ state at 821 KeV has no experimental counterpart. Finally the two states observed at 905 and 945 KeV with uncertain spin assignments $(1/2, 3/2)^+$ may correspond to the calculated levels at 954 and 975 KeV with spins $1/2^+$ and $3/2^+$ respectively, suggesting the spin sequence $1/2^+$, $3/2^+$ respectively for the two experimental levels at 905 and 945 KeV.

The state vectors of some of the observed levels in ^{129}Xe as obtained from the best fit are given in Table 5. The calculated nuclear properties of the levels in ^{129}Xe are given in Table 6.

The magnetic moments of the ground and 39 KeV states in ^{129}Xe have been measured experimentally and the calculated values are in excellent agreement with the data.

The measured quadrupole moment value of $q = -0.40$ barns for the first excited state in ^{129}Xe is in serious disagreement with the calculated value of -0.14 barns based on a $\langle K \rangle$ value of 40 MeV. This again indicates that a lower $\langle K \rangle$ value might be more appropriate. Table 2 shows that the experimental value of the stiffness parameter C is not available from the neighbouring to ^{129}Xe even-even Xe nuclei.

Table 5

Calculated state vectors of some ^{129}Xe excited states

$ E; I^\pi\rangle$	$ 0; 1/2^+\rangle$	$ 601; 1/2^+\rangle$	$ 954; 1/2^+\rangle$	$ 39; 3/2^+\rangle$	$ 481; 3/2^+\rangle$	$ 626; 3/2^+\rangle$	$ 975; 3/2^+\rangle$	$ 340; 5/2^+\rangle$
$ j; NR\rangle$								
$ 1/2; 00\rangle$	0.807	0.501	0.151					
$ 1/2; 12\rangle$				0.447	0.567	0.289	-0.263	0.766
$ 1/2; 20\rangle$	0.149	-0.518	0.658					
$ 1/2; 22\rangle$				-0.138	0.422	-0.356	0.444	-0.071
$ 1/2; 24\rangle$								
$ 1/2; 30\rangle$	-0.034	0.140	0.289					
$ 1/2; 32\rangle$				0.052	0.067	0.222	0.333	
$ 1/2; 33\rangle$								0.118
$ 1/2; 34\rangle$								0.094
$ 1/2; 36\rangle$								
$ 3/2; 00\rangle$				0.757	-0.051	-0.563	0.128	
$ 3/2; 12\rangle$	-0.540	0.429	0.265	-0.392	0.542	-0.276	0.025	0.236
$ 3/2; 20\rangle$				0.158	0.007	0.441	0.660	
$ 3/2; 22\rangle$	0.168	-0.417	-0.524	0.144	0.379	0.288	-0.223	-0.157
$ 3/2; 24\rangle$								-0.538
$ 3/2; 30\rangle$				-0.039	0.008	-0.143	0.223	
$ 3/2; 32\rangle$	-0.062	0.318	-0.337	-0.049	0.064	-0.215	-0.225	0.043
$ 3/2; 33\rangle$				-0.001	-0.220	0.021	-0.109	0.074
$ 3/2; 34\rangle$								0.081

However, if an average value for C of about 60 MeV is used, a value obtained from the available data on ^{126}Xe and ^{132}Xe , the corresponding value of the parameter $\langle K \rangle$ becomes $\langle K \rangle \sim 16$ MeV. With this value for the parameter $\langle K \rangle$ the calculated quadrupole moment turns out to be $q = -0.35$ barns, in good agreement with the experimental value.

The calculated transition probability for the predominant M1 39 KeV transition is 50 times lower than the experimental value. M1 transition probabilities are very sensitive to the choice of the g_s parameter. The observed discrepancy may be due to the inadequate choice of the g_s parameter for this particular transition. Since the g_s parameter in general is dependent on the particular states involved in a transition, the substitution of an average g_s value may be a source of error in the estimation of some M1 transition probabilities especially if $3/2^+ \rightarrow 1/2^+$ transitions are involved. It may also be noted that the effect of the exact choice of the g_s parameter is more critical in transitions involving neutrons than in transitions involving protons since the presence of the $g_p = 1$ factor for the protons will reduce the importance of the g_s factor.

In Table 6 (c) the branching ratios of transitions deexciting some ^{129}Xe states are calculated and compared with the experimental data. The 411 KeV state has been assumed to have a spin $3/2^+$ or $1/2^+$. The corresponding wavefunctions of the calculated states at 481 KeV ($3/2^+$) and 601 KeV ($1/2^+$) have been obtained from Table 5 (columns 5 and 2 respectively). The results indicate that the $3/2^+$ spin assignment for

Table 6

Calculated properties of some ^{129}Xe nuclear states

a) Moments

State E in KeV	I^π	μ calc in (nm)	μ exp in (nm) (a)	q calc in barns	q exp in barns
ground	$1/2^+$	-0.76	-0.77		
39	$3/2^+$	+0.77	+0.68 \pm 0.30 (b)	-0.14(-0.35) (d)	-0.40 \pm 0.07 (c)

(a) = from ref. (15)

(b) = from ref. (23)

(c) = from ref. (24)

(d) = calculated with $\langle K \rangle = 16$ MeV

b) Electromagnetic transitions

Initial state E in KeV	I^π	Final state E in KeV	I^π	E in KeV	T(M1)calc in tr/sec	T(M1)exp in tr/sec (e)	T(E2)calc in tr/sec	T(E2)exp in tr/sec (e)	δ^2 calc
39	$3/2^+$	ground	$1/2^+$	39	1.5×10^6	$\sim 5.0 \times 10^7$	1×10^4	2×10^6	0.007
411	$3/2^+$	39	$3/2^+$	372	6.5×10^9		4.1×10^8		0.064
411	$1/2^+$	39	$3/2^+$	372	1.1×10^9		4.8×10^8		0.438
411	$3/2^+$	ground	$1/2^+$	411	7.2×10^8		6.2×10^8		0.865
411	$1/2^+$	ground	$1/2^+$	411	1.15×10^{11}				0.000
589	$3/2^+$	ground	$1/2^+$	589	9.2×10^8		1.38×10^9		1.500
589	$3/2^+$	39	$3/2^+$	550	4.32×10^9		1.43×10^9		0.332

(e) = from ref. (18)

Table 6 (continued)

c) Branching ratios

Initial state		Final state		Transition KeV	Branching calculated	(a) Branching experimental
E in KeV	I^π	E in KeV	I^π			
411	$3/2^+$	ground	$1/2^+$	411	0.165	0.410
		39	$3/2^+$	372	0.835	0.590
411	$1/2^+$	ground	$1/2^+$	411	0.987	0.410
		39	$3/2^+$	372	0.013	0.590
589	$3/2^+$	ground	$1/2^+$	589	0.287	0.145
		39	$3/2^+$	550	0.713	0.855

d) Total half lives of some excited states in ^{129}Xe

Level in KeV	I^π	Calculated $T_{1/2}$ in sec	Experimental $T_{1/2}$ in sec
39	$3/2^+$	3.6×10^{-8}	1.10^{-9} (b)
411	$3/2^+$	8.0×10^{-11}	10^{-9} (b)
411	$1/2^+$	6.0×10^{-12}	10^{-9} (b)
589	$3/2^+$	8.6×10^{-11}	

(a) = from refs. (18, 22)

(b) = from ref. (18)

the 411 KeV level gives a more adequate description of the branching ratios of the transitions deexciting this level. In particular the calculations indicate that the 372 KeV transition is about 5 times more intense than the 411 KeV transition, contrary to the assumption of a $1/2^+$ 411 KeV level which indicates a 411 KeV transition about 100 times more intense than the 372 KeV transition. These results (22) may be compared with the experimental data indicating that the 372 KeV transition is about 1.5 times more intense than the 411 KeV transition.

Finally the calculated branching ratios of the transitions deexciting the 589 KeV level are in good agreement with the experimental data.

3.6. Level structure of ^{131}Xe

The experimental data suggest that in ^{131}Xe the ground state is a $3/2^+$ state with the first excited state lying at 80 KeV with a $1/2^+$ spin assignment. From a pure single particle picture, it must be assumed that for some reason the $2d_{3/2}$ state, in ^{131}Xe and as well in ^{133}Xe and ^{135}Xe , is lowered with respect to the $3s_{1/2}$ state. Thus in the ground state of the Xe isotopes with $A \geq 131$, 3 neutrons occupy the $2d_{3/2}$ state, and the odd neutron has available half the $2d_{3/2}$ states and both the higher lying $3s_{1/2}$ states. In accordance, then, with the arguments presented in section 2.9, a statistical factor is introduced for the odd neutron.

The statistical factor for the $2d_{3/2}$ state is chosen to be $\frac{1}{\sqrt{2}}$

and for the $3s_{1/2}$ state 1. Thus the matrix elements between $j=3/2$ states are multiplied by $1/2$ and the matrix elements between $j=1/2$ and $j=3/2$ states are multiplied by $\frac{1}{\sqrt{2}}$.

The calculated final spectrum is shown in Fig. (3A). The values of the adjustable constants obtained from the best fit to the experimental spectrum are $\epsilon_{3/2}-\epsilon_{1/2} = 185$ KeV, $\hbar\omega = 372$ KeV and $\xi \cong 3.25$.

All the observed experimental levels have a calculated counterpart. The calculated spectrum indicates a $5/2^+$ level at 366 KeV corresponding to the experimental $5/2^+$ level at 365 KeV. The model further predicts a $3/2^+$ level corresponding to the level observed at 405 KeV with $1/2^+$ or $3/2^+$ spin assignment. The model also predicts a $7/2^+$ level and a $5/2^+$ level at 321 and 437 KeV respectively. No experimental counterparts to these levels have been observed as yet. Two levels predicted at 503 and 547 KeV with $3/2^+$ and $1/2^+$ spins respectively have not been observed in the experimental spectrum of ^{131}Xe . Finally the two experimental states at $7/2^+$ and $5/2^+$ at 637 and 723 KeV respectively are explained well by the two levels at 700 and 740 KeV of the calculated spectrum. The state vectors deduced from the best fit are listed for a number of ^{131}Xe states in Table 7.

The calculated electromagnetic properties of several levels in ^{131}Xe are shown in Table 8. The calculated magnetic moment for the ground state of ^{131}Xe is in very good agreement with the experimental value available. The calculated quadrupole moment for the ^{131}Xe ground state is in good agreement with the experimental quadrupole moment of the same state.

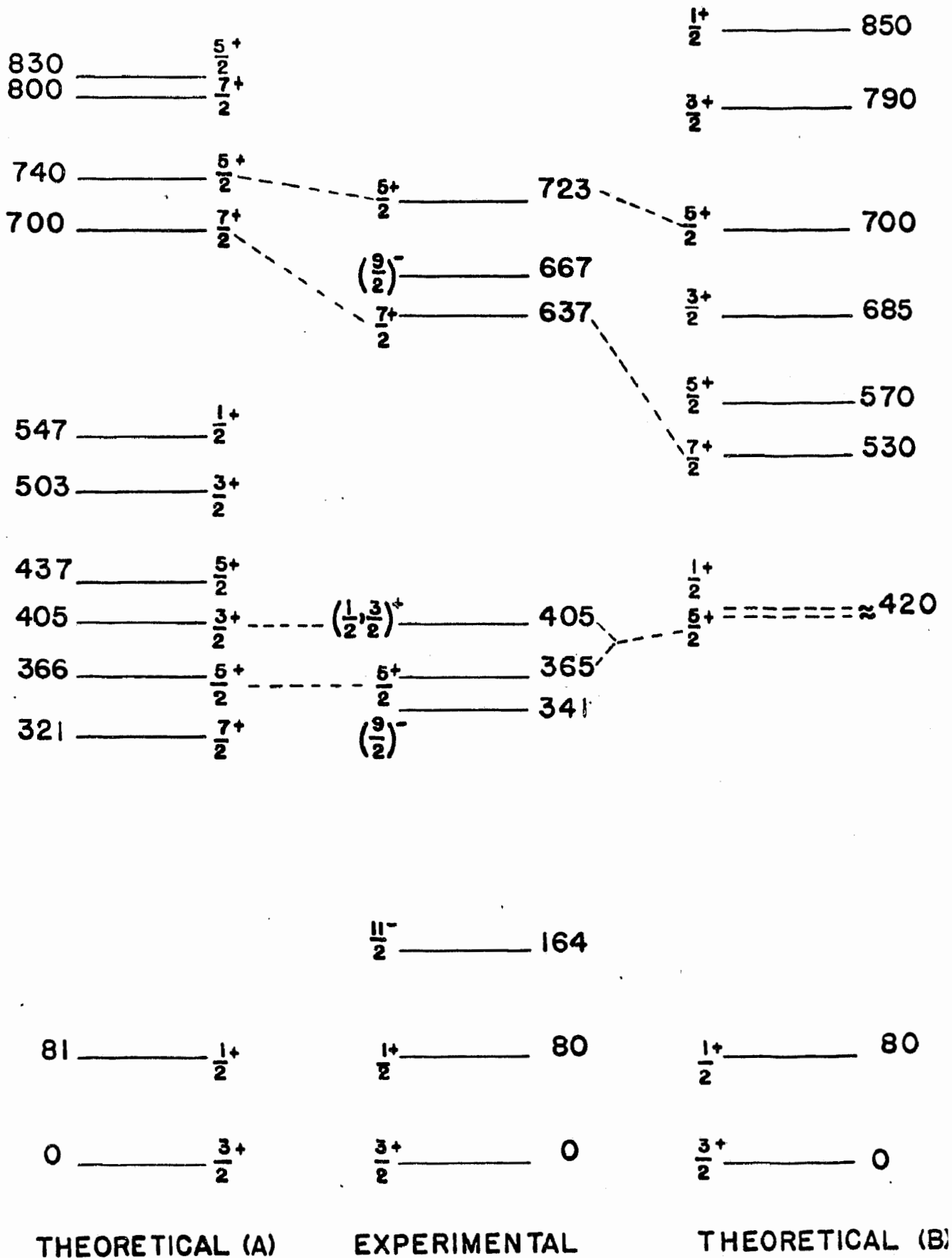


Fig. 3. The calculated spectra of ^{131}Xe . Spectrum A has been calculated with $\hbar\omega = 372$ KeV, while spectrum B with $\hbar\omega = 610$ KeV. The experimental spectrum is obtained from Refs (22,25).

Table 7

Calculated state vectors of some excited states in ^{131}Xe (I)

$ E;I^\pi\rangle$	$ 0;3/2^+\rangle$	$ 405;3/2^+\rangle$	$ 82;1/2^+\rangle$	$ 364;5/2^+\rangle$	$ 364^i;5/2^+\rangle$	$ 775;5/2^+\rangle$	$ 856;5/2^+\rangle$	$ 705;7/2^-\rangle$
$ j;NR\rangle$								
$ 1/2;00\rangle$			0.764					
$ 1/2;12\rangle$	0.301	0.234		0.475		0.006	0.113	
$ 1/2;20\rangle$			0.124					
$ 1/2;22\rangle$	-0.069	+0.366		-0.153		0.643	-0.400	
$ 1/2;24\rangle$								0.064
$ 1/2;30\rangle$			-0.021					
$ 1/2;32\rangle$	0.020	-0.011		0.073			0.021	
$ 1/2;33\rangle$				0.054		0.134	0.192	-0.101
$ 1/2;34\rangle$								0.301
$ 3/2;00\rangle$	0.894	0.229						
$ 3/2;12\rangle$	-0.298	0.835	-0.615	0.696	0.851	-0.006	-0.382	0.130
$ 3/2;20\rangle$	0.081	-0.129						
$ 3/2;22\rangle$	0.084	0.144	0.137	-0.041	0.382	0.502	0.658	
$ 3/2;24\rangle$				-0.498	-0.340	-0.203	-0.194	0.887
$ 3/2;30\rangle$	-0.015	0.048						0.048
$ 3/2;32\rangle$	-0.017	0.079	-0.044	-0.049	0.092	0.001	0.213	
$ 3/2;33\rangle$	0.001	-0.119		0.005	-0.003	0.245	-0.329	-0.032
$ 3/2;34\rangle$				0.064	-0.050	-0.463	0.131	0.203
								-0.210

Table 8

Calculated properties of some ^{131}Xe nuclear states (I)

a) Moments

State	I^π	μ calc in (nm)	μ exp in (nm) (a)	q calc in barns	q exp in barns (a)
ground	$3/2^+$	+0.75	+0.69	-0.10	-0.12
81	$1/2^+$	-0.66	---		

(a) = from ref. (15)

b) Electromagnetic transitions

Initial state E in KeV	I^π	Final state E in KeV	I^π	E in KeV	T(M1)calc	T(M1)exp	T(E2)calc	T(E2)exp	δ^2 calc	δ^2 exp
					in tr/sec	in tr/sec	in tr/sec	in tr/sec		
80	$1/2^+$	ground	$3/2^+$	80	8.1×10^6	$\sim 4.0 \times 10^8$ ^(b)	5×10^5	3.6×10^7 ^(b)	0.06	0.17 ^(d)
364	$5/2^+$	ground	$3/2^+$	364	2.2×10^{10}	2.8×10^8 ^(c)	9.2×10^7	1.36×10^{10} ^(c)	0.004	49 ^(d)
364	$5/2^+$	80	$1/2^+$	284			2.6×10^8	9.8×10^8 ^(c)	∞	∞ ^(d)
(i)364	$5/2^+$	ground	$3/2^+$	364	4.1×10^8	2.8×10^8 ^(c)	4.2×10^9	1.36×10^{10} ^(c)	10	49 ^(d)
(i)364	$5/2^+$	80	$1/2^+$	284			3.6×10^8	9.8×10^8 ^(c)	∞	∞
637	$7/2^+$	ground	$3/2^+$	637			3.8×10^8	2.3×10^{12} ^(b)	∞	∞
637	$7/2^+$	364	$5/2$	272	7.2×10^7		3.9×10^7		0.54	--

(b) = from ref. (15)

(c) = from ref. (26)

(d) = from ref. (22)

Table 8 (continued)

c) Branching ratios

Initial state E in KeV I ^π	Final state E in KeV I ^π	Transition in KeV	Branching calculated	Branching (a) experimental
364 5/2 ⁺	ground 3/2 ⁺	364	0.988	0.935
	80 1/2 ⁺	284	0.012	0.065
364(i) 5/2 ⁺	ground 3/2 ⁺	364	0.939	0.935
	80 1/2 ⁺	284	0.061	0.065
637 7/2 ⁺	ground 3/2 ⁺	637	0.775	0.99
	364 5/2 ⁺	272	0.225	0.01

(a) = from refs (22,25)

d) Total half lives of some excited states in ¹³¹Xe

Level in KeV	I ^π	Calculated T _{1/2} in sec	Experimental T _{1/2} in sec
80	1/2 ⁺	3x10 ⁻⁸	6x10 ⁻¹⁰ (b)
364	5/2 ⁺	3.0x10 ⁻¹¹	5.0x10 ⁻¹¹ (c)
364(i)	5/2 ⁺	1.4x10 ⁻¹⁰	5.0x10 ⁻¹¹ (c)
637	7/2 ⁺	1.5x10 ⁻⁹	3x10 ⁻¹³ (b)

(b) = from ref. (15)

(c) = from ref. (26)

The transition probability predicted by the model for the M1 80 KeV transition deexciting the first excited state of ^{131}Xe is again lower than the experimental value probably for the same reasons as in the case of ^{129}Xe .

The transition probabilities of the transitions deexciting the 364 KeV level in ^{131}Xe lead to the correct half life for this level (see Table 8 (d)) but fail to determine the correct multipolarity of the 364 KeV transition. This transition is an E2 transition with a (22) 2% admixture. Thus it seems that the wavefunctions deduced from the best fit cannot explain the structure of this level. It seems very probable in this case that the contribution of the $3s_{1/2}$ state to the structure of this level is overestimated in the present model. As the state vectors indicate (Table 7, column 4) the 364 KeV level is composed approximately 70% of $2d_{3/2}$ particle states and 20% $3s_{1/2}$ particle states. If the statistical factor used for the $3s_{1/2}$ state is higher than it should be, the contribution of the $3s_{1/2}$ particle state to the structure of the 364 KeV level will be higher. If, for example, it is assumed that the $3s_{1/2}$ state has very little influence on the 364 KeV level, the state vector for the 364 KeV state may be computed with only the $2d_{3/2}$ state contributing. This state vector is shown in Table 7 as $|364^i, 5/2^+\rangle$ (column 5 of Table 7). With this state vector the transition probability for the 364 KeV transition turns out to be in excellent agreement with the experimental data as shown in Table 8.

The branching ratio of transitions deexciting the 364 KeV level are shown in Table 8 (c). The results shown are obtained by using both state vectors (columns 4 and 5 of Table 7). The results obtained using the state vector of the 364 KeV level where the contributions of only the $2d_{3/2}$ state are included are in excellent agreement with the experimental data. Nevertheless the model fails to reproduce the properties of the $7/2^+$ 637 KeV level. This level has been observed experimentally ⁽¹⁵⁾ to have a half life of 3×10^{-13} sec. The present results cannot account for this presumably pure E2 transition. Basically no model can explain such a high transition probability for an E2 transition. It is very probable that either the reported half life of this level is wrong or that the spin of this level is not $7/2^+$ but $5/2^+$. If it is so, then the preceding transition will be M1 in character, and the observed half life of this level may be accounted for.

One point which needs further discussion is the low phonon energy value of 370 KeV derived from the best fit. The neighbouring even-even Xe nuclei (see Table 1) have much higher oscillation energies.

This apparent discrepancy might indicate that in the description of the ^{131}Xe nucleus the last three neutrons participate in the extra core motion. Under such conditions it may be possible that the three neutrons behave like one effective neutron equivalent to the one considered above. Such a hypothesis will require, to a first approximation, that the derived coupling constant is an effective one for the

three particles and that the single particle Hamiltonian should include the contribution resulting from the mutual interaction between the three neutron pairs. The realization of a ^{128}Xe core in the ^{131}Xe nucleus may possibly explain the lower phonon energy derived from the best fit. In order to investigate the effect of a higher phonon energy in the resulting spectrum of ^{131}Xe the calculations were repeated with the following assumptions:

- (1) The 364 KeV level originates from the coupling of a $3/2$ neutron state to the core and
- (2) The oscillation energy is assumed to be $\hbar\omega = 610$ KeV (value obtained from the neighbouring even-even isotopes).

The calculated spectrum under the above assumptions is shown in Fig. (3B). The constants obtained from the best fit are $\epsilon_{3/2}-\epsilon_{1/2} = 198$ KeV and $\xi = 3.25$.

In this description the 364 KeV level originates from the coupling of the $2d_{3/2}$ state to the core and the 405 KeV level can be explained with a similar structure. Indeed, coupling a $2d_{3/2}$ neutron to the core will result in the creation of three closely spaced levels at around 400 KeV with corresponding spin and parity $7/2^+$, $5/2^+$ and $1/2^+$, in order of increasing energy. A residual interaction could split the $5/2^+$ and $1/2^+$ levels by an amount equal to the experimental separation of 40 KeV.

In this second description, the model predicts fewer low lying levels than in the first case, where many levels are calculated without an experimental counterpart. The state vectors deduced from the best fit are

Table 9

Calculated state vectors of some excited states in ^{131}Xe (II)

$ E; I^\pi\rangle$	$ 0; 3/2^+\rangle$	$ 80; 1/2^+\rangle$	$ 364; 5/2^+\rangle$	$ 570; 5/2^+\rangle$	$ 700; 5/2^+\rangle$	$ 530; 7/2^+\rangle$
$ j; NR\rangle$						
$ 1/2; 00\rangle$		0.801				
$ 1/2; 12\rangle$	0.330			0.644	-0.472	
$ 1/2; 20\rangle$		0.118				
$ 1/2; 22\rangle$	-0.073			-0.121	-0.214	
$ 1/2; 24\rangle$						0.381
$ 1/2; 30\rangle$		-0.019				
$ 1/2; 32\rangle$	0.022			0.089	-0.051	
$ 1/2; 33\rangle$				0.048	0.033	-0.023
$ 1/2; 34\rangle$						-0.070
$ 3/2; 00\rangle$	0.884					
$ 3/2; 12\rangle$	-0.293	-0.572	0.851	0.508	0.749	0.861
$ 3/2; 20\rangle$	0.084					
$ 3/2; 22\rangle$	0.092	0.121	0.382	-0.050	0.360	-0.108
$ 3/2; 24\rangle$			-0.340	0.539	0.151	-0.282
$ 3/2; 30\rangle$	-0.016					
$ 3/2; 32\rangle$	-0.018	-0.040	0.092	0.042	0.032	0.085
$ 3/2; 33\rangle$	0.001		-0.003	0.025	-0.105	0.053
$ 3/2; 34\rangle$			-0.050	0.065	0.018	0.074

Table 10

Calculated properties of some ^{131}Xe nuclear states (II)

a) Moments

State	I^π	μ calc in (nm)	μ exp in (nm)	q calc in barns	q exp in barns
ground	$1/2^+$	+0.76	+0.69 ^(a)	-0.16	-0.12 ^(a)
125	$3/2^+$	-0.72			

(a) = from ref. (15)

b) Transition probabilities

Initial state E in KeV	I^π	Final state E in KeV	I^π	E in KeV	T(M1)calc in tr/sec	T(M1)exp in tr/sec	T(E2)calc in tr/sec	T(E2)exp in tr/sec	δ^2 calc	δ^2 exp
80	$1/2^+$	ground	$3/2^+$	80	8.5×10^6	4.0×10^7	1.3×10^6	3.6×10^7 ^(b)	0.15	0.17 ^(d)
364	$5/2^+$	ground	$3/2^+$	364	4.15×10^8	2.8×10^8	4.2×10^9	1.36×10^{10} ^(c)	10	49 ^(d)
364	$5/2^+$	80	$1/2^+$	284			2.9×10^8	9.8×10^8 ^(c)	∞	∞
637	$7/2^+$	ground	$3/2^+$	637			5.7×10^{10}	2.3×10^{12} ^(b)	∞	∞
637	$7/2^+$	364	$5/2^+$	272	3.4×10^9		1×10^7		0.030	--

(b) = from ref. (15)

(c) = from ref. (26)

(d) = from ref. (22)

Table 10 (continued)

c) Branching ratios

Initial state E in KeV	I^π	Final state E in KeV	I^π	Transition in KeV	Branching calculated	Branching (a) Experimental
364	$5/2^+$	ground	$3/2^+$	364	0.939	0.935
		80	$1/2^+$	284	0.061	0.065
637	$7/2^+$	ground	$3/2^+$	637	0.95	0.99
		364	$5/2^+$	272	0.05	0.01

(a) = from refs. (22,25)

d) Total half lives of some excited states in ^{131}Xe

Level in KeV	I^π	Calculated $T_{1/2}$ in sec	Experimental $T_{1/2}$ in sec
80	$1/2^+$	2.8×10^{-8}	6×10^{-10} (b)
364	$5/2^+$	1.4×10^{-10}	5.0×10^{-11} (c)
637	$7/2^+$	1.1×10^{-11}	3×10^{-13} (b)

(b) = from ref. (15)

(c) = from ref. (26)

listed in Table 9 and the calculated electromagnetic properties are listed in Table 10. As shown in Table 10, no significant improvement has been made in the calculated nuclear properties except for the predicted half life of the 637 KeV level, which is closer to the experimental value than in the previous case but still lower by a factor of 10^2 than the experimental value.

From the above discussion it is clear that the first treatment of the ^{131}Xe nucleus is more natural and involves less arbitrary assumptions than in the latter case. Thus the calculated spectrum shown in Fig.(3A) may be considered as the representative calculated spectrum for ^{131}Xe . The same spectrum indicates further the existence of some levels which have not been observed experimentally as yet.

3.7. Level structure of ^{133}Xe

The $3s_{1/2}$ and $2d_{3/2}$ states are again considered to be available for the last odd neutron in ^{133}Xe and the same statistical factor as in the case of ^{131}Xe was used. The experimental separation energy between the $1/2^+$ and $3/2^+$ states in ^{133}Xe was unknown at the time this work was completed. For this reason, the matrices have been diagonalized for several values of the $\epsilon_{3/2}-\epsilon_{1/2}$ separation energy. The best fit was then made using the experimentally observed levels ⁽²⁷⁾ at 529 KeV $(5/2, 7/2)^+$ and 679 KeV $(5/2, 7/2)^+$ and assuming that the 529 KeV is a $7/2^+$ state, that is, it has the same spin as the lowest developed level in the calculated spectra. If this level is not a $7/2^+$ but a $5/2^+$, then some of the levels

of the final spectrum will appear at somewhat lower energies. The final spectrum obtained is shown in Fig. (4). The constants obtained from the best fit are $\epsilon_{3/2} - \epsilon_{1/2} = 545$ KeV, $\hbar\omega = 680$ KeV and $\xi \approx 3.5$. The spectrum derived indicates a $1/2^+$ level at 222KeV. Only very recently ⁽¹⁶⁾ has this level been observed at 264 KeV and it is not shown in the experimental spectrum of ^{133}Xe in Fig. (4). Many other levels are predicted by the model and most of these levels have an experimental counterpart. Although no definite spin assignments have been made for the ^{133}Xe levels, the comparison of the existing data with the predicted levels in Fig. (4) leads to some immediate conclusions. The two low lying levels at 529 and 679 KeV compare favourably with the $7/2^+$ and $5/2^+$ levels at 585 and 680 KeV of the calculated spectrum. Many of the other $3/2^+$, $5/2^+$, $7/2^+$ observed levels may be reproduced by the model. In addition, the model predicts the existence of at least a level with a $9/2^+$ spin at around 1400 KeV. Actually a level at 1385 KeV in ^{133}Xe is observed and the experimental data suggest a $9/2^+$ spin assignment for this level. A level observed at 1592.0 KeV with a probable $9/2^+$ assignment may correspond to a calculated $9/2^+$ level at 1500 KeV or with a calculated $5/2^+$ level at 1630 KeV.

Thus the overall agreement of the level sequences in ^{133}Xe indicates that the present model works particularly well in this nucleus.

The calculated state vectors of some excited states in ^{133}Xe are listed in Table 11. Electromagnetic properties of some excited states in ^{133}Xe have also been computed and listed in Table 12, but no

1592 _____ $(\frac{9^+}{2})$
 1385 _____ $(\frac{9^+}{2})$
 1350 _____ $(\frac{5}{2}, \frac{7}{2})$
 1297 _____ $(\frac{5}{2}, \frac{7^+}{2})$
 1235 _____ $(\frac{5}{2}, \frac{7^+}{2})$

1052 _____ $(\frac{3}{2}, \frac{5}{2})$

875 _____ $(\frac{5}{2}, \frac{7^+}{2})$

679 _____ $(\frac{5}{2}, \frac{7}{2})$

529 _____ $(\frac{5}{2}, \frac{7}{2})^+$

233 _____ $\frac{11^-}{2}$

0 _____ $\frac{3^+}{2}$

EXPERIMENTAL

$\frac{7^+}{2}$ _____ 1800
 $\frac{3^+}{2}$ _____ 1750

$\frac{5^+}{2}$ _____ 1630
 $\frac{1^+}{2}$ _____ 1595

$\frac{7^+}{2}$ _____ 1500
 $\frac{9^+}{2}$ _____ 1475
 $\frac{5^+}{2}$ _____ 1450
 $\frac{9^+}{2}$ _____ 1400

$\frac{7^+}{2}$ _____ 1310

$\frac{1^+}{2}$ _____ 1120

$\frac{3^+}{2}$ _____ 1000

$\frac{5^+}{2}$ _____ 858

$\frac{3^+}{2}$ _____ 767

$\frac{5^+}{2}$ _____ 680

$\frac{7^+}{2}$ _____ 585

$\frac{1^+}{2}$ _____ 222

$\frac{3^+}{2}$ _____ 0

THEORETICAL

Fig. 4. The calculated spectrum of ^{133}Xe in comparison with the experimental spectrum. Ref (27).

Table 11

Calculated state vectors of some ^{133}Xe nuclear states

$ E; I^\pi\rangle$	$ 0; 3/2^+\rangle$	$ 680; 5/2^+\rangle$	$ 853; 5/2^+\rangle$	$ 585; 7/2^+\rangle$
$ j; NR\rangle$				
$ 1/2; 00\rangle$				
$ 1/2; 12\rangle$	0.279	0.309	0.633	
$ 1/2; 20\rangle$				
$ 1/2; 22\rangle$	-0.071	-0.164	0.106	
$ 1/2; 24\rangle$				0.325
$ 1/2; 30\rangle$				
$ 1/2; 32\rangle$	0.020	0.059	0.101	
$ 1/2; 33\rangle$		0.058	-0.005	-0.024
$ 1/2; 34\rangle$				-0.071
$ 3/2; 00\rangle$	0.894			
$ 3/2; 12\rangle$	-0.317	0.804	-0.424	0.872
$ 3/2; 20\rangle$	0.085			
$ 3/2; 22\rangle$	0.084	0.124	-0.404	-0.118
$ 3/2; 24\rangle$		-0.447	-0.463	-0.313
$ 3/2; 30\rangle$	-0.016			
$ 3/2; 32\rangle$	-0.090	0.057	-0.004	0.085
$ 3/2; 33\rangle$	0.002	-0.010	0.129	0.048
$ 3/2; 34\rangle$		0.060	0.041	0.069

Table 12

Calculated properties of some ^{133}Xe excited states

a) Moments

State E in KeV	I^π	μ calc in (nm)	μ exp in (nm)	q calc in barns	q exp in barns
ground	$3/2^+$	+0.73		-0.208	

b) Electromagnetic transitions

Initial state E in KeV	I^π	Final state E in KeV	I^π	E in KeV	T(M1)calc in tr/sec	T(M1)exp in tr/sec	T(E2)calc in tr/sec	T(E2)exp in tr/sec	δ^2 calc
530	$7/2^+$	ground	$3/2^+$	530			2.3×10^{10}		∞
680	$5/2^+$	ground	$3/2^+$	680	4.8×10^{10}		7.3×10^{10}		1.52
875	$1/2^+$	ground	$3/2^+$	875	1.95×10^{11}		4.0×10^9		0.02

c) Total half lives of some excited states

Level in KeV	I^π	Calculated $T_{1/2}$ in sec	Experimental $T_{1/2}$ in sec
530	$7/2^+$	3×10^{-11}	
680	$5/2^+$	5.7×10^{-12}	
875	$5/2^+$	3.5×10^{-12}	

experimental data exist at the present time to allow any meaningful comparison.

3.8. General remarks

The application of the model to the odd Xe isotopes discussed in the previous chapter illustrates the usefulness of the intermediate coupling model in understanding, at least phenomenologically, the nuclear structure of the low lying levels of some spheroidal nuclei. Four Xe isotopes were examined in this work and it was found that the nuclear structure of these isotopes may be adequately explained by the model employed. In some cases the model offered some good guesses about several electromagnetic properties of these nuclei. In Fig. (5) the single particle spacing $\epsilon_{3/2} - \epsilon_{1/2}$ obtained from the best fit is shown as a function of the mass number. The $2d_{3/2}$ state is shown to move from 250 KeV above the $3s_{1/2}$ state in $A=127$ to become the ground state in $A=131$, while the $3s_{1/2}$ state rises from the ground state in $A=129$ to about 600 KeV in $A=133$ above the $2d_{3/2}$ state. According to the discussion in section 2.9, the separation energy between the $3s_{1/2}$ and $2d_{3/2}$ states is determined by the pairing force between the neutrons and the number of neutrons in a given shell. Thus the behavior of the $2d_{3/2}$ and $3s_{1/2}$ states in Xe isotopes predicted by the model employed must be in agreement with the predictions of the pairing theory.

In order to solve the MCS equations for the Xe isotopes, a set of
(10)
single particle energies have been obtained from the Nilson model

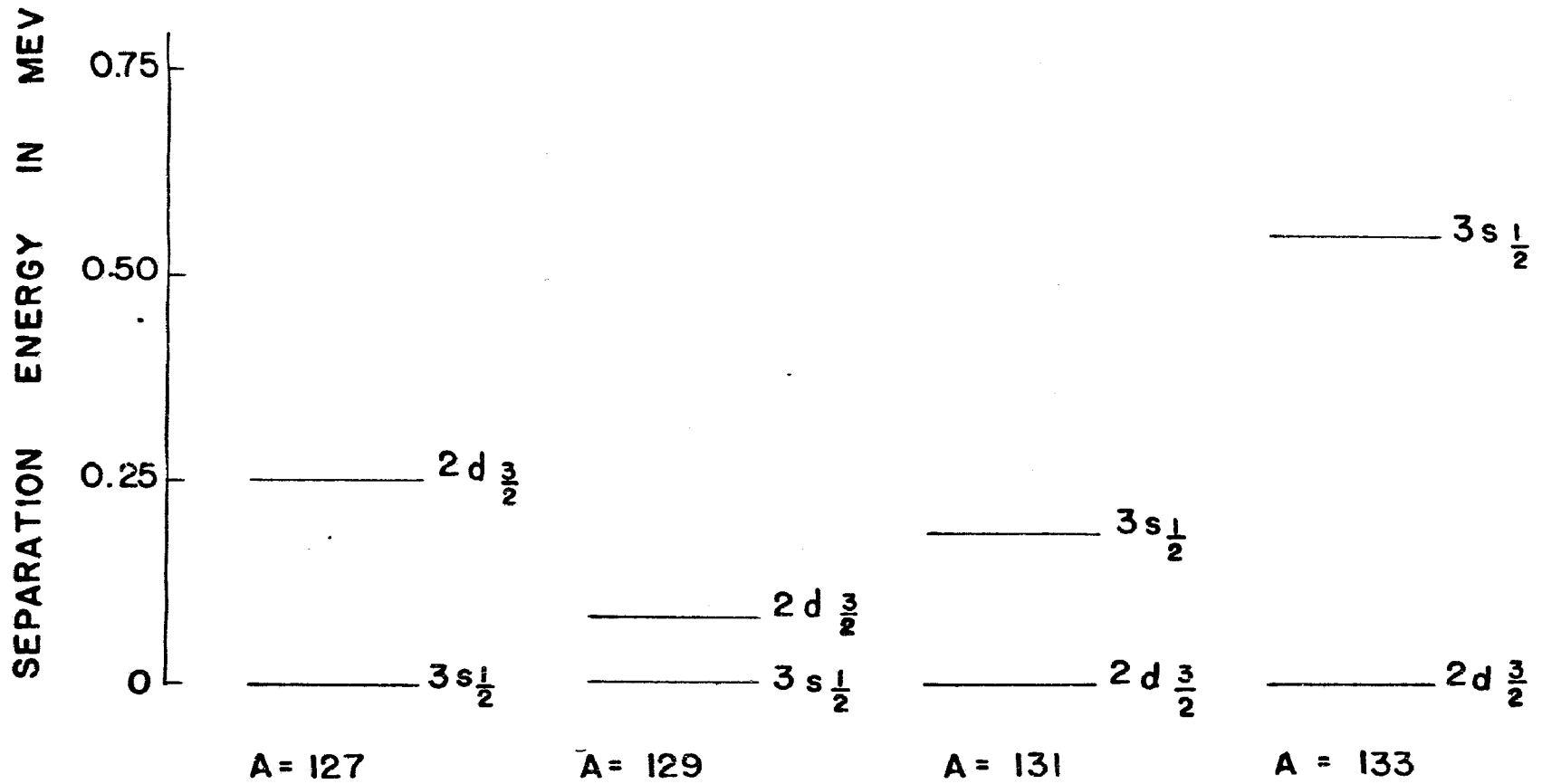


Fig. 5. Calculated single particle spacing in odd Xe isotopes as a function of the mass number.

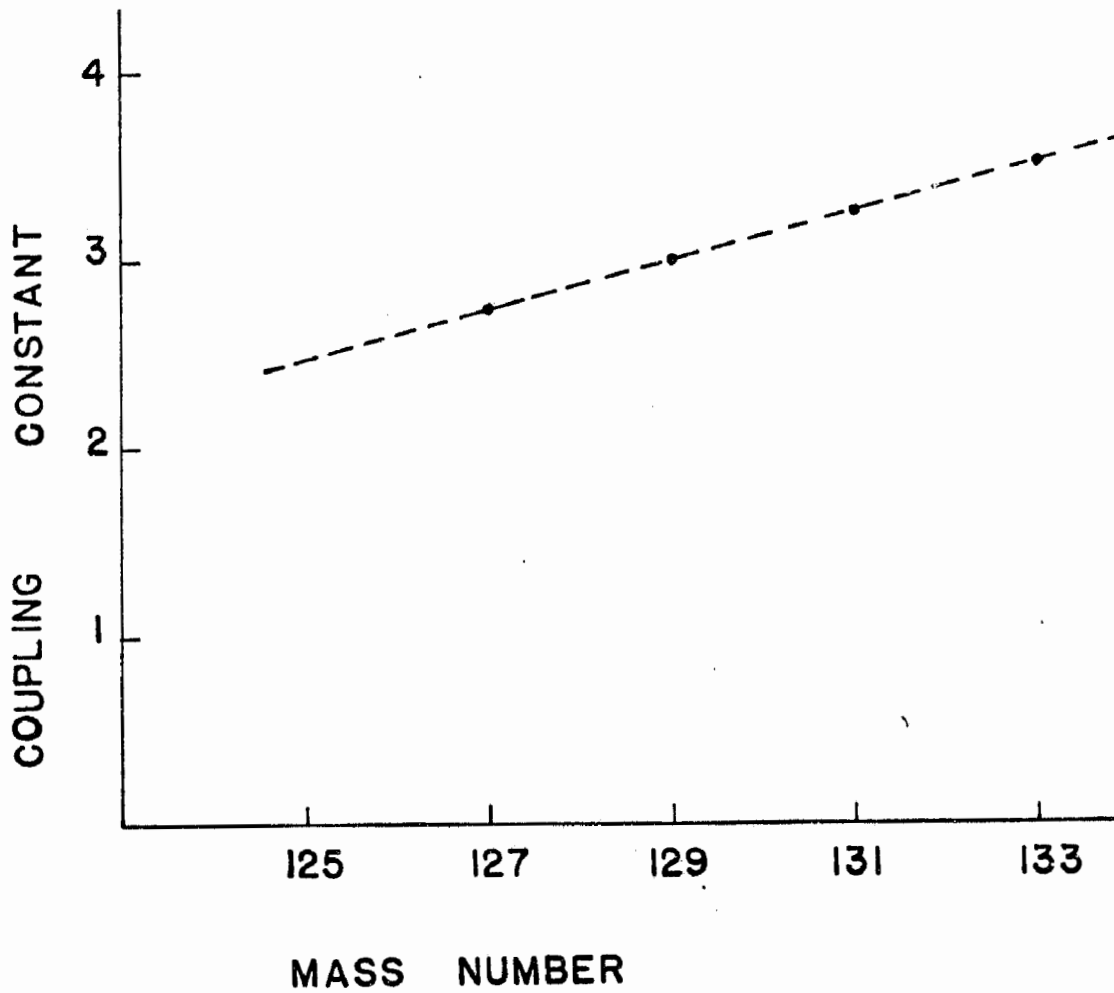


Fig. 6. The calculated coupling constant of odd Xe isotopes as a function of the mass number.

Table 13

a) Single particle energies and G values for some Xe isotopes

Nuclei	G in MeV	2d5/2 in MeV	1g7/2 in MeV	3s1/2 in MeV	2d3/2 in MeV	1h11/2 in MeV
^{127}Xe	0.180	0.0	0.342	2.300	2.942	1.800
^{129}Xe	0.178	0.0	0.340	2.290	2.935	1.850
^{131}Xe	0.176	0.0	0.339	2.280	2.925	1.900
^{133}Xe	0.173	0.0	0.338	2.270	2.920	1.960

b) Energy difference of the 2d3/2 and 3s1/2 states in Xe isotopes

Nucleus	$(\epsilon_{3/2} - \epsilon_{1/2})$ from BCS in KeV	$(\epsilon_{3/2} - \epsilon_{1/2})$ from best fit in KeV
127	-242	-250
129	- 98	- 82
131	+ 97	185
133	+339	+545

for $\delta = 0$ and $K = 7.5 \times 10^{-2}$. This set of single particle energies is listed in Table 13. The pairing force used is also shown in Table 13. This set of values has been obtained from ref. (13).

The results obtained from the solutions of the BCS equations are compared in Table 13 with the values obtained from the best fit. The agreement is reasonable and it seems that the pairing theory explains well the effective particle separation energies derived in the application of this model.

The oscillation energies $\hbar\omega$ derived for the Xe isotopes from the best fit are in good agreement with the values suggested by the neighbouring even-even nuclei, except in the case of ^{131}Xe where it was found suitable to assume the existence of a ^{128}Xe core. Finally, the coupling constant ξ is plotted in Fig. (6) as a function of the mass number. The linear dependence shown in Fig. (6) has also been observed (8) by Heyde and Brussard in the case of the coupling of a proton to an even-even core.

4. EXPERIMENTAL FACILITIES

4.1. Detectors and associated electronics

In the present work the nuclei of interest are investigated by means of high resolution gamma ray spectroscopy. Four types of Ge(Li) detectors were used. In the initial steps a 2 cm³ ORTEC Ge(Li) detector was used. This detector has an active area of 4 cm² and a sensitive depth of 5 mm. The measured total resolution of this detector at the ¹³⁷Cs 661 KeV peak is 2.7 KeV fwhm under a low counting rate. This detector was later exchanged for a 29 cm³ active volume CI Ge(Li) detector. The Ge(Li) crystal of this detector has an active area of 10 cm² and a sensitive depth of 3 cm. The measured total resolution of this detector is 3.1 KeV at 1.33 MeV under low counting rates.

An ORTEC X-ray spectrometer has been also widely used in the present work. This spectrometer consists of a 0.39 cm³ active volume cylindrical Ge(Li) crystal. The active area of this crystal is $1/4\pi$ cm² and has a sensitive depth of 5 mm. The measured resolution of this detector is 0.48 KeV at 14 KeV and about 0.6 KeV at 81 KeV under low counting rates. The front face of the X-ray spectrometer is covered by a thin Be window with a layer of gold about 100 to 200 ^oA thick.

On various occasions a Nuclear Diodes Ge(Li) detector has been used. The crystal of this detector has an active area of 10.3 cm² drifted to 1 cm depth, with a total active volume of (42±1) cm³. All the above mentioned detectors were received from the supplying company with a preamplifier

system mounted on the detector. Pulses from the preamplifier systems have been subsequently amplified and shaped by using CI 1416 and ORTEC 1405 linear amplifiers. These amplifiers have a prompt and a delayed output. The typical length of the output pulses from the linear amplifiers was 4 μ sec. If a part of the obtained pulses spectrum was required in an expanded form, a 1460 CI biased and stretcher amplifier was used. This amplifier can stretch a part of the spectrum up to 20 times. A bias level knob on the amplifier allowed the selection of the desired part of the spectrum to appear in the output of the amplifier. This amplifier is also supplied with a gating input. The presence of a negative pulse (-5 Volts) in the gating input opens the gate and a pulse fed into the biased and stretcher amplifier input will appear in the output.

The pulses from the output of the linear or biased amplifier were then used subsequently fed into the recording system, which consisted of a Northern Scientific 2048 channels analyzer. The 2048 channel analyzer as well as other electronic equipment described here are discussed (25) in detail elsewhere. In some instances a small Victoreen 400 channel analyzer has also been used. The output readout from the analyzer was obtained with a 6550 OMNIGRAPHIC model plotter and a high speed teletype puncher which stored the data on an eight level code.

Gamma-gamma coincidence experiments have been carried out with the electronic arrangement shown in Fig. (7) and discussed in more detail in ref. (25). In the coincidence experiment either two Ge(Li) detectors

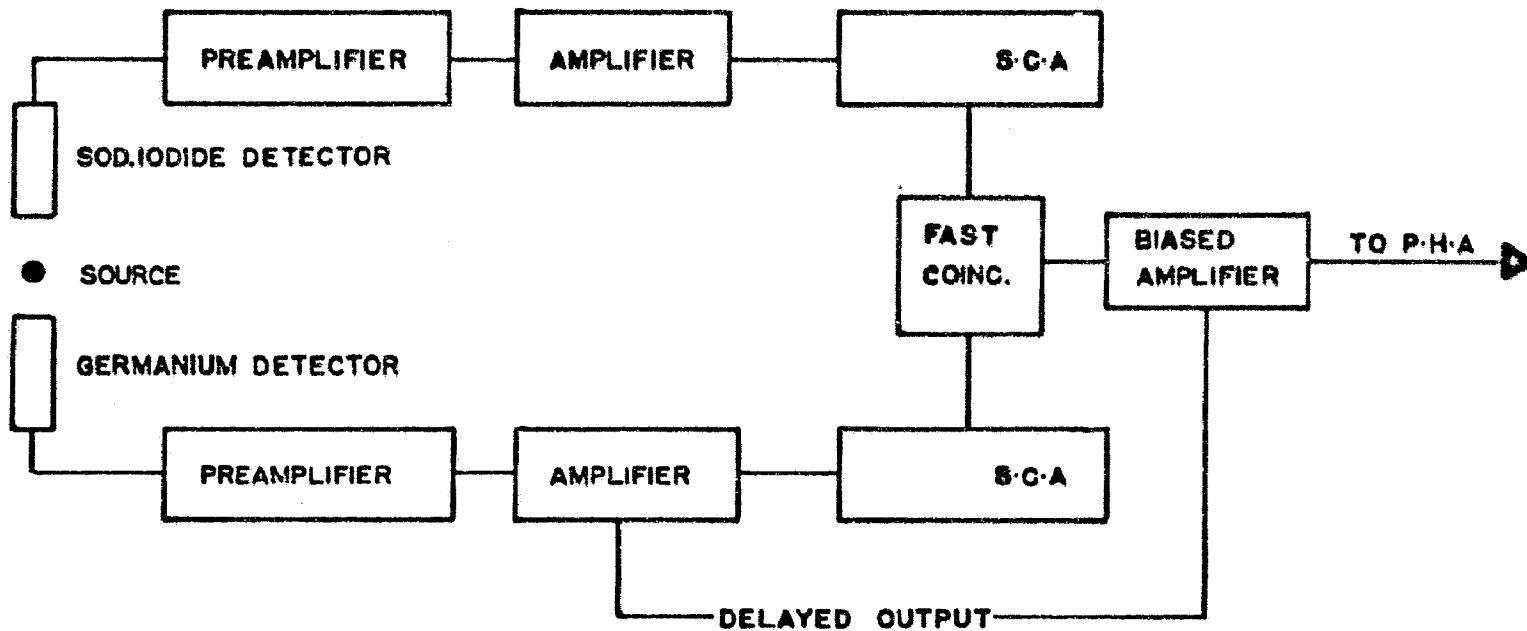


Fig. 7. Block diagram of the coincidence arrangement. (See text for discussion.)

or a Ge(Li) and a NaI detector have been used. The pulses from the two detectors were fed into two CI 1460 amplifiers. The bipolar prompt output of the amplifiers was fed to two CI 1435 single channel analyzers. One of the single channel analyzers was used to gate the required pulses. The output of the two single channel analyzers was fed into a CI 1440 fast coincidence unit. The negative pulses of the fast coincidence unit were used to gate the CI 1460 biased amplifier, the input of which was fed by the delayed pulses of one of the CI linear amplifiers. The coincident pulses were then displayed into the 2048 channel analyzer. The resolving time of the fast coincidence unit could range from 6 to 120 ns. Both the single channel analyzers used were equipped with a variable delay of 1000 ns. The optimum delay settings were determined in practice with the help of a ^{60}Co and a ^{133}Ba source. By varying the delay of one of the two timing SCA, the counting rate of the output of the system was obtained as a function of the delay. The optimum delay was then set at the position of the maximum counting rate. This procedure also determined in practice the true resolving time of the system (25).

4.2. Relative efficiency calibration of the Ge(Li) detectors

The relative efficiency of the detectors described previously has been determined experimentally using the pair point method described by Donnelly et al (28). A set of radioactive sources with photopeaks of well known relative intensities have been employed in the calibration procedures. The sources employed were ^{241}Am , ^{131}Ba , ^{22}Na , ^{57}Co , ^{60}Co , which have a

(15)

very well known decay scheme and photopeaks with intensities known to a good degree of accuracy ⁽¹⁵⁾. ⁷⁵Se and ¹⁵⁴Eu sources have also been used. Both nuclei have some strong gamma rays with relative intensities which are known precisely enough for the present work. All these radioactive nuclei and their corresponding transitions used for calibration purposes are listed in Table 14.

The sources consisted of a small drop of the radioactive material deposited on a Mylar or Al disk. Each source in turn was placed on the axis of the detector at a distance of 5 cm from its front face. The source strength was of the order of a few μC , so that the final counting rate experienced by the detectors was small. For each photopeak at least 10^4 counts were accumulated and each experiment was repeated at least twice. In order to account for the background, a straight line was drawn from the point where the slope of the peak started to the point where the slope of the peak ended.

If A represents the net counts under a given photopeak of energy x , and $\epsilon(x)$ is the efficiency of the detector for the photons of energy x , then A is related to the intensity of the emitted radiation by the relation given by

$$A(x) = K \epsilon(x) I(x) \dots \dots \dots (4.1)$$

where $I(x)$ is the absolute intensity of the emitted photons and K is a constant.

If a radioactive nucleus emits two gamma rays of energy x_1 and x_2

Table 14

Radioactive sources used in efficiency calibration of the Ge(Li) detectors

Source	Energy in KeV	Rel. Int.	Ref.	Source	Energy in KeV	Rel. Int.	Ref.
^{60}Co	1173.2	100	15	^{75}Se	96.75	5.46±0.20	39,40
	1332.5	100			121.12	27.9±0.7	
					135.99	95.2±2.0	
^{24}Na	1368.5	100	15		198.60	2.35±0.06	
	2753.9	100			264.62	100	
					400.70	20.9±2.0	
^{22}Na	511.0	180	15				
	1274.5	100					
				^{154}Eu	248.0	18.5±0.7	29
^{137}Cs	32.1	6.85	15		444.4	1.4±0.05	
	36.5	1.54			591.7	13.6±0.5	
	661.6	100			722.3	55.4±2.2	
					756.8	12.2±0.5	
^{57}Co	14.4	11	15		873.2	32.4±1.3	
	122.0	100			996.3	29.0±1.1	
	136.3	13			1004.8	48.8±1.9	
					1274.4	100	
^{241}Am	11.89	2.2	15				
	13.9	37.5					
	17.8	51.2					
	20.8	13.8					
	26.35	7.0					
	59.5	100					

with corresponding relative intensities $I(x_1)$ and $I(x_2)$, then the net area under the detected photopeaks may be written with the aid of equation (4.1)

$$\frac{A(x_1)}{A(x_2)} = \frac{\epsilon(x_1)}{\epsilon(x_2)} \frac{I(x_1)}{I(x_2)} \dots \dots \dots (4.2)$$

Thus if the relative intensities of the two radiations x_1 and x_2 are known, measurements of the relative areas $A(x_1)$ and $A(x_2)$ under the two registered photopeaks will determine uniquely the ratio $\frac{\epsilon(x_1)}{\epsilon(x_2)}$.

If a source having more than two strong transitions with fairly well known relative intensities is employed, use of equation (4.2) may define a set of points $\epsilon(x_1)$ representing a dependence of the relative efficiency of a particular detector on the energy of the incoming photons. A smooth curve then can be drawn through these experimentally determined points. If a second radioactive source has at least one transition falling in the energy region determined from the previously radioactive source, then the curve drawn may be extended to the energy region covered by the second source. If the second source has more than one transition falling in the energy region covered by the first radioactive source, then it becomes clear that a more accurate curve may be drawn through these points.

In the present application of this method, the efficiency of each detector was assumed to be unity for the energy of incoming photons of 1274.5 KeV. The ^{22}Na source provides the relative efficiency of the detector at 511.0 KeV since the relative intensity of the 1274.5 and 511.0 KeV peaks of ^{22}Na is very well known.

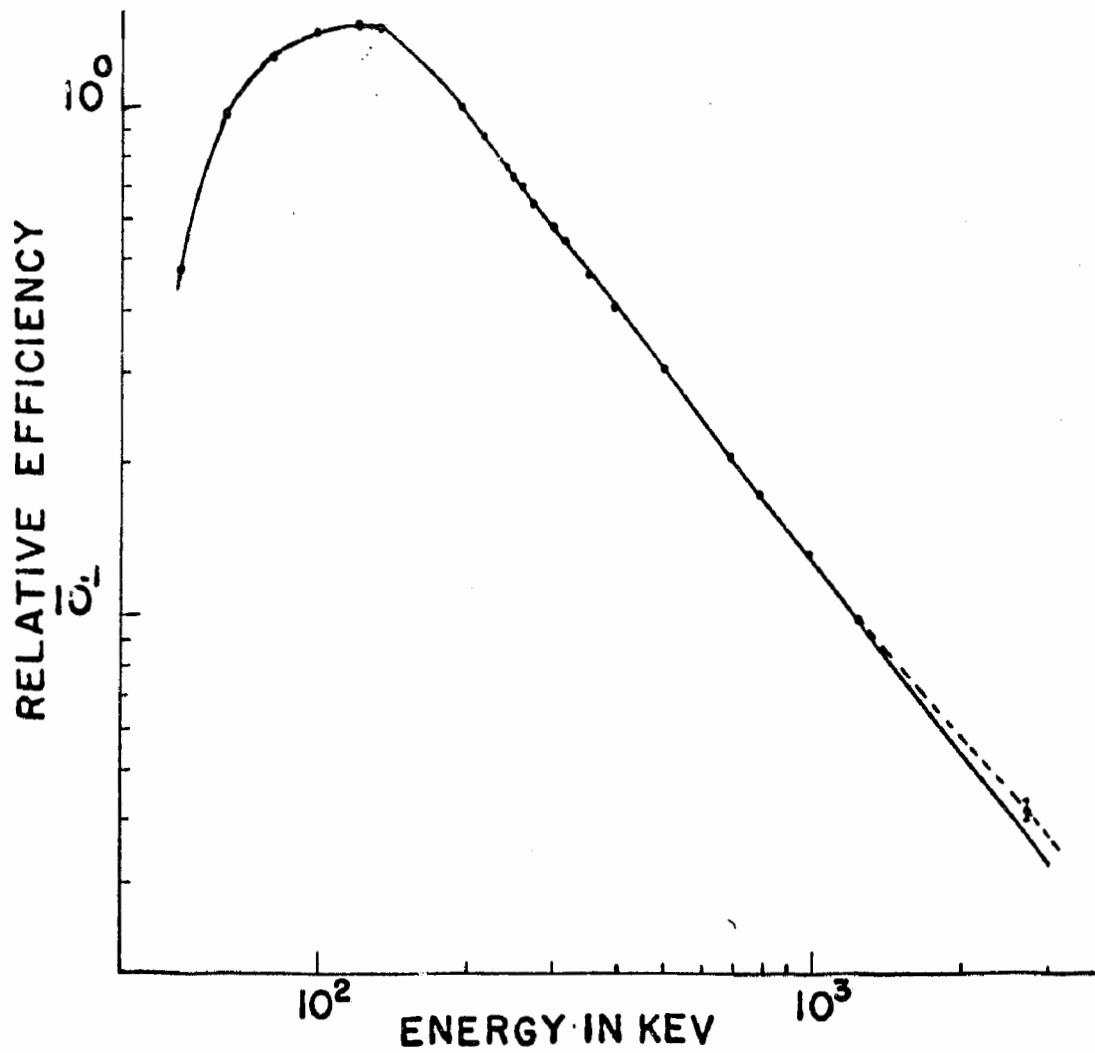


Fig. 8. Log-log dependence of the relative efficiency of the 29cm^3 Ge(Li) detector on the energy • data obtained from least mean squares fit. $\dot{\bar{I}}$ ^{24}Na 275.45 KeV experimental point. Broken lines indicate the experimental curve for energy $E > 1.2\text{MeV}$.

The next source used was ^{154}Eu . As shown in Table 14, the prominent peaks of ^{154}Eu cover a wide energy region. The presence of a prominent 1274.5 KeV transition in ^{154}Eu serves as the starting point, since the efficiency at the ^{22}Na 1274.5 KeV transition was assumed as 1. Thus a first smooth curve may be drawn through these points determined by the ^{22}Na and ^{154}Eu sources. With sources as ^{241}Am , ^{133}Ba , ^{57}Co , ^{75}Se and ^{60}Co , the initial curve may be improved in accuracy and may be extended to cover an energy region from as low as 14 KeV to a maximum of 1.33 MeV.

The points representing the relative efficiency of the Ge(Li) detectors obtained as described above have been plotted in a log-log paper as a function of the energy. It was found then that for the energy region from 0.2 to about 1.3 MeV the dependence of the relative efficiency of each detector was linear with respect to energy. A least-mean-squares fit to the experimental data yielded the desired relative efficiency of each detector. In Fig. (8) the log-log dependence of the relative efficiency curve of the 29 cm³ Ge(Li) detector is shown as a function of energy. A semilog plot of the relative efficiency curves of the 0.39, 2 and 29 cm³ detectors is shown in Figs. (9,10 and 11) respectively. The relative efficiency of the 0.39 cm³ X-ray spectrometer has been measured separately for the energy region from 14 to 121 KeV using ^{241}Am , ^{133}Ba , ^{57}Co , ^{75}Se standard sources. The semilog plot of these measured relative efficiency values is shown in Fig. (12).

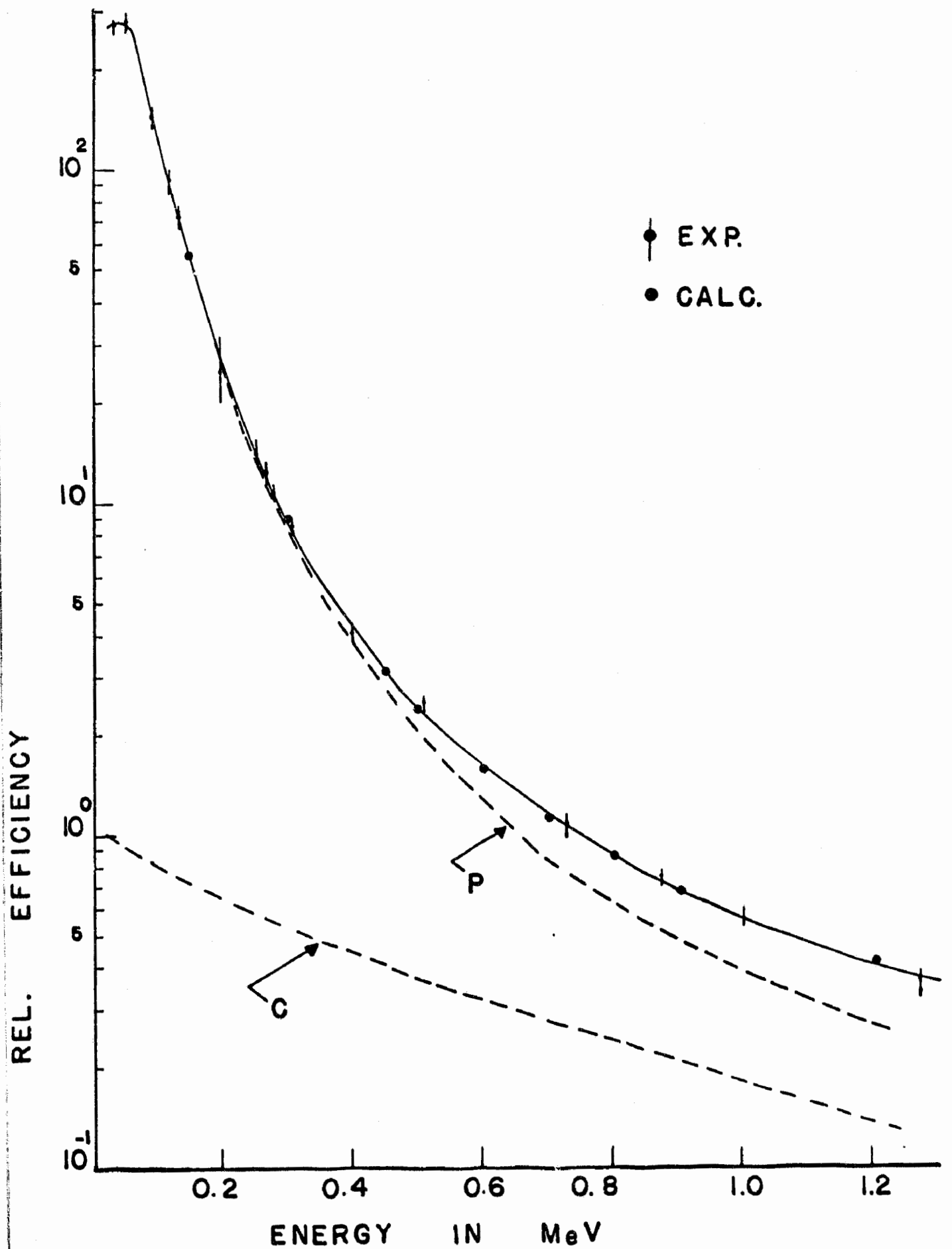


Fig. 9. Relative efficiency curve of the 0.39cm^3 Ge(Li) detector. \dagger Experimental points \bullet calculated points. P=Photoelectric, C=Compton contribution.

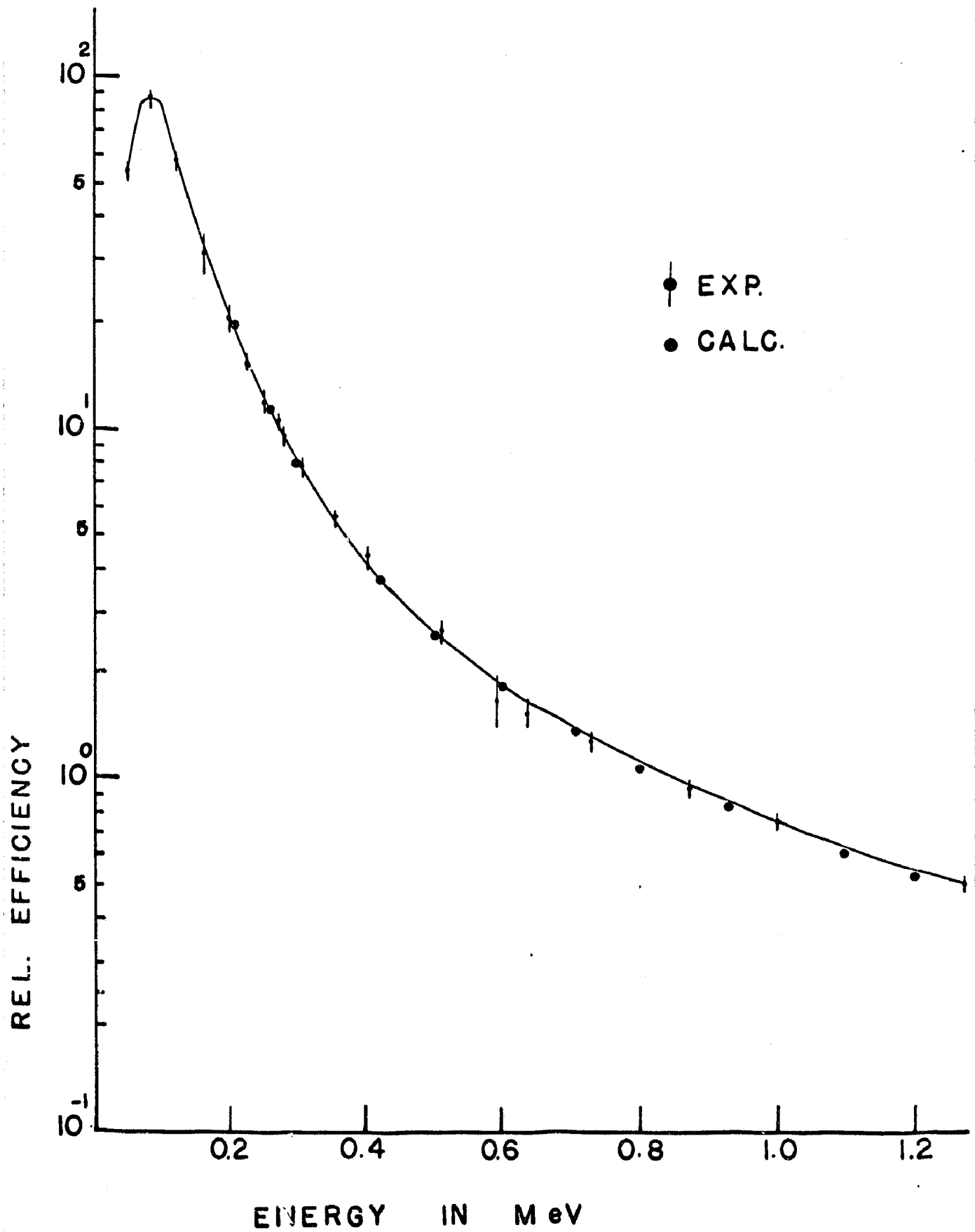


Fig. 10. Relative efficiency curve of the 2 cm³ Ge(Li) detector. † Experimental points, • calculated points.

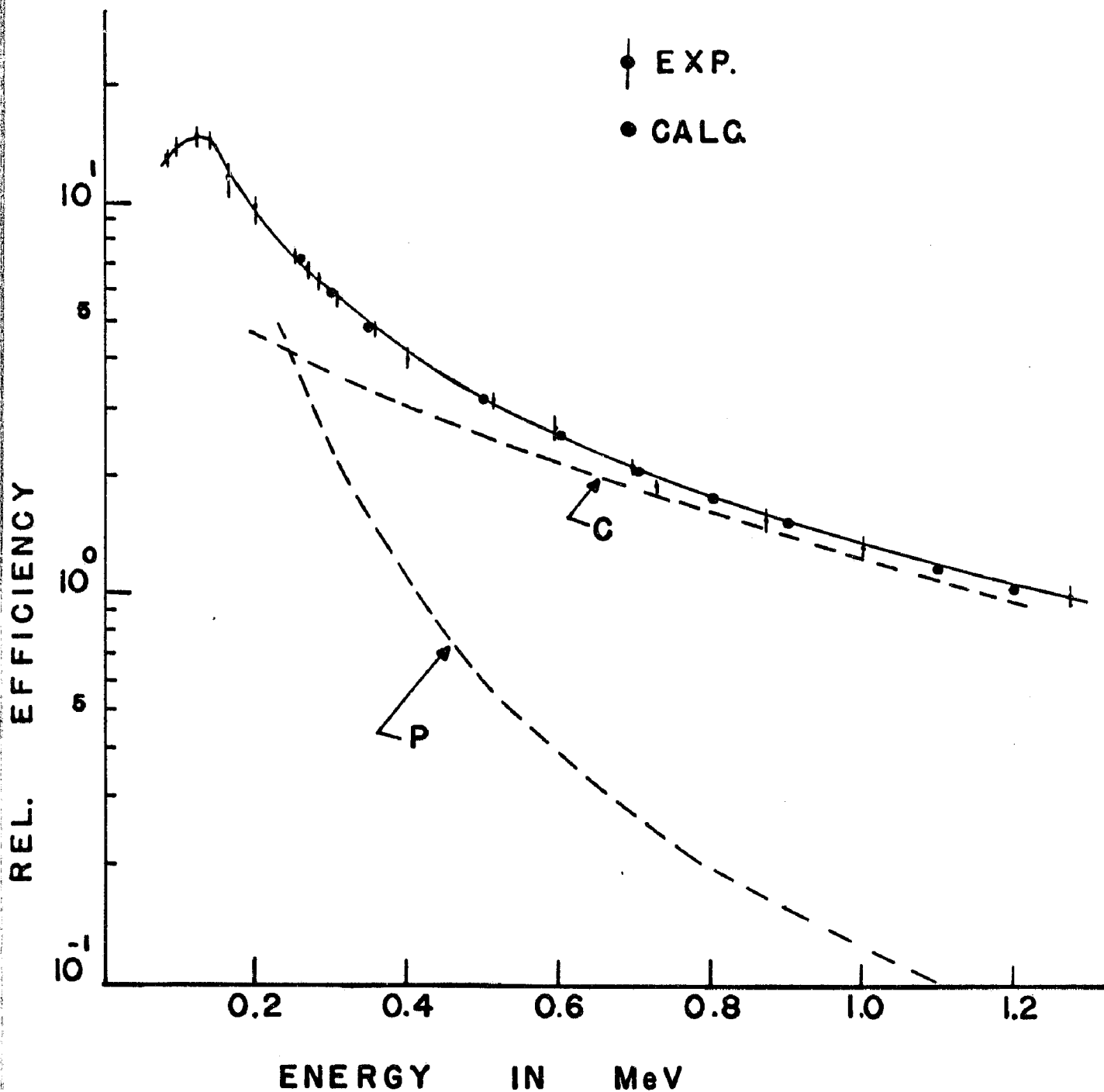


Fig. 11. Relative efficiency curve of the 29 cm³ Ge(Li) detector. ♦ Experimental points, • calculated points. Solid line: least mean squares fit of experimental points. Dotted lines indicated with letters P and C: Contributions to the efficiency curve from the two processes, Photoelectric and Compton respectively.

Extension of the efficiency calibration of the detectors to energy higher than 1.33 MeV was not possible because no suitable sources were available. In more recent experiments using the neutron generator, ^{24}Na activity was produced as contaminant. This nucleus has two prominent peaks at 1368 and 2754 KeV, with a well known intensity ratio (15) . The presence of this contaminant activity in the measured spectra was used to check the efficiency of the 29 cm^3 Ge(Li) detector at 2754 KeV against the value predicted by extrapolation of the curve given in Fig. (8). The experimental relative efficiency at 2754 KeV was found to be 0.42 ± 0.2 against a predicted value of 0.38. The curve which included this experimental point is shown in broken lines in Fig. (8). For energy below 1.9 MeV the relative efficiency values obtained from the extrapolated and the experimentally suggested curve do not show a significant difference. For energies above 1.9 MeV the values obtained from the experimentally determined curve are used. It should be noted here, that for some experiments to be discussed later, the experimental conditions under which these relative efficiency curves have been obtained were not kept the same. Thus in some experiments, the activity under investigation was not in the form of a point source or the distance of the detector to the source was not 5 cm. In these experiments the relative efficiency values were obtained again from the experimentally determined curves, omitting the probable error caused by neglecting the experimental condition under which these curves have been determined.

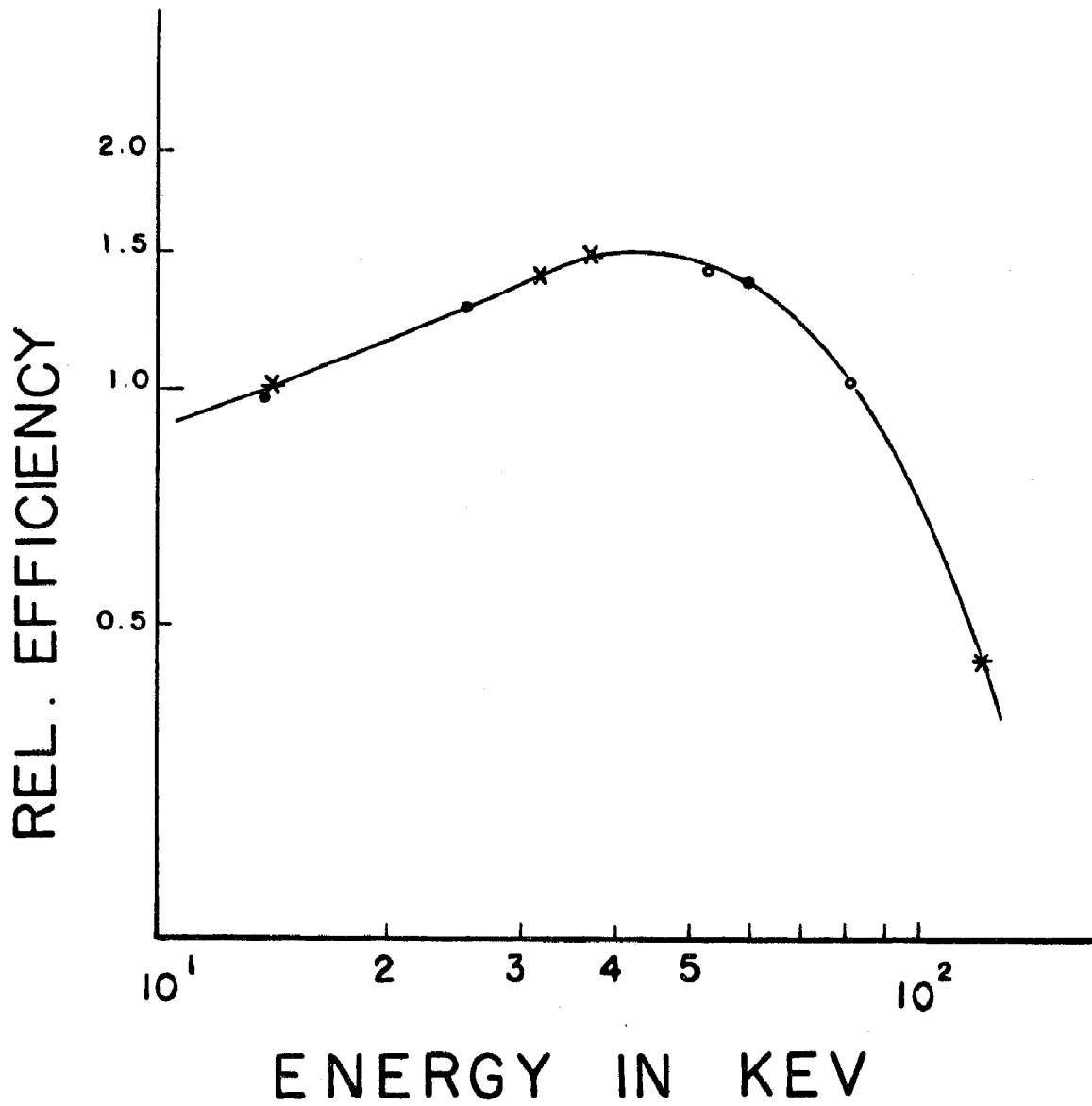


Fig. 12. Relative efficiency curve of the 0.39 cm³ Ge(Li) detector for E < 100 KeV. ○ ¹³³Ba * ⁵⁷Co ● ²⁴¹Am × ¹³⁷Cs.

4.2.1. A semi-empirical efficiency equation for Ge(Li) detectors

(30)

A few years ago Freeman and Jenkins proposed a semi-empirical equation which related the efficiency of a Ge(Li) detector to the photoelectric and Compton coefficient of germanium and the energy of the incoming photons. The equation proposed by these authors has the form given by

$$\epsilon \propto 1 - \exp(-\tau \cdot x) + A\sigma \exp(-BE) \dots \dots \dots (4.3)$$

where τ, σ are the photoelectric and the Compton absorption coefficients of germanium respectively, E is the energy of the detected photons, x is the thickness of the crystal and A and B constants to be determined.

For energy of the incoming photons greater than 500 KeV the product $\tau \cdot x$ is much less than unity and equation (4.3) may be written

$$\epsilon \propto \tau \cdot x + A\sigma \exp(-BE) \dots \dots \dots (4.4)$$

Freeman and Jenkins⁽³⁰⁾ used the relation given by equation (4.4)

in the energy region above 500 KeV and devised a method of determining the two constants A and B for a given detector. Later Topcan and

⁽³¹⁾ Cothern verified that equations (4.3) and (4.4) were in good agreement with their experimental data for a 2 cc Ge(Li) detector down to energies as low as 200 KeV.

The work proposed by the above mentioned workers to determine the constants A and B requires a considerable amount of experimental work, particularly if it is necessary to calibrate a number of detectors. It was tempting then to try to see if the present data obtained from the calibration of our detectors could be fitted to such a semi-empirical

equation. Furthermore, it is very interesting to investigate the possibility that the constants A and B of an equation of the form given by equation (4.3) are simple functions of the geometrical characteristics of a particular detector.

On the basis of the present knowledge of photon interactions with matter it is expected that a certain number of photons incident on a germanium crystal will contribute directly to the full energy peak through the photoelectric process. The percentage ϵ_{τ} of photons detected by a germanium crystal of an effective thickness x may be written in the form

$$\epsilon_{\tau} = 1 - \exp(-0.044 \cdot \tau \cdot x) \dots (4.5)$$

where x is the effective thickness of the detector in cm and τ is the photoelectric coefficient of germanium given in units of barns/at. The numerical factor 0.044 transforms the effective thickness x from cm to at/barns units. The photoelectric coefficient τ is a function of energy and thus equation (4.5) represents the dependence of ϵ_{τ} on the energy of the incoming photons. For $E > 500$ KeV $\tau \cdot x \ll 1$ and (4.5) may be written as

$$\epsilon_{\tau} = 0.044 \tau \cdot x \dots (4.6)$$

A considerable portion of the contribution to the full energy peak of the detected photons arises from the multiple Compton scattering mechanism. A photon of initial energy $h\nu$ is scattered within the crystal transferring an amount of energy $h(\nu - \nu_1)$ to an electron and retaining an amount of energy $h\nu_1$ which is then used to eject a photoelectron

of energy $h\nu - w$ where w is the work function of Ge. If θ_i is the probability that the two electrons with total energy $h(\nu - \nu_i) + h\nu_i - w = h\nu - w$ will add to the full energy photopeak, then the Compton contribution to the efficiency may be written as

$$\epsilon\sigma = C.\theta_i.\sigma \quad \dots \dots \dots (4.7)$$

where σ is the Compton scattering coefficient of Ge and C is a proportionality constant. The contribution from second order multiple scattering involving more than two electrons may be also included in equation (4.7). Then equation (4.7) may be written in the form

$$\epsilon\sigma = C.\sigma.\sum_i \theta_i = C.\sigma.\theta \quad \dots \dots \dots (4.8)$$

where θ is the total probability of the Compton scattering mechanism to contribute to the full energy photopeak. It is not unreasonable to assume in accordance with Freeman and Jenkins (30), that the probability θ defined previously, to be a function of the energy E having the form

$$\theta = D.\exp(-BE) \quad \dots \dots \dots (4.9)$$

where D and E are constants.

Substituting equation (4.9) into equation (4.8), the equations given by

$$\epsilon\sigma = C.B.\sigma.\exp(-BE) \doteq A.\sigma.\exp(-BE) \quad (4.10)$$

where $A = CD$ is obtained.

By combining equation (4.10) with equation (4.5), the total contribution to the photopeak from both processes may be written

$$\epsilon = K \left[1 - \exp(-0.044\tau.x) + A\sigma\exp(-BE) \right] \dots \dots (4.11)$$

Equation (4.11) may also be written as

$$\epsilon = K \left[0.044\tau.x + A\sigma\exp(-BE) \right] \dots \dots \dots (4.12)$$

for energy $E > 500$ KeV.

If ϵ is assumed to be the relative efficiency of a detector at a given energy E , then the constant K in equation (4.11) may be considered as the constant which transforms the relative efficiency of the detector to the absolute efficiency ϵ/K where

$$\epsilon/K \equiv \frac{N \text{ detected}}{N \text{ incoming}} \dots \dots \dots (4.13)$$

where N is the number of photons.

4.2.2. Application of the semi-empirical equation

For a given set of experimental values ϵ_i of the relative efficiency of a detector, and for energies of more than 500 KeV, equation (4.12) may be written

$$\epsilon_i \equiv 0.044\tau_i b + d\sigma_i \exp(-BE_i) \dots \dots \dots (4.14)$$

where

$$b = Kx \quad \text{and} \quad d \equiv KA \dots \dots \dots (4.15)$$

In principle, three of the equations given by equation (4.14) are necessary to determine the unknown quantities b, d , and B . In practice several sets of three equations of the type given in equation (4.14) were used to eliminate the quantities b and d and obtain thus an exponential equation involving the unknown B . The photoelectric and the non-coherent Compton coefficients were obtained from the recent work by Chapman (32). The relative efficiency curves for the 0.39, 2 and 29 cm³

Ge(Li) detectors as determined here have been used to obtain the experimental relative efficiency values ϵ_i required by equation (4.14). In addition, the relative efficiency curve of a 17 cm³ Ge(Li) detector which has been supplied by the chemistry branch of the Chalk River AECL Laboratories ⁽³³⁾ has also been used. This curve is shown in Fig. (13). The exponential equations resulting from equation (4.14) have been solved numerically for all four detectors to determine the constant B. For each detector numerous combinations of the equations (4.14) were solved and yielded values of B which ranged from 0.5 to 1.4. Although the calculated B values for all the detectors were scattered in this range, the average B for each of the detectors used was found to be equal to 0.8. Thus the value of 0.8 was adopted for B and for all the detectors used.

This value for B was then substituted back in equation (4.14) and least-mean-squares methods were employed to determine the parameters b and d for each detector.

Equation (4.11) is written in terms of the constants b and d as

$$\epsilon_i = \frac{b}{x} \left[1 - \exp(-0.044\tau_i x) + d\sigma_i \exp(-BE_i) \right] \dots (4.16)$$

This equation has been used in conjunction with the relative efficiency values for $E > 500 \text{ KeV}$ and the previously determined constants b and d to determine the unknown effective thickness of the detector. With this value of x and the set of equations given by (4.15) the constants K and A are determined uniquely for each detector. The constants A, x and K as determined for each detector are listed in Table 15.

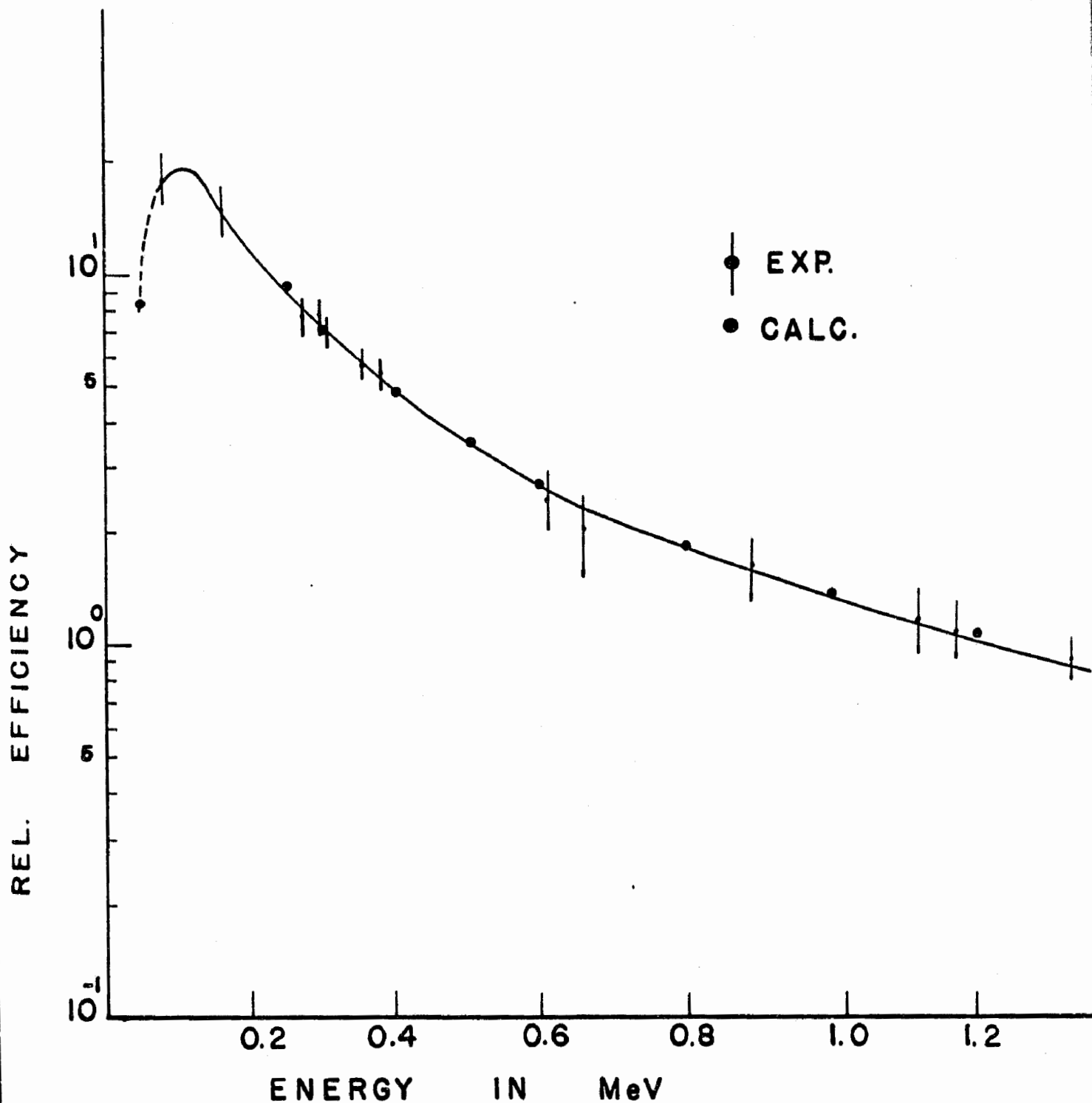


Fig. 13. Relative efficiency curve of the 17 cm³ Ge(Li) detector. † Experimental points, • calculated points. Solid line: Least mean squares fit of experimental points. (See discussion in Section 4.2.1.)

Table 15

Calculated parameters of various detectors

Detector active volume V (cm^3)	B MeV^{-1}	A (at/barn)	A/V (barn/at) 2	x (cm)	$V^{1/3}$ (cm)	K
0.39	0.8	0.0004	0.00103	0.795	0.724	145.7
2.00	0.8	0.0026	0.00130	1.810	1.260	53.0
17.00	0.8	0.0196	0.00115	2.510	2.570	20.90
29.00	0.8	0.0368	0.00127	3.180	3.080	11.09

An immediate conclusion may be drawn from this table. While the constant A is shown to increase with increasing volume of the detector, the ratio $\frac{A}{V}$ for all the detectors is almost constant. An average value of $\frac{A}{V} = 0.00120 \left(\frac{\text{barn}}{\text{atom}}\right)^2$ is obtained which suggests that the constant A for any given detector may be given by

$$A = 0.0012 V \text{ at/barn} \dots\dots\dots(4.17)$$

where V is the active volume of the detector.

Another important conclusion which may be drawn from Table 15 is that the calculated effective thickness of each detector was very close to the cubic root of its volume. Thus the effective thickness of any detector may be written in terms of the active volume of the detector as

$$x = V^{1/3} \text{cm} \dots\dots\dots(4.18)$$

Thus the equation given by equation (4.11) may be written in terms of the expression for A and x given by equations (4.17) and (4.18)

$$\epsilon \equiv K \left[1 - \exp(-0.044\tau.V^{1/3} + 0.0012 V.\sigma \exp(-0.8E)) \right] \dots\dots(4.19)$$

The relative efficiency values calculated by means of equation (4.19) are shown with small black circles in Figs. (9,10,11 and 13) for the four detectors respectively. Some typical calculated values are also shown in Table 16 for the four detectors used. These values are also compared with the experimentally obtained values. It is expected that equation (4.19) will be valid for the range from 200 to 1500 KeV. The presence of absorbing layers in front of the Ge(Li)

Table 16

Relative efficiency values for several Ge(Li) detectors

Detector volume cm ³	Photon energy (MeV)	Experimental relat. effic.	Calculated relat. effic.
0.39	0.2	26.0±2.0	27.2
	0.3	8.6±0.4	9.0
	0.5	2.5±0.1	2.45
	0.8	0.87±0.05	0.88
	1.0	0.56±0.03	0.58
	1.2	0.39±0.03	0.41
2.00	0.2	20.5±0.90	21.0
	0.3	8.0±0.30	8.1
	0.5	2.55±0.09	2.6
	0.8	1.10±0.05	1.09
	1.0	0.76±0.04	0.76
	1.2	0.56±0.02	0.55
17.0	0.25	9.20±0.40	9.45
	0.30	7.20±0.40	7.26
	0.50	3.50±0.20	3.53
	0.80	1.90±0.10	1.91
	1.00	1.32±0.08	1.42
	1.20	1.02±0.08	1.10
29.0	0.25	7.5±0.20	7.60
	0.30	6.0±0.20	6.00
	0.50	3.19±0.08	3.16
	0.70	2.10±0.07	2.10
	0.90	1.54±0.06	1.53
	1.20	1.08±0.05	1.03

crystals is expected to modify the efficiency of the detectors for photons energy lower than 200 KeV. For energies higher than the pair production threshold, deviations are expected from the values given by equation (4.19) since the effect of the pair production contribution is not included in equation (4.19). It is interesting to note here that in the present form of equation (4.19) the contribution from the direct and the multiple Compton process in the efficiency of a detector may be calculated separately. These contributions are calculated and shown in Fig. (9) and (11) for the 0.39 and 29 cm³ Ge(Li) detectors. As expected the contribution to the photopeak efficiency from the Compton effect is predominant in the large 29 cm³ detector while in the 0.39 cm³ detector the direct photoelectric effect contributed most to the observed efficiency.

The 42 cm³ Ge(Li) detector described in section 4.1 was received after the completion of the present work. The experimental relative efficiency curve for this detector is shown in Fig. (14). The values calculated from equation (4.19) are also shown in the same figure. In using equation (4.19) the value of 42 cm³ was substituted for V. Some calculated values are shown also in Table 17 and are compared with the experimental values. The observed agreement supports the validity of the proposed semi-empirical equation given by (4.19).

It will be of interest if the equation given in (4.19) is checked for its validity with a variety of Ge(Li) detectors. Also the nature

Table 17

Experimental and calculated relative efficiency values for the
(42±1) cm³ Ge(Li) detector

Energy (MeV)	Relative efficiency	
	exp	calculated
0.2	10.5±0.2	10.0
0.25	7.8±0.2	7.36
0.30	6.1±0.2	5.93
0.40	4.3±0.1	4.18
0.50	3.25±0.08	3.25
0.60	2.60±0.07	2.65
0.70	2.13±0.07	2.20
0.80	1.80±0.06	1.90
0.90	1.55±0.06	1.62
1.00	1.36±0.06	1.44
1.10	1.23±0.05	1.25
1.20	1.08±0.04	1.09

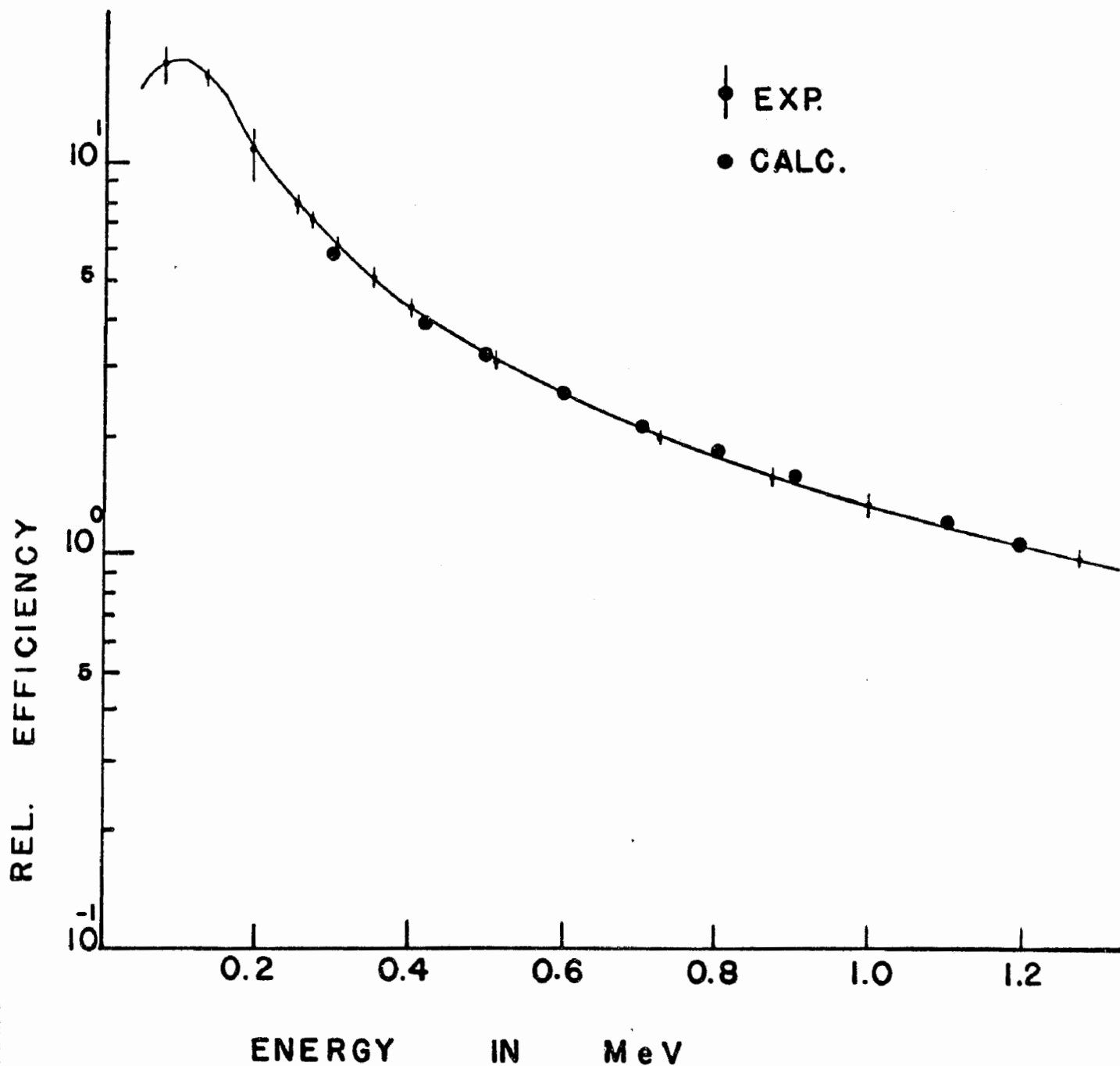


Fig. 14. Relative efficiency curve of the 42 cm³ Ge(Li) detector. † Experimental points. ● Calculated points. Solid line: Least mean squares fit to the experimental data.

of the constants $\frac{A}{V}$ and B may be investigated more accurately under several geometries, especially with the help of collimated photon beams.

Finally the importance of the constant K which appears in equation (4.19) is briefly discussed. As equation (4.13) indicates the values ϵ/K derived correspond to the absolute efficiency of the particular detector at the energy E of the incoming photons.

The absolute efficiency for the 0.39 cm³ Ge(Li) detector has been measured by using a ²²Na source at 511 KeV. Many measurements have been carried out and the results indicated that the absolute efficiency of this detector at 511 KeV is $(1.2 \pm 0.3) \times 10^{-2}$. The value ϵ/K obtained from Tables 15 and 16 for the 0.39 cm³ detector is 1.6×10^{-2} in fair agreement with the experimental value.

For the 29 cm³ Ge(Li) detector the experimental absolute efficiency for the ²²Na 511 KeV photons was found to be $(10 \pm 1) \times 10^{-2}$. The value ϵ/K obtained using the data of Table 15 and 16 is 28×10^{-2} almost three times larger than the experimental value. This discrepancy may be explained by simple geometric considerations.

The two cases illustrated in Fig. (15) are considered. Photons are entering the two detectors A and B respectively. In both cases photons entering the crystal within the solid angle \underline{O}_2 have a larger probability of interacting with the crystal than through the funnel $\underline{O}_1 - \underline{O}_2$ simply because their path length in the material is larger. Assuming that \underline{O}_2 is chosen as the appropriate experimental solid angle

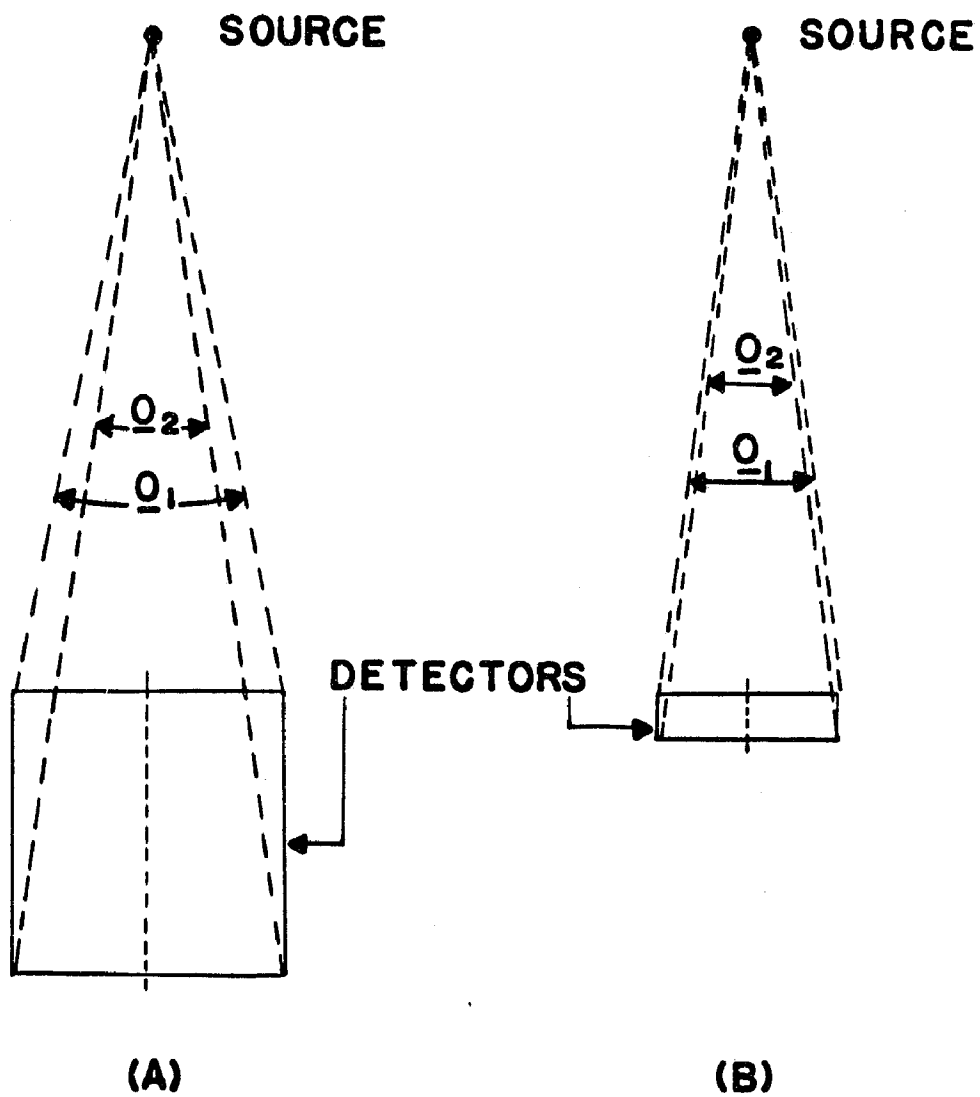


Fig. 15. Horizontal cross section of a source and detector. A: Large crystal, B: Small crystal.

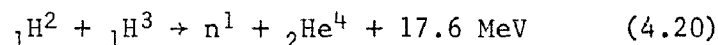
sustained by the source and the detector instead of the angle \underline{O}_1 , the experimental absolute efficiency of the 29 cm³ Ge(Li) detector becomes $(22\pm 3)\times 10^{-2}$ at 511 KeV in fair agreement with the calculated value of 28×10^{-2} . In the case of the small detector (Fig. (17B)) $\underline{O}_1 \approx \underline{O}_2$ and no serious discrepancy is observed between experimental and calculated values.

4.3. Energy calibration

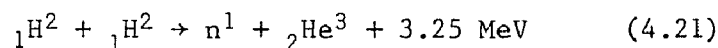
The energy calibration of the spectra observed with the Ge(Li) detectors are performed with a variety of standard sources with peaks of well known energy. In Chapter 5 where the details of the experimental work are given, the energy calibration procedure is discussed in more detail for each case of interest.

4.4. The neutron generator

The Texas 9900 neutron generator acquired recently by the USRC is designed specifically to produce high current beams of protons or deuterons. The fast neutrons are produced via the reactions



and



In the case given by equation (4.20) momentum and energy conservation principles indicate that the energy of the released neutrons at zero angle to the beam direction is 14.7 MeV.

A detailed description of the design and the operation procedures of the neutron generator is given in ref. (34).

The tritium targets used in the present work produce a total yield of 4×10^{10} neutrons per second. The target is separated from the sample to be irradiated by a cooling jacket with a thickness of approximately 1.3 cm. If another 0.5 cm for the thickness of the irradiated sample is allowed, it can be easily found that the total neutron flux through the sample is approximately 10^9 n cm⁻² sec⁻¹. Larger tritium targets may also be used. These targets produce a yield of $\sim 10^{11}$ n/sec. Such targets have not been used in the present work. If the cross section for a given reaction is σ the activity produced by irradiating a sample of weight g in grams for a time t is given by

$$R = \frac{A \cdot \sigma \cdot f \cdot g \cdot F}{W} [1 - \exp(-t \cdot \lambda)] \quad (4.22)$$

where R =disint/second is the activity of the produced nuclei, A is Avogadro's number, W is the atomic weight of the irradiated sample, f is the abundance of the isotope of interest in the sample, F is the neutron flux and λ is the decay constant of the produced activity.

5. EXPERIMENTAL WORK

5.1. The decay of ^{75}Se

The ^{75}Se nucleus decays with a half life of 120 days by electron capture to the excited states of ^{75}As . In the past an extensive study of the decay of ^{75}Se has been made using beta (35-37) and gamma (38-40) ray spectrometers.

The main features of the ^{75}Se decay are well established but some particular points require further discussion. Grigoriev and Zolotavin (35) observed a 24.4 KeV transition in the conversion electron spectrum of ^{75}Se . These workers deduced from their conversion electron spectra an intensity of 0.05 ± 0.02 for the corresponding 24.4 KeV gamma transition (normalized to 100 for the intensity of the 264.6 KeV gamma ray). (40) However Rao et al (40) did not observe this transition in a search with a proportional counter, and they set an upper limit of 10^{-3} for the intensity of this transition.

In the past, Grigoriev and Zolotavin (35), as well as de Croes et al (36) reported a 80.8 KeV transition observed in the conversion electron spectra of ^{75}Se . The intensity value of the corresponding gamma transition reported by these workers differs appreciably. Grigoriev (35) and Zolotavin (36) report a value of 0.025 ± 0.004 for the intensity of this gamma transition, while de Croes et al (40) report a value of 0.050 ± 0.010 . Rao et al (40) have not observed this transition in their gamma ray spectra obtained with a Ge(Li) detector and they set an upper limit of 10^{-5} for the intensity of this transition. However,

(42)
in a more recent work, Gasior et al have made a careful investigation of the conversion electron spectrum of ^{75}Se using a double, iron free toroidal beta spectrometer. Their measurements, which are supported by coincidence experiments, indicate that the 80.8 KeV transition exists. The intensity of the corresponding gamma transition is estimated to be 0.014 ± 0.002 . Recently (41) a 373 KeV gamma ray with intensity 0.03 ± 0.02 was deduced from gamma ray spectra but has not been observed by other workers. A 468 KeV transition was suspected (35-42) in the ^{75}Se gamma ray spectrum but no direct observation of this transition is reported. Instead various upper limits for the intensity of this transition are set to about $8 \cdot 10^{-3}$.

The radioactive ^{75}Se used in the present work was purchased from Amersham, England. Two sources were prepared from the stock solution about six months after receiving the material. The first source was made directly from the stock solution. The second was prepared after chemical purification of the remainder of the stock solution. In both cases two drops of the radioactive solution were deposited on an Al disk and dried under an infrared lamp. After drying, the sources were covered with a thin Mylar sheet.

From the long counting periods required to investigate the extremely weak transitions occurring in the decay of ^{75}Se above the 400 KeV region, it was found that the chemical purification was not necessary.

5.1.1. Single gamma ray spectroscopy

The low energy gamma ray spectrum of ^{75}Se was measured with the ORTEC 0.39 cm^3 Ge(Li) detector. In these measurements the amplifier gain was set to record all gamma rays of energy less than 130 KeV. The source was placed on the axis of the detector at a distance of 5 cm from the front face. A typical spectrum including gamma rays up to 100 KeV is shown in Fig. (16). For energy calibration ^{133}Ba and ^{57}Co sources were used. The two prominent peaks at 66.0 and 96.7 KeV are well known ⁽³⁵⁻⁴²⁾ gamma rays of ^{75}Se . At about 11 KeV, the K_α and K_β X-ray peaks of ^{75}As are observed. A peak at 24.4 KeV is observed which should correspond to the 24.4 KeV transition observed in the conversion electron ⁽³⁵⁾ spectrum by Grigoriev and Zolotavin . The deduced intensity for this transition is in good agreement with the value deduced by ⁽³⁵⁾ Grigoriev and Zolotavin .

The energy and the relative intensity of these transitions, with respect to the 121.1 KeV transition are given in Table 18. To determine the intensity of these transitions three spectra have been recorded. For each spectrum the area under a photopeak has been determined and normalized to the area under the 121.1 KeV photopeak. The corresponding area ratios obtained from the three spectra have been averaged and then corrected for the efficiency of the Ge(Li) detector used. The values obtained are presented in Table 18. The error in the estimation of the relative intensity is one standard

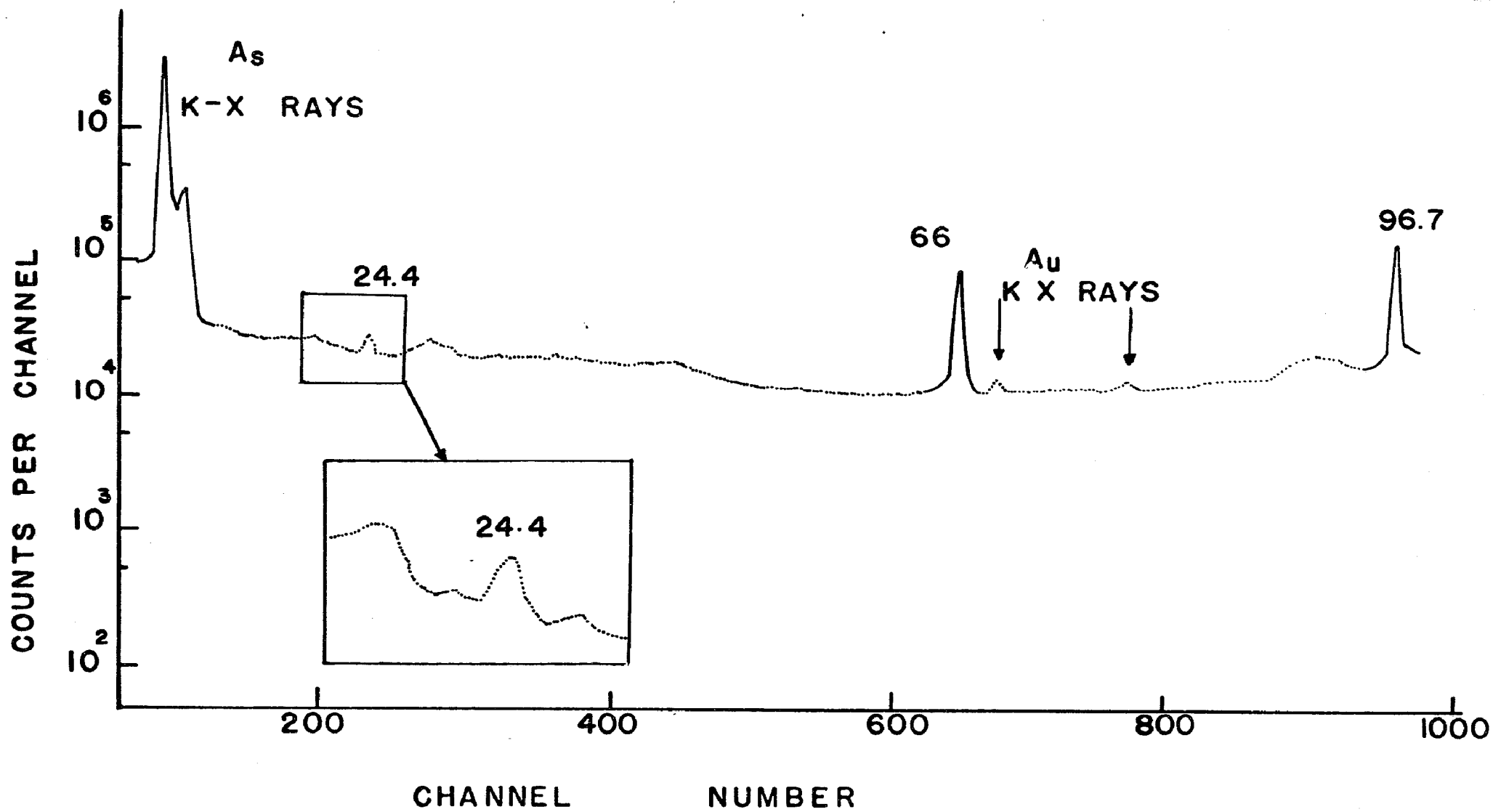


Fig. 16. Gamma ray spectrum of ^{75}Se observed with the 0.39 cm^3 Ge(Li) detector. (Energy: up to 100 KeV.)

Table 18

Energy and intensity of the low energy gamma rays in ^{75}Se

Energy in KeV	Intensity
K X-rays	326±7
24.4±0.1	0.159±0.020
66.0±0.1	6.2±0.2
96.7±0.1	18.5±0.5
121.1±0.1	100

deviation of the average result. Since the final intensity values are normalized to the 264.4 KeV transition, all intensity data quoted in Table 18 are multiplied by the relative intensity of the 121.1 KeV gamma ray with respect to the 264 KeV transition as derived later, and then presented in Table 19. The 80.8 KeV transition did not appear at all in the single spectra. Instead the K_{α} and K_{β} X-rays of gold were observed at 67.0, 68.8, 78 and 80.1 KeV. Their presence is explained as fluorescence emission from the gold layer of the Be window of the X-ray spectrometer due to the presence of the strongly exciting 96.7, 121.1 and 136.0 KeV gamma rays of ^{75}Se . The presence of the 80.1 KeV X-ray, and the Compton peaks of the higher lying strong transitions which occur in the same energy region made the identification of the 80.8 KeV gamma ray difficult because of the apparent weakness of this transition. The spectrum of Fig. (16) suggests an upper limit of 0.06 - 0.10 for the intensity of this gamma ray.

The 2 cc ORTEC Ge(Li) detector which has a good resolution in this energy region was also used. The spectrum obtained with this detector is shown in Fig. (17) in the energy region from 70 to 100 KeV. The spectrum is again badly distorted due to the high Compton peaks resulting from the presence of the 96.7, 121.1 and 136 KeV gamma rays. Detection of the 81 KeV gamma ray was again prevented because of the distortion of the spectrum. An upper limit of 0.1 for the intensity of this transition may be derived from the data.

The higher energy gamma ray spectrum of ^{75}Se was observed with the

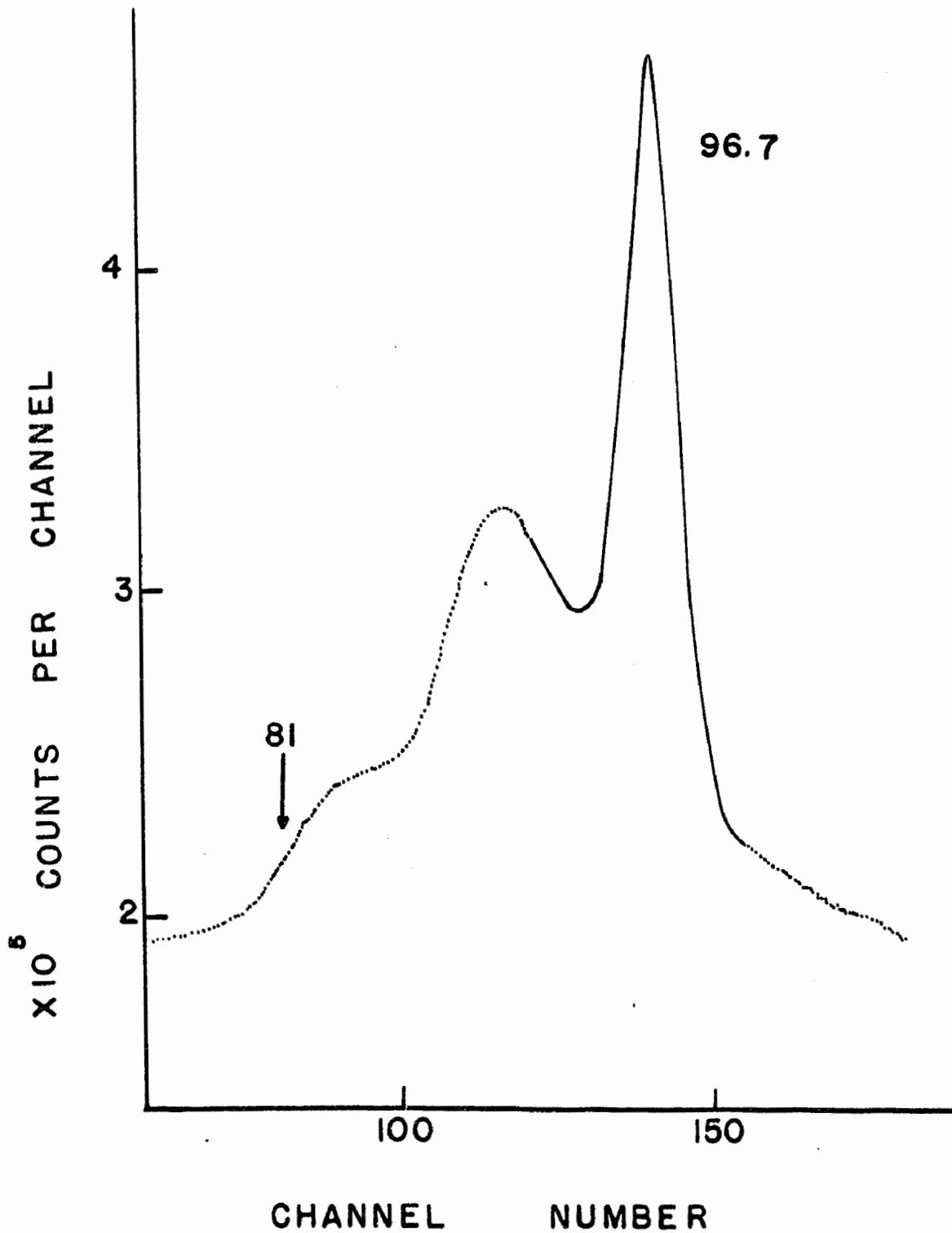


Fig. 17. Gamma ray spectrum of ^{75}Se obtained with the 2 cm^3 Ge(Li) detector. (Energy region from 75 to 100 KeV.) The arrow indicates the position of the unobserved 81 KeV transition.

29 cm³ CI detector. Figure (18) shows a typical spectrum of the energy region below the 400 KeV. Seven gamma rays are observed in this energy region. Their energies and intensities are listed in Table 19 and are compared with the results of other workers. The gamma ray reported ⁽⁴¹⁾ at 373 KeV has not been observed. An upper limit of 0.006 is indicated by the present data for the intensity of this transition. The procedure followed here to derive the intensities of the various peaks is the same as that described previously for obtaining the intensity of the peaks of the lower energy region.

During the investigation of the high energy region with the 29 cm³ detector, a lead absorber of 1.15 cm thickness was used to reduce the summing effects of the lower energy gamma rays. This way chance summing peaks above the 400 KeV energy region were avoided.

Due to the long counting periods required for this experiment, the internal zero level and gain stabilizer of the multichannel analyzer were used to avoid peak shifts.

The spectrum obtained after a 48 hour counting period and total background radiation subtraction is shown in Fig. (19). The peaks at 400.5, 419.3, 572.6 and 617.7 KeV are well known peaks of ⁷⁵Se. A small peak observed at 468.6±0.4 KeV is believed to belong to ⁷⁵Se.

In Fig. (20) the spectrum obtained after a 48 hour counting period is shown for the energy region above the 400 KeV. Except for the three known ⁷⁵Se transitions at 419.3, 572.6 and 617.7 KeV, the peaks observed were identified as impurities due to the presence of Th and Ra traces

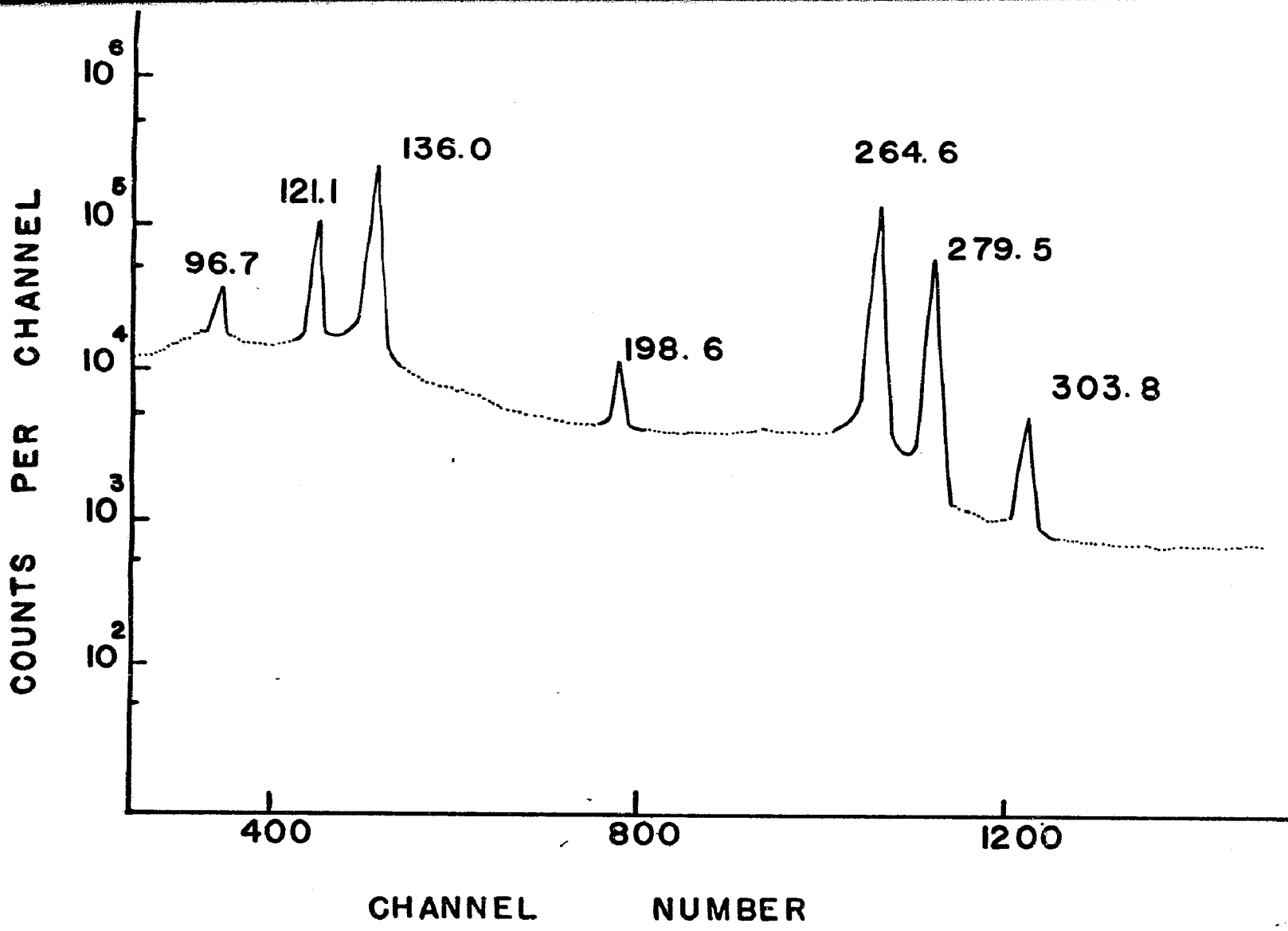


Fig. 18. Gamma ray spectrum of ^{75}Se obtained with the 29 cm^3 Ge(Li) detector. (Energy region 100-400 KeV, background has been subtracted.)

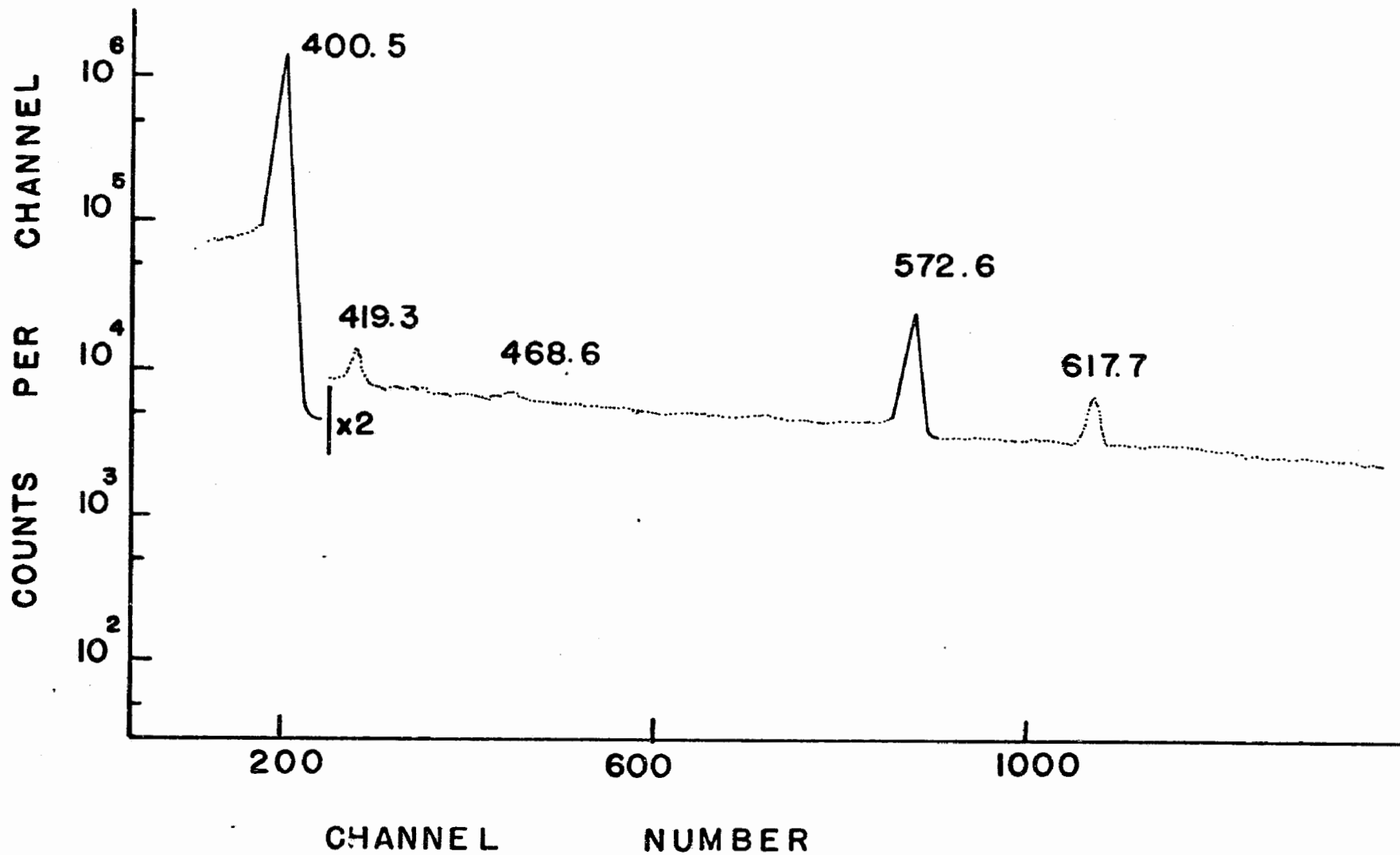


Fig. 19. Gamma ray singles spectrum of ^{75}Se obtained with the 29 cm^3 Ge(Li) detector. (Energy region: 400-700 KeV, background has been subtracted.)

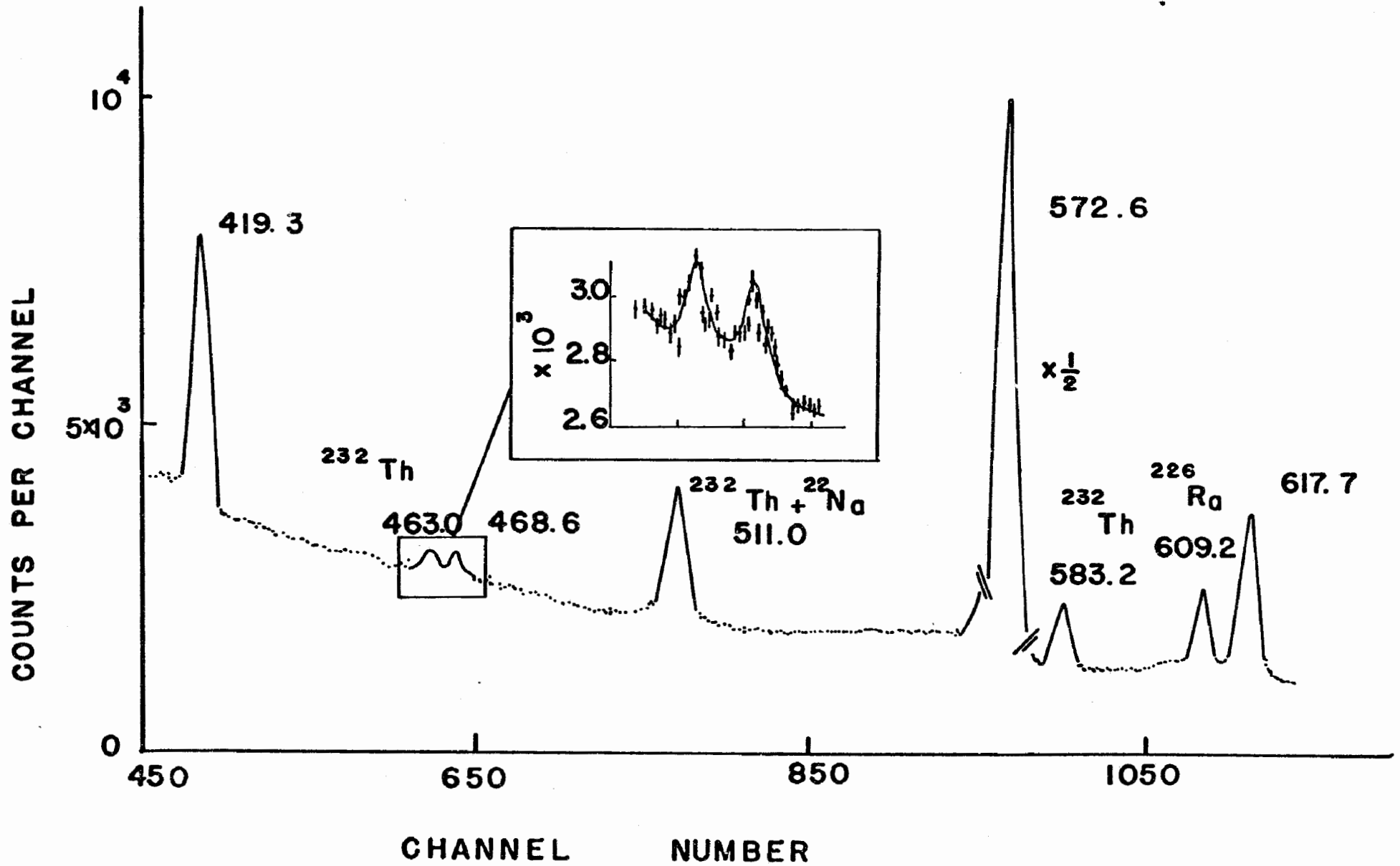


Fig. 20. Expanded gamma ray spectrum of ^{75}Se in the energy region 400 to 620 KeV as obtained with the $29\text{ cm}^3\text{ Ge(Li)}$ detector (48 hours counting period).

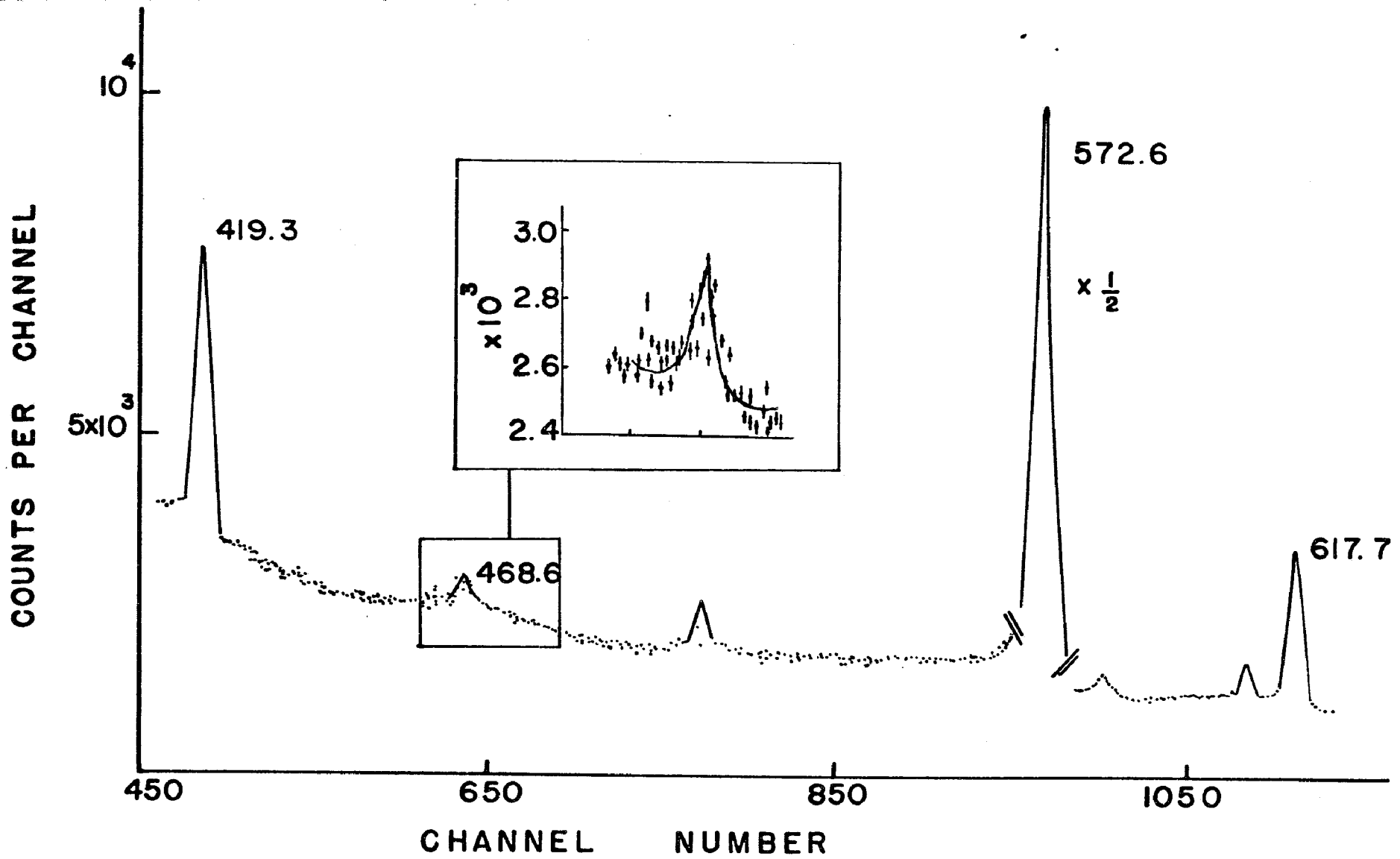


Fig. 21. The spectrum of Fig. 20 after a 32 hours subtraction period.

in the lead sheets used to shield the detector from the lower energy gamma rays. In Fig. (21), the same spectrum is shown after a 32 hour subtraction period. All the peaks which have been previously assigned to background activity are greatly reduced. The 463.0 KeV transition almost disappears while the 468.6 KeV peak has the same area ratio with respect to the 419.3 KeV transition. On these grounds the transition at 468.6 KeV is assigned to the decay of ^{78}Se . Ra and Th and daughter sources were used for energy calibration in this region. Intensities of the observed peaks were calculated from the relative areas under the photopeaks obtained from three different spectra. The areas under the photopeaks had been corrected for lead absorption using the Pb absorption coefficients obtained from ref. (43) and for the relative efficiency of the Ge(Li) detector. The energy and intensity values derived are listed in Table 19 and are compared with the results of other workers. The upper limit for any other transition above 600 KeV still unobserved is 0.001.

5.1.2. Coincidence experiments

The level structure of ^{75}As is well known from previous studies and coincidence experiments are not expected to yield any impressive new results. In the present work coincidence experiments have been carried out. In two of these experiments a careful search for the still unobserved 81 KeV transition has been made. In the third experiment an attempt was made to establish the newly observed 24.4 KeV transition.

Table 19

Energy and intensity of gamma rays in ^{75}Se

(40)

(39)

(41)

Present work		Rao et al	Edward and Galagher	USSR Lab of Neutron Physics
Energy in KeV	Intensity (a)	Intensity	Intensity	Intensity
K X-rays	90.3±2.6	94.0±2.4	---	81±10
24.4±0.1	0.044±0.006	<10 ⁻³	---	---
66.0±0.1	1.72±0.04	1.64±0.05	1.6±0.6	1.7±0.1
81.0±0.2	0.015±0.003 (b)	<10 ⁻⁵		<0.15
96.7±0.1	5.12±0.10	5.33±0.16	5.6±0.2	5.7±0.2
121.1±0.1	27.70±0.50	27.8±0.8	28.0±0.6	26.5±1.0
136.0±0.1	95.00±1.80	94.9±2.0	95.5±1.8	91.8±2.0
198.6±0.1	2.38±0.07	2.28±0.05	2.4±0.1	2.6±0.2
264.6±0.1	100.0	100.0	100.0	100.0
279.5±0.2	42.0±0.80	43.0±0.9	42.2±0.6	43.7±2.0
303.8±0.2	2.19±0.07	2.39±0.05	2.29±0.14	2.25±0.1
373.0	<0.006	----	---	0.3±0.22
400.5±0.2	20.4±0.50	22.3±0.5	19.5±0.6	18.6±1.0
419.0±0.3	0.023±0.002	0.0326±0.0060	---	----
468.6±0.4	0.001±0.0005 (c)	---	---	<0.008
572.6±0.2	0.063±0.002	0.0636±0.0013		0.07
617.7±0.2	0.0075±0.0002	0.0077±0002		0.01

(a) Errors quoted are one standard deviation of the mean results

(b) Value deduced from coincidence experiments

(c) Error quoted here is the uncertainty

It is apparent from the singles spectroscopy experiments described in the previous section that the inability to observe the weak 81 KeV transition of ^{75}Se is mainly due to strong Compton peaks arising from the 121 and 136 KeV transitions which mask completely the transition under consideration.

If a coincidence experiment is planned in such a way that the Compton peaks are suppressed while the 81 KeV transition is unaffected, then in principle it should be possible to observe this transition. To do that it is useful to have a closer look at the decay scheme of ^{75}Se shown in Fig. (25). For a long time it was established that the first excited state in ^{75}As is the 198.6 KeV level which deexcites through the 198.6 KeV transition. This level is fed through two weak transitions (35-42) at 419.3 and 66.0 KeV. If the 81 KeV transition (35-42) exists it may also feed this level. Thus, in a coincidence experiment in which a gate is set on the 198.6 KeV transition, it is expected that these three weak transitions will appear in the final coincidence spectrum. The 66 KeV transition, as it is shown in Fig.(25) is in cascade with the strong 136 KeV transition, through the 264.6 KeV level. But since the branching ratio for the 66 KeV transition is very small, the contribution made by the 136 KeV transition in the coincidence spectrum through this cascade is small and hence may lead to a very diminished Compton peak in the final spectrum.

In the coincidence experiment, the 29 cm³ Ge(Li) detector and the 0.39 cm³ Ge(Li) X-ray spectrometer were used. The 29 cm³ detector was used to gate the 198.6 KeV gamma ray while the coincidence spectrum was

observed with the X-ray spectrometer. The source was placed between the two detectors and at a distance of about 5 cm from each detector. The detectors were in a face to face geometry. No special precautions were taken in this experiment to avoid crystal to crystal scattering. The resolving time of the coincidence unit was set at about 120 ns. The ratio of true to chance coincidences was 10:1. The spectrum obtained after 80 hours counting period is shown in Fig. (22). A peak is observed in the final spectrum, at 81.0 ± 0.2 KeV which is probably the 80.9 KeV transition observed in the conversion electron spectra of ^{75}As . After subtraction of the random events and the contribution due to Compton photons scattered in the gate, the intensity of this newly observed transition was determined by comparison with the area and intensity of the 66 KeV transition (see Appendix E). The value obtained for the intensity of the 81.0 KeV transition observed here is 0.017 ± 0.003 (relative to the 264 KeV transition(100)). This value compares favourably with the value of 0.014 ± 0.002 obtained in the conversion electron investigation of ^{75}Se by Gasior et al ⁽⁴²⁾.

Due to the long counting periods necessary for this experiment, precautions were taken with respect to the stability of the system. During the experiment, the gate and output of the X-ray spectrometer were monitored frequently against drifts with the aid of a 400 channel analyzer. No noticeable change was detected in both the gain and the zero level of the electronic system of the two detectors. The possibility that the observed 81.0 KeV peak is due entirely or to a great

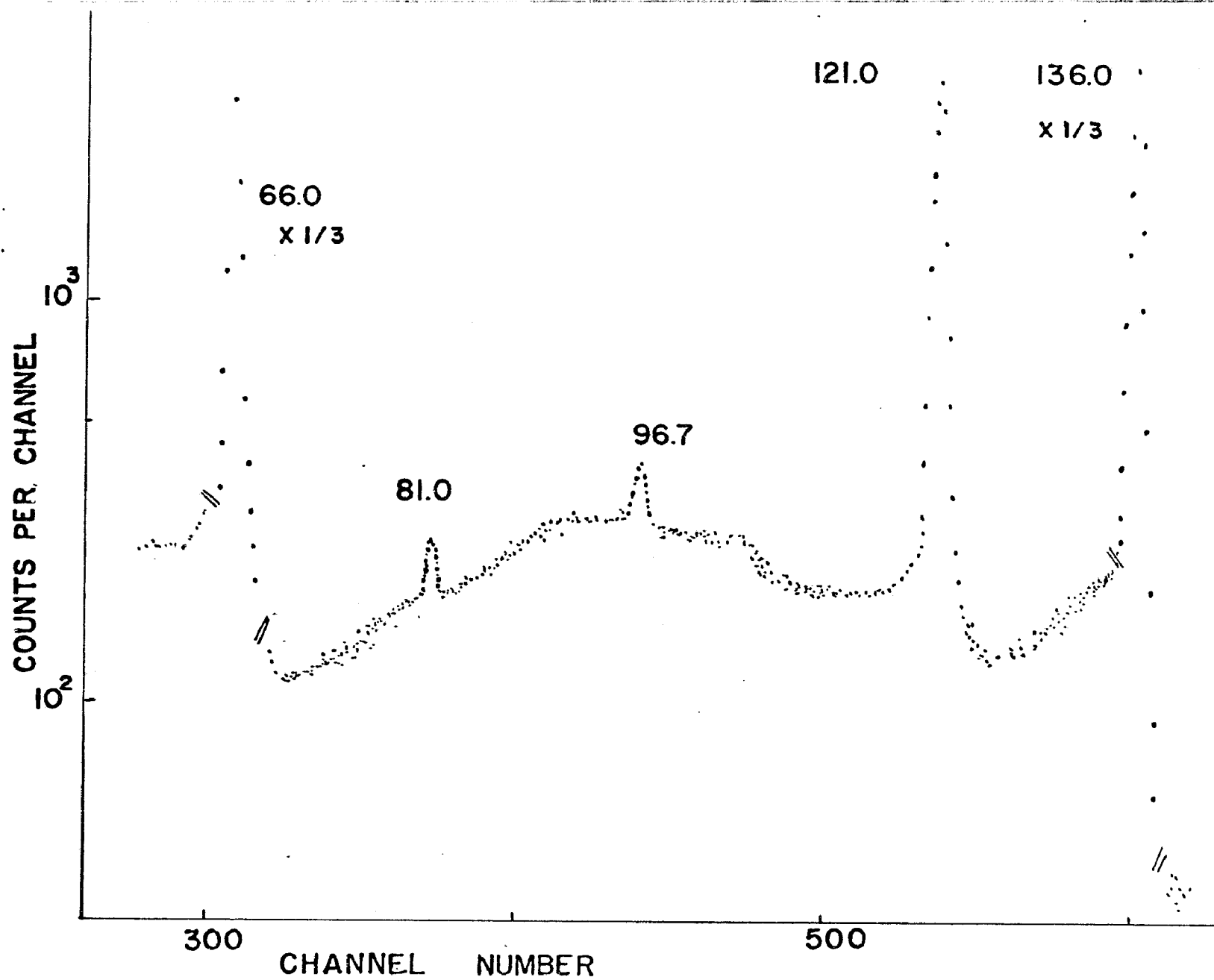


Fig. 22. Gamma rays in ^{75}Se in coincidence with the 1986 KeV transition. Only the part of the spectrum from 66 to 121 KeV is shown.

extent to 81.0 KeV Compton photons arising from crystal to crystal scattering of the 279.5 KeV gamma ray is considered to be very small due to the strong absorption of the 81 KeV quanta by the Ge(Li) crystal.

Nevertheless a second coincidence experiment was carried out to test the assumption made. In this experiment a lead absorber of 1 cm thickness with a 5 mm hole in diameter at the center was used to shield the front face of the 29 cm³ Ge(Li) detector. The source was centered at the hole facing the X-ray spectrometer which was set at a distance of about 3 cm from the source. The resulting counting rate was much lower than in the former experiment. During the long period necessary for this experiment precautions were also taken, similar to the ones described previously, to monitor probable shifts. The spectrum obtained after 160 hours of counting period is shown in Fig. (23). The 81.0 KeV peak is again observed. The intensity of this transition as deduced from this experiment after the necessary corrections is 0.013 ± 0.004 , in agreement with the value obtained previously. The average value of 0.015 ± 0.003 is adopted in this work for the intensity of this transition. This value is listed in Table 19.

Finally in order to establish the newly observed 24.4 KeV transition, a new coincidence experiment was carried out. The gate was set at the 29 cm³ Ge(Li) detector on the 279.5 KeV peak. The coincidence spectrum was obtained with the X-ray spectrometer. The spectrum obtained after 48 hours of counting is shown in Fig. (24). The same spectrum indicates also that the 121.1 KeV transition is in strong

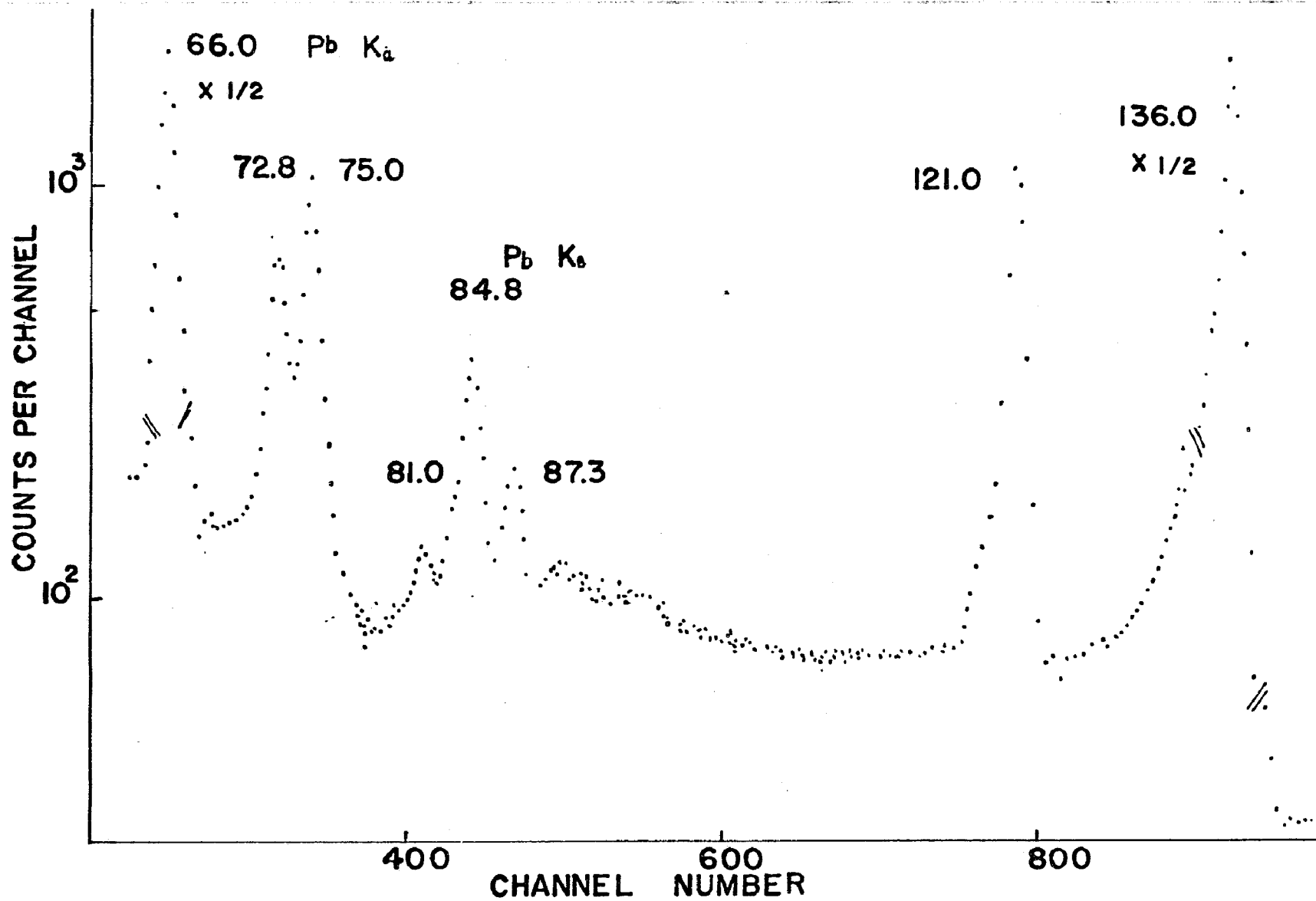


Fig. 23. Gamma rays in ^{75}Se in coincidence with the 1986 KeV transition. In this experiment a lead absorber was used to shield the two detectors. (See text for discussion.)

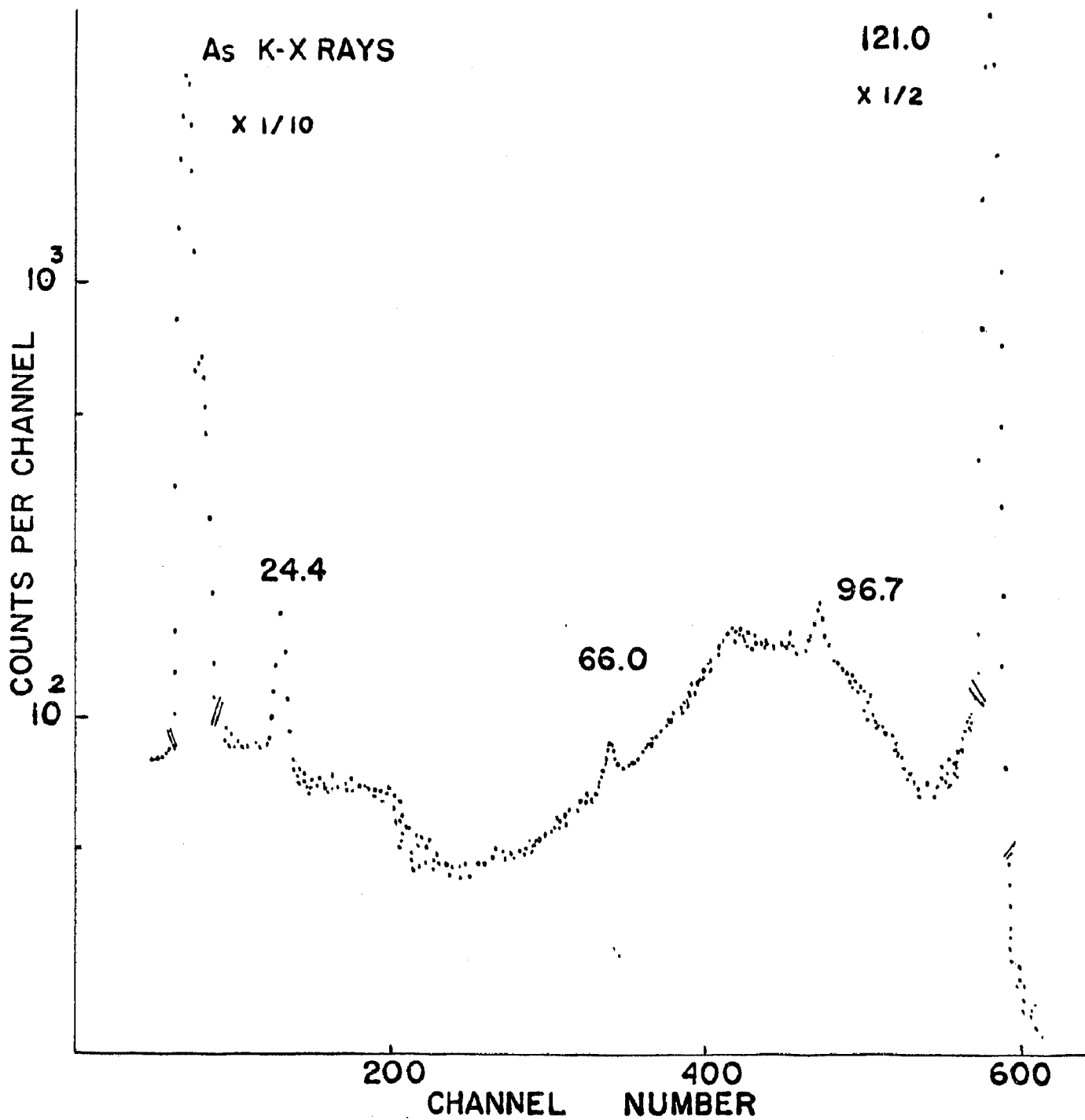


Fig. 24. Gamma rays of ^{75}Se in coincidence with the 2795 KeV transitions. The part of the spectrum up to 125 KeV is only shown.

coincidence with the 279.5 KeV gamma ray. After the necessary corrections, the value for the intensity of the 24.4 KeV transition as obtained from this coincidence experiment is found to be 0.045 ± 0.008 , in agreement with the value of 0.044 ± 0.006 obtained from the singles spectra.

5.1.3. Internal conversion coefficients

The accurate intensity measurements of the transitions in ^{75}As as obtained in this work may be used to obtain the internal conversion coefficients of these transitions.

From the definition of the electron K-conversion coefficient

$$a_k = \frac{I_k^e}{I_\gamma} \quad \dots \quad (5.1)$$

the ratio of the electron intensity of two transitions may be obtained and is given by

$$\frac{I_k^e(x_1)}{I_k^e(x_2)} = \frac{I_\gamma(x_1)\alpha_k(x_1)}{I_\gamma(x_2)\alpha_k(x_2)} \quad \dots \quad (5.2)$$

The intensities of the conversion electron transitions in ^{75}As were obtained from the data of Grigoriev and Zolotavin ⁽³⁵⁾, Edwards and Gallagher ⁽³⁹⁾ and Gasior et al ⁽⁴²⁾. The reported intensities were averaged out and the obtained values are given in Table 20. The intensities listed in Table 20 are normalized to 100 for the intensity of the 264 KeV transition. The K-conversion coefficient for the ^(35,36,39,42) 264.6 KeV transition has been measured by several workers

Table 20

(a)

Internal conversion electron intensities

Transition in KEv	K	L+M
24.3	1250±150 (b)	375±39 (b)
66.05	72.3±1.0	1.6±0.4
80.90	4.0±0.5 (c)	
96.70	724±69	118±18
121.1	174±17	21.3±3.4
136.0	399±32	49.4±4.3
198.6	7.36±0.41	0.86±0.04
264.6	100.0	10.4±0.7
279.6	52.5±2.3	6.5±0.2
303.8	16.6±0.5	2.56±0.23
400.7	3.71±0.04	0.433±0.011
419.6	0.0066±0.0007 (c)	0.0013±0.0004 (c)
572.5	0.0099±0.0009	
618.0	0.00085±0.0009 (c)	

(a) Unless otherwise specified these are the average of the values reported in refs. (35,39,42). Errors quoted are one s.d. of the average.

(b) = from ref. (35)

(c) = from ref. (42)

The average value of $(6.22 \pm 0.13) \times 10^{-3}$ of these measurements is used for the conversion coefficient of the 264.6 KeV transition.

The K-conversion electron intensities listed in Table 20, the $a_k(264) = (6.22 \pm 0.13) \times 10^{-3}$ value and the gamma ray intensity measurements of the present work listed in Table 19 are used in equation (5.2) to determine the K-conversion coefficients of the various ^{75}As transitions. The calculated values are listed in Table 21, and are compared with the results of other workers. In Table 22 the theoretical K-conversion coefficients ⁽⁴⁴⁾ for E1, E2, M1, and M2 transitions are also given. By comparing the calculated with the theoretical K-conversion coefficients, the possible multipolarities of the transitions are deduced and listed also in Table 22.

The results obtained indicate the possible pure E1 character of the 121.1, 136 and 400.5 KeV transitions. The K-conversion coefficient for the 24.4 KeV transition indicates a pure M2 transition, while the coefficients for the 81 KeV and 303 KeV transitions indicate a pure E2 and E3 character respectively.

The experimental error of the K-conversion coefficient of the 96.7 KeV transition does not allow a choice between an E2 and M2 character. On the grounds of other nuclear properties of the 400.5 KeV level which is deexcited partly through the 96.7 KeV transition, the M2 character for this transition may be ruled out, as shown in more detail later.

The calculated multipolarities M1 + 0.2% E2 and M1 + 20.0% E2

Table 21

K conversion coefficients of the transitions in ^{75}As

Transition in KeV	Experimental K conversion coefficient			Present work
	Grigoriev et al ⁽³⁵⁾	Edwards et al ⁽³⁹⁾	M. Gasior et al ⁽⁴²⁾	
24.4	----	----	----	178±31
66.0	$(3.0\pm 0.3)\times 10^{-1}$	$(3.6\pm 0.5)\times 10^{-1}$	$(2.66\pm 0.10)\times 10^{-1}$	$(2.63\pm 0.1)\times 10^{-1}$
81.0	----	----	----	1.65±0.35
96.7	$(7.6\pm 0.5)\times 10^{-1}$	$(8.1\pm 0.7)\times 10^{-1}$	$(8.3\pm 0.2)\times 10^{-1}$	$(8.8\pm 1.0)\times 10^{-1}$
121.1	3.7×10^{-2}	4.06×10^{-2}	$(3.0\pm 0.3)\times 10^{-2}$	$(4.05\pm 0.17)\times 10^{-2}$
136.0	2.5×10^{-2}	2.4×10^{-2}	$(2.74\pm 0.10)\times 10^{-2}$	$(2.86\pm 0.11)\times 10^{-2}$
198.6	$(1.8\pm 0.2)\times 10^{-2}$	$(1.8\pm 0.2)\times 10^{-2}$	$(1.95\pm 0.15)\times 10^{-2}$	$(1.92\pm 0.12)\times 10^{-2}$
264.6	$(6.5\pm 0.4)\times 10^{-3}$	$(6.0\pm 0.5)\times 10^{-3}$	$(6.0\pm 0.2)\times 10^{-3}$	$(6.22\pm 0.13)\times 10^{-3}$ (a)
279.5	$(7.8\pm 0.8)\times 10^{-3}$	$(7.6\pm 0.9)\times 10^{-3}$	$(7.9\pm 0.4)\times 10^{-3}$	$(7.78\pm 0.40)\times 10^{-3}$
303.8	$(4.3\pm 0.6)\times 10^{-2}$	$(4.5\pm 0.6)\times 10^{-2}$	$(4.3\pm 0.4)\times 10^{-2}$	$(4.72\pm 0.23)\times 10^{-2}$
400.5	1.1×10^{-3}	$(1.1\pm 0.1)\times 10^{-3}$	$(1.05\pm 0.10)\times 10^{-3}$	$(1.14\pm 0.04)\times 10^{-3}$
419.3	----	----	$(1.36\pm 0.15)\times 10^{-3}$	$(1.79\pm 0.36)\times 10^{-3}$
572.6	$(1.9\pm 1.3)\times 10^{-3}$	----	$(1.0\pm 0.1)\times 10^{-3}$	$(1.00\pm 0.10)\times 10^{-3}$
617.7	----	----	$(6\pm 1)\times 10^{-4}$	$(7.0\pm 1.0)\times 10^{-4}$

(a) average of several available experimental values as listed in refs. (35,36,39,42)

Table 22

Experimental and theoretical K conversion coefficients in ^{75}As
(a)

Transition in KeV	Present work	Theoretical K conversion coefficient				Multipolarity
		E1	M1	E2	M2	
24.4	178±31	4.0	4.5	80	168	M2
66.0	(2.63±0.1)×10 ⁻¹	2.25×10 ⁻¹	2.5×10 ⁻¹	3.1	3.9	M1 + 0.5% E2
81.0	1.65±0.35	1.2×10 ⁻¹	1.4×10 ⁻¹	1.45	17.0	E2
96.7	(8.8±1.0)×10 ⁻¹	7.2×10 ⁻²	8.7×10 ⁻²	7.8×10 ⁻¹	9.5×10 ⁻¹	E2
121.1	(4.05±0.17)×10 ⁻²	3.6×10 ⁻²	4.8×10 ⁻²	3.4×10 ⁻¹	4.8×10 ⁻²	E1
136.0	(2.86±0.11)×10 ⁻²	2.6×10 ⁻²	3.5×10 ⁻²			E1
198.6	(1.92±0.12)×10 ⁻²	9×10 ⁻³	1.3×10 ⁻²	5.6×10 ⁻²	8×10 ⁻²	M1 + 14.5% E2
264.6	(6.22±0.13)×10 ⁻³	3.65×10 ⁻³	6.2×10 ⁻³	1.9×10 ⁻²	3.2×10 ⁻²	M1 + 0.2% E2
279.5	(7.78±0.40)×10 ⁻³	3.15×10 ⁻³	5.5×10 ⁻³	1.6×10 ⁻²	2.6×10 ⁻²	M1 + 20% E2
303.8	(4.72±0.23)×10 ⁻²					E3
400.5	(1.14±0.04)×10 ⁻³	1.2×10 ⁻³	2.3×10 ⁻³	4.7×10 ⁻³	8.4×10 ⁻³	E1
410.3	(1.79±0.36)×10 ⁻³	1.05×10 ⁻³	2.05×10 ⁻³	4×10 ⁻³	7.1×10 ⁻³	M1 + 5% E2
572.6	(1.00±0.10)×10 ⁻³	4.5×10 ⁻⁴	1.02×10 ⁻³	1.52×10 ⁻³	3.0×10 ⁻³	M1
617.7	(7.0±1.0)×10 ⁻⁴	3.9×10 ⁻⁴	8.0×10 ⁻⁴	1.3×10 ⁻³	2.6×10 ⁻³	M1

(a) obtained from ref. (44)

(b) average of several available experimental values as listed in refs.(35,39,42)

for the 264.6 and 279.1 KeV transitions are in very good agreement
 (45)
 with the recently reported values $M1 + 0.2\% E2$ and $M1 + (13.5 \pm 8.6)\% E2$
 obtained from angular correlation experiments.

The present data further support a $M1 + 14.5\% E2$ multipolarity for
 the 198.6 KeV transition. The two weak transitions at 572.6 and 617.7
 KeV have a K-conversion coefficient compatible with an M1 character.
 Finally the calculated conversion coefficient for the 419.3 KeV transi-
 tion indicates an M1 character with a possible 5% maximum E2 admixture.

The internal conversion coefficients may be calculated from the
 K ICC by employing the relation given by

$$a_t = a_k \frac{(K+L+M+\dots)}{K} \dots \dots \dots (5.3)$$

The conversion intensity ratios $\frac{K+L+M+\dots}{K}$ were obtained either from
 the experimental data of Table 20 or from the theoretical data of
 ref. (44). Wherever experimental data were used, the ratio included
 only L and M intensities. The influence of the omitted N, O... inten-
 sities is expected to be of second order and of no importance for the
 present results. These ratios and the calculated total conversion
 coefficients are given in Table 23.

5.1.4. The disintegration of ^{75}Se

The data obtained in this work are in good agreement with those of
 others. The decay scheme for ^{75}Se , which is supported from the present
 data is shown in Fig. (25). The weak transition observed for the first

Table 23

Conversion intensity ratios and internal conversion coefficients

in ^{75}As

Transition in KeV	K+L+M/K	a_t
24.4	(a) 1.21	216±37
66.0	(b) 1.16	0.305±0.012
81.0	(c) 1.17	1.92±0.45
96.7	(b) 1.16	1.02±0.12
121.1	(b) 1.12	(4.36±0.45)×10 ⁻²
136.0	(b) 1.12	(2.91±0.22)×10 ⁻²
198.6	(b) 1.12	(2.14±0.13)×10 ⁻²
264.6	(b) 1.10	(6.84±0.14)×10 ⁻³
279.5	(b) 1.12	(8.71±0.45)×10 ⁻³
303.8	(b) 1.16	(5.46±0.26)×10 ⁻²
400.5	(d) 1.12	(1.28±0.05)×10 ⁻³
419.3	(d) 1.10	(1.97±0.37)×10 ⁻³
572.6	(d) 1.10	(1.10±0.11)×10 ⁻³
617.7	(d) 1.10	(7.7±1.1)×10 ⁻³

(a) Theoretical value for an M2 transition. The only available experimental result is by Grigoriev et al.⁽³⁵⁾ and is 1.43±0.30.

(b) Experimental value obtained from Table 20.

(c) Theoretical value obtained from ref.(44) for a pure E2 transition.

(d) Theoretical value for M1 transition obtained from ref. (44).

time in this work at 468.6 KeV is shown in Fig. (25) to deexcite a newly introduced level at 468.6 KeV. Data obtained by Scharadt (46) and Welker (47) in the decay of ^{75}Se and Robinson et al in Coulomb excitation experiments support the existence in ^{75}As of a 468.6 KeV level with a probable spin and parity assignment $(1/2^-)$.

The 24.4 KeV transition observed in this work fits exactly between the 303.8 and 279.5 KeV levels. Finally the weak transition observed in the coincidence spectra with an energy of 81.0 KeV fits exactly between the 279.5 and 198.6 KeV levels. Both these assignments are in agreement with the present coincidence data.

The spin and parity of most of the observed levels in ^{75}As (35-42) have been well established in the past (15). The ^{75}As ground state spin has been measured and found to be $3/2^-$.

The multipolarities of transitions of energy less than 400 KeV as determined in Table 22 are consistent with the spin assignments shown in the decay scheme of Fig. (25). The 96.7 KeV transition proceeds from the $5/2^+$ 400 KeV level to the 303.8 KeV $9/2^+$ level and thus the suggested multipolarity for this transition is a mixture of E2 and M3. The K-conversion coefficient value obtained from Table 21 for the 96.7 KeV transition suggests an E2 multipolarity.

The $5/2^-$ spin and parity assignment for the 572.6 KeV level (see Fig. (25)) is compatible with the M1 character of this transition suggested by the data presented in Table 22.

The 617.7 KeV level is deexcited through the 419.6 KeV and 617.7 KeV transitions. The data of Table 22 suggest an M1 and possibly some E2 admixture for the multipolarity of the 419.3 KeV transition, which feeds the $1/2^-$ 198.6 KeV level. This indicates a spin change 0,1 between the 617.7 and 198.6 KeV level, suggesting $1/2^-$, $3/2^-$ spin and parity assignment for the 617.7 KeV level. The data of Table 22 suggest an M1 character for the 617.7 KeV transition which is compatible with a ($1/2^-$, $3/2^-$, $5/2^-$) spin and parity assignment of the 617.7 KeV level. Thus the possible spin and parity assignment for this level is either $1/2^-$ or $3/2^-$.

(48)

Recent data by Nagpal indicate transitions at 335.1, 415.0, 419.9, 485.8, 528.5, 535.8, 543.03 and 556.6 KeV in the decay of ^{75}Se . None of the above transitions has been observed in the present work. Some of these peaks have been observed initially but they have been eliminated as soon as lead absorbers and the gain stabilizer were utilized. Thus it is concluded that the above mentioned peaks are a result of chance summing and instrumental drifting. Recently the same conclusions have been independently reached by D. Raeside et al .

(45)

The electron capture branching to the excited states of ^{75}As has been calculated using the gamma ray intensities obtained in this work and the total conversion-conversion coefficients obtained from Table 23.

The number of electron captures x_i which lead to an ^{75}As level x_i may be calculated by the relationship given by

$$x_i \equiv \sum_i I^i [1 + a_t(i)] \cdot K - \sum_{i'} I^{i'} [1 + a_t(i')] \cdot K \dots (5.4)$$

where I^i and $I^{i'}$ are the relative intensities of the transitions depopulating and populating a given level respectively. The constant K transforms the relative intensity I of a given transition to the absolute transition $I \cdot K$ per 100 disintegrations of the parent nucleus.

Here the constant K may be calculated from the known relative intensity of the K X-rays. If the K -capture probability to a level x of ^{75}As is $p_i(x)$ and the fluorescence yield of the K X-rays of As is f_k , then it can be easily established that

$$100 p_i f_k + \sum_i I^i \alpha_k \cdot K \cdot f_k = I_x \cdot K \dots (5.5)$$

The value $p_i(400) = 0.885$ for the K -capture probability to the (40) 400 KeV level of ^{75}As has been measured by Rao et al. In this work this value is adopted for all K -captures leading to any of the other levels in As . The value of $f_k = 0.52$ was obtained from ref.(15). Using the relative intensity and K conversion coefficients for the As transitions from Tables 19 and 21, equation (5.5) yields the value of $K = 0.568 \pm 0.016$.

Equation (5.5) is thus used and the branching ratios to the ^{75}As levels are calculated. The values obtained are listed in Table 24 and compared with the results of other workers. The data indicate a weak feeding of the ground state in ^{75}As . Almost 90% of the transitions feed the $5/2^+$ 400.5 KeV level. Evidences of a weak feeding of the $1/2^-$

Table 24

Electron capture branching ratios in ^{75}Se

^{75}As level in KeV	Branch % This work	Branch % Rao et al ⁽⁴⁰⁾	Branch % USSR Lab of Neutron Phys (41)	Logft (this work)
0	(4.0±3.0)	5.8±1.8	<8	7.9
198.6	0.07±0.05	0.05±0.04	<0.2	>9.2
264.6	3.1±1.1	2.8±1.7	3.0	7.65
279.5	2.3±0.9	4.9±0.8	2.0	7.75
303.8	0.88±0.71	0.36±0.57	<2	>8.0
400.5	89.6±3.0	86.1±2.0	94	6.0
468.6	0.0007±0.0003		<0.005	>10.8
572.6	0.036±0.001	0.035±0.001	0.06	9.0
617.7	0.017±0.001	0.022±0.001	0.02	9.2

198.6 KeV, and 303.8 KeV levels are also indicated.

The branching ratios deduced in this work have been used to calculate the logft values of the EC transitions from ^{75}Se to the levels of ^{75}As . The energy available for the EC is 865 KeV, a value obtained from ref. (15). The Moszkowski diagrams from ref.(15) were used to calculate the logft values listed in Table 24.

The spin and parity of the ground state of ^{75}Se has been measured ⁽¹⁵⁾, and it was found to be $5/2^+$. The logft value of 6.0 for the transition ⁽⁴⁸⁾ to the $5/2^+$ level in ^{75}As is then consistent with an allowed transition. The logft values for the transitions to the $3/2^-$ ground state, $3/2^-$ 264.4 and $5/2^-$ 279.5 KeV levels are in good agreement with the ⁽⁴⁹⁾ expected logft value of 7 ± 1 for a first forbidden transition.

The derived logft values for the transition leading to the 198.6 KeV level in ^{75}As are in good agreement with the expected value for a unique first forbidden transition. The derived logft value to the 468.6 KeV level is somewhat larger than the expected value for a unique first forbidden transition suggested by the probable $(1/2)^-$ spin and parity assignments for this level, but is not unreasonable. The logft values to the 572.6 and 617.7 KeV levels are somewhat larger than the values suggested by a first forbidden transition indicated by the possible spin and parity assignments of these levels, but again they cannot be considered as totally unreasonable.

Finally the $9/2^+$ spin assignment for the 303.8 KeV level indicates that the transition leading to this As level may be a second forbidden

Table 25

Absolute intensities of the ^{75}As gamma rays
(per hundred disintegrations of the parent nucleus)

Energy in KeV	Intensity
K X-rays	51.4±2.1
24.4	0.025±0.003
66.0	0.976±0.038
81.0	0.0097±0.0002
96.7	2.91±0.10
121.1	15.62±0.53
136.0	54.00±1.9
198.6	1.36±0.05
264.6	56.8±1.6
279.5	23.9±0.8
303.8	1.24±0.05
400.5	11.6±0.4
419.3	0.013±0.001
468.6	0.0006±0.0003
572.6	0.036±0.002
617.7	0.0043±0.0002

(49)
 transition with an expected $\log ft \approx 13$. The derived $\log ft$ value is about 8.0 but the large experimental error associated with the branching estimate indicates that the $\log ft$ may be a few orders of magnitude larger.

With the calculated value of the constant K, the absolute intensities of the ^{75}Se gamma rays are estimated. The absolute intensities obtained are given in Table 25.

5.1.5. Transition rates in ^{75}As

Recently the half lives of the 198.6, 264.6 and 280 KeV levels (50) (15) have been accurately measured. These data and the previously known half lives of the 400.5 and 303.8 KeV levels may provide useful information about the transition rates in ^{75}As .

Of special interest are the transition rates of M1 and E2 character occurring in ^{75}As . The transition probability of a given gamma transition L deexciting a given level with a measured half life $T_{1/2}$, is given by

$$T(L) = \frac{0.69}{T_{1/2}} \times \frac{I^L}{\sum_i I_i [1 + \alpha_L(i)]} \dots \dots \dots (5.6)$$

where the various symbols are defined as in equation (5.4).

With the known mixing ratio δ^2 of the L transition where δ^2 is given by

$$\delta^2 = \frac{T(E2)}{T(M1)} \equiv \frac{x}{100-x} \dots \dots \dots (5.7)$$

where x is the percentage of E2 admixture in the L transition, the partial transition probabilities for the corresponding M1 and E2 members of the transition L may be obtained from the equations given by

$$T(L) = \frac{\delta^2}{1+\delta^2} T(L) = \frac{x}{100} T(L) \dots \dots \dots (5.8)$$

and

$$T(M1) = \frac{1}{1+\delta^2} T(L) = \frac{1-x}{100} T(L) \dots \dots \dots (5.9)$$

The transition probabilities of the E2 and M2 transitions in ⁷⁵As have been calculated with the above equations and the pertinent quantities obtained from Tables 19 and 21. The results are shown in Table 26. In the same table the single particle estimates for the corresponding M1 and E2 transitions are given. The single particle estimates T(L) are obtained from the equations given by (17) Moszkowski . For these equations the statistical factor S was set equal to 1. In the same table the ratio of the experimental to the single particle estimates of the transition probabilities of the E2 transitions is given (enhancement factor) as well as the ratio of the single particle over the experimental transition probabilities for the M1 transitions (retardation factor).

The data of Table 26 indicate that the transition rates of the E2 transitions at 81, 96.7, 198.6 and 280 KeV are strongly enhanced, thus indicating the existence of strong collective effects. The small enhancement factor of the E2 264 KeV transition indicates a rather

Table 26

(a)

Transition rates of M1 and E2 gamma rays observed in ^{75}As

Transition E in KeV	δ^2 Present work	δ^2 Other sources	T(M1)exp tr/sec	T(M1)sp tr/sec	$\frac{T(M1)sp}{T(M1)exp}$	T(E2)exp tr/sec	T(E2)sp tr/sec	$\frac{T(E2)exp}{T(E2)sp}$
66	$(5 \pm \frac{3}{5}) \times 10^{-3}$	---	1.05×10^9	8.3×10^9	7.9	$<< 10^7$	3.0×10^4	---
81	pure E2	---	---	---	---	9.3×10^5	8.2×10^4	11
96.7	pure E2	---	---	---	---	1.2×10^7	2.0×10^5	60
198.6	$(1.7 \pm 0.3) \times 10^{-1}$	1.9×10^{-1} (b)	$(6.6 \pm 1.2) \times 10^8$	2.1×10^{11}	318	$(1.1 \pm 0.1) \times 10^8$	6.9×10^6	16 ± 2
264.6	$(2 \pm \frac{8}{2}) \times 10^{-3}$	$(2 \pm \frac{2.9}{1.6}) \times 10^{-3}$ (c)	6.1×10^{10}	5.2×10^{11}	8.5	1.2×10^8	3.0×10^7	4
280.0	$(2.5 \pm \frac{0.5}{0.7}) \times 10^{-1}$	$(1.5 \pm \frac{0.16}{0.08}) \times 10^{-1}$	$(2.0 \pm 0.3) \times 10^9$	6.2×10^{11}	310	$(3.0 \pm 0.5) \times 10^8$	4.0×10^7	7.5 ± 1.5

(a) The half lives of the levels have been obtained from ref. (15) and (50).

(b) = from ref. (15)

(c) = from ref. (45).

small collective character of this level.

The retardation factor for the 198.6 and 280 KeV levels is approximately 310, indicating again strong collective effects in the levels involved in these transitions. The retardation factor for the M1 66 and 264.6 KeV transitions is only about 8, indicating that these two transitions do not experience a strong influence of collective effects. The E2 component of the 264.6 KeV transition also indicated a very small influence of collective effects. Both the 66 and 264.6 KeV transitions deexcite the 264.6 KeV level. This level according to the data of Table 26 may be considered to have a structure close to one given by a single particle picture and thus the influence of collective effects on the 264.6 KeV level, if any, may be considered small.

The other transitions listed in Table 26 deexcite the 198.6, 280 and 400.5 KeV levels in ^{75}As . All three levels may be considered as collective in nature due to the large observed enhancement and retardation factors of the E2 and M1 transitions deexciting these levels.

Thus the level structure of ^{75}As may be well explained in the framework of the intermediate coupling model. This subject is discussed in full detail in Chapter 6.

5.2. The decay of ^{78}As

^{78}As decays with the emission of negatrons to the excited states
(15)
of ^{78}Se with a half life of 90 minutes. The decay of ^{78}As has been

studied in the past by Van Lieshout ⁽⁵¹⁾, Nemilov et al ⁽⁵²⁾ and
other workers ⁽⁵³⁾ with the help of NaI(Tl) and plastic detectors.

All the beta-decay data of ⁷⁸As exhibit numerous discrepancies.

With the exception of the well known levels at 614 and 1310 KeV in
⁷⁸Se, the previous studies of the decay of ⁷⁸As offered little infor-
mation on the level structure of ⁷⁸Se as compared with the information
available from (p,p'), (d,d') and (d,p) reactions ⁽⁵³⁾.

In the present work radioactive ⁷⁸As was produced by neutron acti-
vation of samples containing Br and Se. The 14 MeV neutron flux of the
USRC neutron generator was used. In the case of Br the reaction
⁸¹Br(n, α)⁷⁸As was used. The cross section value reported for this reac-
tion ⁽⁵⁴⁾ is 14 mb. From Se the ⁷⁸As activity is produced by the
⁷⁸Se(n,p)⁷⁸As reaction. The cross section value reported for this
reaction ⁽⁵⁵⁾ is (22 \pm 2) mb.

In both cases natural Br and Se were used in the form of spec. pure
NaBr and SeO₂. Amounts up to six grams were used. A plastic vial con-
taining the sample to be activated was placed in front of the target of
the neutron generator.

The sample was receiving a neutron flux of 10⁹ncm⁻² sec⁻¹. Irra-
diating periods ranging from 30 to 80 minutes were used. The duration
of the irradiation was determined mainly by the vacuum condition of the
neutron generator assembly. After the end of the irradiation, the vial
containing the produced radioactivity was transferred to the counting
room and placed close to the front face of the 29 cm³ CI Ge(Li) detector.
A lucite absorber in the form of a disk of 1 cm thickness was used.

This lucite disk was placed in contact with the detector completely covering its face, in order to absorb electrons of low energy, thus preventing possible distortion of the lower gamma ray spectrum. The radioactive source in most cases was in contact with the lucite disk.

The pulses from the amplifier were fed into the biased amplifier. The settings of the amplifier were adjusted so that the desired part of the spectrum could be displayed in the 2048 channel analyzer by adjusting the bias level and the stretcher dials of the biased and stretcher amplifier. When irradiated samples of SeO_2 were used, two positions of the bias and stretcher dials were chosen so that the energy regions from 0 to 1.6 MeV and 1 MeV to 3.2 MeV could be displayed in the analyzer. In the case of the Br targets a somewhat similar procedure was followed. This choice of the energy settings reduces the resolution of the system somewhat but at the same time lowers the cost of the experiment by reducing the number of necessary irradiations without affecting the reliability of the results. The total resolution of the system was about 4.0 KeV at 1332 KeV. In the Br irradiation experiments the main impurities detected were ^{80}Br and ^{82}Br with corresponding half lives of 4.4 and 36 hours respectively. Both isotopes have a fairly well known decay scheme ⁽¹⁵⁾. The most prominent peak of ^{80}Br is the strong 617.0 KeV gamma ray which interferes with the 614.0 KeV prominent peak of ^{78}As . For this reason it is difficult to normalize the intensity of the gamma rays of ^{78}As directly to the 614.0 KeV transition in ^{78}As , when ^{78}As is produced via the $^{81}\text{Br}(n,\alpha)^{78}\text{As}$ reaction.

In the Se irradiation experiments $^{81m,8}\text{Se}$, ^{77}Ge , $^{73g-m}\text{Se}$ and ^{76}As impurities are produced with half lives of 57 minutes, 18.5 minutes, 11.3 hours, 42 minutes, 7 hours and 26.5 hours respectively. From the singles spectra obtained in these experiments it was found that the amounts of ^{77}Ge and ^{76}As were small, less than 10% of the produced ^{78}As activity, one hour after the end of irradiation. Both of these activities are easily recognized because of their long half lives. From the other activities produced, the ^{81}Se activity was the most prominent. The well known half life and decay scheme (56,57) of ^{81}Se simplified the identification of the components of this activity.

The general procedure used in the present experiments was the identification of the peaks by half life measurements. For this purpose the activated target was counted over periods of four to five half lives. The duration of each counting interval was longer than the preceding one, in order to accumulate a satisfactory number of counts under each photopeak. Half life measurements were systematically used when ^{78}As activity was produced via the $^{78}\text{Se}(n,p)^{78}\text{As}$ reaction. The $^{81}\text{Br}(n,\alpha)^{78}\text{As}$ reaction was used mainly to check the results obtained from the $^{78}\text{Se}(n,p)^{78}\text{As}$ reaction.

5.2.1. Low energy single spectroscopy (<1 MeV)

The spectrum obtained from the irradiated SeO_2 target for the energy region from 0.5 to 1 MeV after a 20 minute counting period is shown in Fig. (26). The peaks at 614.1 and 694.8 KeV are well known

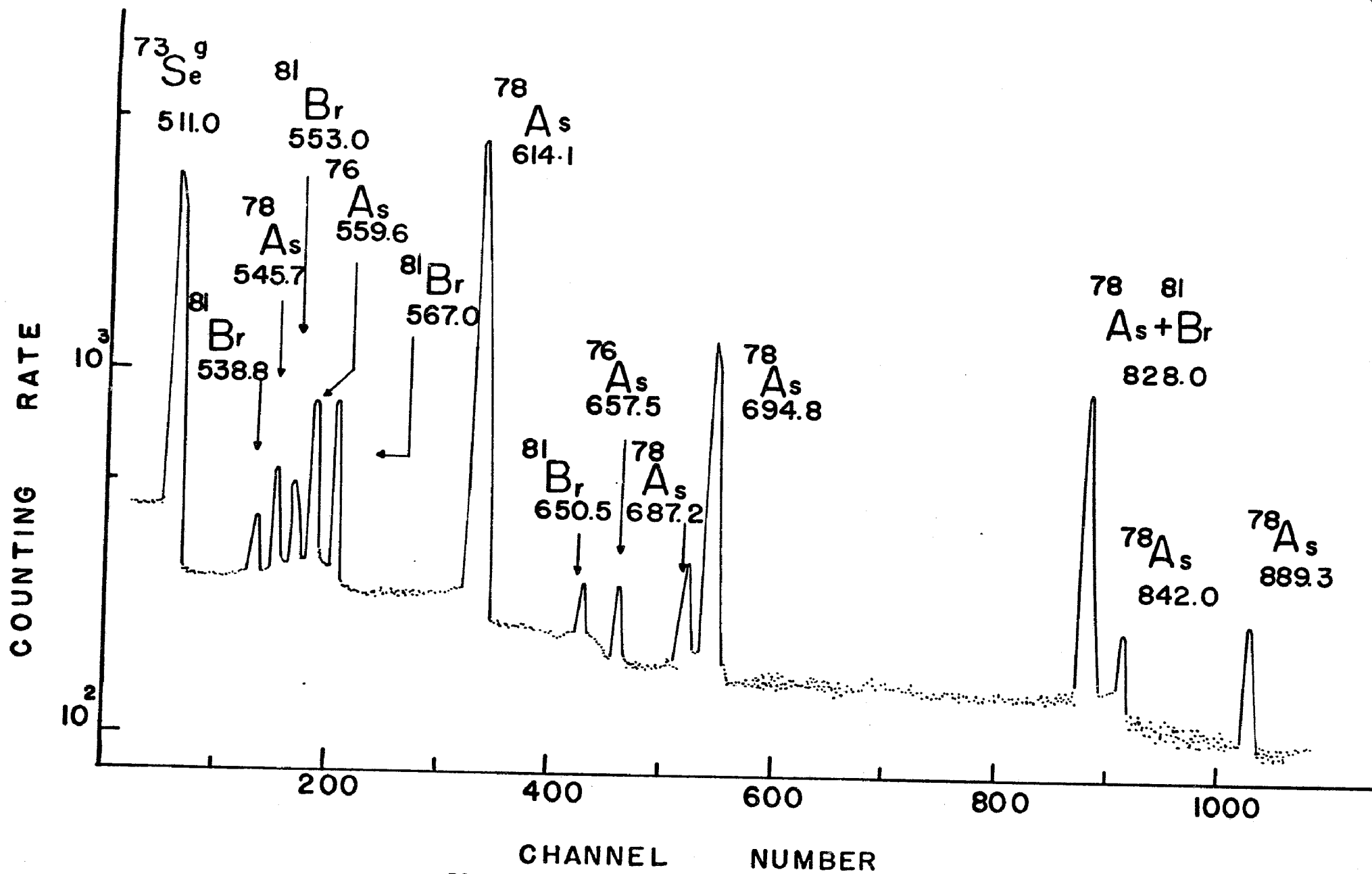


Fig. 26. Gamma ray spectrum of ^{78}As observed with the 20 cm^3 $\text{Ce}(\text{Li})$ detector in the energy region 0.5-1.0 MeV (activity produced by irradiation of a SeO_2 target).

transitions belonging to the decay of ^{78}As . The counting rates of these photopeaks as a function of time are shown in Fig. (27). As shown in Fig. (27), the peaks at 545.7 and 687.2 KeV also follow the half life of ^{78}As and they are assigned to the decay of ^{78}As . The peaks at 538.8, 553.0, 567.0 and 650.6 KeV are assigned to ^{81}Se (56,57) on the basis of their half life, energy and relative intensity. The peaks at 559.6 and 657.5 KeV are assigned to the decay of ^{76}As on the basis of their long half lives, energies and relative intensities (15).

The peak at 828.0 KeV appears to be a composite one. Since ^{81}Se (56) activity is formed via the $^{82}\text{Se}(n,2n)^{81m,8}\text{Se}$ reaction it is expected that a transition at 828.0 KeV will appear in the spectrum. The intensity of the 828.0 KeV transition observed in the present spectra (15,56) is almost twice the reported intensity value for the ^{81}Se 828.0 KeV transition. The observed counting rate of this photopeak as a function of time is shown in Fig. (28). Since the relative intensities (56,57) of the ^{81}Se gamma rays are well known, the contribution of the ^{81}Se in the observed composite 828.0 KeV photopeak may be easily found. The counting rate of the ^{81}Se contribution in this photopeak is plotted versus time and yields a straight line with a slope corresponding to a half life value of 62 minutes, in good agreement with the expected value of 57 minutes. Subtracting this curve from the total decay curve obtained for the composite 828.0 KeV peak, a single decay curve is obtained with a slope corresponding to a half life value of 97 minutes (see Fig. (28)).

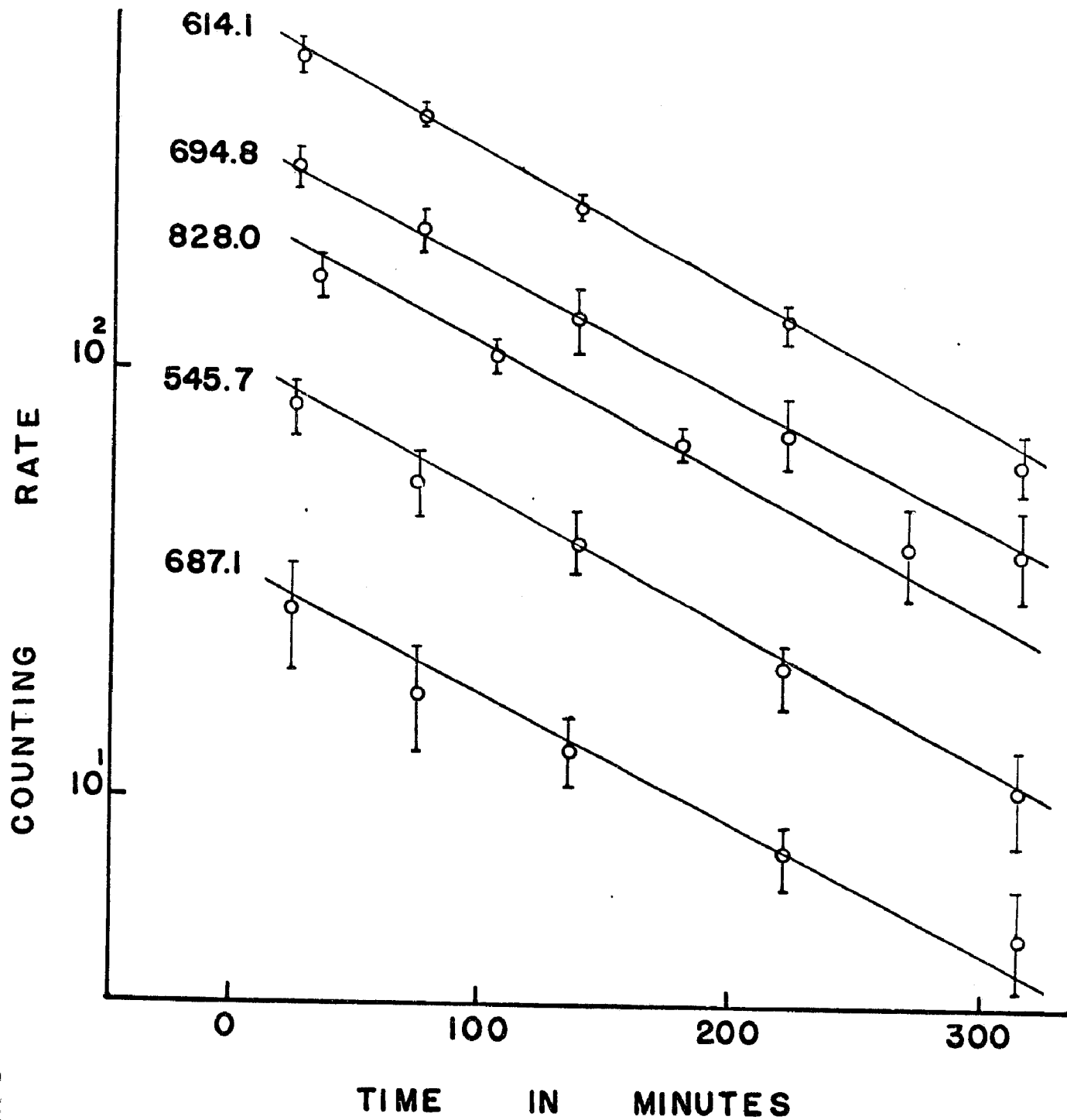


Fig. 27. The decay curves of some ^{78}As gamma rays.

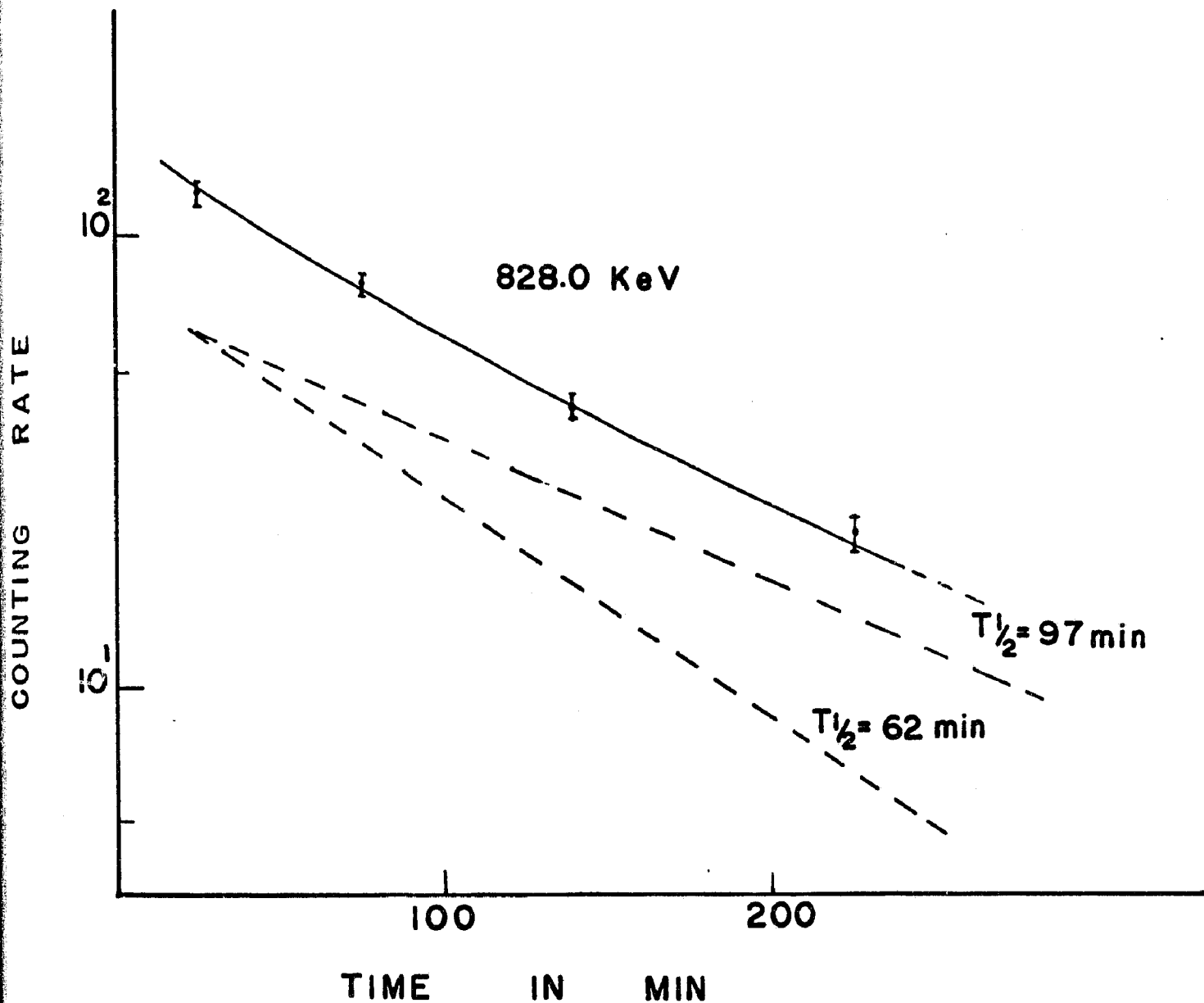


Fig. 28. The decay of the composite 828 KeV gamma ray as observed in the activity produced by irradiation of a SeO_2 target.
 (The error in the estimation of the half lives is ± 10 min)

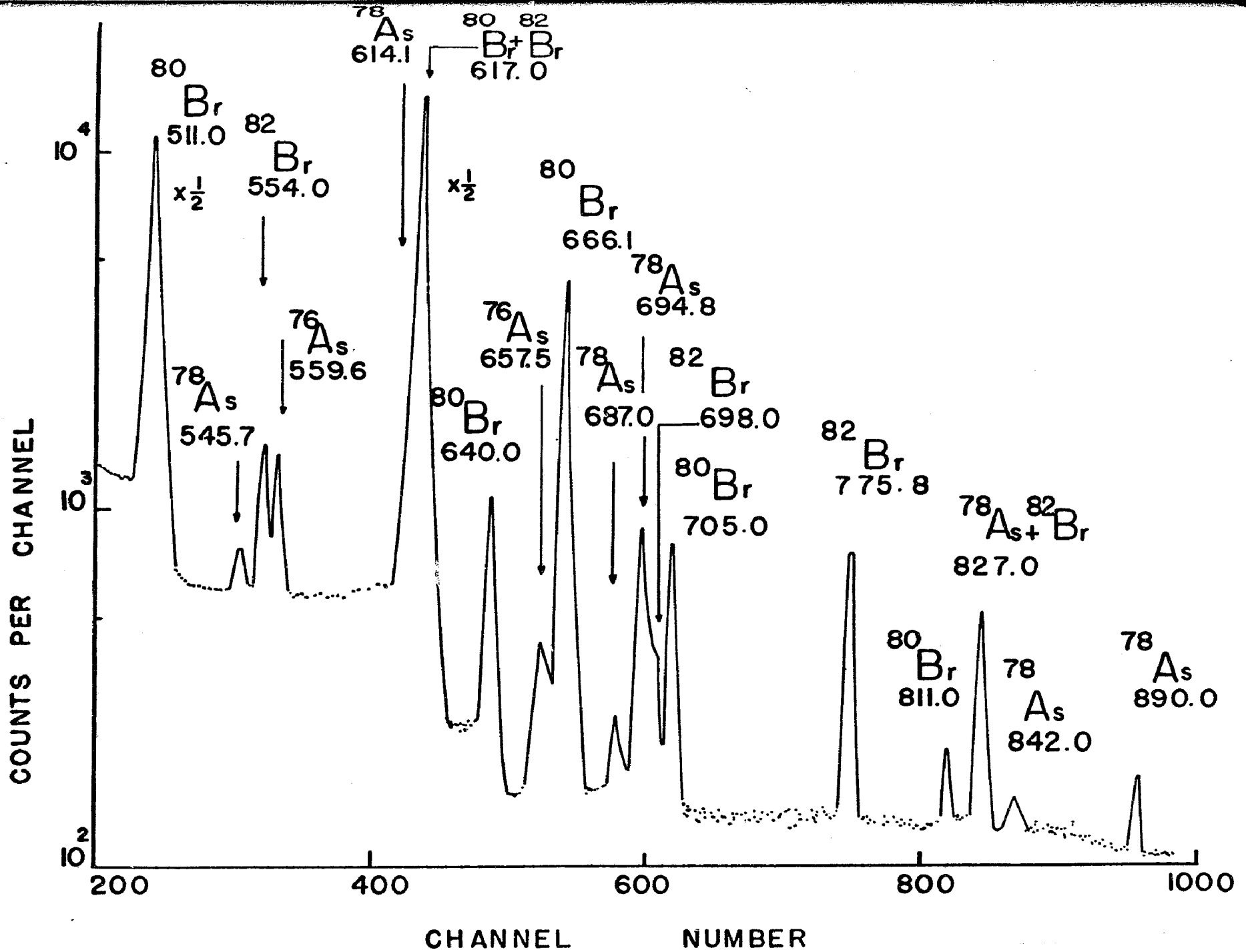


Fig. 29. Gamma ray spectrum of ^{78}As . Activity produced by irradiation of a Br target (0.5-1.0 Mev).

The 97 minute component of the composite peak at 828.0 KeV is thus assigned to the ^{78}As activity. The two weak transitions at 842.0 and 889.3 KeV appear to follow the half life of ^{78}As but the experimental error associated with their half life determination is large enough to prevent any definite assignment of these peaks.

The singles spectrum obtained from the irradiation of a NaBr sample is shown in Fig. (29). Except for the well known transitions which belong to the decay of ^{82}Br , ^{80}Br and ^{76}As , the transitions at 545.7, 687.0 and 694.8 KeV previously assigned to the decay of ^{78}As are observed and their respective relative intensities are the same as in the case of the Se target (see Table 27). The two transitions at 842.0 and 889.0 KeV observed in the Se target are also observed in this spectrum. The relative intensity of these transitions as compared with the other ^{78}As transitions is the same in the spectra shown in Figs. (26 and 27) (see Tables 27 and 28). This may be considered as supporting evidence for the assignment of these transitions to the decay of ^{78}As . The 828.0 KeV photopeak observed in the spectrum shown in Fig. (29) is also a composite one. The one component of this photopeak follows the decay of ^{78}As while the other component is due to ^{82}Br ($T_{1/2} = 36$ hours) impurity. After subtraction of the small ^{82}Br contribution, the counting rate of the remaining component of this composite photopeak is shown as a function of time in Fig. (27). The deduced half life for this component again supports the assignment of this transition to the decay of ^{78}As .

Initially the intensities of the observed transitions in ^{78}As were

calculated from the measured spectra in experiments involving Se and Br targets. However, the intensities obtained from the irradiated SeO_2 spectra indicated much better statistical accuracy. These spectra were then used throughout this work for the determination of the adopted relative intensities of the transitions in ^{78}As . The calculated energy and intensity values of the ^{78}As gamma rays are listed in Table 28 and are compared with the results of VanLieshout (51). The errors associated with the intensity values listed in Tables 27 and 28 include the error in estimating the area under the photopeaks and the error of the relative efficiency values used.

Energy calibrations were performed in two stages. Some prominent transitions of ^{78}As were first measured by using standard sources such as ^{60}Co , ^{22}Na , Ra and daughters and Th and daughters. These calibrated peaks were then used for the subsequent calibration of the weaker transitions. Errors in the energy values listed in Tables 27 and 28 include errors associated with the uncertainty in the position of the centroid of a photopeak, as well as the error associated with the channel to energy conversion factor. No other peak belonging to the decay of ^{78}As , of energy less than 500 KeV, has been observed in the present work. The data reported by Leishout (51) indicate transitions at 620, 700, and 830 KeV in ^{78}As which may be considered to correspond to the respective 614.1, 694.8 and 828.0 KeV transitions observed in the present work. Their intensity values are comparable with those obtained in this work. The transitions at 545.7, 687.2, 842 and 889.3 KeV are reported for the first time.

The half life of ^{78}As has also been measured by following the decay of the prominent 614.1 KeV photopeak. Computer analysis of the accumulated data indicated a half life value $T_{1/2} = (87 \pm 3)$ minutes, (15,53) in good agreement with the accepted value of $T_{1/2} = 90$ minutes.

5.2.2. Intermediate energy region singles spectroscopy ($1 < \text{MeV} < E < 2 \text{ MeV}$)

Typical spectra obtained from the irradiated SeO_2 target, in the energy region up to 2 MeV are shown in Figs. (30 and 31). The decay of the most prominent peaks was followed by measuring the area under the photopeaks of three spectra taken in three time intervals. The results of these measurements are shown in Figs. (32 and 33). All the measured photopeaks in this energy region seem to follow quite accurately the decay of ^{78}As . The weak photopeaks at 1199.0, 1228.0, 1440.4 and 1720.0 KeV also seem to follow the decay of ^{78}As but their assignment into the decay of ^{78}As is by no means assured by the present data. The weak transitions at 1214.0 KeV shown with a question mark in the spectrum of Fig.(30) belong to a long lived activity. This peak probably corresponds to the ^{76}As transition at 1214 KeV reported by other workers (15). The relative intensity of this photopeak with respect to the prominent 559.3 KeV ^{76}As transition (15) is 10. All other ^{76}As transitions have a relative intensity of less than 1 except for a 1228.0 KeV transition with a reported relative intensity of 2.3.

As a result, only a small interference is anticipated from the 1228.0 KeV transition of the ^{76}As impurity in this energy region. However,

Table 27

Gamma rays observed in the decay of ^{78}As produced via the $^{81}\text{Br}(n,\alpha)^{78}\text{As}$ reaction

(a) Energy in KeV	(b) Rel. Intensity
545.7	6.0±1.0
687.2	2.4±0.6
694.8	32.0±3.0
828.0	16.0±3.0
842.5	2.5±0.3
887.0	4.0±0.8
1074.0	3.5±0.6
1144.7	3.6±0.6
1199.0	2.0±0.04
1228.0	1.0±0.3
1240.5	12.0±1.8
1308.8	22.7
1372.5	8.0±2.5
1381.0	0.9±0.4
1440.4	0.7±0.4
1529.5	4.5±1.0
1714.5	4.0±1.0
1720.0	2.0±0.3
1791.0	1.8±0.4
1838.0	3.0±0.6
1893.0	1.1±0.2
1921.0	3.0±0.4
1996.0	2.8±0.4
2067.5	2.0±0.5
2183.0	0.5±0.2
2218.3	1.5±0.5

(a) Energy values listed here are obtained from Table 28.

(b) normalized to 22.7 for the 1308.8 KeV transition

Table 28

Gamma rays observed in the decay of ^{78}As produced via the
 $^{78}\text{Se}(n,p)^{78}\text{As}$ reaction (Adopted values) (51)

Present work		R. Van Leishout	
Energy in KeV	Intensity	Energy in KeV	Intensity
545.7 ± 0.3	5.3 ± 0.3		
614.1 ± 0.1	100.0	620	100
687.2 ± 0.8	2.5 ± 0.4		
694.8 ± 0.3	31.4 ± 0.9	700	37.5
828.0 ± 0.6	15.0 ± 3.0	830	19.5
842.5 ± 0.7	2.3 ± 0.6		
889.0 ± 1.5	3.6 ± 0.5		
1074.0 ± 0.4	3.8 ± 0.4	990	5.4
1144.7 ± 0.3	3.1 ± 0.3	1100	7.15
1199.0 ± 0.2	1.3 ± 0.3		
1228.0 ± 1.0	0.8 ± 0.2		
1240.5 ± 0.2	11.0 ± 0.8	1210	11.0
1308.8 ± 0.2	22.7 ± 1.0	1310	25.0
1372.5 ± 0.4	9.0 ± 0.6		
1381.0 ± 2.0	1.2 ± 0.1		
1440.5 ± 0.7	0.75 ± 0.07		
1529.5 ± 1.0	5.0 ± 0.4	1490	5.4
1714.5 ± 1.0	4.3 ± 0.5	1700	3.6
1720.0 ± 2.0	0.9 ± 0.2		
1791.0 ± 1.0	2.1 ± 0.2		
1838.0 ± 2.0	3.0 ± 0.4	1820	3.6
1893.0 ± 1.5	1.2 ± 0.2		
1921.0 ± 1.0	3.8 ± 0.4		
1996.0 ± 1.0	3.0 ± 0.3	1940	3.6
2067.5 ± 1.0	1.6 ± 0.1	2050	2.3
2183.0 ± 1.5	0.6 ± 0.1		
2218.3 ± 1.5	1.6 ± 0.3	2240	2.3
2683.5 ± 3.0	2.8 ± 0.3	2650	3.6
2798.5 ± 3.0	0.3 ± 0.1		
2843.5 ± 3.0 ^(a)	0.18 ± 0.08		
3103.5 ± 6.0	0.10 ± 0.05		

(a) This transition has not been assigned definitely to the decay of ^{78}As .

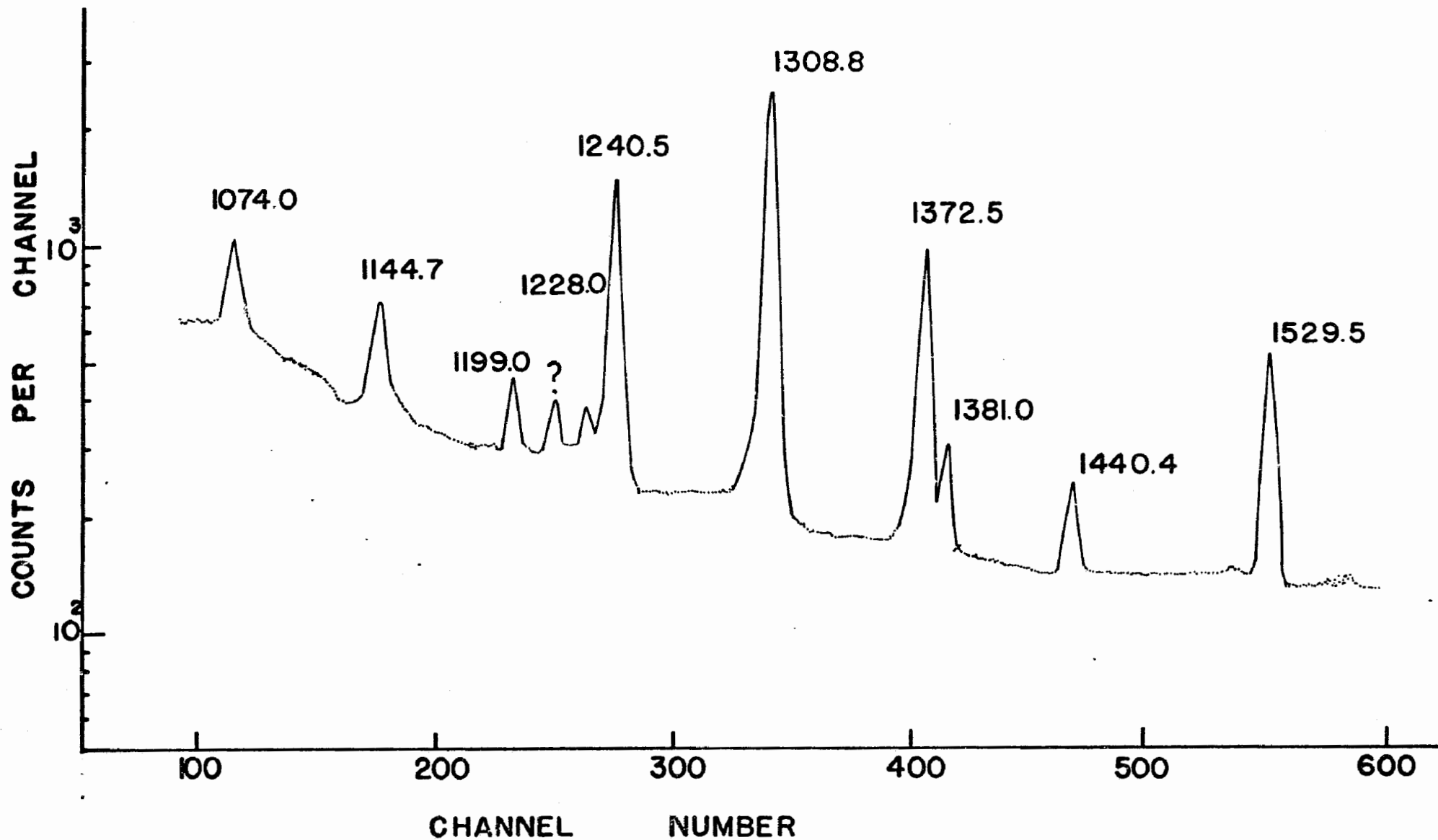


Fig. 30. Gamma ray spectrum of ^{78}As observed with the 29 cm^3 Ge(Li) detector. Activity produced by irradiation of a Se target. (Energy region: 1.0-1.6 MeV.)

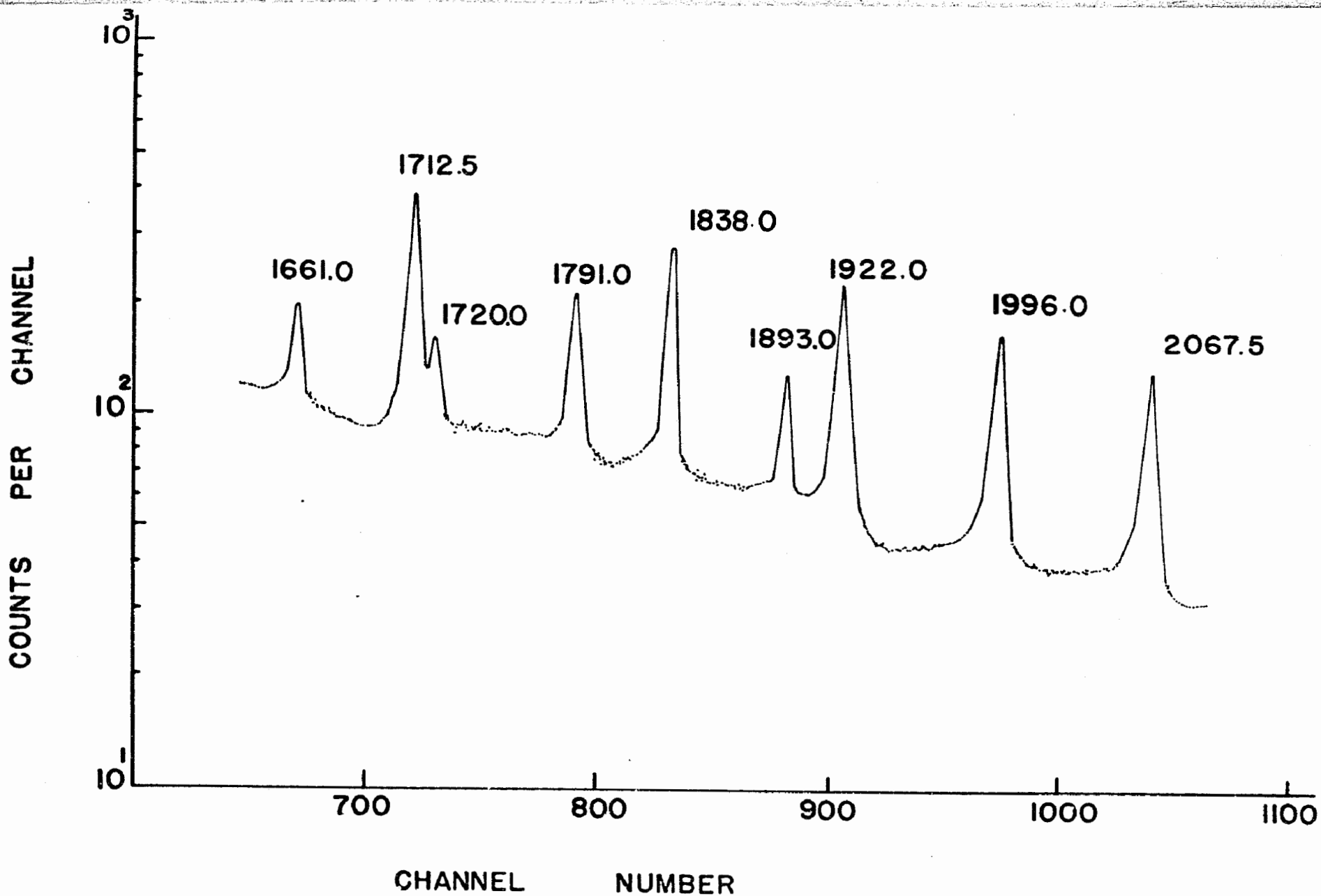


Fig. 31. Gamma ray spectrum of ^{78}As observed with the 29 cm^3 Ge(Li) detector. Activity produced by irradiation of a Se target. (Energy region: 1.6-2.1 MeV.)

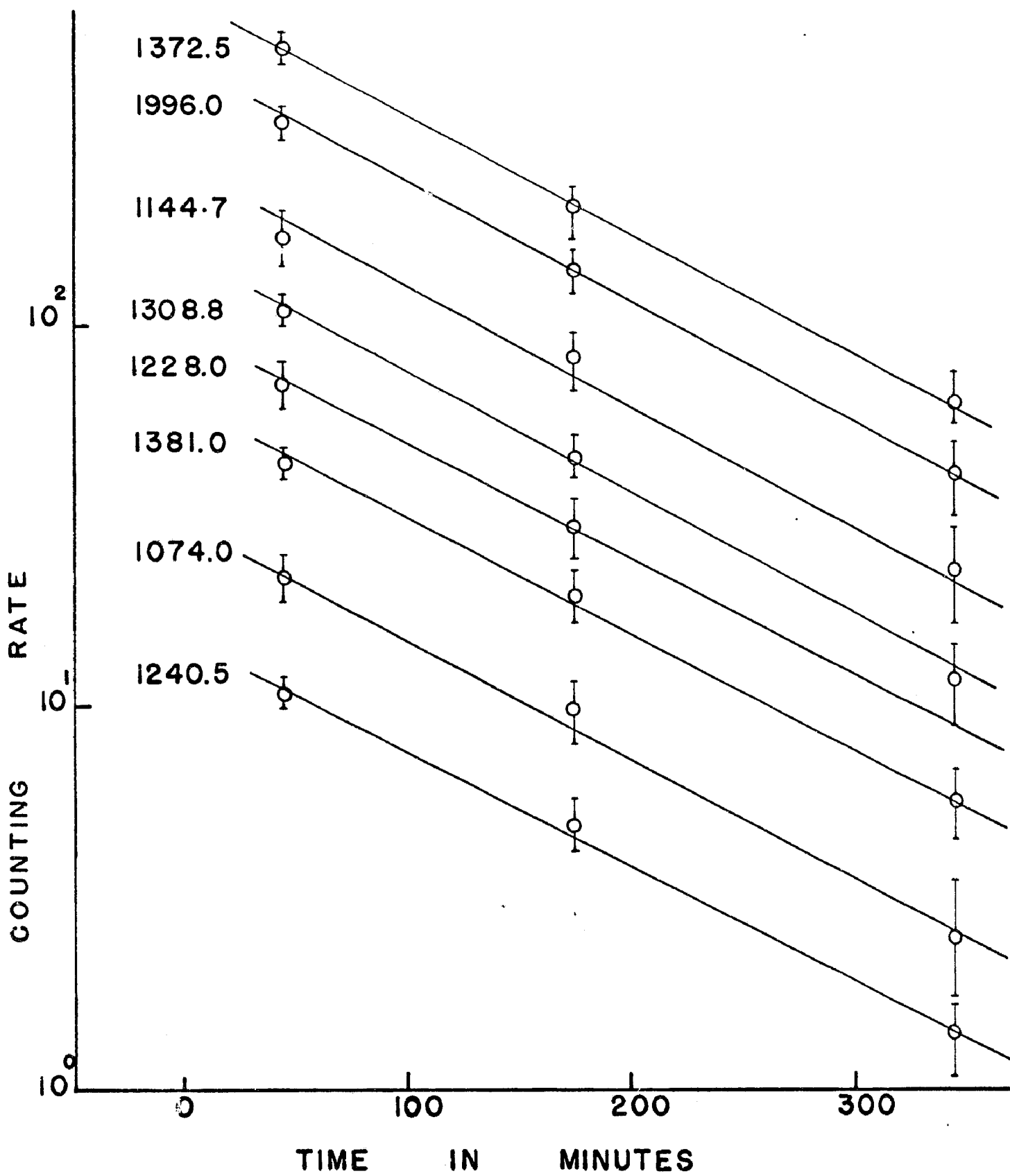


Fig. 32. The decay curves of some ^{78}As gamma rays.

COUNTING RATE

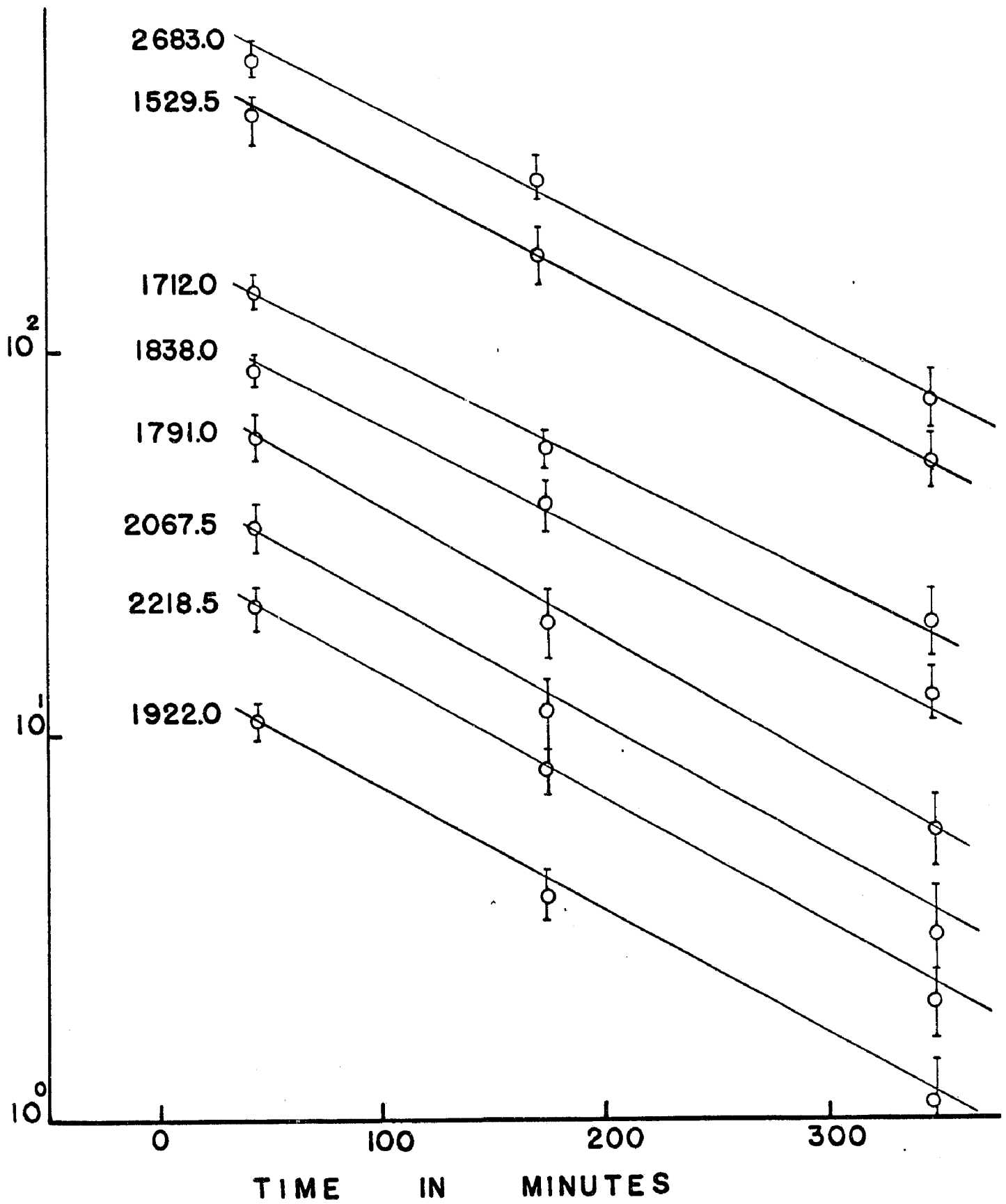


Fig. 33. The decay curves of some ^{78}As gamma rays.

the contribution of the 1228.0 KeV of ^{76}As to the observed photopeak at 1228.0 KeV in the present spectra is found to be 20% (see Table 29).

The photopeak at 1661.0 KeV shown in Fig. (31) belongs to the decay of ^{78}As . It is a second escape peak arising from a strong photopeak observed at 2683.0 KeV, as discussed in the next section. The part of the observed spectrum in the energy region 1 - 1.3 MeV obtained by counting a NaBr irradiated target is shown in Fig. (34). The well known ⁽¹⁵⁾ transitions at 1043.0 and 1318.0 KeV of ^{82}Br and the transitions at 1256.0 KeV belonging to the decay ⁽¹⁵⁾ of ^{80}Br are easily observed. The peak observed at 1368.5 KeV is due to ^{24}Na contamination.

The transitions observed in the spectrum of the SeO_2 target, and assigned to the decay of ^{78}As in the energy region under consideration are also observed in the spectrum of the NaBr target at 1074.0, 1145.0, 1240.5, 1308.8, 1372.5 and 1381.0 KeV. Their relative intensity values with respect to the 1308.8 KeV transition are listed in Table 27 and they are in agreement with those obtained in the SeO_2 target measurements (Table 28).

The ^{76}As photopeak at 1214.0 KeV is also observed in this NaBr spectrum. The weak transitions at 1199.0 and 1228.0 KeV observed in the Se target spectra are also observed in the Br target spectra. The relative intensities of these two transitions with respect to the 1308.8 KeV transition in ^{78}As are in agreement with the corresponding data obtained from the measurements of the SeO_2 target, as indicated in Tables 27 and 28. Thus these two weak transitions are assigned to the decay of ^{78}As .

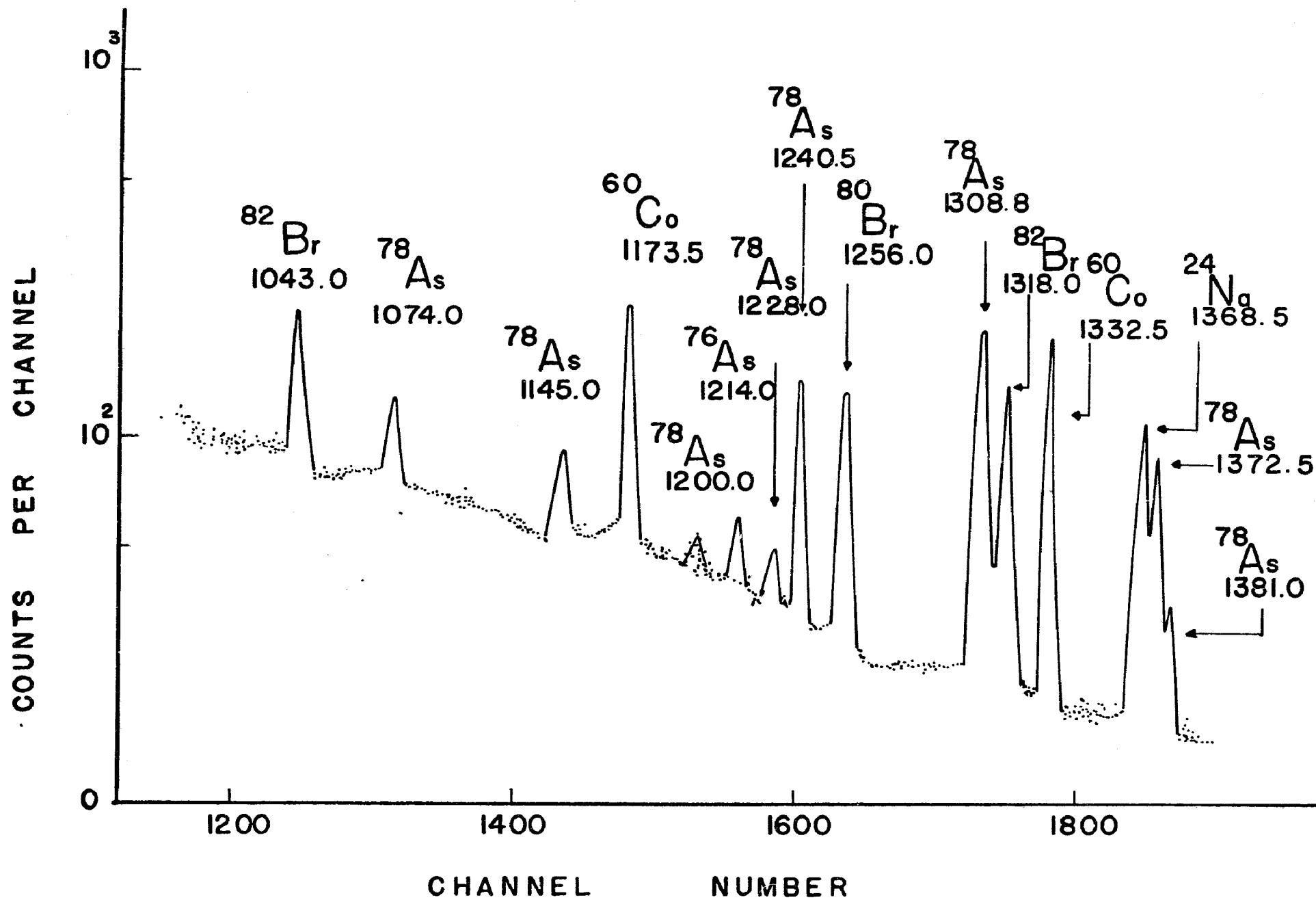


Fig. 34. Gamma ray spectrum of ^{78}As observed with the 29 cm^3 Ge(Li) detector. Activity produced by irradiation of a Br target. (Energy region: 1.0-1.4 MeV.)

In Table 29 the corrections for the contribution of the ^{76}As 1228.0 KeV transition in both Se and Br targets spectra are shown.

The spectrum of the NaBr target obtained in the energy region up to 2 MeV is shown in Fig. (35). The peak at 1473.0 KeV is a well known transition of the decay of ^{82}Br . The peak at 1733.0 KeV is the double escape peak arising from the 2754.0 KeV transition of the ^{24}Na contamination. All the transitions assigned to the decay of ^{78}As on the basis of the results obtained from the analysis of the Se irradiated target are also observed here. The two weak transitions at 1440.5 and 1720.0 KeV, observed in the SeO_2 target spectra, are observed in Fig. (35) with the same relative intensity with respect to the neighbouring ^{78}As peaks. This correspondence supports the assignment of these transitions to the decay of ^{78}As . The relative intensities of the peaks observed in the spectrum of the NaBr target in the energy region from 1.3 to 2 MeV are also listed in Table 27.

(51)

The results obtained by V. Lieshout using NaI detectors indicate transitions in the energy region under investigation at 990, 1100, 1210, 1310, 1490, 1700, 1820, 1940 and 2050 KeV. These may correspond to the transitions observed in this work at 889.3, 1074.0, 1144.7, 1240.5, 1308.8, 1529.5, 1714.5, 1838, 1921.0, 1996.0 and 2067.5 KeV respectively. The corresponding intensity values are in reasonable agreement with the present data as shown in Table 28.

Table 29

Contributions of the 1228.0 KeV ^{76}As photopeak to the
1228.0 KeV ^{78}As photopeak

a) in $^{78}\text{Se}(n,p)^{78}\text{As}$ spectra

Energy in KeV	Rel. Intensity
^{76}As 1214	1.0±0.2
$^{76}\text{As} + ^{78}\text{As}$ 1228	1.0±0.2 (a)
^{76}As 1228	0.2
^{78}As 1228	0.8±0.2

b) in $^{81}\text{Br}(n,\alpha)^{78}\text{As}$ spectra

Energy in KeV	Rel. Intensity
^{76}As 1214	1.8±0.3
$^{76}\text{As} + ^{78}\text{As}$ 1228	1.4±0.3 (a)
^{76}As 1228	0.4
^{78}As 1228	1.0±0.3

(a) based on the value $\frac{I(1228)}{I(1214)} = 0.23$ in ^{76}As obtained from ref. (15).

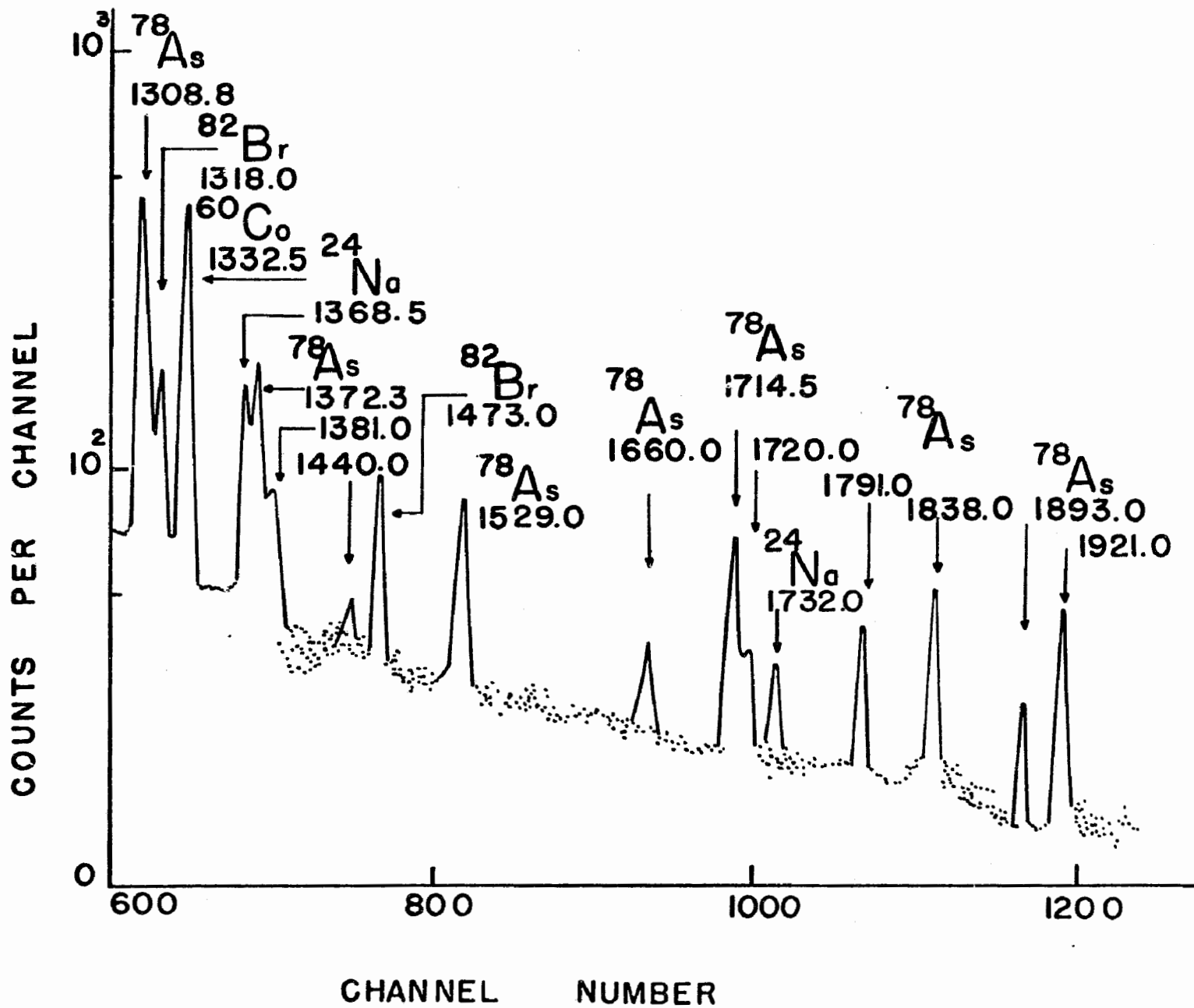


Fig. 35. Gamma ray spectrum of ⁷⁸As observed with the 29 cm³ Ge(Li) detector. Activity produced by irradiation of a Br target. (Energy region: 1.4-1.9 MeV.)

5.2.3. High energy region singles spectroscopy ($E > 2$ MeV)

The spectra of the irradiated SeO_2 target have been used to investigate the energy region from 2 to 3.2 MeV. The spectrum obtained after a 90 minute counting period is shown in Fig. (36). Eight transitions were observed in this energy region with the most prominent one at (2683.5 ± 3.0) KeV. This peak follows the half life of ^{78}As , as shown in Fig. (33). The peak observed at (2218.3 ± 1.5) KeV also follows the decay of ^{78}As , and this is shown in Fig. (33). The peak at (2758.0 ± 3.0) KeV was found to belong to a long lived activity and is probably due to traces of ^{24}Na impurity.

It is shown later (see section 5.2.5) that the peaks at 2798.5, 2183.5 and 3103.5 KeV may be fitted exactly into the decay scheme and on this ground only are considered to belong to the decay of ^{78}As . The gamma ray at (2843.5 ± 3.0) KeV can also be fitted into the proposed decay scheme, but the assignment of this transition to the decay of ^{78}As is somewhat doubtful.

Finally, the peak observed at (2166 ± 4.0) KeV cannot be accommodated into the decay scheme and is omitted along with the 2758.0 KeV transition. The 2166.0 KeV peak is probably the weak single escape peak of the (2683.5 ± 3.0) KeV transition which is expected to appear at around (2672.5 ± 3.0) KeV. The part of the spectrum which includes gamma transitions between 1.9 and 2.5 MeV, obtained by measuring the Br target, is shown in Fig. (37). The peaks assigned to ^{78}As on the basis of the data of the SeO_2 target, namely the 2183.0 and 2218.3

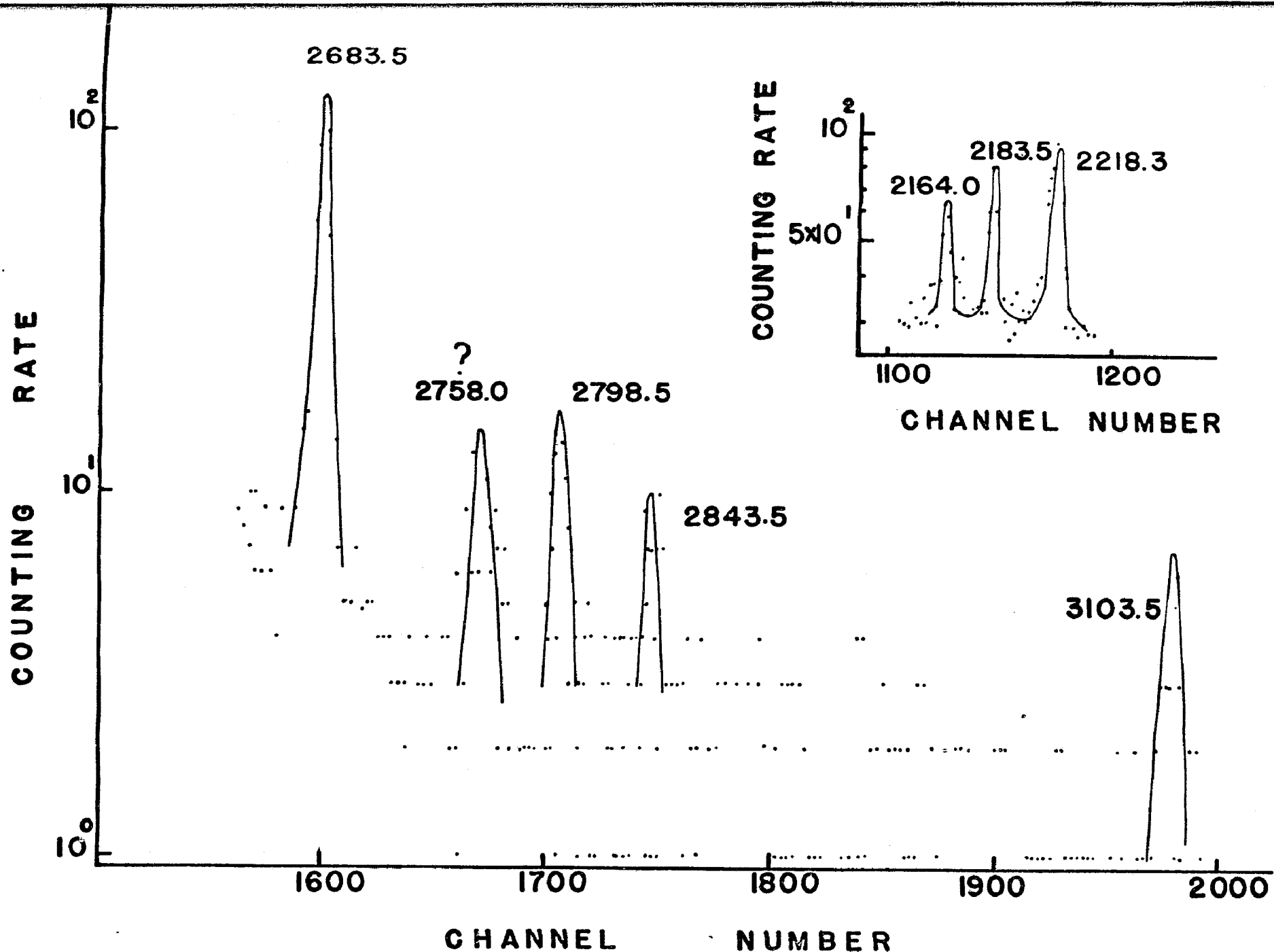


Fig. 36. Gamma ray spectrum of ^{78}As observed with the $29 \text{ cm}^3 \text{ Ge(Li)}$ detector. Activity produced by irradiation of a Se target. (Energy region: 2.1-3.1 MeV.)

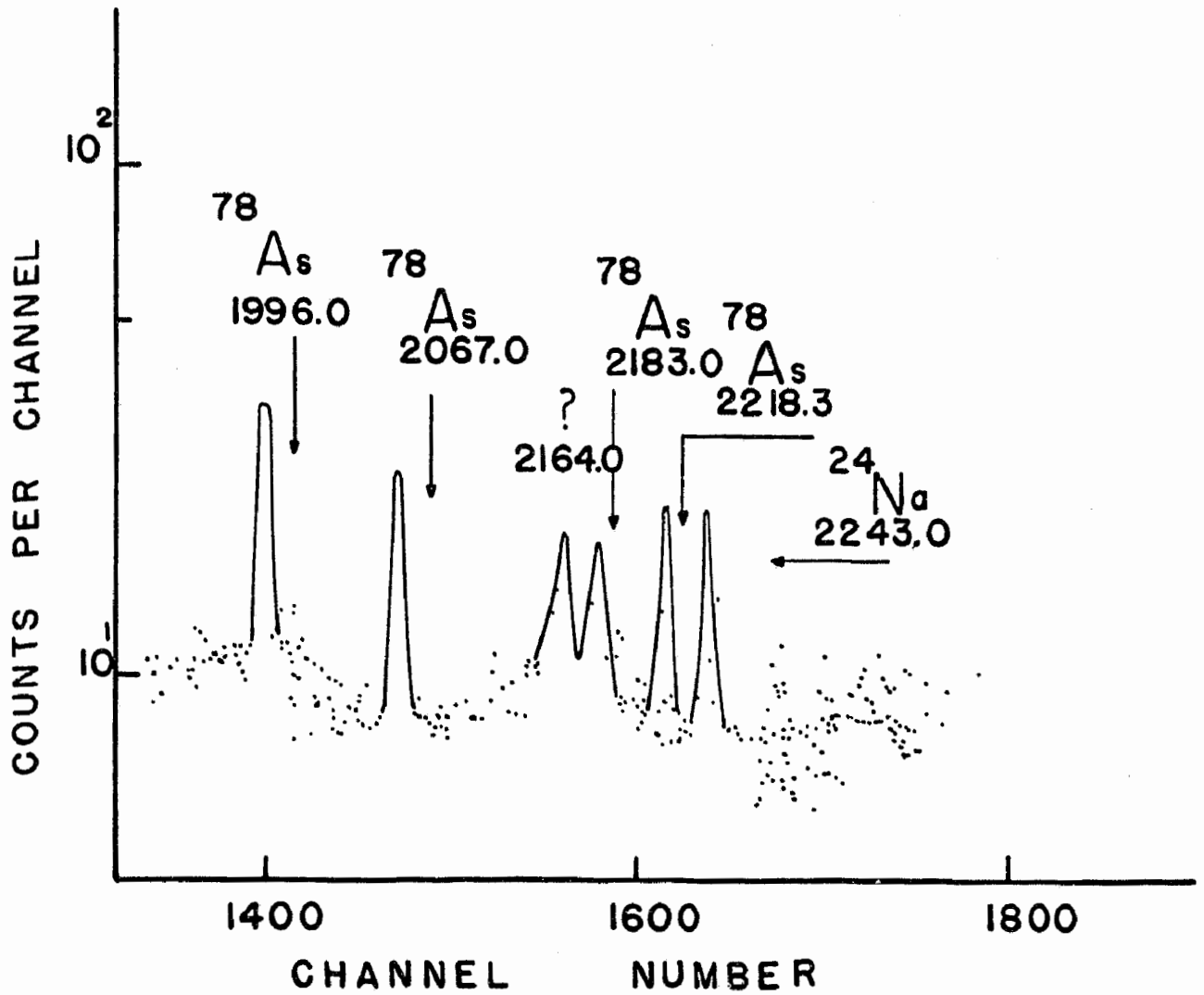


Fig. 37. Gamma ray spectrum of ^{78}As observed with the $29\text{ cm}^3\text{ Ge(Li)}$ detector. Activity produced by irradiation of a Br target. Energy region: 1.9-2.3 MeV.

KeV transitions, appear in the NaBr target spectra with the same relative intensity. The calculated energy and intensity of the transitions observed in this energy region are also listed in Table (51) 27. The results of V. Lieshout indicate two transitions in this energy region at 2240 and 2650 KeV, which should correspond to the 2218.3 and 2683.5 KeV transitions observed in the present study.

5.2.4. Coincidence measurements

The coincidence experiments were carried out by utilizing the 29 cm³ Ge(Li) detector and a NaI(Tl) crystal. The NaI detector was used to gate the desired energy region, while the coincidence spectra were obtained with the Ge(Li) detector. The two detectors were placed into a face to face geometry, as close to each other as the plastic vial containing the irradiated target would permit. The resolving time of the coincidence unit was set at 60 ns.

In these experiments the ⁷⁸As activity was produced exclusively by irradiating SeO₂ targets. The resulting coincidence counting rate was rather low and in two of the three coincidence experiments described below it was found necessary to use two irradiations of the target for each experiment and to add the resulting coincidence spectra, in order to obtain better statistics.

In a preliminary experiment, the gate on the NaI detector was centered at the 614.1 KeV ⁷⁸As gamma ray. The width of the gate was

approximately 100 KeV. Thus, it is expected that the 545.7, 687.2 and 694.2 KeV transitions in ^{78}As , as well as the strong 614.1 KeV transition, will contribute partly to the gated energy region. The Ge(Li) detector pulses were displayed on the 2048 channel analyzer to cover the energy region from 100 to 700 KeV. The part of the resulting spectrum which includes events from 300 to 700 KeV is shown in Fig. (38). The transitions at 545.7, 614.1 and 694.8 KeV are shown to be in strong coincidence with the gated region which includes the very same transitions, indicating that these transitions are somehow in coincidence with each other. No other transition has been observed with energy less than 540 KeV to be in coincidence with the gated energy region.

The higher energy transitions which are in coincidence with the same gate have been measured in a separate experiment. With the help of the biased and stretcher amplifier the energy region from 0.8 to 2.7 MeV as observed by the Ge(Li) detector was displayed in the analyzer. In this experiment, after the end of the counting period of the irradiated target, the analyzer was stopped, the target was irradiated again and the counting was continued for about 5 hours. The obtained spectrum of the ^{78}As transitions, which is in coincidence with the 545.7, 614.1, 687.2 and 694.8 KeV transitions, is shown in Fig. (39) and (40). The spectrum of Fig. (39) indicates that all the transitions observed in the singles ^{78}As spectra in the energy region from 800 to 1500 KeV are in coincidence with the transitions included in the gated region. The

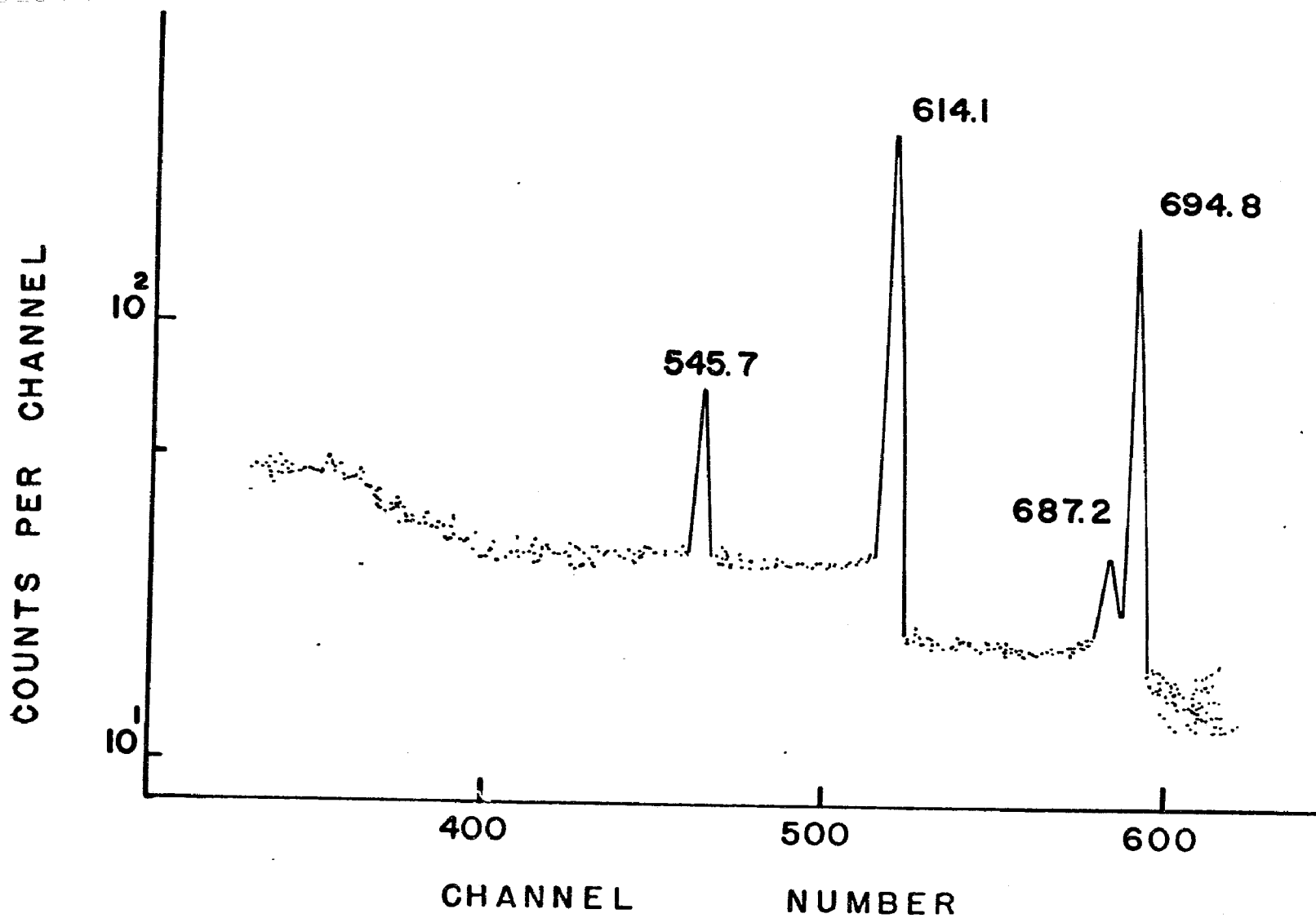


Fig. 38. ^{78}As gamma rays with $E < 700$ KeV in coincidence with a 100 KeV wide gate centered at the 614 KeV transition.

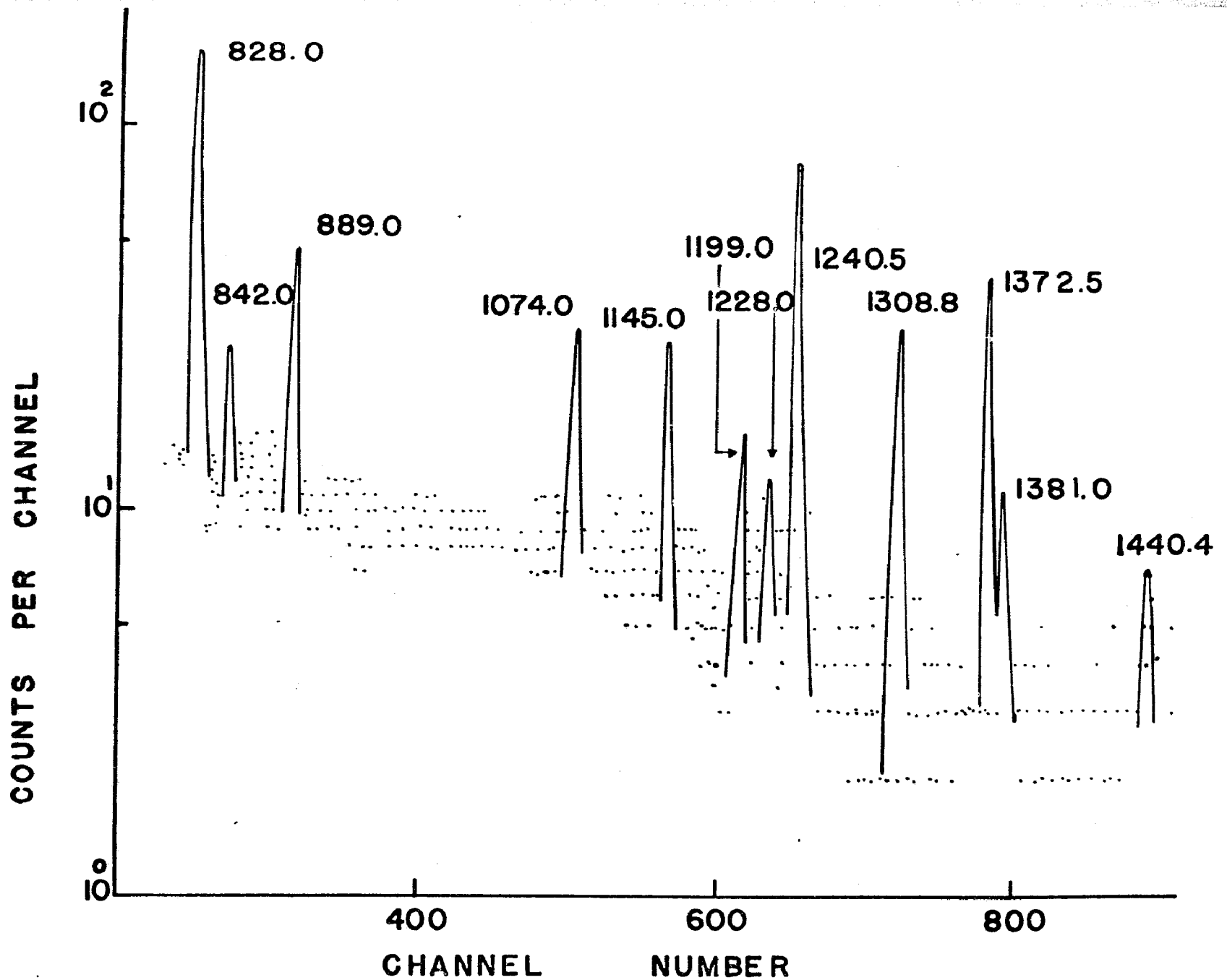


Fig. 39. ^{78}As gamma rays in coincidence with the gate which includes the 614 KeV transition. (Energy region: 0.8-1.5 MeV.)

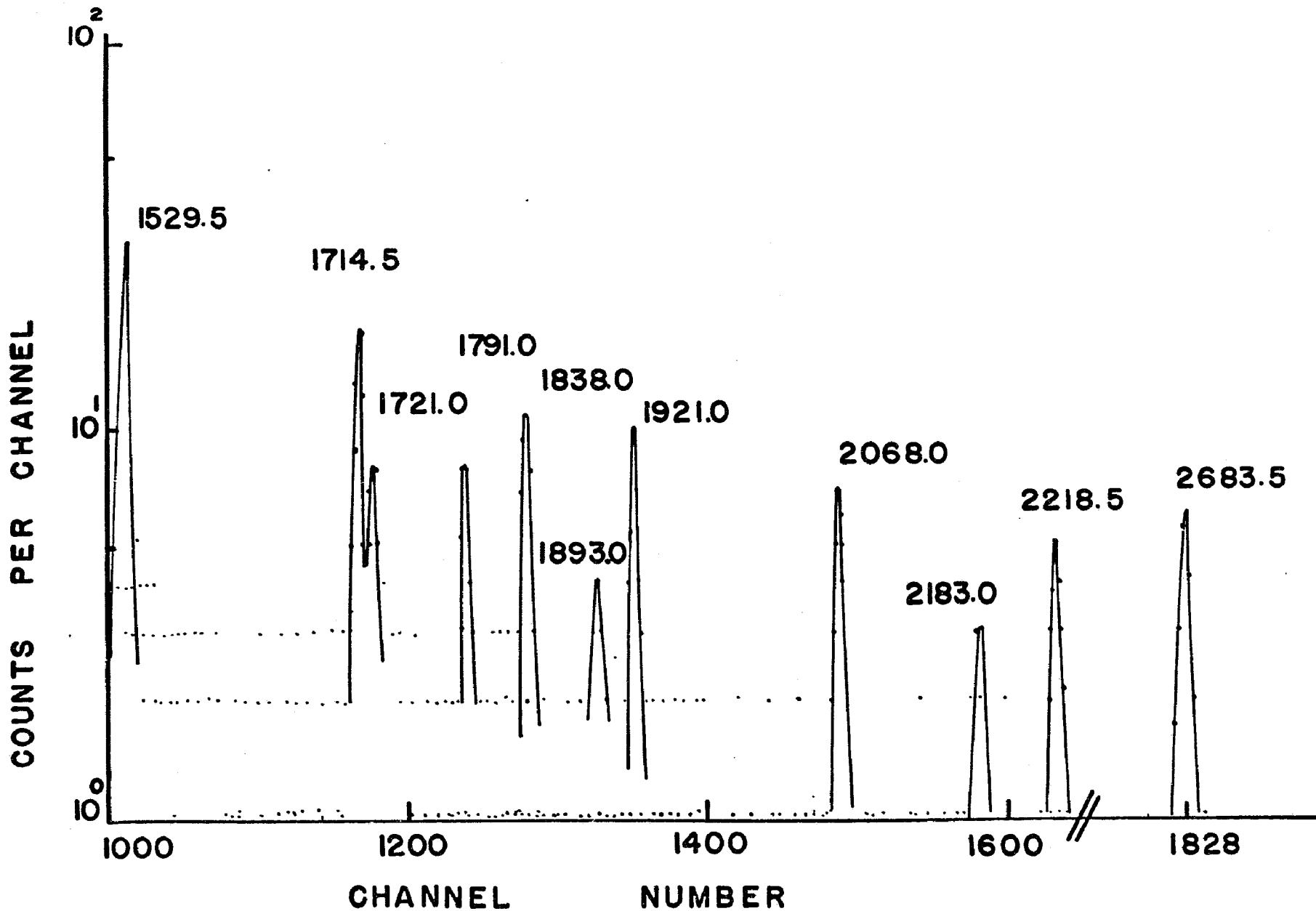


Fig. 40. ⁷⁸As gamma rays in coincidence with the gate which includes the 614 KeV transition. (Energy region: 1.5-3 MeV.)

intensity of the 1308.8 KeV transition is shown in Fig. (39) to be greatly reduced in comparison with the neighbouring peaks at 1240.5 and 1372.5 KeV. This suggests that the 1308.8 KeV transition is not in coincidence with the strong 614.1 and 694.8 KeV transitions, but rather is in coincidence with either of the 687.2 or 545.7 KeV transitions or both.

In the same spectrum, the 1240.5 KeV transition appears in strong coincidence with the gated region, indicating that the transition is probably in coincidence with the 614.1 KeV transition. The part of the observed coincidence spectrum which includes transitions of energy higher than 1.4 MeV is shown in Fig. (40). This spectrum indicates that most of the transitions observed in this energy region in the singles spectra are in coincidence with the transitions included in the gated region. The intense transition at 1996.0 KeV observed in the single spectra is not in coincidence with the gated region. This indicates that this transition is either a transition feeding directly the ground state or it is in coincidence with another transition which in turn feeds the ^{78}Se ground state. Since no transition of intensity comparable to the 1996.0 KeV transition is missing in the observed coincidence spectrum except the 1996.0 KeV transition itself, it may be concluded that the former case is the most probable.

The relative intensity of the transitions observed in coincidence with the gated region (Figs. (39) and (40)), have been calculated and listed in Table 30. The intensities shown in Table 30 are normalized

Table 30

Coincidence intensities of gamma rays in ^{78}As

(The gate includes the 614.1 KeV transition and part of the 545.7, 687.2 and 694.8 KeV transitions.)

Energy in KeV	Relative coincidence intensity ^(a)	(b)	
		Ratio	$\frac{I \text{ coinc.}}{I \text{ single}}$
828.0	11.7±0.7		0.78±0.05
842.5	1.0±0.4		0.40±0.16
889.3	4.0±0.4		1.1±0.1
1074.0	2.4±0.5		0.63±0.13
1144.7	2.4±0.5		0.76±0.13
1199.0	<1.0		
1228.0	very weak		
1240.5	11.0	1.0	
1308.8	3.1±0.4		0.14±0.02
1372.5	6.3±0.5		0.70±0.05
1381.0	1.4±0.3		1.10±0.22
1440.7	very weak		
1529.5	3.5±0.4		0.70±0.08
1714.5	4.0±0.5		0.94±0.11
1791.0	2.0±0.4		0.95±0.19
1838.0	2.6±0.5		0.87±0.16
1921.0	3.6±0.5		0.98±0.13
2067.5	1.7±0.3		1.05±0.18
2218.3	1.4±0.3		0.88±0.18
2683.5	2.6±0.4		0.93±0.15

(a) normalized to 11.0 for the 1240.5 KeV transition

(b) quoted error includes error in estimating the coincidence intensity only.

with respect to the 1240.5 KeV transition which has an intensity of 11.0 relative to the 614.1 KeV transition (see Table 28).

With the considerations concerning the coincidence intensity data discussed in Appendix E, some useful results may be obtained from the coincidence data shown in Table 30. The intensity and the $\frac{I_{\text{coinc}}}{I_{\text{singles}}}$ ratios of the transitions at 889.0, 1381.0, 1714.5, 1921.0, 2067.5 and 2683.5 KeV, indicate that these transitions are directly feeding the same level as the 1240.5 KeV transition. Because of the strong intensity of this transition in the coincidence spectrum, it was assumed that it feeds the 614.1 KeV level of ^{78}Se . Thus the above mentioned transitions may be in direct coincidence with the 614 KeV transition, although the possibility of coincidence due to the other transitions present in the gate cannot be excluded (see Appendix E).
(53)
Of these transitions the 694.8 KeV transition is known to deexcite the second level in ^{78}Se at 1308.8 KeV level. From the intensity of the 694.8 and 1308.8 KeV transitions listed in Table 28, the value 0.58 is found for the branching ratio of the 694.8 KeV transition. The other two weak transitions at 687.2 and 545.7 KeV should feed or deexcite levels above the 614.1 KeV level. At best they deexcite levels at 1159 and 1301 KeV with branching ratio 1, but their intensity cannot account for but one or two of the transitions listed in Table 30, should these transitions feed these hypothetical 1159 and 1301 KeV levels.

For the remaining transitions, little information can be obtained

from Table 30. There are a few transitions which have the same ratio 0.70. If these transitions are in coincidence with the 614.1 KeV transition through the 694.8 KeV transition, they should exhibit a ratio of 0.58. However, since a part of the 694.8 KeV transition contributes in the gated region, some additional counts may be added in these peaks and thus their intensity might appear higher.

The known width of the gate (~100 KeV) suggests that the 694.6 KeV transition should contribute about 20% of its total intensity to the coincidence spectrum. This contribution will increase the apparent ratio of coincidence to single intensity for the transitions of interest from 0.58 to 0.70. Thus the gamma rays which exhibit this ratio in Table 30 may very well be in coincidence with the 614.1 KeV transition through the 694.8 KeV transition. However, a more complicated structure (for example, contribution through several gamma rays present in the gate or transitions being indirectly in coincidence with the 614.1 KeV transition) may result in the very same ratio 0.7. To conclude these remarks, it may be noted that the two transitions at 1074.0 and 1144.7 KeV which have almost equal intensity in the singles spectra, as well as the 828.0, 1372.5 and 1529.5 KeV transitions are probably also in coincidence with the 694.8 - 614.1 KeV cascade. All these transitions have a coincidence to single intensity ratio of about 0.7. The transition at 1308.8 KeV has a very low intensity in the coincidence spectra. The observed intensity indicates

that probably both transitions at 545.7 and 687.2 in the gated region are in coincidence with the 1308.8 KeV transition.

In order to obtain more information on the level structure of ^{78}Se , one more coincidence experiment was carried out. In this experiment the gate on the NaI side was set to include the 1308.8 and the 1372.5 KeV transitions. The gate was centered at around 1340 KeV with a width of approximately 140 KeV. Thus except for the main contributions to the gated region from the two strong transitions at 1308.8 and 1372.5 KeV, contributions are expected from the 1240.5 KeV and 1381.0 KeV transitions. The Ge(Li) detector was set up to accept events extending from 0.5 to 2.1 MeV. The obtained spectrum is shown in Figs. (41) and (42).

The first thing to be noted is the apparent equality of the intensities of the 1308.8 and 1372.5 KeV transitions. Since these two transitions are the main contributors to the gating region, it is expected that they are in cascade. Since the 1308.8 KeV transition is known ⁽⁵³⁾ to deexcite the 1308.8 KeV level, the 1372.5 KeV may feed this level directly. These two transitions may have the same intensity in the coincidence spectrum, as indicated in equation (E-3). The intensities of the transitions observed in this coincidence experiment are listed in Table 31, and are normalized to the 1372.5 KeV transition ($I = 9.0$).

As indicated in Table 31, the transitions at 545.7, 687.2, 828.0,

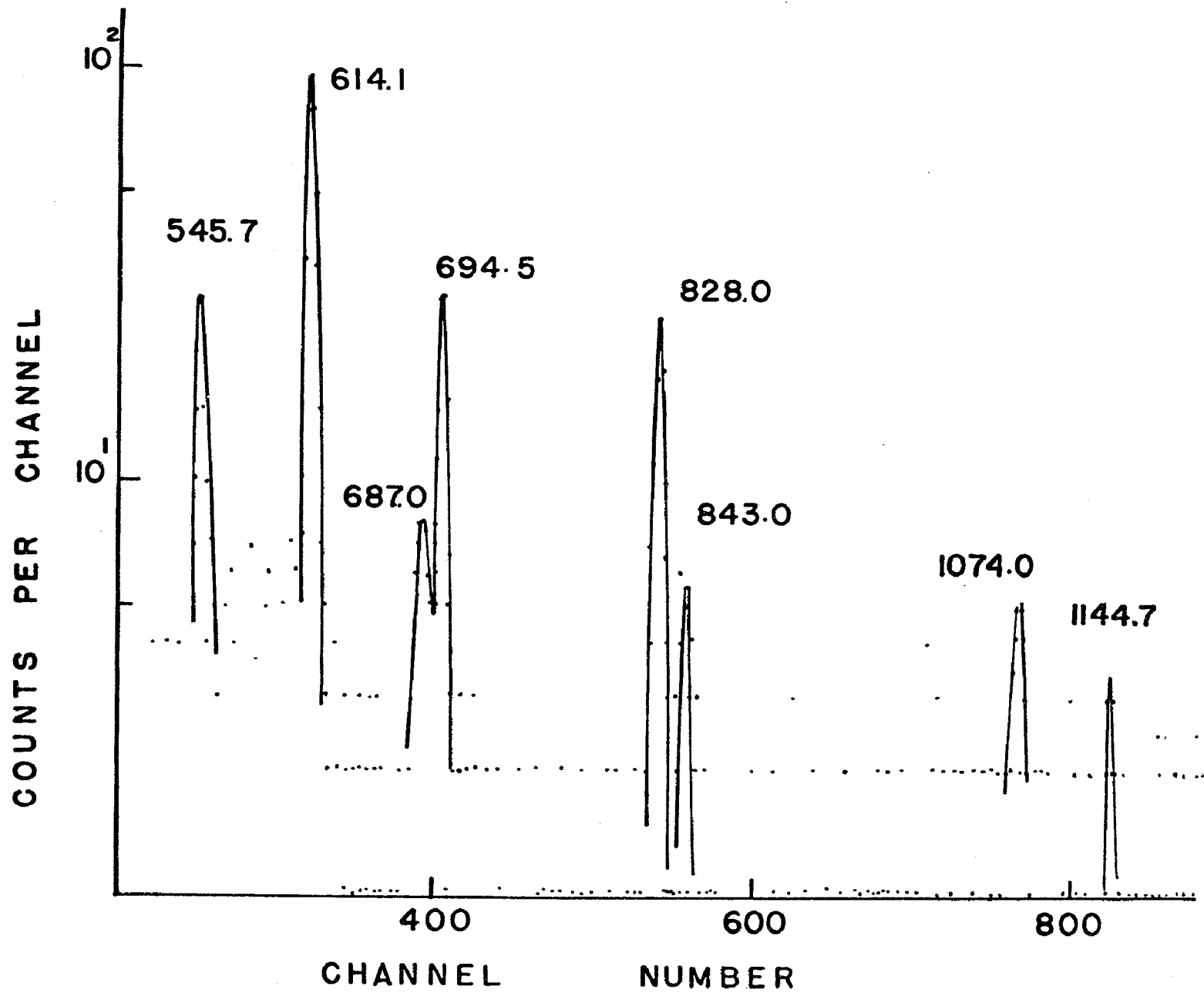


Fig. 41. ^{78}As gamma rays in coincidence with the gate which includes the 1373 and 1308 KeV transitions. (Energy region: 0.5-1.2 MeV.)

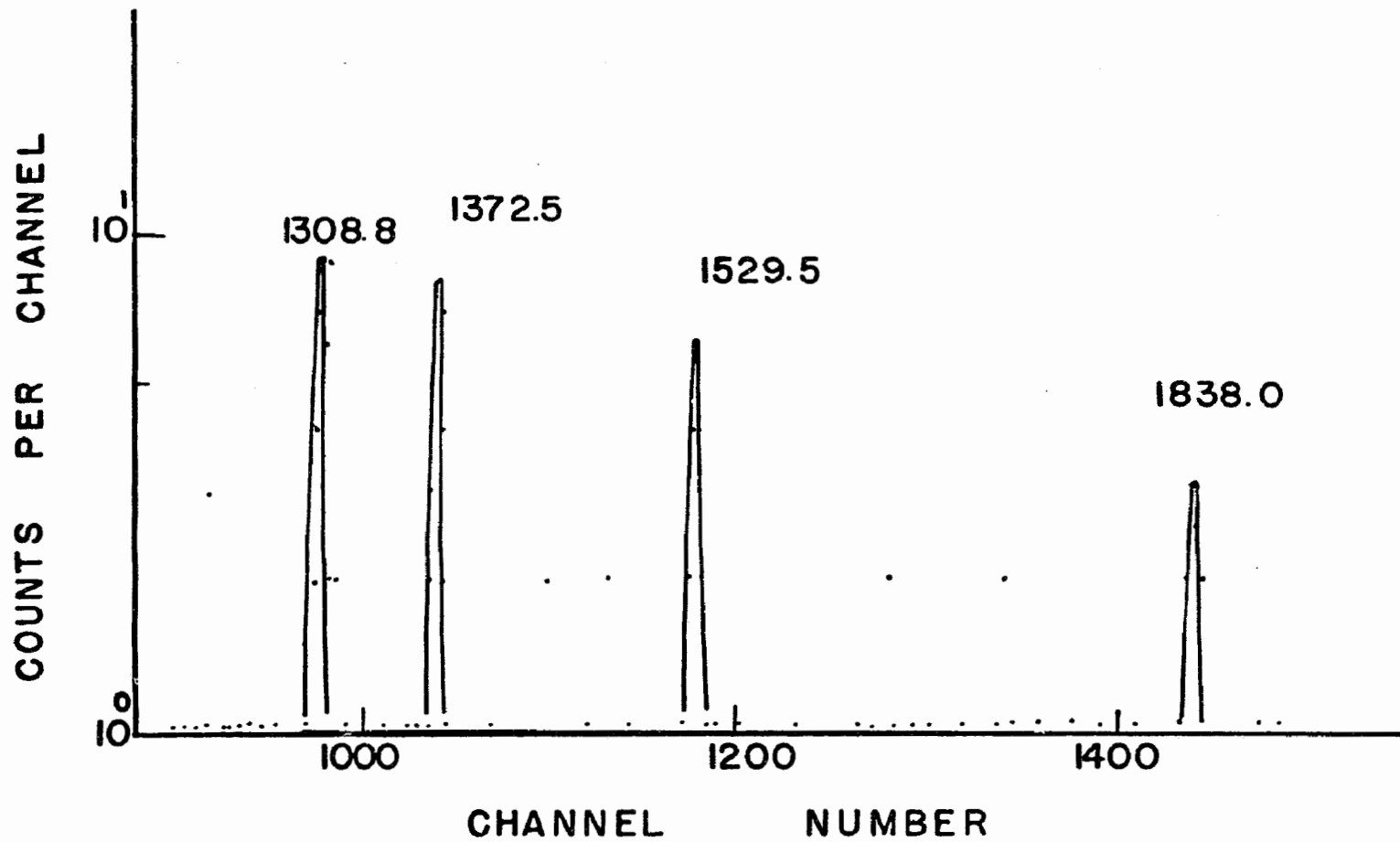


Fig. 42. ^{78}As gamma rays in coincidence with the gate which includes the 1373 and 1308 KeV transitions. (Energy region: 1.3-1.9 MeV.)

Table 31

Coincidence intensities of gamma rays in ^{78}As

(The gate includes the 1308.8 KeV, 1372.5 KeV transitions and part of the 1240.5 and 1381.0 KeV transitions.)

Energy in KeV	Relative coincidence Intensity ^(a)	(b)	
		Ratio	$\frac{I \text{ coinc.}}{I \text{ single}}$
545.7	6.0±1.0		1.13±0.18
614.1	37.5±5.5		0.375±0.055
687.2	2.3±1.1		0.92±0.44
694.8	14.0±2.5		0.45±0.08
828.0	15.0±2.7		1.00±0.18
842.0	1.3±0.6		0.5±0.3
1074.0	3.0±0.9		0.78±0.21
1140.4	2.6±0.9		0.83±0.20
1308.8	10.0±1.7		0.49±0.07
1372.5	9.0		1.0
1529.5	6.0±1.5		1.2±0.3
1838.0	3.6±0.9		1.2±0.3

(a) normalized to 9 for the 1372.5 KeV transition

(b) quoted error includes error in estimating the coincidence intensity only.

1529.5 and 1838.0 KeV may be in coincidence with the 1308.8 KeV transition on the grounds of the same $\frac{I \text{ coinc}}{I \text{ single}}$ ratio. The 545.7 and 687.2 KeV transitions have also been found to be in coincidence with the 694.8 KeV transition, as previously discussed (see Table 30). Thus it is probable that both weak transitions feed the level at 1308.8 KeV. The transitions at 1529.5 and 1838.0 KeV very likely feed the 1308.8 KeV level. This is supported by the previous discussion and the data shown in Table 31. The 694.8 KeV coincidence intensity and part of the 614.1 KeV as listed in Table 31, arises through coincidences of the 1372.5 KeV transition with these two transitions.

5.2.5. Construction of the decay scheme of ^{78}As

There is no doubt that the well known 614.1 KeV transition deexcites the 614.1 KeV 2^+ level in ^{78}Se . The second vibrational state, which has been observed (51-53) at 1320 KeV, should correspond to the 1308.8 KeV level which is deexcited through the 1308.8 KeV transition proceeding between this level and the ground state of ^{78}Se , and through the 694.8 KeV transition which proceeds between the 1308.8 KeV and the 614.1 KeV levels. Both assignments are in agreement with the coincidence data discussed in section 5.2.4.

The transition at 1240.5 KeV has been observed to be in strong coincidence with the 614.1 KeV transition (see Table 30). If this transition then deexcites a level at $614.1 + 1240.5 = 1854.6$ KeV, then it is possible

to place the 545.7 KeV transition between the 1854.6 KeV level and the 1308.8 KeV level. Such an accommodation is in good agreement with the coincidence data presented in Tables 30 and 31, which suggest that the 545.7 KeV transition is in coincidence with the 1308.8 and 694.8 KeV transitions. In (d,p), (p,p') and (d,d') reactions a level at 1.88 MeV is reported, which may correspond to the level observed here at 1854.6 KeV. (58-59)

The 1996.0 KeV transition has not been observed in the coincidence spectra of this work (see section 5.2.4), suggesting that this transition directly feeds the ^{78}Se ground state. Thus a 1996.0 KeV level may be introduced which in turn deexcites through the 1996.0 KeV transition. The observed 1381.0 and 687.2 KeV transitions then may be placed exactly between the 1996.0, 614.1 and the 1308.8 KeV level, respectively. The placement of these transitions as indicated above is in excellent agreement with the coincidence data of this work. The data presented in Table 30 support a direct 1381.0 and 614.1 KeV cascade, while the data of Tables 30 and 31 support the coincidence of the 687.2 KeV transition with the 1308.8 and 694.8 KeV transitions. A level at 2.03 MeV has been observed in (p,p') and (d,d') reactions and it may correspond to the 1996.0 KeV level introduced in this work. (59)

The strong coincidence observed between the 1372.5 and 1308.8 KeV transitions indicates that the 1372.5 KeV transition may deexcite a level at $(1372.5 + 1308.8)$ KeV = 2681.3 KeV. The difference in energy between this new level and the 614.1 KeV level is 2067.2 KeV.

Leaf 191 omitted in page numbering.

The transition at 2067.5 KeV observed in the singles spectra was found to be in direct coincidence with the 614.1 KeV level (see Table 30). For this reason, this transition may be placed between the 2681.3 KeV and the 614.1 KeV level. The 827.0 KeV energy difference between the 614.1 KeV level and the previously introduced 1854.6 KeV level, accommodates nicely the 828.0 KeV transition. The coincidence data of Table 30 and 31 indicate that this transition may be in coincidence with the 1308.8 or 694.8 transitions. However, the possibility that this transition is in coincidence with other transitions (for example, the 1240.5 KeV transition) could not be excluded. Nevertheless, the assumption that the 828.0 KeV transition proceeds between the previously mentioned levels indicates that this transition is in coincidence with the 1240.5, 545.7, 1308.8, 694.8 and 614.1 KeV transitions. Application of the data presented in Tables 30 and 31 in equation (E-3) indicates a good agreement of the assumption made with the coincidence data. Finally, a transition observed in the singles spectra at (2683.5 ± 3.0) KeV can proceed between the 2683.5 KeV level and the ground state of ^{78}Se . However, this is highly doubtful on the grounds that this transition has been observed in coincidence with the 614.1 KeV transition (Table 30). This suggests the introduction of a level at 3296.0 KeV which deexcites to the 614.1 KeV level through the 2683.5 KeV transition. This level has been observed in both (p,p') and (d,p) experiments (58,59) at 3.36 and 3.33 MeV, respectively. Further support for the existence of this level may be the fitting of the observed transition at 1440.4 KeV between this level and the 1854.6

KeV level.

In Table 30 it is indicated that the transition observed at 889.0 KeV is in strong coincidence with the 614.1 KeV level. It is very tempting to interpret this transition as deexciting a level at $(614.1 + 889.0) \text{ KeV} = 1503.1 \text{ KeV}$. This interpretation is possible because in (p,p') , (d,p) and (d,d') experiments a level at 1.51 MeV has been observed. One can assume this level to be the 0^+ or 4^+ member of the 2 phonon group. Assuming then that the 889.0 KeV transition deexcites the 1503.0 KeV level, the observed 1791.0 KeV transition may be fitted between the previously introduced 3296.0 KeV and the 1503.0 KeV levels. This is strongly supported by the coincidence data of Table 30, where the 889.0 KeV transition appears in strong coincidence with the 614.1 KeV transition. The transition at 1714.5 KeV, which is shown in Table 30 to be in strong coincidence with the 614.1 KeV transition, is assumed to deexcite a level at 2328.6 KeV. A level at 2.33 or 2.36 MeV has been observed in all (p,p') , (d,p) and (d,d') experiments .

The transition at 1529.5 KeV is shown in Table 31 to be in coincidence with the 1308.8 KeV transition. If this is taken into account, a level may be introduced at 2838.3 KeV which deexcites through the 1529.5 KeV transition. The observed weak 842.5 KeV transition may then be placed between this new level and the 1996.0 KeV level. The weak transition observed at (2843.5 ± 3.0) may also be placed between this level and the ground state. The difference in energy between this transition

and the adopted value of 2838.3 KeV for the newly introduced level is higher than the experimental error involved. This fact makes the assignment of this very weak transition into the decay of ^{78}As uncertain.

The coincidence data presented in Table 30 indicate that the 1921.0 KeV transition may be in strong coincidence with the 614.1 KeV level. The introduction of a $(1921.0 + 614.1)$ KeV = 2535.0 KeV level, may accommodate the weak 1228.0 KeV transition between this new level and the 1308.8 KeV level. The two weak transitions which are observed at 1893.0 and 1199.0 KeV have a difference in energy of (694.0 ± 1.7) KeV. This consideration introduces a level at 2508.0 KeV which in turn deexcites through the 1893.0 and 1199.0 KeV transitions, feeding the levels at 614.1 KeV and 1308.8 KeV, respectively.

The very weak transitions observed in the singles spectra at 3104.0 KeV may feed either the ground state of ^{78}Se or the first excited state at 614.1 KeV. Any other combination with a state above the 614.1 KeV level will lead to levels with energy higher than that allowed by the $Q = 4.1$ MeV value ^(15,53). If the second case is accepted, a 3718.0 KeV level may then be introduced. This state may correspond to a level at 3.7 MeV observed in (d,p) reaction experiments ⁽⁵⁸⁾. The observed weak transition in the singles spectra at 1720.0 KeV may then be placed between the 3718.0 and 1996.0 KeV levels.

The two weak transitions at 2798.5 and 2183.5 KeV have an energy difference of (615 ± 4.5) KeV. The 2183.5 KeV transition may be placed

between a new level at 2798.0 KeV and the 614.1 KeV level, while the 2798.5 KeV transition may feed the ground state of ^{78}Se .

The transition at 2218.3 KeV is observed to be in **coincidence** with either the 614.1 KeV or 694.8 KeV transition. The coincidence intensity suggests coincidence with the 694.8 KeV, but the error is too large for definite conclusions. If this transition is assumed to feed the 614.1 KeV level then it may deexcite a level at 2832.4 KeV. This is approximately 6 KeV lower than the 2838.3 KeV level introduced previously. If the 2218.3 KeV transition is assumed to feed the 1308.8 KeV level, then a level is introduced at 3527.0 KeV. This choice is closer to the coincidence observation described previously. If it is assumed that the transition at 1074.0 KeV deexcites this new level and feeds a level at 2453.5 KeV, then in turn the 2453.5 KeV level may be deexcited through the observed 1144.7 KeV transition feeding the 1308.8 KeV level. This assumption is supported by the coincidence data. These two transitions are observed to be in coincidence with the 1308.8 KeV and 694.8 KeV transitions (see Tables 30 and 31). Furthermore, they exhibit comparable intensities (see Table 28). Here it should be noted that the deexcitation order of the 3528.0 KeV level may be inverted with the 1144.7 KeV level, deexciting first the 3528.0 KeV level and the 1074.0 KeV transition deexciting a 2383 KeV level. Both possibilities are equally probable, and there is no way to decide which one is the most favourable. The existence of the 3528.0 KeV level is further supported by the observation of a 3.55 MeV level in (d,p)

(58)

experiments . The transition observed at 1838.0 KeV may also deexcite the level at 2453.5 KeV introduced previously. But the coincidence data presented in Table 30 indicate that this transition is in coincidence with either the 614.1 or the 694.8 KeV transitions. The data of Table 31 indicate that this transition is in coincidence with the 1308.8 KeV level. For this reason only, the 1838.0 KeV transition is considered to deexcite a level at $(1838.0 + 1308.8) \text{ KeV} = 3146.8 \text{ KeV}$, rather than deexciting the 2453.5 KeV level. In the final decay scheme shown in Fig. (43), the 2453.5 KeV level only is shown, instead of the equally probable 2386 KeV level. The only reason for this choice is the remote possibility that the 1838.0 KeV transition deexcites this level. Finally, the last level introduced at 3147.0 KeV has been observed in both (p,p') and (d,p) experiments at 3.14 MeV.

The levels of ^{78}Se deduced in the present work (Fig. (43)) are shown in Fig. (44) in comparison with the results of (p,p'), (d,p) and (d,d') experiments as obtained from refs. (53,58,59). Using the intensity values listed in Table 28 for the gamma rays of ^{78}As (15, 53) and the assumption that 25% of the transitions feed the ^{78}Se ground state, the feeding to the different levels of ^{78}Se has been calculated and are also shown in Fig. (43). Assuming that the Q value of ^{78}As is 4.1 MeV and using the half life value of 87 minutes for ^{78}As , the logft values have been calculated from the Moszkowski diagrams (15). These values are also shown in Fig. (43).

From the As systematics it is expected that the ground state of ^{78}As has a 2^- spin assignment. The $\log ft$ values of the transitions to the well known 2^+ levels at 614.1 and 1308.8 KeV support this assignment. The calculated $\log ft$ values are 7.7 and 7.6 respectively for these two levels, indicating ⁽⁴⁹⁾ a first forbidden transition which has typical values of 7 ± 1 . This in turn indicates spin and parity changes of 0,1 yes. Thus, the ^{78}As ground state spin is probably 2^- or 1^- . The $\log ft$ value for the transition to the 0^+ ^{78}Se ground state is 8.1. If the assumption ⁽⁵³⁾ of a 25% feeding of the ^{78}Se ground state is accepted, a unique first forbidden transition which has typical values ⁽⁴⁹⁾ of 8.5 ± 0.5 is indicated. The resulting spin and parity changes are 2 yes, favouring a 2^- ^{78}As ground state spin assignment. It is then reasonable to adopt a 2^- assignment for the ^{78}As ground state.

The $\log ft$ value for the transition to the 1503.0 KeV level is 8.6, indicating a unique first forbidden transition. Thus, a spin ⁽⁵⁹⁾ 0^+ , 4^+ is favoured for this level. The results of (d,p) experiments favour a 0^+ spin assignment. The $\log ft$ value to the 1854.6 KeV level ⁽⁵⁸⁾ favours a 0^+ or 4^+ assignment. Lin interpreting the results of (d,p) experiments assigned a 2^+ or 3^+ spin and parity for the observed 1.88 MeV level. The level at 1996.0 KeV with a 7.9 $\log ft$ value is probably a $(1,2 \text{ or } 3)^+$ level. The existence of the ground state 1996.0 KeV transition excludes the 3^+ assignment. Single particle estimates indicate that the 687.2 KeV transition is one multiple order lower

than the 1996.0 KeV transition. This supports a 2^+ assignment for this level. Since the existence of two close lying 2^+ levels is not very usual (but not impossible), a 3^+ assignment for the 1854.6 KeV level is strongly indicated.

Beta transitions to the 2328.6 KeV level have a $\log ft$ value of 7.6 indicating a $(2,1,3)^+$ assignment. Data from (d,p) experiments suggest a $(0^+,2^+)$ spin assignment. Thus, the most likely spin assignment for this level is 2^+ . The three levels at 2453.5, 2508.0, 2535.0 KeV have not been observed in (d,p) or (p,p') experiments. The $\log ft$ values for the 2508.0 and 2535.0 KeV levels indicate a positive parity and spin assignment $(1,2,3)^+$. The level at 2453.5 2386.0 KeV is very weakly fed or not fed at all. It may be a 0^+ , 4^+ level. The level at 2681.5 KeV is strongly populated and the calculated $\log ft$ value of 6.2 indicates an allowed or a first forbidden transition. Thus, from the $(1,2,3)^{\pm}$ spin and parity assignments, the 3^- is the most likely. On the basis of ^{78}Se systematics, a negative 3^- octupole vibrational state is expected to appear at this energy. In (d,p) and (d,d') as well as (p,p') experiments a 3^- level is observed at around 2.56 MeV which probably corresponds to the 2681.5 KeV level observed in this work. The state at 2798.0 KeV is observed in (p,p') experiments as a positive parity state, but has not been observed in (d,p) experiments. The $\log ft$ value of 7.5 for the transitions to this level indicates a $(1,2,3)^+$ spin and parity assignment. However, since the 2798.5 KeV transition

originating from this level feeds the ground state, the 3^+ assignment may be excluded. Thus, the probable assignment is $(1^+, 2^+)$. The level at 2838.3 KeV is observed in (p, p') experiments as a negative parity state. The logft value of 6.7 for this level indicates a negative parity state, although positive parity cannot be excluded. A 2^- spin assignment is not very improbable.

The levels at 3148.0 and 3296.0 KeV have been observed in both (p, p') and (d, p) experiments ^(58, 59). In the (p, p') experiments these levels appear as negative parity levels, and in (d, p) experiments ⁽⁵⁸⁾ as $(0, 2)^+$. The logft values obtained in this work are in favour of a negative parity assignment.

Finally, the two levels at 3528.0 and 3718 KeV have been observed in (d, p) experiments as positive and negative states, respectively. The logft values in this work suggest negative parity assignments for these states. The $(2^-, 3^-)$ assignments for the 3718 KeV level by Lin ⁽⁵⁸⁾ are in agreement with the assignment suggested by the logft value obtained in this work.

5.3. The decay of ^{92}Y

The ^{92}Y nucleus decays with a half life of 3.5 hours ⁽¹⁵⁾ by electron emission to the excited states of ^{92}Zr . The decay of ^{92}Y has been extensively studied by Bunker et al ⁽⁶⁰⁾. These workers have separated ^{92}Y activities from ^{235}U fission products and measured their gamma and beta ray spectra with the help of NaI(Tl) and plastic detectors. The

proposed decay scheme of ^{92}Zr by Bunker et al ⁽⁶⁰⁾ included six levels. The results obtained by these authors have been later confirmed by (p,p') and (d,p) experiments ⁽⁶¹⁾. Very recent (p,p') and (d,p) experiments ^(62,63) revealed the existence of excited states ⁽⁶⁰⁾ in ^{92}Zr up to 5 MeV. Although the results of Bunker et al are consistent with the results of (d,p) and (p,p') experiments, it is tempting to investigate the beta decay of ^{92}Y by means of a high resolution Ge(Li) detector. The need for such investigation is further supported by the lack of any work in the literature involving a Ge(Li) detector investigation of the decay of ^{92}Y .

The ^{92}Y activity was produced via the $^{92}\text{Zr}(n,p)^{92}\text{Y}$ reaction using the 14 MeV neutron flux of the USRC neutron generator. A sample of 300 mg of isotopically enriched ^{92}Zr was purchased from the Commercial Products division of the Oak-Ridge Nat. Lab., Tenn., USA. The chemical analysis provided by the supplier indicated the following isotopic composition:

$^{92}\text{Zr}(94.5\%)$, $^{90}\text{Zr}(3\%)$, $^{91}\text{Zr}(1.3\%)$, $^{94}\text{Zr}(1.2\%)$ and $^{96}\text{Zr}(0.15\%)$. ⁽⁶⁴⁾

The cross section reported ⁽⁶⁴⁾ for the $^{92}\text{Zr}(n,p)^{92}\text{Y}$ reaction is (22 ± 4) mb. This cross section value for the $^{92}\text{Zr}(n,p)^{92}\text{Y}$ reaction is used in equation (4.22) and the ^{92}Zr activity expected to be produced after a 60 minute irradiation of the ^{92}Zr sample is estimated to be about 0.2 μC . The results of Bunker et al ⁽⁶⁰⁾ indicate that 85% of the decay of ^{92}Y feeds the ^{92}Zr ground state. Taking this into account together with the low efficiency of the Ge(Li) detectors, one has no

difficulty in deciding that the expected counting rate for the gamma spectrum of ^{92}Zr is very low.

These considerations have been substantiated by preliminary experiments where the counting rate was found to be low to allow a good statistical analysis of the weak ^{92}Zr peaks. After the end of one irradiation, the sample was measured for a period of approximately one half life. After the end of this counting period, the analyzer was stopped and the obtained spectrum was punched on a tape. The sample was irradiated again, and the counting of the sample was continued after the end of this new irradiation. This procedure was repeated four times and the total counting period used was 23 hours. In this way about 6×10^4 counts were obtained under the prominent 934.5 KeV peak of ^{92}Zr . After the end of the counting period, the background radiation has been subtracted.

Because of the presence of the ^{90}Zr and ^{92}Zr isotopic impurities $^{89\text{m}}\text{Zr}$, $^{89\text{g}}\text{Zr}$, $^{90\text{m}}\text{Y}$ and $^{87\text{m}}\text{Sr}$ activities are expected to be present in the gamma spectrum of the irradiated target. The expected contaminants were easily identified in the low energy gamma spectrum of the target.

The single gamma spectra were obtained using the $29 \text{ cm}^3 \text{ Ge(Li)}$ detector. The front face of the detector was covered with a lucite absorber of 1 cm thickness. The amplifier and the stretcher were set in such a way that the energy region from 0.3 to 2.3 MeV was displayed in the 2048 channel analyzer. The combined energy resolution was about 4 KeV fwhm at 1.33 MeV. Energy and intensity calibration have been

made in the same way as described in the previous sections.

5.3.1. Gamma ray singles spectra for $E < 1$ MeV

The spectrum obtained after the 23 hours counting period is shown in Fig. (45) for the energy region below 1 MeV. The background radiation has been subtracted from the spectrum shown in Fig. (45). Also in this spectrum part of the intense 909.5 KeV ^{89}Zr peak has been subtracted as is later discussed. In this subtraction process the irradiated sample was used after all the ^{92}Y has decayed. The ^{89}Zr activity has a relatively long half life (78 hours).

In the spectrum of Fig. (45) the two peaks at 511.0 and 909.5 KeV are assigned ⁽¹⁵⁾ to the ^{89}Zr impurity. The peaks at 480.3 and 556.0 KeV are assigned ⁽¹⁵⁾ to the $^{90\text{m}}\text{Y}$ and $^{91\text{m}}\text{Y}$ activity respectively. The $^{90\text{m}}\text{Y}$ activity is produced via the $^{90}\text{Zr}(n,p)^{90}\text{Y}$ reaction while the $^{91\text{m}}\text{Y}$ activity is formed via the $^{91}\text{Zr}(n,p)^{91}\text{Y}$ reaction. The peak at 591.0 KeV labelled with a question mark in the spectrum of Fig. (45) may well be the $^{89\text{m}}\text{Zr}$ isomeric transition. The $^{89\text{m}}\text{Zr}$ isomer has a half life of about four minutes. The presence of the $^{89\text{m}}\text{Zr}$ in the spectrum is explained since the time between the end of each irradiation and the beginning of each counting period was less than 10 minutes.

The peaks at 450.7, 492.0, 560.7, 844.0 and 934.5 KeV cannot be assigned to any other isotopic impurity and are considered to belong to the decay of ^{92}Y . The peaks observed here agree well with the results ⁽⁶⁰⁾ of Bunker et al who report peaks at 448, 490, 560, 840 and 932 KeV

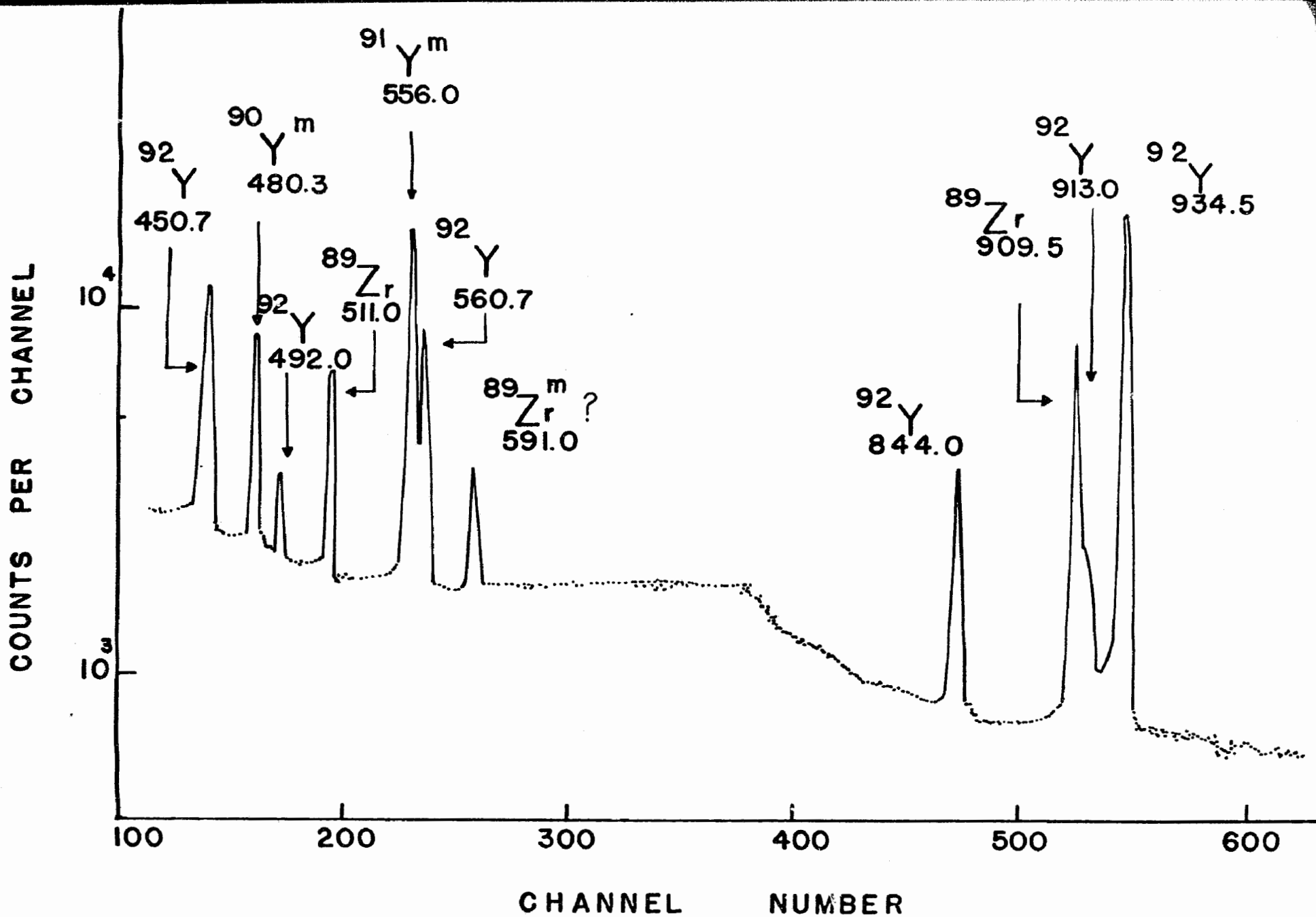


Fig. 45. Gamma ray spectrum of ^{92}Y as observed with the 29 cm^3 Ge(Li) detector. (Energy region: 0.4-1.0 MeV.)

in the same energy region. The energy and intensity values obtained in the present experiments are listed in Table 32 and are compared with the data of Bunker et al ⁽⁶⁰⁾. There is in general good agreement in the reported energies and intensities.

The data obtained by Bunker et al ⁽⁶⁰⁾ support the existence of a 900 ± 10 KeV transition in this part of the spectrum. The deduction of this transition according to Bunker et al ⁽⁶⁰⁾ is based on coincidence data. The part of the spectrum which includes the 910 and 934 KeV transitions as obtained after the 23 hours counting period (before any subtraction) is shown in Fig. (46A).

The ^{89}Zr 909.5 KeV peak is shown to be as intense as the 934.0 KeV transition of ^{92}Y . No 900 KeV transition is observed in this spectrum. Comparison of the 909.5 KeV peak with the neighbouring 934.5 KeV peak shows a broadening in the right foot of the 909.5 KeV peak. This observation may be an indication that the peak observed by Bunker et al ⁽⁶⁰⁾ at 900 ± 10 KeV exists but its energy is about 912 KeV.

In an attempt to locate the position of this peak more precisely, the remaining ^{89}Zr activity in the irradiated spectrum has been subtracted from the spectrum of Fig. (46A). The spectrum obtained after 15 hours of subtraction is shown in Fig. (46B). As can be seen in Fig. (46B), ⁽⁶⁰⁾ the transition observed by Bunker et al ⁽⁶⁰⁾ is formed at 913.0 ± 0.8 KeV, provided no channel drifts occurred during the subtraction period. The intensity value obtained from this spectrum for this 913.0 KeV transition is (5.2 ± 1.2) relative to the 934.5 KeV transition. In

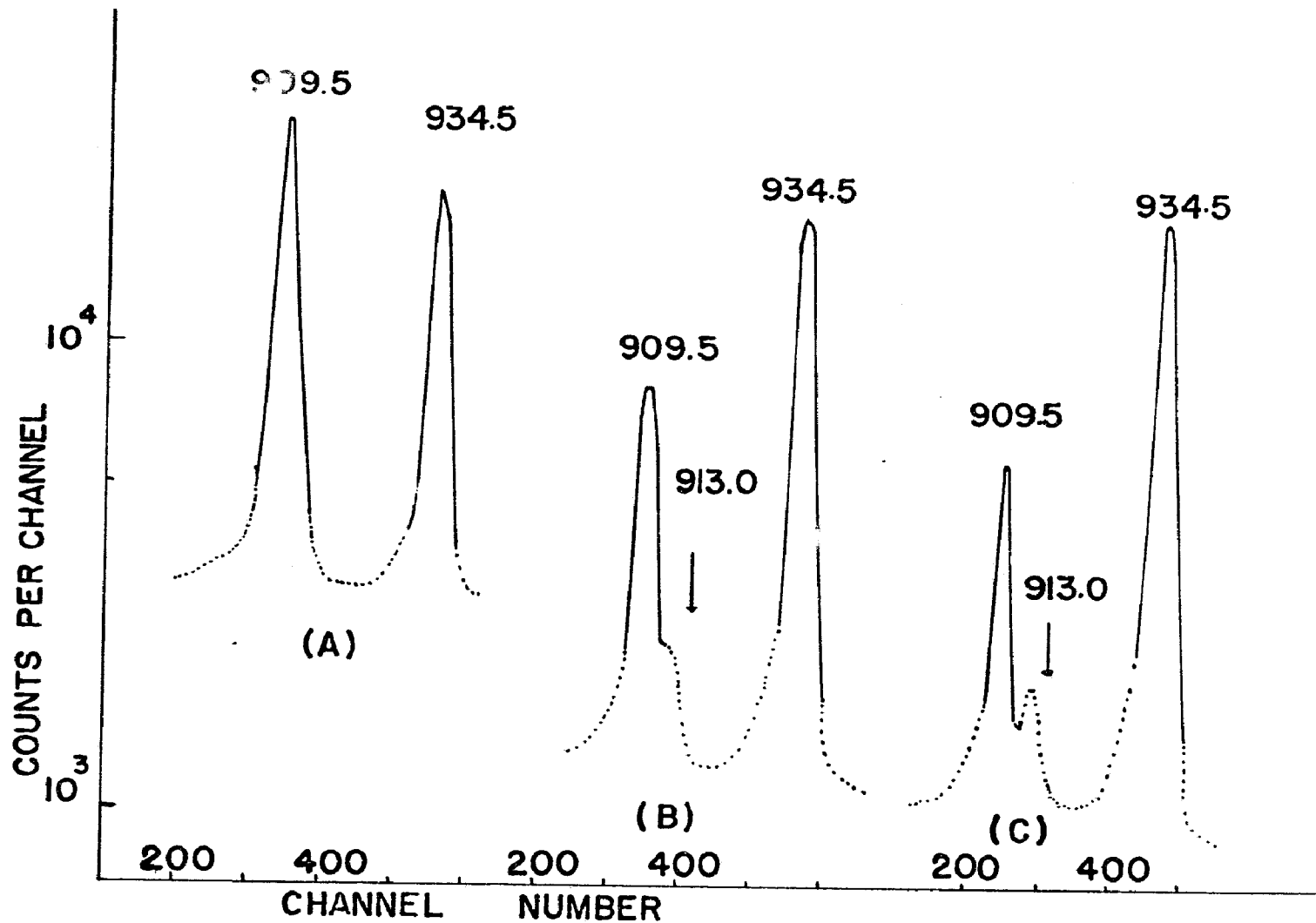


Fig. 46. The 909 and 934 KeV transitions observed in the irradiated Zr target. (A) The spectrum after a 23 hours counting period. (B) The spectrum after a 15 hours subtraction of the remaining ^{89}Zr activity. (C) The spectrum after 18 hours subtraction period.

Fig. (46C) the spectrum obtained after 18 hours subtraction period is shown. The 913.0 KeV peak is more clearly shown. Again the assumption is made that the subtraction was done properly, without channel drifts. The intensity values obtained for this transition from the spectrum shown in Fig.45 are (5.0 ± 1.0) . The results of this work support the data of Bunker et al ⁽⁶⁰⁾ for the existence of the (913 ± 0.8) KeV transition. The intensity value of this transition may be taken as (5.1 ± 1.1) , i.e., the average of the two previously obtained values.

5.3.2. Gamma ray singles spectra for $E > 1$ MeV

The part of the observed spectrum which includes transitions from 1 to 1.5 MeV is shown in Fig. (47). Part of the background radiation has been subtracted. Except for the well known ^{60}Co and ^{40}K peaks at 1173.2, 1132.5 and 1460.0 KeV, which occur as background radiation, the strong peak at 1368.5 KeV is due to ^{24}Na contamination. The strong transition at 1404.6 KeV and the weak transition observed at 1132.6 KeV cannot be attributed to any background or contamination activity and they are assigned to the ^{92}Y activity. The strong transition observed at 1404.6 KeV with an intensity of 32 with respect to the 934.5 transition may correspond to the 1395 KeV transition observed by Bunker in the decay of ^{92}Y with an intensity of 34.

The only transition observed by Bunker et al ⁽⁶⁰⁾ which is comparable to the presently observed 1132.6 KeV transition is the 1120 ± 10 KeV transition. The intensity value of this transition as obtained by

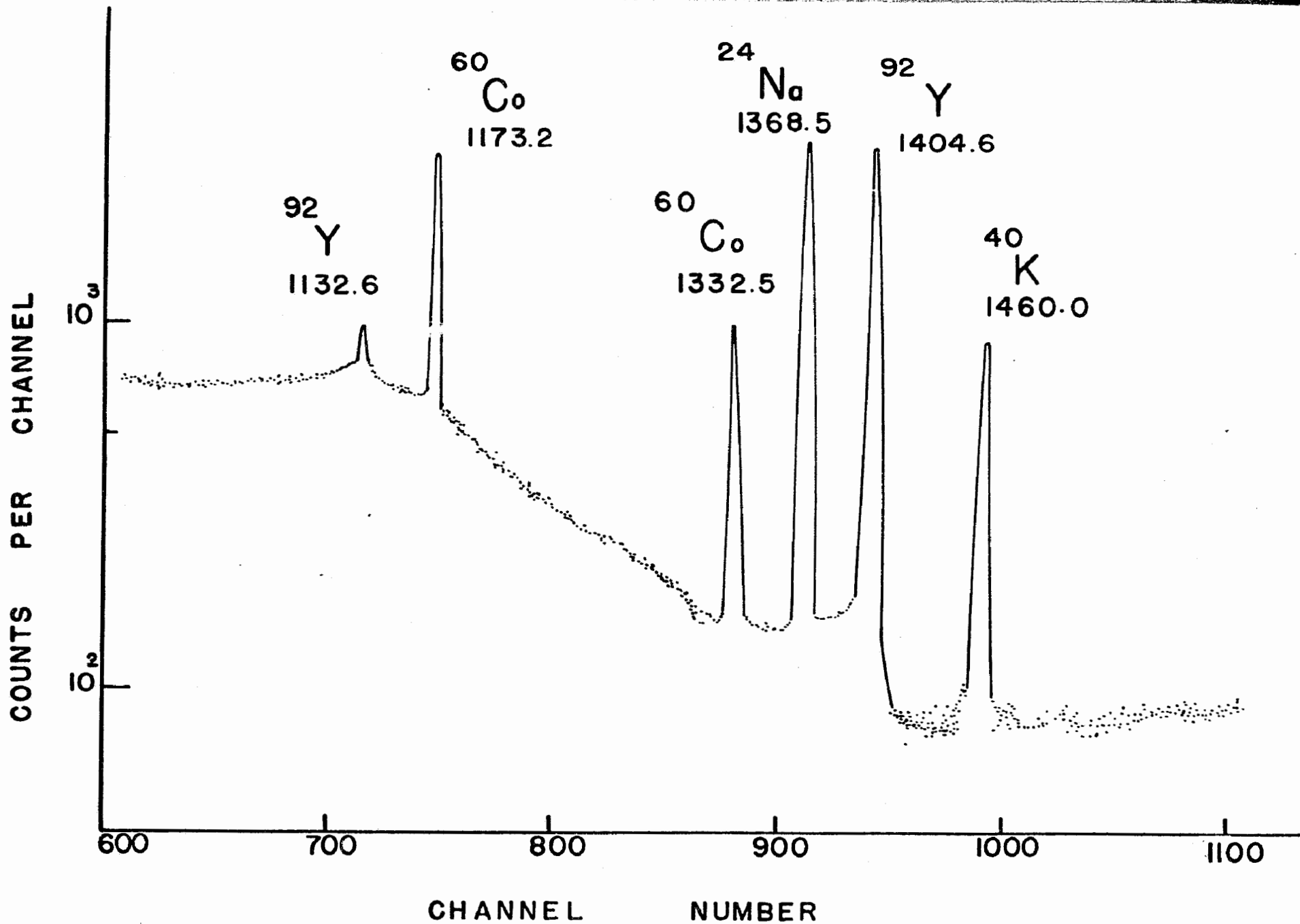


Fig. 47. Gamma ray spectrum of ^{92}Y as observed with the 29 cm^3 Ge(Li) detector. (Energy region: 1.0-1.5 MeV.)

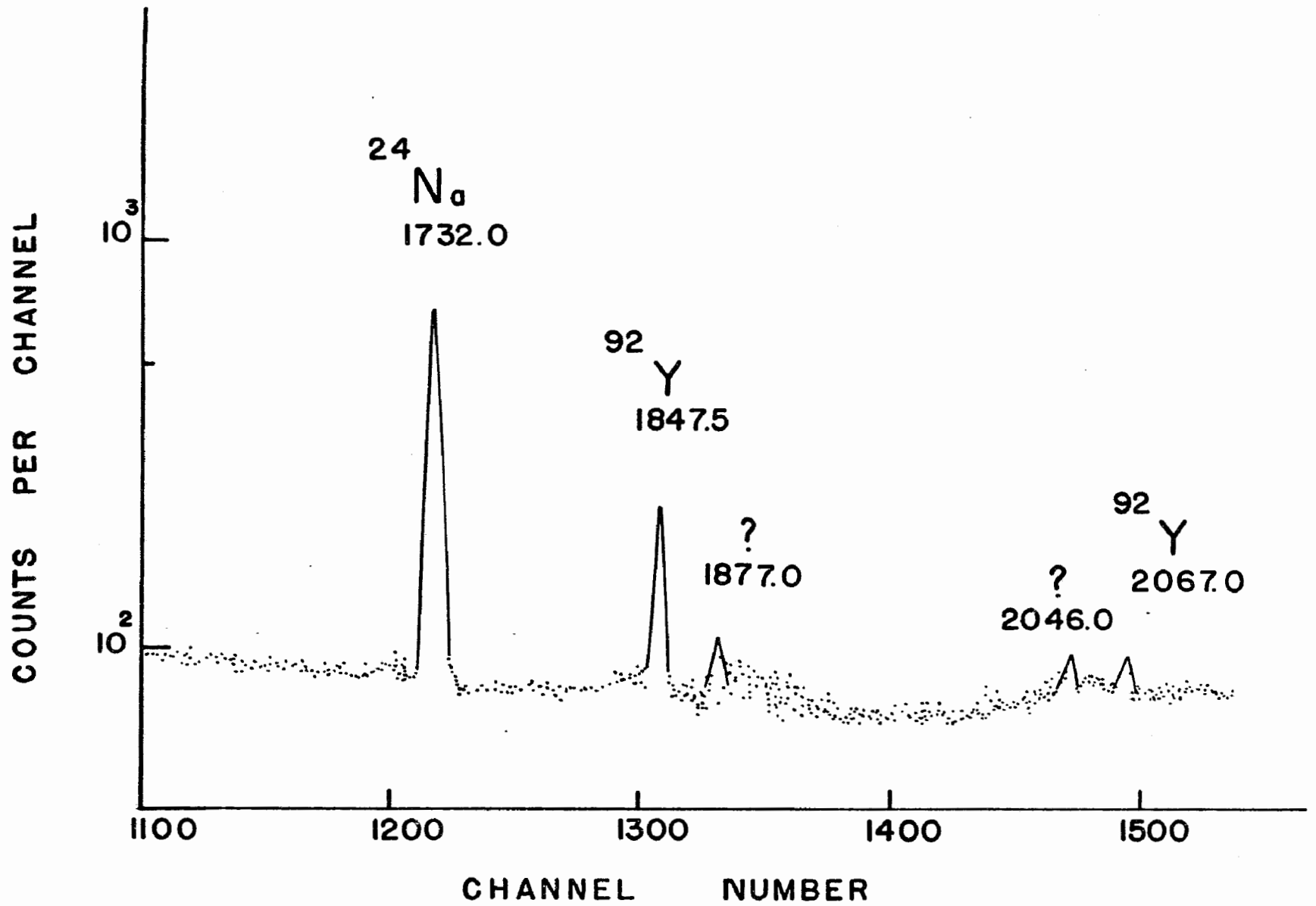


Fig. 48. Gamma ray spectrum of ^{92}Y as observed with the $29\text{ cm}^3\text{ Ge(Li)}$ detector. (Energy region: 1.5-2.1 MeV.)

Table 32

Energy and intensity of gamma rays observed in the decay of ^{92}Y
(60)

Present work		Bunker et al	
Transition(a) in KeV	Intensity ^(b)	Transition in KeV	Intensity
450.7±0.5	18.2±0.6	448±2	16.5±1.3
492.0±1.0	3.4±0.3	490±10	3.3±0.4
560.7±0.4	18.3±0.9	560±2	19.0±1.5
844.0±0.4	10.7±0.7	840±10	8.0±1.0
913.0±0.7	5.8±1.0 ^(c)	900±10	6.0±0.7
934.5±0.1	100.0	932±2	100.0
1132.6±1.0	1.9±0.2	1120±10	1.7±0.2
1404.6±0.3	32.0±0.7	1395±10	34±2
1847.5±0.5	2.4±0.2	1830±10	2.8±0.3
2067.0±3.0	0.3±0.10	2060±20	0.3±0.1
1877.0±2.0 ^(d)	0.5±0.2		
2046.0±3.0 ^(d)	0.25±0.10		

(a) Errors quoted include uncertainty in the determination of the centroid position of the peaks as well as uncertainty in the channel to energy conversion factor.

(b) Errors quoted include uncertainty in the determination of the areas of the photopeaks as well as uncertainty in the relative efficiency factor.

(c) Average value obtained from singles and coincidence experiments.

(d) This transition has not been established with certainty as belonging to the decay of ^{92}Y .

